Illuminating Coronavirus-Host Interactions

Matthijs Raaben

Cover design by W. Bartelink
Printed by Ipskamp, Amsterdam
ISBN: 978-90-393-5138-3

Illuminating Coronavirus-Host Interactions

Nieuw licht op
coronavirus-gastheer interacties
(met een samenvatting in het Nederlands)

Proefschrift

ter verkrijging van de graad van doctor aan de Universiteit Utrecht
op gezag van de rector magnificus, prof.dr. J.C. Stoof,
ingevolge het besluit van het college voor promoties
in het openbaar te verdedigen op
donderdag 3 september 2009 des middags te 2.30 uur

door

Matthijs Raaben
geboren op 13 oktober 1980 te Groenlo

Promotor:

Prof.dr. P.J.M. Rottier

Co-promotor:

Dr. C.A.M. de Haan

The research described in this thesis was financed by grants from the The Netherlands Organization for Scientific Research (NWO) and the M.W. Beijerinck Virology Fund, Royal Netherlands Academy of Arts and Sciences. Printing of this thesis was financially supported by Biotrading Benelux, Promega Benelux, and the Eijkman Graduate School.

Contents

Chapter 1

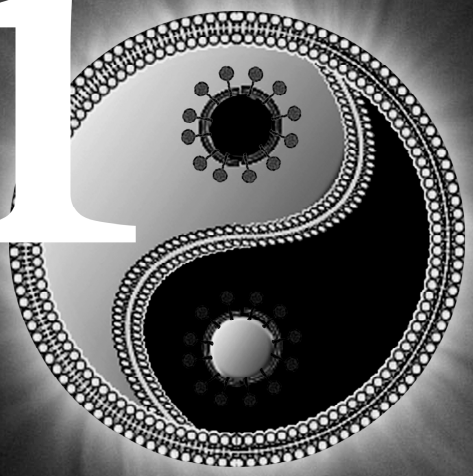

General Introduction

General Introduction

Viruses are infectious agents incapable of growing or reproducing outside a host cell. They are completely dependent on the cellular machinery of the host for their multiplication. On the other hand, however, viruses also have to deal with the immune defences of the host. Apparently, viruses are walking a thin line between hijacking the cellular machinery of the host and at the same time escaping from its defences. This thesis deals with these virus-host interactions at the cellular level, but also at the level of the organism.

Table 1. The *Nidovirales*: their family members, main representatives, hosts, and principal associated diseases.

Virus family	Genus	Main representatives	Host	Disease
Arteriviridae	Arterivirus	Equine Arteris Virus (EAV)	Horse,	Respiratory infection
Coronaviridae	Coronavirus			
	group 1	Feline Coronavirus (FCoV)	Cat	Enteritis/Peritonitis
		Transmissible GastroEnteritis Virus (TGEV)	Pig	Enteritis
		Porcine Respiratory Coronavirus (PRCoV)	Pig	Respiratory infection
		Canine Coronavirus (CCoV)	Dog	Enteritis
		Human Coronavirus (HCoV)-229E	Human	Respiratory infection
	group 2a	Mouse Hepatitis Virus (MHV)	Mouse	Respiratory infection/ Hepatitis/Encephalitis/Enteritis
		Bovine Coronavirus (BCoV)	Cow	Enteritis
		Human Coronavirus (HCoV)-OC43	Human	Respiratory infection
		Hemagglutinating Encephalomyelitis Virus (HEV)	Pig	Respiratory infection
		Turkey Coronavirus (TCoV)	Turkey	Enteritis
	group 2b	Severe Acute Respiratory Syndrome Virus (SARS-CoV)	Human	Respiratory infection
	group 3	Infectious Bronchitis Virus (IBV)	Chicken	Respiratory infection
	Torovirus	Equine Torovirus (EToV)	Horse	Enteritis
Roniviridae	Okavirus	Gill-Associated Virus (GAV)	Prawn	Lymphoid hypertrophy

The Coronavirus Family

Coronaviruses (CoVs) are enveloped, positive-sense, RNA viruses, which together with the Torovirus genus, constitute the family of *Coronaviridae*. These viruses are grouped with two other virus families (i.e. the *Arteriviridae* and the *Roniviridae*) into the order *Nidovirales* (11). The classification of these virus families is not based on structural similarities, but on general features of genome organization and gene expression (42). Nidus in Latin means nest, which refers to the nested set of subgenomic RNAs that all of these viruses produce during infection. The CoVs themselves are again subdivided into three different phylogenetic groups, which are classified on the basis of serological and

genetic properties (Table 1). In view of the recent increase in the number of newly discovered CoVs and available sequence data, a new taxonomic organization has recently been proposed (Fig.1), in which the three different CoV phylogenetic groups are converted into genera designated Alpha-, Beta and Gammacoronavirus. As a consequence, the genus Torovirus has been allocated to a subfamily (27). This proposal has yet to be formally approved (15).

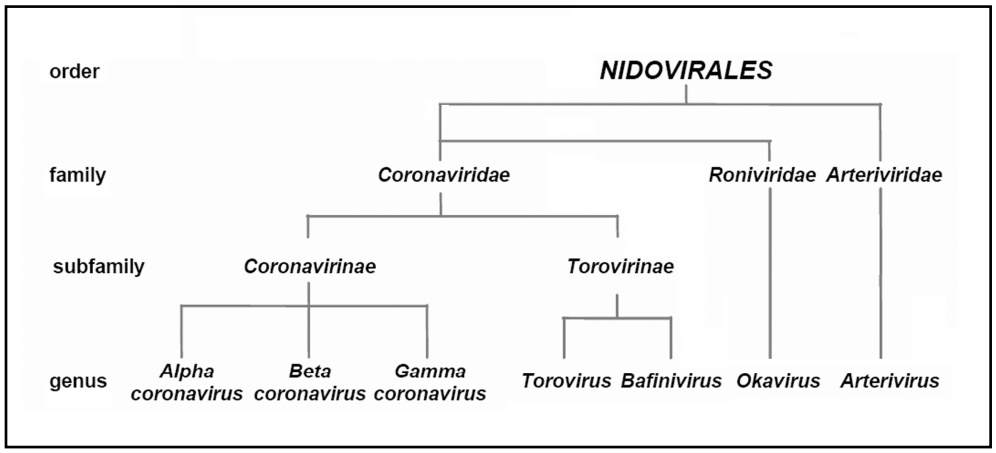

Fig.1. Newly proposed taxonomic organization of the *Nidovirales*.

The Coronavirion and its Structural Components

CoV particles are about 80-160 nm in diameter and have a characteristic crown-like appearance -hence the name coronavirus- when examined with an electron microscope. This phenotype is caused by prominent, petal-shaped spike (S) glycoproteins that extend (20 nm-long) from the viral envelope, generating the solar image as shown in Fig.2A. Fixed within the viral envelope, the S protein is responsible for both virus cell attachment and subsequent membrane fusion. In addition to the S protein, CoVs have at least two other proteins anchored in their envelope: the triple-spanning membrane protein M, and the small hydrophobic membrane protein E, which both play crucial roles in virus budding. Viruses from group 2 like BCoV, HCoV-OC43, and several MHV strains, have an additional membrane protein; the hemagglutinin-esterase glycoprotein HE. These viruses exhibit additional surface protrusions alongside the spikes (Fig.2B) (8, 37, 79). A schematic representation of the coronavirion is drawn in Fig.2C, showing both the viral envelope and the ribonucleoprotein (RNP) structure, which contains a copy of the viral genome packaged

into a helical arrangement by numerous copies of the nucleocapsid protein N. In a recent study, it was shown that the core structure is flexible and extensively folded upon itself within the coronavirion. This flexibility may well be essential for CoVs to tolerate the packaging of its very large RNA genome (1).

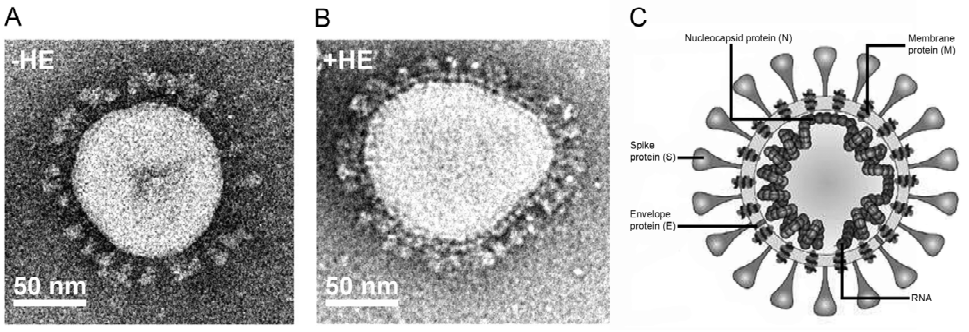

Fig.2. Structure of the coronavirion. Electron micrographs of MHV virus lacking (A) or containing (B) the HE envelope protein (adapted from Lissenberg *et al*. 2005 [46]). A schematic representation of the coronavirion is depicted in panel C. The viral genomic RNA is packaged by the N protein forming the helical ribonucleoprotein core. This nucleocapsid is surrounded by a lipid bilayer in which the S (trimer), M, and E proteins are incorporated. A few group 2 CoVs contain an additional membrane protein, namely the HE protein (dimer).

Coronavirus Genome Organization

CoVs contain a plus-stranded RNA genome of approximately 30 kilobases in size, which is the largest non-segmented viral genome identified to date. The genomic RNA contains a cap structure at the 5' end and is polyadenylated at its 3' end, which makes it structurally equivalent to a host mRNA. Both of these termini contain untranslated regions (UTRs) that harbour cis-acting elements, which are essential for viral replication and transcription. The CoV genome organization is extremely conserved, encoding a specific set of genes that always occur in the following order: 5'UTR-replicase-S-E-M-N-3'UTR (Fig.3). Interspersed in between these conserved structural genes so-called accessory genes are present, which vary between CoVs from the different phylogenetic groups. The replicase gene, which actually consists of two large open reading frames (ORFs), accounts for more than two-thirds of the CoV genome. These ORFs are translated from the genomic RNA, generating two large polyproteins designated as polyprotein (pp) 1a and 1ab. ORF1b is only translated after translational read-through via a -1 frameshift, which is mediated by a RNA pseudoknot structure (9, 57, 81). The genes downstream of the polymerase gene are

translated from a nested set of subgenomic (sg)RNAs, which are produced by a process of discontinous transcription (41, 70, 73, 75). Transcriptional regulating sequences (TRSs), which are present in the CoV genome upstream of each gene, are used as signals for the generation of this set of sgRNAs. Although these sgRNAs are structurally polycistronic, only the most 5' gene of each is generally translated. As a result of this rather complex transcription mechanism, the sgRNA encoding the N protein is most abundantly transcribed, whereas the sgRNA for the more upstream located S gene is far less expressed (52).

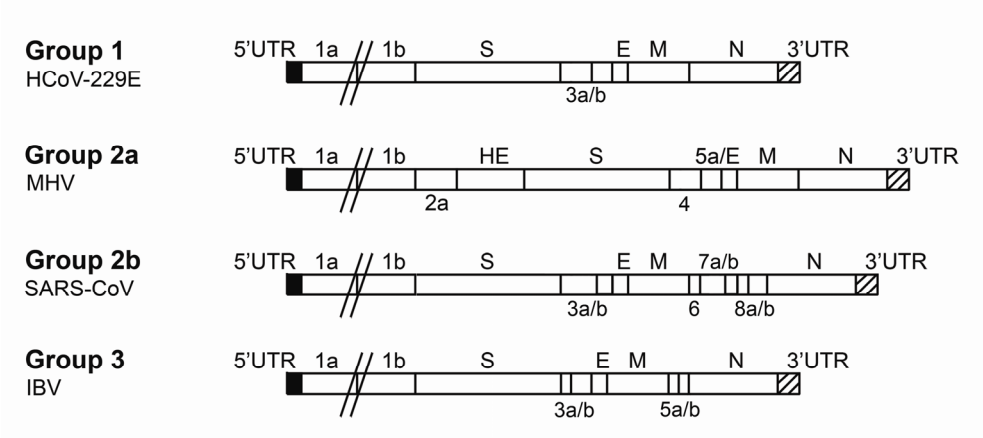

Fig.3. The genome organization of coronaviruses. Representatives of group 1 (HCoV-229E), group 2a (MHV), group 2b (SARS-CoV), and group 3 (IBV) are shown. Note that the order of the polymerase and structural genes is strictly conserved between the different groups. Also the accessory genes from the different CoVs, which flank the structural genes, are indicated.

The Coronavirus Infectious Cycle

Attachment & Entry

The first step in any virus infection cycle involves the attachment to a target cell. The viral tropism is obviously largely mediated by virus-receptor interactions. The majority of CoVs display restricted species specificity: porcine, human, and feline CoVs exploit the cell membrane-bound metalloprotease, aminopeptidase N (APN) from their respective host species as a receptor; MHV can bind to murine glycoproteins from the carcinoembryonic antigen (CEA) family; and some CoVs can interact with carbohydrate moieties on the cell surface (34). The binding of virus particles to these cellular receptors is mediated by the S protein. Subsequently, this interaction will trigger conformational changes in the S protein,

which result in the fusion of the viral envelope with a limiting cellular membrane (7). While several CoVs appear to enter cells via endocytic pathways, others are able to induce fusion independently of low pH at the plasma membrane (4, 12, 22, 30, 87, 92).

Replication and Transcription

After the initial entry/fusion event, the nucleocapsid is released into the cellular cytoplasm where disassembly of the ribonucleoprotein complex takes place, thereby allowing the genomic RNA to immediately serve as a template for the synthesis of pp1a and pp1ab. These two polyproteins are subsequently proteolytically processed by an internal chymotrypsin-like proteinase and one or two papain-like proteinases, yielding 16 mature non-structural proteins (i.e. nsp1-16) (Fig.4) (94).

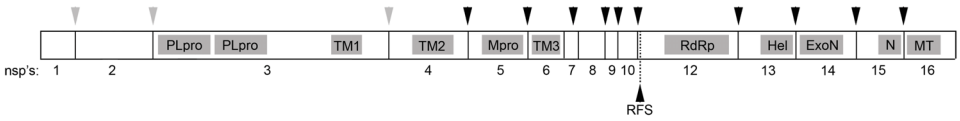

Fig.4. A schematic representation of the coronavirus replicase. The cleavage products (nsp's) of pp1ab are depicted by the numbers (1-16), whereas the location of the pseudoknot structure, separating the polymerase gene in ORF1a and ORF1b, is indicated as RFS (ribosomal frameshift). The actual protease cleavage sites are also depicted: cleavage by the papain-like proteinases (PLpro) (grey arrowheads), or cleavage by the main proteinase (Mpro) (black arrowheads). Within several nsp's, essential domains are highlighted, including the putative transmembrane domains (TMs), RNA dependent RNA polymerase (RdRp), helicase (Hel), exonuclease (ExoN), endoribonuclease (N), and methyltransferase (MT).

Together, these nsp's assemble into membrane-bound viral replication complexes (RCs), which serve as the factories for *de novo* viral RNA synthesis (72, 84). In addition, the viral N protein is also recruited to the RCs as well as some cellular proteins (71). In infected cells, the RCs are detected in the perinuclear region, being anchored to virus-induced double-membrane vesicles (DMVs) (26, 28). For MHV and SARS-CoV, the cleavage products nsp3, nsp4, and nsp6 contain hydrophobic domains, which presumably function in the membrane-anchoring of the viral RCs (31, 63, 94, 95). The subcellular origin of the DMVs has not been clearly defined yet, but a number of organelles (i.e. the ER, and Golgi complex) and cellular transport pathways (i.e. endosomal trafficking, and the autophagic pathway) have been implicated in the formation of the RCs (68, 72, 74, 83).

Recent studies, however, designate the ER as the most likely source of the membranes (63, 74). How the intracellular transport pathways are exactly utilized by CoVs remains to be elucidated (for a review on host factors involved in CoV replication see (17)).

Assembly & Release

When the structural proteins have been synthesized from their sgRNAs and novel RNA genome equivalents have been produced, the assembly of new virions can start. The actual budding events are thought to take place at the membranes of the ER-to-Golgi intermediate compartment (ERGIC) (38, 39). The M protein plays a central role in CoV particle assembly. It is the most abundant envelope protein with a molar ratio between the M and S proteins in the virion of about 16:1, whereas the E protein is only present at very low levels within the viral membrane (78). The M protein can interact with itself (19, 48) and with all other structural proteins (14, 18, 25, 62, 64), mediating both the incorporation of the S protein and the packaging of the genomic RNA into the coronavirion via M-N and M-RNP interactions (1, 32, 49, 58, 59). For the production of virus-like particles (VLPs; lacking the genomic RNA), co-expression of the M and E protein is sufficient to drive their formation, whereas the S protein is also incorporated when simultaneously expressed (78). Co-expression of the N protein facilitates VLP formation in some experimental systems (6, 35), whereas the integration of N into the virions is dependent on the presence of (defective) genomic RNA containing the appropriate packaging signal (5, 50). It has been proposed that the E protein is responsible for the induction of membrane curvature and/or the actual pinching off-mechanism of coronavirions (86). Surprisingly, however, deletion of the E gene from the MHV or SARS-CoV genome appeared to be non-lethal (20, 40). During budding, the complete RNP is incorporated into the new virion, after which the assembled viruses exit the cells through the cellular secretory pathway. A schematic representation of the complete CoV life cycle is depicted in Fig.5.

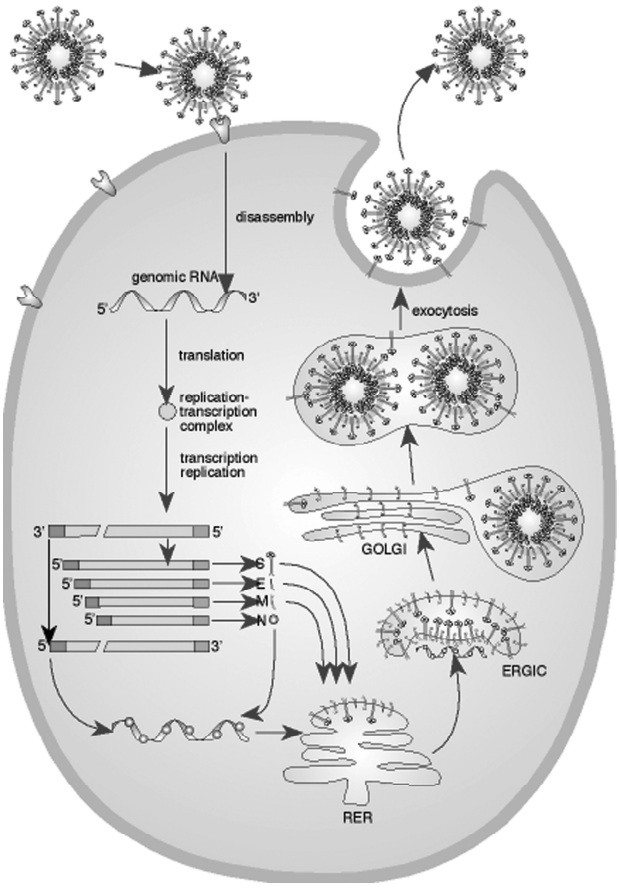

Fig.5. The coronavirus infectious cycle. After attachment to a target cell, the virus envelope fuses with a cellular limiting membrane. The nucleocapsid is released into the cytoplasm where, after disassembly, the genomic RNA becomes translated into the 16 different replicase proteins. These so-called nsp's form the replication-transcription complex which mediates the replication of the genomic RNA as well as the production of the sgRNAs encoding the structural proteins S, E, M, and N. These proteins accumulate in the ERGIC where budding of new coronavirions take place. The newly formed viruses are released from the cell by the secretory pathway.

Coronavirus Pathogenesis and Immunity: MHV as a Model

The pathogenesis of several CoVs has been intensively studied since the 1970s. However, with the discovery of the human pathogenic SARS-CoV in the spring of 2003 (21), CoVs became much more recognized and were even classified as "emerging pathogens". Since the SARS epidemic, two new human respiratory CoVs have been described (i.e. HCoV-NL63 and HCoV-HKU) (82, 89). Several of the animal viruses, such as TGEV, FCoV,

BCoV, and IBV, are of veterinary importance. MHV is frequently studied as a prototype CoV. Various MHV strains have been described, demonstrating different tropisms and levels of virulence. The universally used laboratory strains infect mainly the liver and the central nervous system (CNS), providing practical animal models for encephalitis, hepatitis, and also immune-mediated demyelinating disease that can develop during later stages of infection. MHV infection is considered to be one of the best animal (mouse) models for the study of multiple sclerosis (53).

The role of the immune response to MHV infection in viral clearance and pathogenesis is quite well characterized, especially in the CNS. Antibody- as well as cell-mediated immune responses are essential to guard against CoV infections (3, 51, 56). In addition, interferon-(both type I and type II) and perforin-mediated mechanisms are involved in the clearance of MHV from different cell types (88). Clearance of virus during acute infection is predominantly regulated by a typical expression pattern of proinflammatory chemokines that attract CD8+ and CD4+ T lymphocytes to sites of infection (24, 43). So far, several MHV T-cell epitopes have been mapped to some of the structural proteins. $CD8^+$ and $CD4^+$ T-cell epitopes have been identified in the S, M, and N proteins (2, 13, 85, 90). Whereas MHV infection is primarily cleared by a cell-mediated immune response, antibodies are indispensable to prevent re-emergence of the virus in the CNS after initial clearance. This requirement however, does not hold true for virus replication and clearance in the liver (45, 54), suggesting that each tissue may require different immune effector mechanisms to clear MHV infection. The kinetics and the extent of the host immune response are important in determining survival of the host, which aims to limit the production of infectious virus and viral spread without inducing extensive deleterious effects. Infectious virus is usually cleared from MHV-infected mice within two weeks, but most animals still do not obtain completely sterile immunity, since viral RNA can still persist within the CNS. The latter has been associated with chronic inflammation and ongoing demyelination, although it has become evident that also the host immune response plays an important role in the induction of this demyelinating disease in MHV-infected animals (44, 47, 77).

Coronavirus Virulence Factors

The level of virulence as well as the tropism of MHV strains is depending on different viral and host factors (88). With the use of different, mainly chimeric, recombinant CoVs, it has been established that the S protein is the most important determinant of virulence (10, 33, 66, 69). MHV strain JHM is highly neurotropic and can cause severe encephalitis, while the A59 strain causes moderate hepatitis and is only mildly neurovirulent. The replacement of the MHV-A59 S gene by that of the most highly neurotropic isolate of strain JHM renders this chimeric virus highly neurovirulent (67). The high neurovirulence conferred by the JHM S protein is associated with rapid spread through the CNS, which may occur independently of the entry receptor, since CEACAM1a knock-out mice were still susceptible to MHV-JHM infection (55). However, the recombinant MHV-A59 virus bearing JHM spikes is not as virulent as the parental JHM (36). Overall, these data indicate that also other genes, besides the S gene, play a role in CoV pathogenesis. However, the replicase genes of MHV strain JHM and A59 appeared to be interchangeable without loss of virulence, indicating that probably the other structural genes and/or the group-specific genes are also mediators of tropism and virulence (60). The functions of most of the group-specific genes are currently not known, but they are dispensable for viral replication in tissue culture. Therefore, they are also frequently referred to as accessory proteins. However, their deletion has a clear attenuating effect on virus replication *in vivo*, supporting the idea that they are virulence factors (16, 29, 65, 76, 91). In addition, taking into account the high rate of mutation and recombination of RNA viruses, these group-specific genes would not have been maintained in the viral genomes if they were not beneficial for virus replication in the natural host. For example, the accessory ORF6 of SARS-CoV has recently been shown to increase virulence, probably by interference with the innate immune response of the host (23, 61, 80, 93). Overall, these observations imply that the functional significance of the accessory genes relates to their function in virus–host interactions (i.e. modulating the host immune response).

Outline of this Thesis

As described in this introduction, CoVs, just like any other virus, interact at multiple levels with their host: at the cellular level, as they exploit the cellular machinery for their own propagation, as well as at the level of the organism by manipulating/evading host immune responses. Although a lot is known about the molecular biology of CoVs, our knowledge about these CoV-host interactions is still rudimentary. The aim of this thesis was to gain further insight into these interactions, both at the molecular/cellular level and at the level of the organism, the host. In chapter 2 we describe an improved microarray protocol for whole-genome gene expression profiling of virus-infected cells, which allowed us to subsequently study the reaction of the cell's transcriptome to CoV infection, as described in chapter 3. In chapter 4, 5 and 6 the involvement of several host cellular pathways/proteins in the replication of MHV in cell culture is described in detail. In chapter 7, bioluminescence imaging was used as a new tool for studying several aspects of CoV-host interactions in living mice. Chapter 8 describes the whole-genome gene expression profiling of mice of different genetic backgrounds, providing more insight into type I IFN-independent and -dependent transcriptional responses after infection with MHV.

References

1. **Barcena, M., G. T. Oostergetel, W. Bartelink, F. G. Faas, A. Verkleij, P. J. Rottier, A. J. Koster, and B. J. Bosch.** 2009. Cryo-electron tomography of mouse hepatitis virus: Insights into the structure of the coronavirion. Proc Natl Acad Sci U S A 106:582-7.

2. **Bergmann, C., M. McMillan, and S. Stohlman.** 1993. Characterization of the Ld-restricted cytotoxic T-lymphocyte epitope in the mouse hepatitis virus nucleocapsid protein. J Virol 67:7041-9.

3. **Bergmann, C. C., N. W. Marten, D. R. Hinton, B. Parra, and S. A. Stohlman.** 2001. CD8 T cell mediated immunity to neurotropic MHV infection. Adv Exp Med Biol 494:299-308.

4. **Blau, D. M., and K. V. Holmes.** 2001. Human coronavirus HCoV-229E enters susceptible cells via the endocytic pathway. Adv Exp Med Biol 494:193-8.

5. **Bos, E. C., J. C. Dobbe, W. Luytjes, and W. J. Spaan.** 1997. A subgenomic mRNA transcript of the coronavirus mouse hepatitis virus strain A59 defective interfering (DI) RNA is packaged when it contains the DI packaging signal. J Virol 71:5684-7.

6. **Boscarino, J. A., H. L. Logan, J. J. Lacny, and T. M. Gallagher.** 2008. Envelope protein palmitoylations are crucial for murine coronavirus assembly. J Virol 82:2989-99.

7. **Bosch, B. J., R. van der Zee, C. A. de Haan, and P. J. Rottier.** 2003. The coronavirus spike protein is a class I virus fusion protein: structural and functional characterization of the fusion core complex. J Virol 77:8801-11.

8. **Bridger, J. C., E. O. Caul, and S. I. Egglestone.** 1978. Replication of an enteric bovine coronavirus in intestinal organ cultures. Arch Virol 57:43-51.

9. **Brierley, I.** 1995. Ribosomal frameshifting viral RNAs. J Gen Virol 76 (Pt 8):1885-92.

10. **Casais, R., B. Dove, D. Cavanagh, and P. Britton.** 2003. Recombinant avian infectious bronchitis virus expressing a heterologous spike gene demonstrates that the spike protein is a determinant of cell tropism. J Virol 77:9084-9.

11. **Cavanagh, D.** 1997. Nidovirales: a new order comprising Coronaviridae and Arteriviridae. Arch Virol 142:629-33.

12. **Chu, V. C., L. J. McElroy, A. D. Ferguson, B. E. Bauman, and G. R. Whittaker.** 2006. Avian infectious bronchitis virus enters cells via the endocytic pathway. Adv Exp Med Biol 581:309-12.

13. **Chua, M. M., J. J. Phillips, S. H. Seo, E. Lavi, and S. R. Weiss.** 2001. Mutation of the immunodominant CD8+ epitope in the MHV-4 spike protein. Adv Exp Med Biol 494:121-5.

14. **Corse, E., and C. E. Machamer.** 2003. The cytoplasmic tails of infectious bronchitis virus E and M proteins mediate their interaction. Virology 312:25-34.

15. **de Groot, R. J.** 2008. Taxonomic proposal to the ICTV Executive Committee: Revision of the family Coronaviridae. The Coronavirus Study Group: Raoul J. de Groot, John Ziebuhr, Leo L. Poon, Patrick C.Woo, Pierre Talbot, Peter J.M. Rottier, Kathryn V. Holmes, Ralph Baric, Stanley Perlman, Luis Enjuanes, and Alexander E. Gorbalenya. Personal communication.

16. **de Haan, C. A., P. S. Masters, X. Shen, S. Weiss, and P. J. Rottier.** 2002. The group-specific murine coronavirus genes are not essential, but their deletion, by reverse genetics, is attenuating in the natural host. Virology 296:177-89.

17. **de Haan, C. A., and P. J. Rottier.** 2006. Hosting the severe acute respiratory syndrome coronavirus: specific cell factors required for infection. Cell Microbiol 8:1211-8.

18. **de Haan, C. A., M. Smeets, F. Vernooij, H. Vennema, and P. J. Rottier.** 1999. Mapping of the coronavirus membrane protein domains involved in interaction with the spike protein. J Virol 73:7441-52.

19. **de Haan, C. A., H. Vennema, and P. J. Rottier.** 2000. Assembly of the coronavirus envelope: homotypic interactions between the M proteins. J Virol 74:4967-78.

20. **DeDiego, M. L., E. Alvarez, F. Almazan, M. T. Rejas, E. Lamirande, A. Roberts, W. J. Shieh, S. R. Zaki, K. Subbarao, and L. Enjuanes.** 2007. A severe acute respiratory syndrome coronavirus that lacks the E gene is attenuated *in vitro* and *in vivo*. J Virol 81:1701-13.

21. **Drosten, C., S. Gunther, W. Preiser, S. van der Werf, H. R. Brodt, S. Becker, H. Rabenau, M. Panning, L. Kolesnikova, R. A. Fouchier, A. Berger, A. M. Burguiere, J. Cinatl, M. Eickmann, N. Escriou, K. Grywna, S. Kramme, J. C. Manuguerra, S. Muller, V. Rickerts, M. Sturmer, S. Vieth, H. D. Klenk, A. D. Osterhaus, H. Schmitz, and H. W. Doerr.** 2003. Identification of a novel coronavirus in patients with severe acute respiratory syndrome. N Engl J Med 348:1967-76.

22. **EIFart, P., K. Ludwig, C. Bottcher, C. A. de Haan, P. J. Rottier, T. Korte, and A. Herrmann.** 2007. Role of endocytosis and low pH in murine hepatitis virus strain A59 cell entry. J Virol 81:10758-68.

23. **Frieman, M., B. Yount, M. Heise, S. A. Kopecky-Bromberg, P. Palese, and R. S. Baric.** 2007. Severe acute respiratory syndrome coronavirus ORF6 antagonizes STAT1 function by sequestering nuclear import factors on the rough endoplasmic reticulum/Golgi membrane. J Virol 81:9812-24.

24. **Glass, W. G., B. P. Chen, M. T. Liu, and T. E. Lane.** 2002. Mouse hepatitis virus infection of the central nervous system: chemokine-mediated regulation of host defense and disease. Viral Immunol 15:261-72.

25. **Godeke, G. J., C. A. de Haan, J. W. Rossen, H. Vennema, and P. J. Rottier.** 2000. Assembly of spikes into coronavirus particles is mediated by the carboxy-terminal domain of the spike protein. J Virol 74:1566-71.

26. **Goldsmith, C. S., K. M. Tatti, T. G. Ksiazek, P. E. Rollin, J. A. Comer, W. W. Lee, P. A. Rota, B. Bankamp, W. J. Bellini, and S. R. Zaki.** 2004. Ultrastructural characterization of SARS coronavirus. Emerg Infect Dis 10:320-6.

27. **Gonzalez, J. M., P. Gomez-Puertas, D. Cavanagh, A. E. Gorbalenya, and L. Enjuanes.** 2003. A comparative sequence analysis to revise the current taxonomy of the family Coronaviridae. Arch Virol 148:2207-35.

28. **Gosert, R., A. Kanjanahaluethai, D. Egger, K. Bienz, and S. C. Baker.** 2002. RNA replication of mouse hepatitis virus takes place at double-membrane vesicles. J Virol 76:3697-708.

29. **Haijema, B. J., H. Volders, and P. J. Rottier.** 2004. Live, attenuated coronavirus vaccines through the directed deletion of group-specific genes provide protection against feline infectious peritonitis. J Virol 78:3863-71.

30. **Hansen, G. H., B. Delmas, L. Besnardeau, L. K. Vogel, H. Laude, H. Sjostrom, and O. Noren.** 1998. The coronavirus transmissible gastroenteritis virus causes infection after receptor-mediated endocytosis and acid-dependent fusion with an intracellular compartment. J Virol 72:527-34.

31. **Harcourt, B. H., D. Jukneliene, A. Kanjanahaluethai, J. Bechill, K. M. Severson, C. M. Smith, P. A. Rota, and S. C. Baker.** 2004. Identification of severe acute respiratory syndrome coronavirus replicase products and characterization of papain-like protease activity. J Virol 78:13600-12.

32. **He, R., A. Leeson, M. Ballantine, A. Andonov, L. Baker, F. Dobie, Y. Li, N. Bastien, H. Feldmann, U. Strocher, S. Theriault, T. Cutts, J. Cao, T. F. Booth, F. A. Plummer, S. Tyler, and X. Li.** 2004. Characterization of protein-protein interactions between the nucleocapsid protein and membrane protein of the SARS coronavirus. Virus Res 105:121-5.

33. **Hodgson, T., R. Casais, B. Dove, P. Britton, and D. Cavanagh.** 2004. Recombinant infectious bronchitis coronavirus Beaudette with the spike protein gene of the pathogenic M41 strain remains attenuated but induces protective immunity. J Virol 78:13804-11.

34. **Holmes, K. V., D. B. Tresnan, and B. D. Zelus.** 1997. Virus-receptor interactions in the enteric tract. Virus-receptor interactions. Adv Exp Med Biol 412:125-33.

35. **Huang, Y., Z. Y. Yang, W. P. Kong, and G. J. Nabel.** 2004. Generation of synthetic severe acute respiratory syndrome coronavirus pseudoparticles: implications for assembly and vaccine production. J Virol 78:12557-65.

36. **Iacono, K. T., L. Kazi, and S. R. Weiss.** 2006. Both spike and background genes contribute to murine coronavirus neurovirulence. J Virol 80:6834-43.

37. **King, B., B. J. Potts, and D. A. Brian.** 1985. Bovine coronavirus hemagglutinin protein. Virus Res 2:53-9.

38. **Klumperman, J., J. K. Locker, A. Meijer, M. C. Horzinek, H. J. Geuze, and P. J. Rottier.** 1994. Coronavirus M proteins accumulate in the Golgi complex beyond the site of virion budding. J Virol 68:6523-34.

39. **Krijnse-Locker, J., M. Ericsson, P. J. Rottier, and G. Griffiths.** 1994. Characterization of the budding compartment of mouse hepatitis virus: evidence that transport from the RER to the Golgi complex requires only one vesicular transport step. J Cell Biol 124:55-70.

40. **Kuo, L., and P. S. Masters.** 2003. The small envelope protein E is not essential for murine coronavirus replication. J Virol 77:4597-608.

41. **Lai, M. M.** 1990. Coronavirus: organization, replication and expression of genome. Annu Rev Microbiol 44:303-33.

42. **Lai, M. M., and D. Cavanagh.** 1997. The molecular biology of coronaviruses. Adv Virus Res 48:1-100.

43. **Lane, T. E., J. L. Hardison, and K. B. Walsh.** 2006. Functional diversity of chemokines and chemokine receptors in response to viral infection of the central nervous system. Curr Top Microbiol Immunol 303:1-27.

44. **Lane, T. E., M. T. Liu, B. P. Chen, V. C. Asensio, R. M. Samawi, A. D. Paoletti, I. L. Campbell, S. L. Kunkel, H. S. Fox, and M. J. Buchmeier.** 2000. A central role for CD4(+) T cells and RANTES in virus-induced central nervous system inflammation and demyelination. J Virol 74:1415-24.

45. **Lin, M. T., D. R. Hinton, N. W. Marten, C. C. Bergmann, and S. A. Stohlman.** 1999. Antibody prevents virus reactivation within the central nervous system. J Immunol 162:7358-68.

46. **Lissenberg, A., M. M. Vrolijk, A. L. van Vliet, M. A. Langereis, J. D. de Groot-Mijnes, P. J. Rottier, and R. J. de Groot.** 2005. Luxury at a cost? Recombinant mouse hepatitis viruses expressing the accessory hemagglutinin esterase protein display reduced fitness *in vitro*. J Virol 79:15054-63.

47. **Liu, M. T., H. S. Keirstead, and T. E. Lane.** 2001. Neutralization of the chemokine CXCL10 reduces inflammatory cell invasion and demyelination and improves neurological function in a viral model of multiple sclerosis. J Immunol 167:4091-7.

48. **Locker, J. K., D. J. Opstelten, M. Ericsson, M. C. Horzinek, and P. J. Rottier.** 1995. Oligomerization of a trans-Golgi/trans-Golgi network retained protein occurs in the Golgi complex and may be part of its retention. J Biol Chem 270:8815-21.

49. **Luo, H., D. Wu, C. Shen, K. Chen, X. Shen, and H. Jiang.** 2006. Severe acute respiratory syndrome coronavirus membrane protein interacts with nucleocapsid protein mostly through their carboxyl termini by electrostatic attraction. Int J Biochem Cell Biol 38:589-99.

50. **Makino, S., K. Yokomori, and M. M. Lai.** 1990. Analysis of efficiently packaged defective interfering RNAs of murine coronavirus: localization of a possible RNA-packaging signal. J Virol 64:6045-53.

51. **Marten, N. W., S. A. Stohlman, and C. C. Bergmann.** 2001. MHV infection of the CNS: mechanisms of immune-mediated control. Viral Immunol 14:1-18.

52. **Masters, P. S., C. A. Koetzner, C. A. Kerr, and Y. Heo.** 1994. Optimization of targeted RNA recombination and mapping of a novel nucleocapsid gene mutation in the coronavirus mouse hepatitis virus. J Virol 68:328-37.

53. **Matthews, A. E., S. R. Weiss, and Y. Paterson.** 2002. Murine hepatitis virus--a model for virus-induced CNS demyelination. J Neurovirol 8:76-85.

54. **Matthews, A. E., S. R. Weiss, M. J. Shlomchik, L. G. Hannum, J. L. Gombold, and Y. Paterson.** 2001. Antibody is required for clearance of infectious murine hepatitis virus A59 from the central nervous system, but not the liver. J Immunol 167:5254-63.

55. **Miura, T. A., E. A. Travanty, L. Oko, H. Bielefeldt-Ohmann, S. R. Weiss, N. Beauchemin, and K. V. Holmes.** 2008. The spike glycoprotein of murine coronavirus MHV-JHM mediates receptor-independent infection and spread in the central nervous systems of Ceacam1a$^{-/-}$ Mice. J Virol 82:755-63.

56. **Morales, S., B. Parra, C. Ramakrishna, D. M. Blau, and S. A. Stohlman.** 2001. B-cell-mediated lysis of cells infected with the neurotropic JHM strain of mouse hepatitis virus. Virology 286:160-7.

57. **Namy, O., S. J. Moran, D. I. Stuart, R. J. Gilbert, and I. Brierley.** 2006. A mechanical explanation of RNA pseudoknot function in programmed ribosomal frameshifting. Nature 441:244-7.

58. **Narayanan, K., A. Maeda, J. Maeda, and S. Makino.** 2000. Characterization of the coronavirus M protein and nucleocapsid interaction in infected cells. J Virol 74:8127-34.

59. **Narayanan, K., and S. Makino.** 2001. Cooperation of an RNA packaging signal and a viral envelope protein in coronavirus RNA packaging. J Virol 75:9059-67.

60. **Navas-Martin, S., M. Brom, M. M. Chua, R. Watson, Z. Qiu, and S. R. Weiss.** 2007. Replicase genes of murine coronavirus strains A59 and JHM are interchangeable: differences in pathogenesis map to the 3' one-third of the genome. J Virol 81:1022-6.

61. **Netland, J., D. Ferraro, L. Pewe, H. Olivares, T. Gallagher, and S. Perlman.** 2007. Enhancement of murine coronavirus replication by severe acute respiratory syndrome coronavirus protein 6 requires the N-terminal hydrophobic region but not C-terminal sorting motifs. J Virol 81:11520-5.

62. **Nguyen, V. P., and B. G. Hogue.** 1997. Protein interactions during coronavirus assembly. J Virol 71:9278-84.

63. **Oostra, M., E. G. te Lintelo, M. Deijs, M. H. Verheije, P. J. Rottier, and C. A. de Haan.** 2007. Localization and membrane topology of coronavirus non-structuralprotein 4: involvement of the early secretory pathway in replication. J Virol 81:12323-36.

64. **Opstelten, D. J., M. J. Raamsman, K. Wolfs, M. C. Horzinek, and P. J. Rottier.** 1995. Envelope glycoprotein interactions in coronavirus assembly. J Cell Biol 131:339-49.

65. **Ortego, J., I. Sola, F. Almazan, J. E. Ceriani, C. Riquelme, M. Balasch, J. Plana, and L. Enjuanes.** 2003. Transmissible gastroenteritis coronavirus gene 7 is not essential but influences *in vivo* virus replication and virulence. Virology 308:13-22.

66. **Phillips, J. J., M. Chua, S. H. Seo, and S. R. Weiss.** 2001. Multiple regions of the murine coronavirus spike glycoprotein influence neurovirulence. J Neurovirol 7:421-31.

67. **Phillips, J. J., M. M. Chua, E. Lavi, and S. R. Weiss.** 1999. Pathogenesis of chimeric MHV4/MHV-A59 recombinant viruses: the murine coronavirus spike protein is a major determinant of neurovirulence. J Virol 73:7752-60.

68. **Prentice, E., W. G. Jerome, T. Yoshimori, N. Mizushima, and M. R. Denison.** 2004. Coronavirus replication complex formation utilizes components of cellular autophagy. J Biol Chem 279:10136-41.

69. **Sanchez, C. M., A. Izeta, J. M. Sanchez-Morgado, S. Alonso, I. Sola, M. Balasch, J. Plana-Duran, and L. Enjuanes.** 1999. Targeted recombination demonstrates that the spike gene of transmissible gastroenteritis coronavirus is a determinant of its enteric tropism and virulence. J Virol 73:7607-18.

70. **Sawicki, S. G., and D. L. Sawicki.** 1998. A new model for coronavirus transcription. Adv Exp Med Biol 440:215-9.

71. **Shi, S. T., and M. M. Lai.** 2005. Viral and cellular proteins involved in coronavirus replication. Curr Top Microbiol Immunol 287:95-131.

72. **Shi, S. T., J. J. Schiller, A. Kanjanahaluethai, S. C. Baker, J. W. Oh, and M. M. Lai.** 1999. Colocalization and membrane association of murine hepatitis virus gene 1 products and De novo-synthesized viral RNA in infected cells. J Virol 73:5957-69.

73. **Snijder, E. J., M. C. Horzinek, and W. J. Spaan.** 1990. A 3'-coterminal nested set of independently transcribed mRNAs is generated during Berne virus replication. J Virol 64:331-8.

74. **Snijder, E. J., Y. van der Meer, J. Zevenhoven-Dobbe, J. J. Onderwater, J. van der Meulen, H. K. Koerten, and A. M. Mommaas.** 2006. Ultrastructure and origin of membrane vesicles associated with the severe acute respiratory syndrome coronavirus replication complex. J Virol 80:5927-40.

75. **Spaan, W., D. Cavanagh, and M. C. Horzinek.** 1988. Coronaviruses: structure and genome expression. J Gen Virol 69 (Pt 12):2939-52.

76. **Sperry, S. M., L. Kazi, R. L. Graham, R. S. Baric, S. R. Weiss, and M. R. Denison.** 2005. Single-amino-acid substitutions in open reading frame (ORF) 1b-nsp14 and ORF 2a proteins of the coronavirus mouse hepatitis virus are attenuating in mice. J Virol 79:3391-400.

77. **Stohlman, S. A., and L. P. Weiner.** 1981. Chronic central nervous system demyelination in mice after JHM virus infection. Neurology 31:38-44.

78. **Sturman, L. S., K. V. Holmes, and J. Behnke.** 1980. Isolation of coronavirus envelope glycoproteins and interaction with the viral nucleocapsid. J Virol 33:449-62.

79. **Sugiyama, K., and Y. Amano.** 1981. Morphological and biological properties of a new coronavirus associated with diarrhea in infant mice. Arch Virol 67:241-51.

80. **Tangudu, C., H. Olivares, J. Netland, S. Perlman, and T. Gallagher.** 2007. Severe acute respiratory syndrome coronavirus protein 6 accelerates murine coronavirus infections. J Virol 81:1220-9.

81. **Thiel, V., K. A. Ivanov, A. Putics, T. Hertzig, B. Schelle, S. Bayer, B. Weissbrich, E. J. Snijder, H. Rabenau, H. W. Doerr, A. E. Gorbalenya, and J. Ziebuhr.** 2003. Mechanisms and enzymes involved in SARS coronavirus genome expression. J Gen Virol 84:2305-15.

82. **van der Hoek, L., K. Pyrc, M. F. Jebbink, W. Vermeulen-Oost, R. J. Berkhout, K. C. Wolthers, P. M. Wertheim-van Dillen, J. Kaandorp, J. Spaargaren, and B. Berkhout.** 2004. Identification of a new human coronavirus. Nat Med 10:368-73.

83. **van der Meer, Y., E. J. Snijder, J. C. Dobbe, S. Schleich, M. R. Denison, W. J. Spaan, and J. K. Locker.** 1999. Localization of mouse hepatitis virus non-structuralproteins and RNA synthesis indicates a role for late endosomes in viral replication. J Virol 73:7641-57.

84. **van der Meer, Y., H. van Tol, J. K. Locker, and E. J. Snijder.** 1998. ORF1a-encoded replicase subunits are involved in the membrane association of the arterivirus replication complex. J Virol 72:6689-98.

85. **van der Veen, R. C.** 1996. Immunogenicity of JHM virus proteins: characterization of a CD4+ T cell epitope on nucleocapsid protein which induces different T-helper cell subsets. Virology 225:339-46.

86. **Vennema, H., G. J. Godeke, J. W. Rossen, W. F. Voorhout, M. C. Horzinek, D. J. Opstelten, and P. J. Rottier.** 1996. Nucleocapsid-independent assembly of coronavirus-like particles by co-expression of viral envelope protein genes. Embo J 15:2020-8.

87. **Wang, H., P. Yang, K. Liu, F. Guo, Y. Zhang, G. Zhang, and C. Jiang.** 2008. SARS coronavirus entry into host cells through a novel clathrin- and caveolae-independent endocytic pathway. Cell Res 18:290-301.

88. **Weiss, S. R., and S. Navas-Martin.** 2005. Coronavirus pathogenesis and the emerging pathogen severe acute respiratory syndrome coronavirus. Microbiol Mol Biol Rev 69:635-64.

89. **Woo, P. C., S. K. Lau, C. M. Chu, K. H. Chan, H. W. Tsoi, Y. Huang, B. H. Wong, R. W. Poon, J. J. Cai, W. K. Luk, L. L. Poon, S. S. Wong, Y. Guan, J. S. Peiris, and K. Y. Yuen.** 2005. Characterization and complete genome sequence of a novel coronavirus, coronavirus HKU1, from patients with pneumonia. J Virol 79:884-95.

90. **Xue, S., A. Jaszewski, and S. Perlman.** 1995. Identification of a CD4+ T cell epitope within the M protein of a neurotropic coronavirus. Virology 208:173-9.

91. **Youn, S., J. L. Leibowitz, and E. W. Collisson.** 2005. *In vitro* assembled, recombinant infectious bronchitis viruses demonstrate that the 5a open reading frame is not essential for replication. Virology 332:206-15.

92. **Yu, G. Y., and M. M. Lai.** 2005. The ubiquitin-proteasome system facilitates the transfer of murine coronavirus from endosome to cytoplasm during virus entry. J Virol 79:644-8.

93. **Zhao, J., A. Falcon, H. Zhou, J. Netland, L. Enjuanes, P. Perez Brena, and S. Perlman.** 2009. Severe acute respiratory syndrome coronavirus protein 6 is required for optimal replication. J Virol 83:2368-73.

94. **Ziebuhr, J.** 2005. The coronavirus replicase. Curr Top Microbiol Immunol 287:57-94.

95. **Ziebuhr, J.** 2004. Molecular biology of severe acute respiratory syndrome coronavirus. Curr Opin Microbiol 7:412-9.

Chapter 2

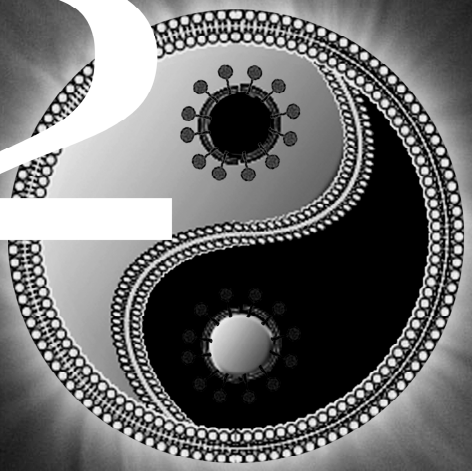

Improved Microarray Gene Expression Profiling of Virus-Infected Cells after Removal of Viral RNA

Matthijs Raaben
Penn Whitley
Diane Bouwmeester
Robert A. Setterquist
Peter J.M. Rottier
Cornelis A.M. de Haan

BMC Genomics; 2008 May 14;9:221.

Abstract

Sensitivity and accuracy are key points when using microarrays to detect alterations in gene expression under different conditions. Critical to the acquisition of reliable results is the preparation of the RNA. In the field of virology, when analyzing the host cell's reaction to infection, the often high representation of viral RNA (vRNA) within total RNA preparations from infected cells is likely to interfere with microarray analysis. Yet, this effect has not been investigated despite the many reports that describe gene expression profiling of virus-infected cells using microarrays. In this study we used coronaviruses as a model to show that vRNA indeed interferes with microarray analysis, decreasing both sensitivity and accuracy. We also demonstrate that the removal of vRNA from total RNA samples, by means of virus-specific oligonucleotide capturing, significantly reduced the number of false-positive hits and increased the sensitivity of the method as tested on different array platforms. We therefore recommend the specific removal of vRNA, or of any other abundant 'contaminating' RNAs, from total RNA samples to improve the quality and reliability of microarray analyses.

Introduction

In various research fields, microarray analysis is frequently being used as a tool to analyze alterations of the transcriptome in response to different stimuli. However, this technology often has serious limitations related to its sensitivity, specificity and reproducibility (17). A key step in the generation of reliable data involves the isolation and processing of the RNA, since high quality RNA is needed to obtain accurate results.

In the field of virology, microarrays are often used as a diagnostic tool to detect the presence of certain viruses within biological samples or to discover new viruses (32, 33). In addition, microarray analysis is regularly applied to identify host genes of which the expression is altered upon virus infection. Whole-genome profiling of virus-infected cells, in combination with other large-scale, high-throughput technology, rapidly increases our knowledge of virus-host interactions and may eventually lead to the production of new antivirals (26). Often these screens are performed using cultured cells with high doses of virus in order to infect all the cells present. As most viruses replicate and transcribe their genome very efficiently, the resulting high levels of viral RNA (vRNA) may be expected to interfere with the microarray analysis. The potential interference of vRNA with array procedures is of particular concern when the vRNAs are polyadenylated, given that most microarray protocols involve mRNA amplification using oligo(dT) primers, thereby hence also amplifying viral mRNAs. This potential problem especially holds true for RNA viruses, including coronaviruses (CoV), the replication of which has been shown to result in an exponential increase in vRNA levels within hours after inoculation of the cells (5, 8, 21).

CoVs are enveloped, positive-stranded RNA viruses and are well-known pathogens in man and animals. Their relevance has increased significantly with the current surfacing of new human CoVs (HCoVs), such as the severe acute respiratory syndrome (SARS)-CoV (7), HCoV-NL63 (30), and HCoV-HKU1 (34). CoVs replicate exclusively within the cytoplasm of their target cells, producing a nested set of subgenomic mRNAs (Fig.1), which contain identical 5’ and 3’ terminal sequences (19). These mRNAs are transcribed by a discontinuous transcription mechanism; they acquire a 5’ cap structure and become 3’ polyadenylated, which makes them equivalent to host cellular mRNAs (24). Gene expression profiling of CoV-infected cells has been performed in several microrarray

studies in order to get more insight in the CoV-host interactions that contribute to pathogenesis (14, 21, 27, 31).

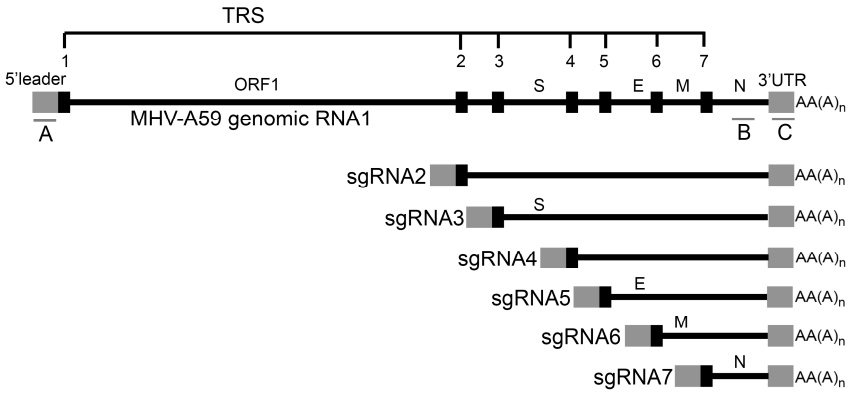

Fig.1. Coronavirus RNA replication strategy. MHV-A59 produces a nested set of subgenomic mRNAs (sgRNAs) that all have identical 5' and 3' terminal ends. Via discontinuous transcription, during the synthesis of the minus strand, sgRNAs obtain the 5' leader sequence fused to a transcriptional regulating sequence (TRS, indicated by the numbered small black boxes), followed by a protein-coding region that is flanked at the 3' terminus by an untranslated region (3'UTR) and a polyA-tail (indicated as AA(A)n). Note that the nucleocapsid (N) gene is present in all sgRNAs. The three biotinylated oligonucleotides, which are used in the vRNA removal procedure and which are complementary to three regions in the viral genome, are indicated by the underscores and the letters A, B, and C (see Table 1 for the nucleotide sequences).

Although large numbers of genes with altered expression have been identified in virus-infected cells, no report exists, which addresses to what extent the high levels of vRNA affect microarray performance. Therefore we investigated the potentially disturbing effect of vRNA overrepresentation on array outcome by using the mouse hepatitis coronavirus (MHV) as a model and by employing two different microarray platforms. Our observations indeed show that the presence of vRNAs in the preparation interferes quite dramatically with the genechip assays. Removal of vRNAs from the total RNA pool before the processing of the RNA for subsequent array hybridization drastically decreased the number of false positive hits for one platform and increased overall sensitivity in both systems. We conclude that depleting vRNAs from infected cell total RNA extracts is beneficial for the microarray analysis not only of cornavirus infection but probably for many other virus infections as well. In addition, the approach is likely to be equally advantageous in other

circumstances where 'contaminating' (viral) RNAs constitute a significant fraction of the target RNA to be processed for microrarray analysis.

Results

vRNA Interferes with Microarray Analysis

In order to investigate the potential interference of vRNA during microarray procedures, we first analyzed in detail the synthesis of vRNA during the course of an MHV infection and the subsequent effect of the presence of vRNA on the mRNA amplification plots. To this end, we infected LR7 cells with MHV-A59 (MOI 10) and determined the amount of vRNA at different time-points post infection (p.i.) using quantitative Taqman RT-PCR. As is shown in Fig.2A, early in infection there is an exponential increase of the vRNA levels. The 4 h and 6 h p.i. time-points, which differ approximately 100-fold in their amounts of vRNA, were chosen for further analysis. Total RNA extracts obtained from mock- and MHV-infected cells were subjected to the mRNA amplification protocol, after which the resulting cRNA was analyzed with the Bioanalyzer. As previously mentioned, coronaviral RNAs are polyadenylated, and should therefore also be amplified with the oligo(dT) primers. Whereas amplification of mRNA of mock- and MHV-infected cells at 4 h p.i. resulted in similar Bioanalyzer profiles, aberrant peaks were observed after amplification of the mRNA derived from MHV-infected cells at 6 h p.i. (Fig.2B). The most abundant peak within the latter amplification plot corresponded in size with the most abundant subgenomic RNA of MHV (16), which encodes the N protein (Fig.1). Determination of the peak surface area showed that at least 40% of the amplified mRNA pool is of viral origin.

Next, microarray experiments were performed to study the effect of these huge amounts of vRNA present in the target cRNA samples. First, 70-mer oligonucleotide arrays, which are routinely used in the Utrecht microarray facility, were used as proof of principle. As shown in the scatter plots in Fig.2C, expression of only few genes was upregulated at 4 h p.i., whereas there appeared to be a dramatic increase in the number of genes, the expression of which was upregulated at 6 h p.i. However, quantitative RT-PCR could not confirm the differential expression of several of these genes (see Supplementary data; False-positive hits).

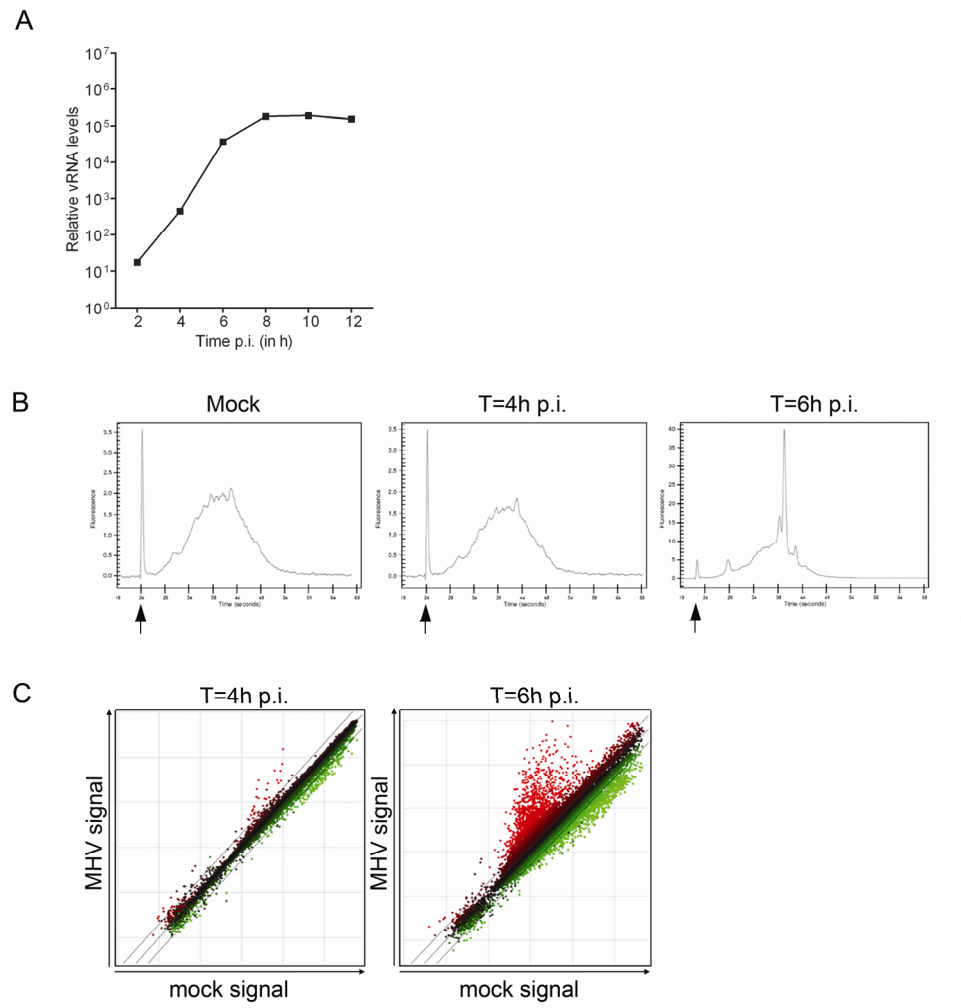

Fig.2. Microarray analysis of MHV-infected LR7 cells. (A) Genomic viral RNA (vRNA) levels in MHV-infected LR7 cells (MOI 10) were measured by quantitative RT-PCR at the indicated time-points. The data are presented as relative vRNA levels. (B) Successful amplification of the mRNA within the individual samples was monitored by analyzing the cRNA samples with a Bioanalyzer (Agilent), according to the manufacturer's instructions. Representative mRNA amplification plots of total RNA samples obtained from mock- or MHV-infected cells at 4 h and 6 h p.i. are shown. The indicated plots represent the size distribution of the total mRNA content present in the samples. The marker peak is indicated by the arrow. Note that the scaling is different between the plots in order to visualize the complete profile. (C) Total RNA was isolated and processed for microarray analysis as described in the Methods section. The scatter plots display the average expression values from independent dye-swap hybridizations (n = 6) for each gene present on the arrays at the indicated time-points p.i. Red spots represent upregulated gene transcripts while green spots represent downregulated gene transcripts upon infection of cells with MHV. The dashed lines indicate the 2-fold change cut-off.

For example, the very high level of expression of the Usp2 gene in MHV-infected cells at 6 h p.i., according to the array analysis, could not be validated by quantitative RT-PCR. In addition, expression of several other genes, which were identified as highly upregulated by the array analysis, could not be detected by Taqman RT-PCR both in infected and mock-infected cells. Interestingly, when the nucleotide sequences of the oligonucleotides on the arrays, of these apparently false-positive hits, where compared to the N gene nucleotide sequence, small stretches (10-15 nucleotides) of identical sequences were observed (data not shown), substantiating the suggestion of cross-hybridization of vRNA to specific sequences on the arrays.

Cross-Hybridization of vRNA to Arrays

The cross-hybridization of vRNAs to the arrays was further explored by performing a similar experiment as described above. Only now, the mock- and MHV-infected cells were treated with ActD, which blocks cellular transcription but not MHV replication (13, 22). By using this inhibitor of cellular transcription we were able to discriminate between genuine upregulation of gene expression and cross-hybridization. Apparent upregulation of gene expression in the presence of ActD, is most likely caused by cross-hybridization of vRNAs to the arrays. Amplification of the mRNA obtained from the MHV-infected, ActD-treated cells again resulted in the appearance of aberrant peaks, which were not observed in the amplification plots of the mock-infected cells (Fig.3A). The subsequent microarray experiment (Fig.3B) gave similar results to the one shown in Fig.2C. Almost 2000 genes were upregulated under both conditions, indicating that most genes identified by the array analysis are indeed the result of cross-hybridization and not of induction of gene expression (Fig.3C). Moreover, 2290 genes were specifically identified in the experiment with ActD. Since viral mRNA is efficiently replicated and transcribed in the presence of ActD, while cellular transcription is blocked, the identification of these genes probably results from a relative increase in the amount of vRNA within the target cRNA samples. Indeed, comparison of the Bioanalyzer profiles presented in Fig.3A and Fig.2B showed that the aberrant peak is higher after treatment with ActD. Interestingly, there is also a significant number of genes downregulated in the absence and presence of ActD, indicating that a post-transcriptional mRNA decay pathway is induced during MHV infection, a phenomenon which we described recently (21).

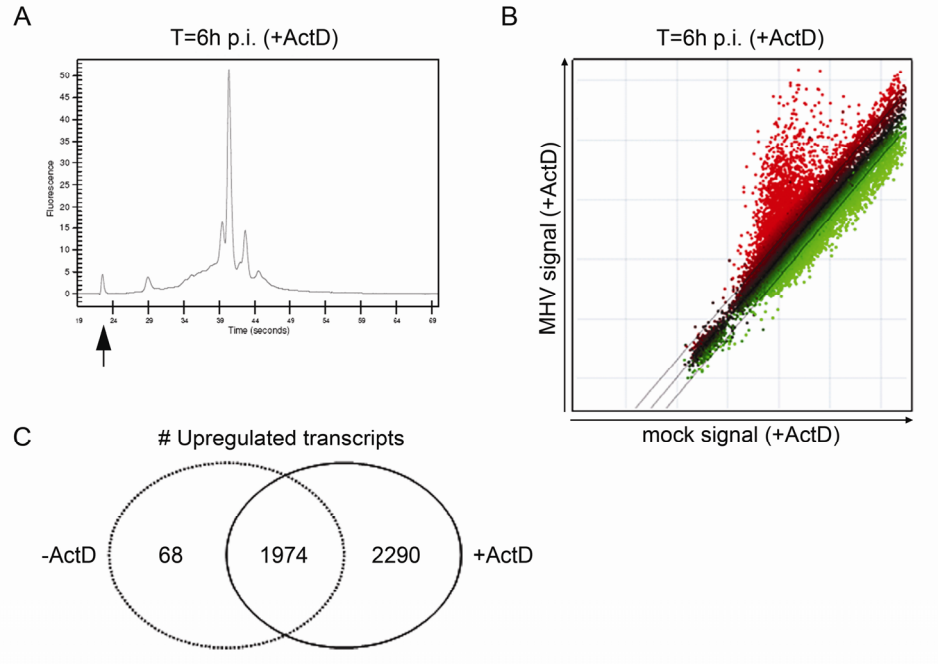

Fig.3. Cross-hybridization of vRNA to array specific sequences. LR7 cells were either mock-infected or infected with MHV (MOI 10). The cells were incubated with ActD (20 µg/ml) 1 h prior to infection, and maintained in the presence of this drug throughout the experiment. Total RNA was isolated from mock- or MHV-infected cells at 6 h p.i. (A) A representative mRNA amplification plot of a total RNA sample derived from MHV-infected, ActD-treated cells at 6 h p.i. The arrow indicates the marker peak. (B) The scatter plot displays the average expression values from independent dye-swap hybridizations (n = 6) for each gene present on the arrays as described in legend of Fig.2. (C) The Venn diagram shows a comparison between the experiments in the absence or presence of ActD.

Extraction of vRNA from Total RNA Improves Microarray Analysis

Since the vRNAs appear to affect the array analysis significantly, we employed a technology to remove these RNAs from the total RNA pool before processing of the samples for microarray analysis (i.e. mRNA amplification, labeling, and hybridization). For this purpose, biotinylated oligonucleotides (27-30 nt in length) complementary to three regions of the MHV-A59 genomic and subgenomic RNAs (the 5' leader, N, and 3' UTR region; Fig.1) were designed (see Methods for nucleotide sequences). The same RNA samples as described above were now subjected to the vRNA removal protocol. In short, the RNA samples were incubated with the MHV-specific oligo's under stringent

hybridization conditions, after which the captured vRNAs were bound to streptavidin-coated beads, and removed. Quantitative RT-PCR targeting the viral N gene, which is present in all MHV-encoded RNAs, demonstrated that approximately 90% of the vRNAs were removed by this procedure (data not shown).

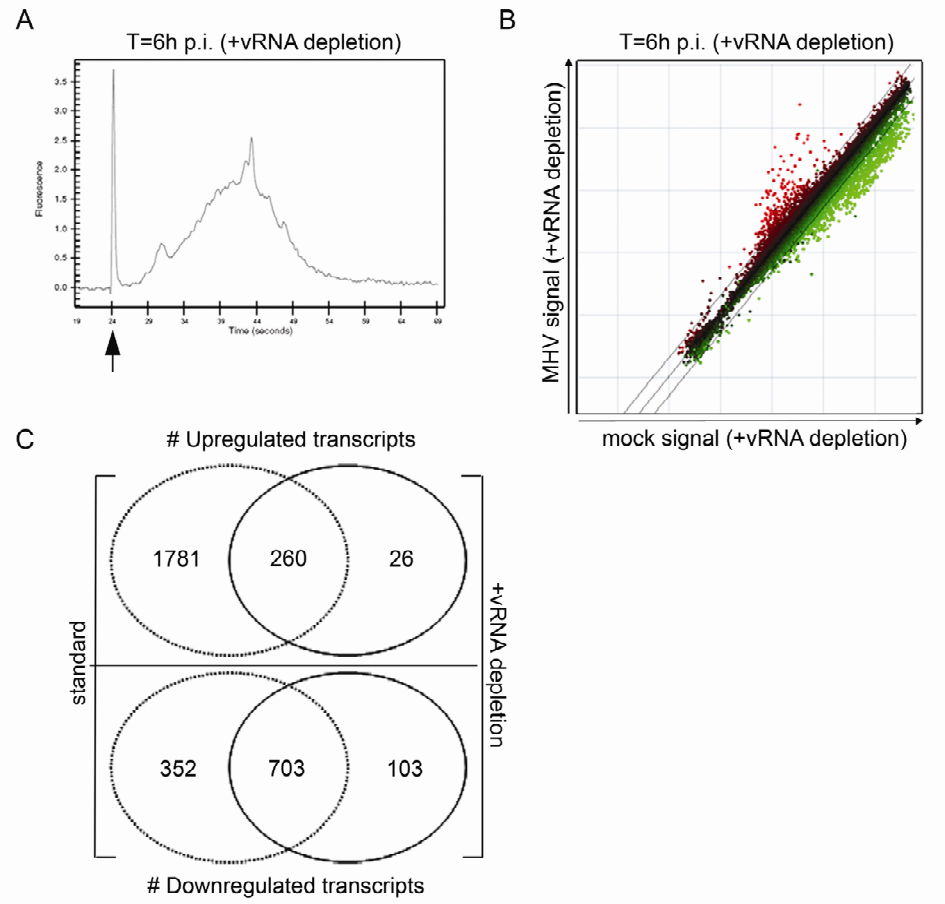

Fig.4. vRNA depletion improves microarray analysis. Total RNA samples were obtained from mock- and MHV-infected LR7 cells at 6 h p.i. were subjected to the vRNA depletion protocol as detailed in the Materials and methods section. (A) Amplification of the mRNA was monitored by analyzing the cRNA samples with a Bioanalyzer. A representative mRNA amplification plot of a total RNA sample derived from MHV-infected cells at 6 h p.i. after vRNA removal is shown. The arrow indicates the marker peak. (B) Total RNA samples were treated with the biotinylated oligo's (indicated as vRNA depleted) and were processed for microarray analysis as described in the Methods section. The scatter plots display the average expression values from independent dye-swap hybridizations (n = 6) for each gene present on the arrays as described in legend of Fig.2. (C) The Venn diagrams show a comparison between the experiments with and without vRNA depletion.

Amplification of mRNAs from the samples treated with the MHV-specific oligo's confirmed the removal of the vRNAs from the total RNA pool as judged from the almost complete absence of the aberrant peaks in the Bioanalyzer profiles (Fig.4A; compare to Fig.2B). Importantly, the vRNA capture procedure did not appear to affect the Bioanalzyer mRNA amplification plots of the mock-infected cells (data not shown). Next, the effect of the vRNA-depletion on the microarray performance was studied. Thus, microarray analysis was performed as described above except that the target samples, derived from both infected and mock-infected cells, were treated with the MHV-specific biotinylated oligo's. The results are shown in Fig.4B. As is evident from the scatter plot, the number of apparently upregulated transcripts was greatly reduced. Increased expression of almost 1800 genes was no longer detected after vRNA depletion when compared to the standard approach (Fig.4C, and compare scatter plots shown in Fig.4B and Fig.2B). This result is consistent with the notion that vRNAs can hybridize to specific sequences on the arrays.

Thus, removal of vRNAs results in a significant reduction of the number of false positive hits. 260 genes were identified under both conditions. This set of genes is likely to contain several hits that are still the result of cross-hybridization, since vRNA depletion was not 100%. For example, Usp2 and Figla, two highly upregulated genes, the differential expression of which could not be confirmed by quantitative RT-PCR, were still present within this collection of genes, although the transcriptional upregulation of these genes as judged from the microarray experiment was much less pronounced (see Supplementary data; False-positive hits). 40 genes out of these 260 hits were not detected in the experiment with ActD, indicating that these genes are specifically upregulated at the transcriptional level upon infection of cells with MHV. Some of these genes were validated by quantitative RT-PCR (see Supplementary data) and have already been described elsewhere (21). Interestingly, transcriptional upregulation of 26 genes could only be detected with the microarray experiment after removal of the vRNA. For some of these genes, we confirmed their differential expression by quantitative RT-PCR (see Supplementary data; Additional hits).

We also compared the number of downregulated transcripts in absence or presence of the vRNA capture procedure. The majority of identified genes overlapped (n = 703) between

both procedures, and downregulation of several transcripts was confirmed by quantitative RT-PCR (21). However, more downregulated transcripts were identified with the standard method (in the presence of vRNA) than with the vRNA depletion approach, 1055 versus 806 genes, respectively (Fig.4C). Downregulation of 352 transcripts was specifically detected with standard method, while 103 genes were exclusively detected with the new approach. The reduced number of downregulated transcripts after removal of the vRNAs is likely caused by the normalization procedure, which relies on the assumption that the bulk of genes are not differentially expressed between samples (36). Thus, a large number of false-positive hits, caused by cross-hybridization of vRNAs, will result in an overrepresentation of downregulated transcripts.

Although we cannot completely exclude that the oligo capture procedure, besides vRNAs, also extracts some cellular mRNAs, it is obvious that this method improves the accuracy and sensitivity of the array analysis significantly. First, the number of false positive hits reduced dramatically, making follow-up analyses much easier to perform. Secondly, the improved microarray approach allowed the additional detection of several differentially expressed genes, which are potentially important targets for further research.

vRNA Extraction Improves Affymetrix Microarray Performance

Next we analyzed whether the removal of vRNA also improves the performance using another array platform. To this end, we used the commonly used Affymetrix GeneChips® Mouse Genome 430 2.0 arrays. The same RNA samples, previously used for the experiments with the 70-mer oligonucleotide arrays, were now processed for analysis on the Affymetrix arrays as described in the Methods section. Using GeneChips®, the standard method detected the upregulation of 144 transcripts upon MHV infection, whereas the vRNA capture procedure resulted in the identification of 241 upregulated transcripts, 133 of which were only detected after vRNA depletion (Fig.5A). The differential expression of some of these genes, which could only be detected after vRNA removal, was validated by quantitative RT-PCR (see Supplementary data; Additional hits). Both with the standard as with the vRNA depletion method, 308 downregulated transcripts were identified. 198 genes were excluded from detection by vRNA depletion, whereas 52 genes were specifically downregulated by using this approach.

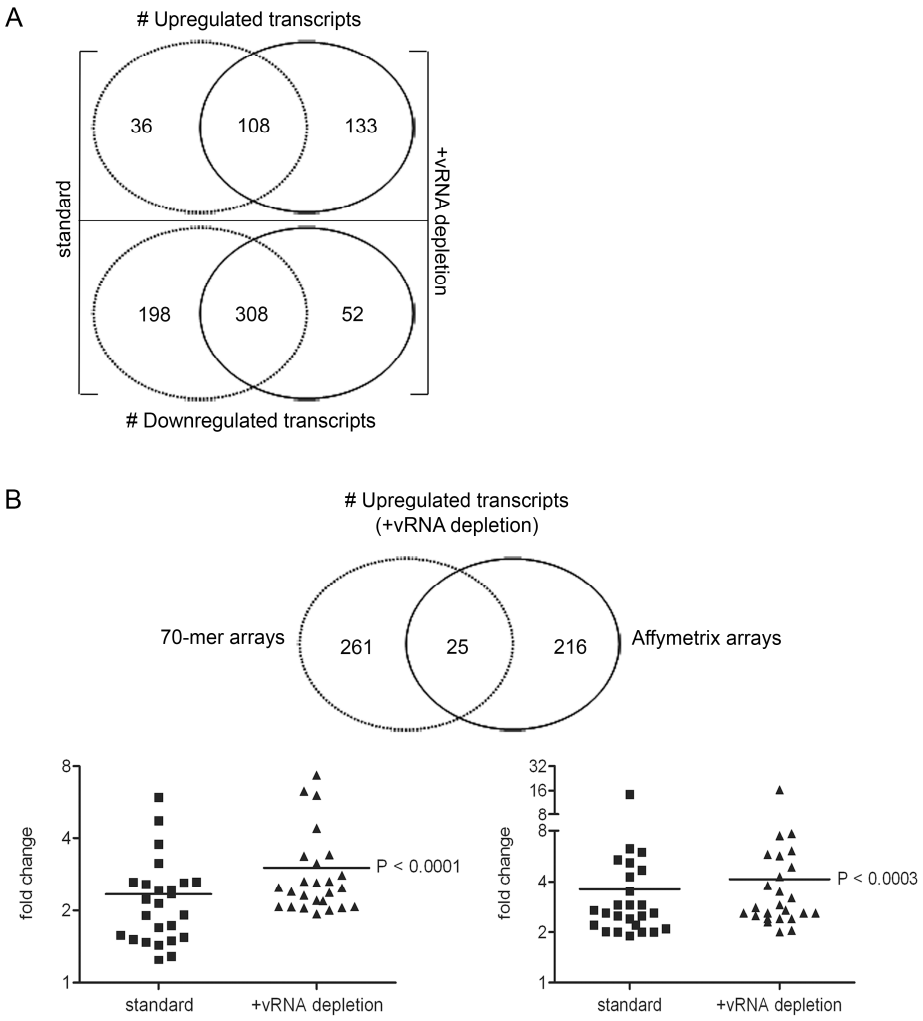

Fig.5. vRNA depletion increases sensitivity on different microarray platforms. (A) Affymetrix arrays were hybridized independently with the same target samples (t = 6 h p.i.; treated with or without vRNA depletion) as described for the 70-mer oligonucleotide arrays. Data analysis was performed as described in the Methods section. The Venn diagram depicts the comparison of the number of upregulated and, separately, the downregulated genes in the two experimental settings (with and without (standard) vRNA depletion). (B) The Venn diagram shows a comparison of the upregulated transcripts obtained with both the 70-mer arrays and the Affymetrix arrays using the vRNA depletion method. The genes within the intersection (n = 25) were selected and the fold changes in gene expression, as discovered by each array analysis, for both methods (standard versus vRNA depleted) are plotted in the graph. Note that the induced expression of several of these genes was validated by quantitative RT-PCR (see Supplementary data). A paired t-test was performed to show the significant difference between both methods for each platform.

Although the problem of cross-hybridization (i.e. false-positive hits) that was observed with the 70-mer oligonucleotide arrays did not become apparent with the Affymetrix arrays, we clearly observed an improved microarray performance with the Affymetrix arrays. Not only more genes were identified of which the expression was induced upon infection, also the fold changes were found to be increased after vRNA clearance. This phenomenon was also observed in the experiments with the 70-mer oligonucleotide arrays. Thus, when the expression levels of the genes, identified by both array platforms using the vRNA depletion method (n = 25), were compared to the expression levels in the experiments without vRNA depletion, a significant increase in the fold changes was observed on both array platforms (Fig.5B). The differential expression of some of these genes was validated by using quantitative RT-PCR (see Supplementary data; Hits by both platforms and both methods). Note that this observation also holds true for most other upregulated transcripts that were detected with only one array platform (data not shown). Conclusively, these results show that the removal of abundant 'contaminating' vRNAs in our CoV system enhanced the ability to detect differential expression of host mRNA using microarray technology.

Discussion

Since microarray technology at the present has progressed towards a point where technical variation, background noise, and a lack of accuracy have greatly improved, the critical step has moved towards the preparation of the RNA sample. Non-specific hybridization is one of the problems that can frequently occur, especially when there is partial degradation of the RNA (25). In addition, high amounts of 'contaminating' RNA are likely to add to this problem and to interfere with microarray analysis. Especially in RNA samples derived from virus-infected cells where high amounts of a limited number of 'contaminating' RNAs are to be expected. In the case of CoVs, replication and transcription results in the formation of a nested set of subgenomic mRNAs that are 5' capped and 3' polyadenylated (Fig.1). In time, the amount of coronavirus vRNA increases exponentially. Most microarray protocols use mRNA amplification, which also results in amplification of CoV RNAs. Indeed, at 6 h p.i., substantial aberrant peaks were observed, when the amplified mRNAs were analyzed with the Bioanalyzer.

The presence of high levels of MHV vRNA affected the microarray analyses, depending on the microarray platform used. On the one hand, the high amounts of vRNA were shown to result in a large number of false-positive hits probably as a result of mishybridization of vRNAs with specific oligonucleotides of the 70-mer oligonucleotide arrays. Indeed, small stretches (10-15 nt) of homologous sequences were observed between vRNAs and the oligonucleotides corresponding with the false-positive hits. On the other hand, the same high number of false positive hits was not observed with the Affymetrix arrays, which contain multiple, much shorter, oligonucleotides per gene. Long nucleotide probes, rather than short (25-mers and shorter), demonstrate less non-specific binding, as is often observed when partially degraded RNA samples are used, due to better hybridization and wash stringency (25). More importantly, however, Affymetrix GeneChips® expression values are calculated by analyzing at least 11 different probes that anneal to the 3' end of each target transcript. Thus, cross-hybridization of vRNA to only one of these probes may not result in an over-estimation of induced gene expression, and will be considered an outlier. However, also for the Affymetrix arrays, the capture and removal of the 'contaminating' vRNAs clearly increased the sensitivity and accuracy of the microarray experiments. Removal of vRNA lowered the threshold for the detection of differentially transcribed genes, thereby identifying potentially important genes for the understanding of virus-host interactions.

MHV-A59 vRNAs were removed from the total RNA samples using the GlobinClear kit (Ambion) with the use of an alternative oligo capture mix, containing three 5' biotinylated oligo's that are complementary to either the 5' leader sequence, the N gene, or the 3' UTR of the MHV-A59 genome. With each of the three oligo's we could target all vRNAs produced in an MHV-infected cell (Fig.1), resulting in a 90% reduction of vRNA present in the total RNA sample. Care was taken in the design of the oligos in order to minimize removal of cellular RNAs. However, the procedure may be optimized further by using alternative capture oligos. This method proved to be better than a Rnase H digestion protocol, in which we tried to remove the poly(A) tail from the vRNAs specifically by using the MHV-specific oligo targeting the 3'UTR. RNAse H would digest vRNA bound to the DNA oligo, thereby preventing subsequent vRNA amplification during cRNA synthesis. Although we could indeed see some improvement of the microarray performance

after RNase H digestion (data not shown), the improvement was less pronounced as compared to direct vRNA removal using the GlobinClear system.

The GlobinClear kit has been designed to remove globin mRNAs from total blood RNA samples. Expression array data generated from whole blood total RNA samples are commonly known to have reduced detection sensitivity compared to data from fractionated blood samples (9). This is mainly caused by the fact that globin mRNA constitutes a large fraction (up to 70%) of the total RNA pool, since globin mRNA is highly expressed in red blood cells and reticulocytes. Microarray analysis has shown that the high amounts of globin mRNA transcripts resulted in decreased sensitivity and increased variation. Similarly, depletion of these abundant 'contaminating' transcripts from whole blood total RNA samples also resulted in increased sensitivity (1, 10, 15, 35). This observed increase in detection sensitivity after targeted RNA depletion could well be a result of decreased competition between the abundant RNA and cellular mRNA for access to the amplification reagents. Removal of these 'contaminating' RNAs will than lead to an increased labeling of host mRNAs, which is detectable by microarray hybridizations. In our experiments, the quality assessment metrics of the Affymetrix arrays indeed showed an increase in the number of detected probe sets after vRNA depletion (see Supplementary data).

High levels of 'contaminating' vRNAs, are not only expected in RNA samples derived from CoV-infected cells, but also from cells infected with other RNA viruses. For flaviviruses, the vRNAs of which do not contain polyadenylated 3'UTRs, mRNA amplification with oligo(dT) primers should be sufficient to diminish the effect of vRNAs on microarray performance. However, the mRNAs synthesized by most other RNA viruses contain poly(A) tails. In case of picorna- or alphaviruses, infection results in the rapid production of high amounts of only 1 or 2 species of polyadenlyated vRNAs (5, 8). Therefore, only a limited set of oligo's is likely to be required to remove these transcripts from total RNA samples by means of the oligo-capture procedure. For orthomyxoviruses, which contain segmented RNA genomes from which different polyadenylated vRNAs are produced (18), a set of oligonucleotides will be required to eliminate all vRNA species. It will be of interest to investigate whether microarray expression profiling studies performed with RNA samples derived from cells infected with other viruses also benefit from the

removal of vRNAs. In conclusion, we show that the presence of abundant viral RNAs interferes with microarray gene expression profiling, affecting both the accuracy and sensitivity of the procedure. Targeted removal of vRNA improved the microarray analyses significantly on different array platforms.

Material & Methods

Cells and viruses

LR7 mouse fibroblast cells (12) were maintained in Dulbecco's Modified Eagle's Medium (DMEM) (Cambrex Bio Science) containing 10% (v/v) fetal calf serum (Bodinco B.V.), 100 U/ml Penicillin, and 100 µg/ml Streptomycin, supplemented with Geneticin G418 (250 µg/ml). MHV strain A59 was grown in and titrated on LR7 cells.

MHV infection and total RNA isolation

LR7 cells were inoculated with MHV-A59 at a multiplicity of infection (MOI) of 10 $TCID_{50}$ (50% tissue culture infectious doses) per cell, in phosphate buffered saline (PBS) containing 50 µg/ml diethylaminoethyl-dextran (PBS-DEAE). When indicated, the cells were incubated with 20 µg/ml of Actinomycin D (ActD; Sigma-Aldrich) from 1 h prior to infection and maintained in the presence of this drug throughout the experiment. After a 1 h inoculation, the cells were washed and the culture medium was replaced by complete DMEM. One hour later, at 2 h p.i., the fusion inhibitory mHR2 peptide (1 µM) was added to the culture medium to inhibit cell-to-cell fusion (4). Total RNA was isolated from mock or MHV-A59 infected cells at the indicated time p.i. using the TRIzol reagent (Invitrogen). RNA was further purified using the RNeasy mini-kit with subsequent DNaseI treatment on the column (Qiagen). RNA concentration and integrity were determined by spectrometry and by a microfluidics-based platform using a UV-mini1240 device (Shimadzu) and a 2100 Bioanalyzer (Agilent Technologies), respectively.

vRNA extraction

MHV-A59 vRNA was removed from the total RNA samples using the GlobinClear kit (Ambion Inc.) with the use of an alternative oligo capture mix that contained three 5' biotinylated oligo's, complementary to the 5' leader sequence, the nucleocapsid (N) gene and the 3' untranslated region (UTR) of the MHV-A59 genome. All subsequent steps were performed according to the manufacturer's protocol. After purification, RNA integrity was analyzed as described above. The sequences of the vRNA capture oligo's are listed in Table 1, and the locations of the complementary sequences in the MHV-A59 genome are depicted in Fig.1.

Table 1. vRNA capture mix.

#	Oligonucleotide sequences (5' to 3')	Locations of complementary nucleotides within the MHV-A59 genome
A	Biotin-CTACAAGAGTTTTAGAGTTGAGAGGGTACG	24-53; 5' leader
B	Biotin-GCACTACGCCATCATCAAGGATCTGAG	30975-31002; N gene
C	Biotin-GGACCTTGCTAACTTCTCTCACACATTCTC	31187-31216; 3' UTR

cRNA synthesis, labeling, and hybridization onto microarrays

70-mer oligonucleotide arrays

mRNA was amplified from 1 µg of total RNA by cDNA synthesis with oligo(dT) double-anchored primers, followed by *in vitro* transcription using Amino Allyl MessageAmp™ II kit (Ambion) as described previously (23). During transcription, 5-(3-aminoallyl)-UTP was incorporated into the single stranded cRNA. Cy3 and Cy5 NHS-esters (Amersham Biosciences) were coupled to 2 µg cRNA. RNA quality was monitored after each successive step using the methods described above. A Mouse Array-Ready Oligo set (version 3.0) was purchased (Operon) and printed on Corning UltraGAPS slides. Mouse slides containing 35,000 spots (32,101 70-mer oligonucleotides, and 2,891 control spots) were hybridized with 1 µg of each alternatively labeled cRNA target at 42oC for 16-20 h using LifterSlips (Erie Scientific) and Corning Hybridization Chambers (29). After hybridization the slides were washed extensively and scanned using the Agilent G2565AA DNA Microarray Scanner.

Affymetrix arrays

mRNA amplification was performed using the MessageAmp™ II Biotin Enhanced kit from Ambion, according to the manufacturer's instructions. Briefly, first-strand cDNA was synthesized by a reverse transcription reaction with T7 oligo(dT) primers. Second-strand cDNA was synthesized with the DNA polymerase mix supplied by the kit to provide double-stranded DNA template for *in vitro* transcription. Biotinylated amplified cRNA was produced by T7 RNA polymerase, after which the cRNA targets were hybridized to Mouse Genome 430 2.0 arrays (Affymetrix, Santa Clara, USA). After extensive washing and subsequent staining, the arrays were scanned using an Affymetrix Genechip® Scanner 3000. All steps were performed as recommended by the manufacturer.

Microarray data analysis

70-mer oligonucleotide arrays

Images were quantified and background corrected using Imagene 5.6 software. The data were normalized using Lowess print-tip normalization as described previously (36). To identify the genes that were significantly different within each experiment, a one-class Significance Analysis of Microrarrays (SAM) (28) was performed on the average of independent dye-swap hybridizations (n = 6), using a false discovery rate (FDR) of 1%. To increase the confidence level, a cut-off at a 2-fold change in expression was applied. The data were subjected to Genespring 7.2 software (Agilent Technologies) for further analysis.

Affymetrix arrays

Images were quantified with Affymetrix Microarray Suite 5.0 (MAS 5.0) software. Quality control (QC) metrics for all arrays are provided as Supplementary data. The robust multichip average (RMA) method (11) was used to process all arrays as a single experiment. A 2-Way ANOVA was used to identify genes that were differentially expressed under the different experimental conditions. The FDR was controlled at 5% using the Benjamini-Hochberg (BH) step-up procedure (3). To increase the confidence level, a cut-off at a 2-fold change in expression was applied. Hierarchical clustering was performed using average linkage clustering with Euclidean Distance. All analyses were performed using Partek® GS software (Copyright, Partek Inc.).

ArrayExpress accession numbers

MIAME-compliant data in MAGE-ML format has been submitted to the public microarray database ArrayExpress (2). Note that the array data obtained from both platforms are submitted as a single experiment. Accession numbers: array designs, A-UMCU-7 and A-AFFY-45; and gene expression data of MHV-infected LR7 cells, E-MEXP-1373. Also included are complete descriptions of protocols for total RNA isolation and mRNA amplification, P-MEXP-34397; vRNA depletion, P-MEXP-114798; cRNA labeling, P-MEXP-34400, P-MEXP-35534, P-MEXP-8712; array hybridization and washing of slides, P-MEXP-34401, P-AFFY-6; scanning of slides, P-MEXP-34430; and data normalization, P-MEXP-34431, P-MEXP-120375.

Quantitative RT-PCR

Altered mRNA expression levels of several genes, which were identified by microarray analysis, were verified by quantitative reverse transcription (RT)-PCR using TaqMan® Gene Expression assays (Applied Biosystems), according to the manufacturer's instructions. Note that from the different groups shown in Supplemental table S1 (i.e. false positive hits, additional hits, and hits by both platforms and both methods) genes were randomly selected for RT-PCR validation. Reactions were performed using an ABI Prism 7000 sequence detection system. The comparative Ct-method was used to determine the fold change for each individual gene. The housekeeping gene GAPDH was used as a reference in all experiments. The amounts of viral genomic and subgenomic RNA were determined by quantitative RT-PCR as described previously (6, 20).

Acknowledgements

We would like to thank Marian Groot Koerkamp and Dik van Leenen from the Microarray Facility (UMC Utrecht, The Netherlands) for technical support, Monique Oostra, Mijke Vogels, and Marne Hagemeijer for stimulating discussions, and Natalie Hernandez and Charmaine San Jose for processing all the samples for the GeneChips®. This work was supported by grants from the M.W. Beijerinck Virology Fund, Royal Netherlands Academy of Arts and Sciences, and The Netherlands Organization for Scientific Research (NWO-VIDI-700.54.421) to C.A.M. de Haan.

Supplementary Data

Supplemental table S1. Validation of microarray data generated by different platforms. Differential expression of a selection of genes after infection with MHV at 6 h p.i. is shown as determined by two different microarray platforms, with or without vRNA depletion, and by quantitative RT-PCR. Note that the genes from the different groups (i.e. false positive hits, additional hits, and hits by both platforms and both methods), were randomly selected for RT-PCR validation.

		Fold induction				
False-positive hits:		Standard	vRNA depletion	Standard	vRNA depletion	RT-PCR
Gene ID	Name	70-mer arrays		Affymetrix arrays		n.d*/n.t**
NM_016808	Usp2	**310.3**	**70.1**	<2	<2	**1.2**
NM_001001809	Olfr218	**210.0**	**12.1**	<2	<2	n.d.
NM_010915	Klk1b4	**209.2**	**22.2**	<2	<2	n.d.
NM_012013	Figla	**162.7**	**23.1**	<2	<2	n.d.
NM_130886	Card14	**9.8**	<2	<2	<2	**1.6**
NM_029562	Cyp2d26	**9.9**	<2	<2	<2	n.d.
NM_175305	Lrrc19	**9.9**	<2	<2	<2	n.d.
NM_174854	Disc1	**9.7**	<2	<2	<2	n.d.
NM_007954	Es1	**9.5**	<2	<2	<2	n.d.
NM_010333	Edg5	**4.8**	<2	**5.5**	<2	**1.0**
NM_178403	Pus7	<2	<2	**4.4**	<2	**1.2**
NM_181400	Wdr47	<2	<2	**2.3**	<2	**1.5**
NM_133753	Errfi1	<2	<2	**2.1**	<2	**1.5**

*n.d. = not detectable, **n.t. = not tested

Supplemental table S1 -continued-

		Fold induction				
Additional hits:		Standard	vRNA depletion	Standard	vRNA depletion	RT-PCR
Gene ID	Name	70-mer arrays		Affymetrix arrays		n.d*/n.t**
NM_010234	Fos	<2	**2.1**	**14.5**	**16.5**	**27.5**
NM_008390	Irf1	<2	**2.4**	**2.2**	**2.4**	**2.8**
NM_008562	Mcl1	<2	**2.3**	**2.1**	**2.0**	**2.1**
NM_013642	Dusp1	<2	**2.4**	**2.6**	**3.8**	n.t.
NM_009344	Phlda1	<2	**2.5**	**2.0**	**2.6**	n.t.
NM_178392	Snapc1	<2	**2.1**	**2.0**	**2.4**	n.t.
NM_010495	Id1	<2	**2.1**	**2.5**	**2.6**	n.t.
NM_008235	Hes1	<2	**2.0**	**2.7**	**2.7**	n.t.
NM_029092	Rg9mtd1	<2	**2.0**	**2.0**	**2.1**	n.t.
NM_010496	Id2	<2	**2.0**	<2	**2.7**	**2.8**
NM_172154	Lcor	<2	**2.0**	<2	**2.7**	**4.2**
NM_011498	Bhlhb2	<2	**2.1**	<2	**2.5**	n.t.
NM_010591	Jun	<2	**2.0**	<2	**2.3**	n.t.
NM_008871	Serpine1	<2	**2.3**	<2	<2	**2.2**
NM_010804	Mllt10	<2	<2	<2	**2.6**	**2.1**

*n.d. = not detectable, **n.t. = not tested

Supplemental table S1 -continued-

		Fold induction				
Hits by both platforms and both methods:		Standard	vRNA depletion	Standard	vRNA depletion	RT-PCR
Gene ID	Name	70-mer arrays		Affymetrix arrays		n.d*/n.t**
NM_010907	Nfkbia	**2.6**	**2.7**	**2.9**	**3.5**	**3.4**
NM_022331	Herpud1	**2.4**	**2.6**	**4.3**	**5.7**	**5.1**
NM_008176	Cxcl1	**5.9**	**7.3**	**6.0**	**6.1**	**10.8**
NM_009140	Cxcl2	**3.8**	**6.3**	**6.3**	**7.7**	**7.2**
NM_013692	Klf10	**4.7**	**6.1**	**5.4**	**5.8**	n.t.
NM_013602	Mt1	**2.2**	**3.1**	**3.5**	**4.3**	n.t.
NM_011803	Klf6	**2.6**	**2.7**	**2.6**	**2.9**	n.t.
NM_153159	Zc3h12a	**2.1**	**3.4**	**2.4**	**2.8**	n.t.
NM_015786	Hist1h1c	**2.6**	**4.4**	**5.2**	**7.5**	n.t.
NM_133662	Ier3	**3.2**	**3.4**	**4.7**	**4.9**	n.t.
NM_008321	Id3	**2.6**	**2.8**	**2.9**	**3.2**	n.t.

*n.d. = not detectable, **n.t. = not tested

Supplemental table S2. QC metrics of Affymetrix Genechips®. Reported QC metrics are shown for each individual array (Chip ID), including scale factor (SF), noise (RawQ), average background signal (Bg Avg), average noise signal (Noise Avg), number of probe sets detected (#P), percent probe sets detected (%P), mean signal for all probe sets (Signal(All)), and β-actin and GAPDH 5'/3' ratios.

(Chip ID)	SF	Raw Q	Bg Avg	Noise Avg	**#P**	**%P**	Signal (All)	Gapdh Ratio	β-Actin Ratio
MHV #A	7,56	1,10	34,31	1,31	**19191**	**42,55**	791,98	0,62	1,82
MHV #B	7,10	1,10	33,45	1,30	**19772**	**43,84**	790,72	0,59	1,65
MHV #C	9,97	0,88	28,83	1,04	**18512**	**41,05**	800,34	0,65	1,59
mock #A	5,25	0,92	29,65	1,14	20432	45,30	801,53	0,67	1,11
mock #B	3,50	1,10	33,61	1,47	21362	47,36	779,64	0,68	1,08
mock #C	3,66	1,11	34,76	1,44	21311	47,25	774,95	0,69	1,14
MHV (vRNA depleted) #A	4,68	1,00	32,44	1,20	**21265***	**47,15***	734,54	0,85	1,81
MHV (vRNA depleted) #B	5,28	0,96	30,42	1,21	**20888***	**46,31***	750,52	0,72	1,59
MHV (vRNA depleted) #C	6,44	1,01	32,21	1,21	**20168***	**44,72***	757,22	0,85	1,92
mock (vRNA depleted) #A	4,77	0,96	31,21	1,20	20722	45,95	797,83	0,79	1,26
mock (vRNA depleted) #B	4,99	1,05	34,41	1,26	20611	45,70	789,74	0,77	1,29
mock (vRNA depleted) #C	3,73	1,06	33,42	1,36	21239	47,09	779,72	0,73	1,19

***Note that the number/percentage of detected probe sets (#P and %P) is increased in the arrays hybridized with cRNA from MHV-infected cells after vRNA depletion. The other QC parameters indicate that the generated data are of high quality.

References

1. **Ambion. 2006.** Improved methods for gene expression profiling from blood samples. Ambion's TechNotes newsletter 13:26-29.

2. **ArrayExpress.** A public repository for microarray data [http://www.ebi.ac.uk/arrayexpress/].

3. **Benjamini, Y., and Y. Hochberg.** 1995. Controlling the false discovery rate – a practical and powerful approach to multiple testing. J Roy Stat Soc B 57:289-300.

4. **Bosch, B. J., R. van der Zee, C. A. de Haan, and P. J. Rottier.** 2003. The coronavirus spike protein is a class I virus fusion protein: structural and functional characterization of the fusion core complex. J Virol 77:8801-11.

5. **Bruton, C. J., and S. I. Kennedy.** 1975. Semliki Forest virus intracellular RNA: properties of the multi-stranded RNA species and kinetics of positive and negative strand synthesis. J Gen Virol 28:111-27.

6. **de Haan, C. A., K. Stadler, G. J. Godeke, B. J. Bosch, and P. J. Rottier.** 2004. Cleavage inhibition of the murine coronavirus spike protein by a furin-like enzyme affects cell-cell but not virus-cell fusion. J Virol 78:6048-54.

7. **Drosten, C., S. Gunther, W. Preiser, S. van der Werf, H. R. Brodt, S. Becker, H. Rabenau, M. Panning, L. Kolesnikova, R. A. Fouchier, A. Berger, A. M. Burguiere, J. Cinatl, M. Eickmann, N. Escriou, K. Grywna, S. Kramme, J. C. Manuguerra, S. Muller, V. Rickerts, M. Sturmer, S. Vieth, H. D. Klenk, A. D. Osterhaus, H. Schmitz, and H. W. Doerr.** 2003. Identification of a novel coronavirus in patients with severe acute respiratory syndrome. N Engl J Med 348:1967-76.

8. **Egger, D., and K. Bienz.** 2005. Intracellular location and translocation of silent and active poliovirus replication complexes. J Gen Virol 86:707-18.

9. **Feezor, R. J., H. V. Baker, M. Mindrinos, D. Hayden, C. L. Tannahill, B. H. Brownstein, A. Fay, S. MacMillan, J. Laramie, W. Xiao, L. L. Moldawer, J. P. Cobb, K. Laudanski, C. L. Miller-Graziano, R. V. Maier, D. Schoenfeld, R. W. Davis, and R. G. Tompkins.** 2004. Whole blood and leukocyte RNA isolation for gene expression analyses. Physiol Genomics 19:247-54.

10. **Field, L. A., R. M. Jordan, J. A. Hadix, M. A. Dunn, C. D. Shriver, R. E. Ellsworth, and D. L. Ellsworth.** 2007. Functional identity of genes detectable in expression profiling assays following globin mRNA reduction of peripheral blood samples. Clin Biochem 40:499-502.

11. **Irizarry, R. A., B. Hobbs, F. Collin, Y. D. Beazer-Barclay, K. J. Antonellis, U. Scherf, and T. P. Speed.** 2003. Exploration, normalization, and summaries of high density oligonucleotide array probe level data. Biostatistics 4:249-64.

12. **Kuo, L., G. J. Godeke, M. J. Raamsman, P. S. Masters, and P. J. Rottier.** 2000. Retargeting of coronavirus by substitution of the spike glycoprotein ectodomain: crossing the host cell species barrier. J Virol 74:1393-406.

13. **Lai, M. M., P. R. Brayton, R. C. Armen, C. D. Patton, C. Pugh, and S. A. Stohlman.** 1981. Mouse hepatitis virus A59: mRNA structure and genetic localization of the sequence divergence from hepatotropic strain MHV-3. J Virol 39:823-34.

14. **Leong, W. F., H. C. Tan, E. E. Ooi, D. R. Koh, and V. T. Chow.** 2005. Microarray and real-time RT-PCR analyses of differential human gene expression patterns induced by severe acute respiratory syndrome (SARS) coronavirus infection of Vero cells. Microbes Infect 7:248-59.

15. **Liu, J., E. Walter, D. Stenger, and D. Thach.** 2006. Effects of globin mRNA reduction methods on gene expression profiles from whole blood. J Mol Diagn 8:551-8.

16. **Masters, P. S., C. A. Koetzner, C. A. Kerr, and Y. Heo.** 1994. Optimization of targeted RNA recombination and mapping of a novel nucleocapsid gene mutation in the coronavirus mouse hepatitis virus. J Virol 68:328-37.

17. **Murphy, D.** 2002. Gene expression studies using microarrays: principles, problems, and prospects. Adv Physiol Educ 26:256-70.

18. **Neumann, G., G. G. Brownlee, E. Fodor, and Y. Kawaoka.** 2004. Orthomyxovirus replication, transcription, and polyadenylation. Curr Top Microbiol Immunol 283:121-43.

19. **Pasternak, A. O., W. J. Spaan, and E. J. Snijder.** 2006. Nidovirus transcription: how to make sense...? J Gen Virol 87:1403-21.

20. **Raaben, M., A. W. Einerhand, L. J. Taminiau, M. van Houdt, J. Bouma, R. H. Raatgeep, H. A. Buller, C. A. de Haan, and J. W. Rossen.** 2007. Cyclooxygenase activity is important for efficient replication of mouse hepatitis virus at an early stage of infection. Virol J 4:55.

21. **Raaben, M., M. J. Groot Koerkamp, P. J. Rottier, and C. A. de Haan.** 2007. Mouse hepatitis coronavirus replication induces host translational shutoff and mRNA decay, with concomitant formation of stress granules and processing bodies. Cell Microbiol 9:2218-29.

22. **Robb, J. A., and C. W. Bond.** 1979. Pathogenic murine coronaviruses. I. Characterization of biological behavior *in vitro* and virus-specific intracellular RNA of strongly neurotropic JHMV and weakly neurotropic A59V viruses. Virology 94:352-70.

23. **Roepman, P., L. F. Wessels, N. Kettelarij, P. Kemmeren, A. J. Miles, P. Lijnzaad, M. G. Tilanus, R. Koole, G. J. Hordijk, P. C. van der Vliet, M. J. Reinders, P. J. Slootweg, and F. C. Holstege.** 2005. An expression profile for diagnosis of lymph node metastases from primary head and neck squamous cell carcinomas. Nat Genet 37:182-6.

24. **Sawicki, S. G., and D. L. Sawicki.** 2005. Coronavirus transcription: a perspective. Curr Top Microbiol Immunol 287:31-55.

25. **Stafford, P., and M. Brun.** 2007. Three methods for optimization of cross-laboratory and cross-platform microarray expression data. Nucleic Acids Res 35:e72.

26. **Tan, S. L., G. Ganji, B. Paeper, S. Proll, and M. G. Katze.** 2007. Systems biology and the host response to viral infection. Nat Biotechnol 25:1383-9.

27. **Tang, B. S., K. H. Chan, V. C. Cheng, P. C. Woo, S. K. Lau, C. C. Lam, T. L. Chan, A. K. Wu, I. F. Hung, S. Y. Leung, and K. Y. Yuen.** 2005. Comparative host gene transcription by microarray analysis early after infection of the Huh7 cell line by severe acute respiratory syndrome coronavirus and human coronavirus 229E. J Virol 79:6180-93.

28. **Tusher, V. G., R. Tibshirani, and G. Chu.** 2001. Significance analysis of microarrays applied to the ionizing radiation response. Proc Natl Acad Sci U S A 98:5116-21.

29. **van de Peppel, J., P. Kemmeren, H. van Bakel, M. Radonjic, D. van Leenen, and F. C. Holstege.** 2003. Monitoring global messenger RNA changes in externally controlled microarray experiments. EMBO Rep 4:387-93.

30. **van der Hoek, L., K. Pyrc, M. F. Jebbink, W. Vermeulen-Oost, R. J. Berkhout, K. C. Wolthers, P. M. Wertheim-van Dillen, J. Kaandorp, J. Spaargaren, and B. Berkhout.** 2004. Identification of a new human coronavirus. Nat Med 10:368-73.

31. **Versteeg, G. A., O. Slobodskaya, and W. J. Spaan.** 2006. Transcriptional profiling of acute cytopathic murine hepatitis virus infection in fibroblast-like cells. J Gen Virol 87:1961-75.

32. **Wang, D., L. Coscoy, M. Zylberberg, P. C. Avila, H. A. Boushey, D. Ganem, and J. L. DeRisi.** 2002. Microarray-based detection and genotyping of viral pathogens. Proc Natl Acad Sci U S A 99:15687-92.

33. **Wang, D., A. Urisman, Y. T. Liu, M. Springer, T. G. Ksiazek, D. D. Erdman, E. R. Mardis, M. Hickenbotham, V. Magrini, J. Eldred, J. P. Latreille, R. K. Wilson, D. Ganem, and J. L. DeRisi.** 2003. Viral discovery and sequence recovery using DNA microarrays. PLoS Biol 1:E2.

34. **Woo, P. C., S. K. Lau, C. M. Chu, K. H. Chan, H. W. Tsoi, Y. Huang, B. H. Wong, R. W. Poon, J. J. Cai, W. K. Luk, L. L. Poon, S. S. Wong, Y. Guan, J. S. Peiris, and K. Y. Yuen.** 2005. Characterization and complete genome sequence of a novel coronavirus, coronavirus HKU1, from patients with pneumonia. J Virol 79:884-95.

35. **Wright, C., D. Bergstrom, H. Dai, M. Marton, M. Morris, G. Tokiwa, Y. Wang, and T. Fare.** 2008. Characterization of globin RNA interference in gene expression profiling of whole-blood samples. Clin Chem 54:396-405.

36. **Yang, Y. H., S. Dudoit, P. Luu, D. M. Lin, V. Peng, J. Ngai, and T. P. Speed.** 2002. Normalization for cDNA microarray data: a robust composite method addressing single and multiple slide systematic variation. Nucleic Acids Res 30:e15.

Chapter 3

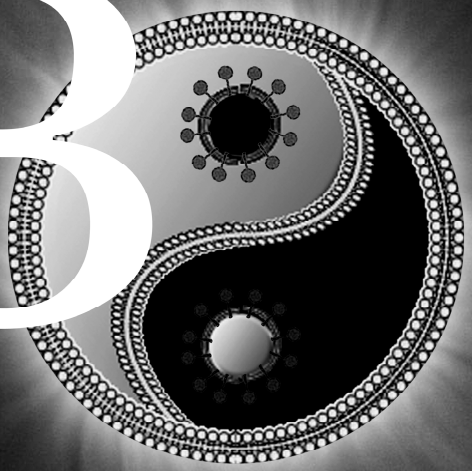

Mouse Hepatitis Coronavirus Replication Induces Host Translational Shutoff and mRNA Decay, with Concomitant Formation of Stress Granules and Processing Bodies

Matthijs Raaben
Marian J.A. Groot Koerkamp
Peter J.M. Rottier
Cornelis A.M. de Haan

Cellular Microbiology; 2007 Sep;9:2218-29.

Abstract

Many viruses, including coronaviruses, induce host translational shutoff, while maintaining synthesis of their own gene products. In this study we performed genome-wide microarray analyses of the expression patterns of mouse hepatitis coronavirus (MHV)-infected cells. At the time of MHV-induced host translational shutoff, downregulation of numerous mRNAs, many of which encode protein translation-related factors, was observed. This downregulation, which is reminiscent of a cellular stress response, was dependent on viral replication and caused by mRNA decay. Concomitantly, phosphorylation of the eukaryotic translation initiation factor 2α was increased in MHV-infected cells. In addition, stress granules and processing bodies appeared, which are sites for mRNA stalling and degradation, respectively. We propose that MHV replication induces host translational shutoff by triggering an integrated stress response. However, MHV replication *per se* does not appear to benefit from the inhibition of host protein synthesis, at least *in vitro*, since viral replication was not negatively affected but rather enhanced in cells with impaired translational shutoff.

Introduction

Virus infections often give rise to a shutoff of host cell translation, while synthesis of viral proteins is maintained. This cellular response provides two advantages for viral replication; it facilitates rapid viral protein synthesis and inhibits the production of antiviral proteins (40). On the other hand, viruses and their hosts share the same translational machinery. Therefore global inhibition of protein synthesis can also be regarded as part of an antiviral response of the host aimed to minimize viral replication.

Coronaviruses (CoVs) are enveloped, positive-stranded RNA viruses and are common pathogens in man and animals. Their relevance has increased considerably with the recent emergence of new human CoVs (HCoVs), such as the severe acute respiratory syndrome (SARS)-CoV (17), HCoV-NL63 (61), and HCoV-HKU1 (63). CoVs replicate entirely within the cytoplasm of their host cells, where they produce a nested set of (sub)genomic mRNAs, containing identical 5'-leader sequences and coterminal 3'-ends (44). These mRNAs, which are transcribed via a discontinuous transcription mechanism, are 5'-capped and 3'-polyadenylated, making them structurally equivalent to host cellular mRNAs (48). Therefore, CoVs must hijack the host translational machinery to produce their own proteins.

The mouse hepatitis CoV (MHV), a close relative of the SARS-CoV (54), and the feline infectious peritonitis virus have been shown to induce host translational shutoff in susceptible cells (25, 47, 52). The mechanism by which this occurs and how CoVs themselves escape from it is not known. As the leader sequence, present on all viral mRNAs, enhances translation in MHV-infected cells, it has been suggested that the apparent downregulation of host protein synthesis is not primarily due to inhibition of translation (56). On the other hand, the reduced host mRNA translation in MHV-infected cells has also been associated with a decrease in the number and size of polysomes and an increase of inactive single 80S ribosomes (25), and with cleavage of 28S ribosomal RNA (3). Furthermore, it has been suggested that a decline in steady-state levels, found for some host cell mRNAs, contributes to the downregulation of host protein translation (25, 33, 56). More recently, the expression of the SARS-CoV non-structural protein 1 (nsp1) was reported to induce mRNA degradation and inhibition of host protein synthesis (27).

Host shutoff is not restricted to virus infected cells, but is induced by various stress stimuli (6). For example, cells deprived of nutrients inhibit protein synthesis to conserve amino acids for essential metabolic processes. In addition, cells also shut down protein synthesis in response to endoplasmic reticulum (ER)-stress, heat, and oxidative stress. These different stress stimuli induce translational shutoff via the increased phosphorylation of eukaryotic initiation factor (eIF)2α (15). In mammalian cells there are at least four eIF2α kinases, including GCN2, PKR, PERK, and HRI, which are activated by amino acid starvation, double stranded RNA, ER stress, and heme depletion, respectively (4, 24, 28, 39). Upon phosphorylation of eIF2α, cytoplasmic structures containing stalled translational preinitiation complexes, frequently referred to as stress granules (SGs), are formed. The actual formation of SGs occurs upon aggregation of the RNA binding proteins TIA-1 (T-cell internal antigen-1) and TIAR (TIA-1-related protein) (30). SGs are thought to recruit specific mRNA transcripts, such as 'housekeeping' protein encoding mRNAs, to regulate their translation in adaptation to altered conditions (2). SGs are also referred to as triage centers since they sort mRNAs for either storage, reinitiation of translation, or degradation (1).

Degradation of mRNA is another way to control gene expression at a post-transcriptional level. While 3'-5' mRNA decay occurs by a complex of exonucleases termed the exosome, 5'-3' mRNA decay takes place in cytoplasmic foci related to SGs, called processing bodies (P bodies) (1). P bodies contain decapping enzymes, the exonuclease Xrn1 and components of the RNA-induced silencing complex, including GW182, which is an RNA binding protein required for microRNA-dependent silencing (11, 20, 26, 38). The formation of P bodies is also induced in response to different stress stimuli including glucose deprivation and osmotic stress. However, unlike SGs their assembly does not require phosphorylation of eIF2α (29, 58).

To get more insight into the interference of CoVs with gene expression of their host, we investigated the global mRNA profiles in MHV-infected cells by using genome-wide microarray analysis. At the time of host shutoff, significant downregulation of many mRNAs, particularly of those encoding translation-related factors, was observed. This downregulation, which is reminiscent of a cellular stress response, was shown to be

dependent on viral replication and to result from mRNA decay. At the same time, increased phosphorylation of eIF2α and the assembly of SGs and P bodies were observed, suggesting that these cellular structures play an important role in the host translational shutoff and mRNA decay, respectively. MHV replication was not negatively affected, but rather enhanced in mouse embryo fibroblast (MEF) cells, in which host translational shutoff and SG formation were impaired by mutation. Apparently, virus replication does not benefit, at least *in vitro*, from the induced translational shutoff.

Results

Kinetics of MHV-Induced Host Translational Shutoff

Before starting with the microarray analyses, the kinetics of the MHV-induced host translational shutoff was determined for the experimental conditions used. To this end, metabolic labeling of MHV-infected LR7 cells was performed at different time-points post infection (p.i.). The results, shown in Fig.1A, clearly demonstrated that host translational was shut down at 6, but not at 4 h p.i., while the viral spike (S), nucleocapsid (N), and membrane (M) proteins were clearly visible at 6 h and at later time-points p.i. Thus, between 4 and 6 h p.i., a shift occurred from host to viral protein synthesis. This conclusion was corroborated by quantification of the radioactivity in the gel (Fig.1B). The data show that there is a continuous rise in expression of the viral protein S, N and M, with the largest increase appearing between 4 and 6 h p.i. The amount of radioactivity in the regions between the viral proteins, representative of host protein synthesis, were also quantified, and confirmed the induction of host shutoff between 4 and 6 h p.i.

Next, the levels of genomic viral RNA in the MHV-infected cells were determined. Total RNA was isolated at different time-points p.i. and viral RNA was quantified using quantitative RT-PCR. The results show that viral RNA accumulated during infection, reaching a steady-state level at approximately 8 h p.i. (Fig.1C). Consistent with the results of the metabolic labeling experiment, the largest relative increase in viral RNA levels was observed between 4 and 6 h p.i. (Fig.1D). Altogether the results demonstrate that, under the experimental conditions used, host translational shutoff is induced in MHV-infected LR7 cells between 4 and 6 h p.i. and is accompanied by a relatively large increase in viral RNA and protein synthesis.

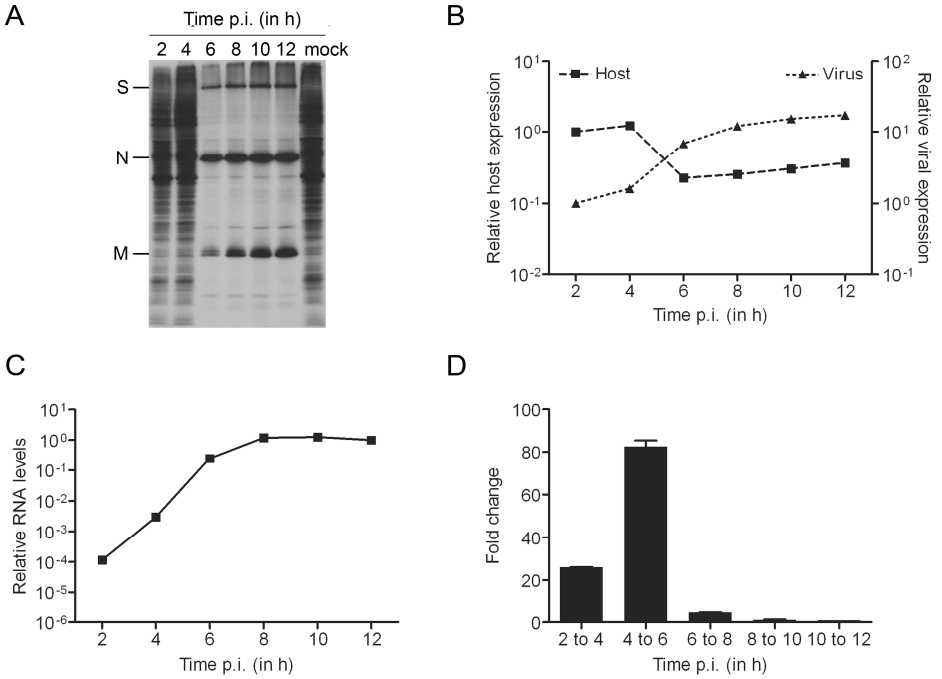

Fig.1. Kinetics of the MHV-induced host translational shutoff. (A) LR7 cells were infected with MHV (MOI 10) and metabolically labeled for 15 min starting at the indicated time-points. Cell lysates were processed and subjected to SDS-PAGE as described in *Material & Methods*. Positions of the viral proteins S, N and M are indicated. (B) The amount of radioactivity in the gel was quantified with a PhosphorImager. For each time point, the amount of radioactivity in the MHV structural proteins S, N and M was combined (viral expression). For the host proteins, the amount of radioactivity in the regions between the MHV proteins was quantified (host expression). The data are presented as relative expression (2 h p.i. = 1). (C and D) Genomic viral RNA levels in MHV-infected LR7 cells (MOI 10) were measured by quantitative RT-PCR at the indicated time-points p.i. The data are presented as relative viral RNA levels (12 h p.i. = 1) in C, or as the fold change increase relative to the previous time point in D. Error bars indicate the standard deviations (n = 3).

Microarray Analysis of MHV-Infected LR7 Cells Reveals Large-Scale mRNA Degradation

To get more insight into the MHV-induced host translational shutoff, we investigated the global mRNA profiles in infected cells by using genome-wide microarray analysis. To this end, parallel cultures of LR7 cells were either mock-infected or infected with MHV-A59 and total RNA was isolated at 4 and 6 h p.i. As will be published elsewhere, at 6 h p.i. viral mRNA constitutes approximately 40% of the total mRNA content in infected cells. By

removing these unwanted transcripts using the oligo capture technique we reduced non-specific hybridization by approximately 80%.

The mRNAs in the infected and uninfected samples were amplified, labeled with either Cy3 or Cy5, and hybridized to the arrays after which they were scanned and analyzed. At 4 h p.i., relatively few changes in the expression profile were observed (Fig.2A). However, at 6 h p.i., a significant number of genes appeared to be altered in their expression (Fig.2B). Besides the apparent upregulation of several mRNAs, a large number of mRNAs (678) was significantly downregulated upon infection. This set of mRNAs is represented by the yellow dots in the different panels of Fig.2. Actinomycin D (ActD), an inhibitor of cellular transcription but not of CoV replication (34, 45), was used to establish whether the observed mRNA downregulation was the result of a transcriptional or a post-transcriptional mechanism. Treatment of both infected and uninfected cells with ActD, did not affect the downregulation of mRNAs, indicating that the observed decrease resulted from post-transcriptional mRNA degradation (Fig.2C). To study the specificity of this virus-induced mRNA degradation, the effect of ActD treatment was analyzed in the absence of a viral infection. Treatment of cells with ActD, or with other transcriptional inhibitors, induced the downregulation of short-lived mRNAs (9). Indeed, downregulation of many mRNAs was observed in ActD-treated cells when compared to mock-treated cells (Fig.2D). However, the mRNA population downregulated by ActD treatment clearly differed from the mRNAs downregulated in response to MHV infection at 6 h p.i. (the latter ones are represented by the yellow dots). In order to determine the role of virus replication in the mRNA decay, cells were inoculated with fusion-competent, replication incompetent, UV-inactivated virus. The results show, that the MHV-induced downregulation of mRNA (shown again as yellow dots) was replication-dependent, as it was not observed after inoculation with the UV-inactivated virus (Fig.2E).

Transcriptional Upregulation of mRNAs

Comparison of the transcriptional profiles of MHV-infected cells in the absence or presence of ActD (Fig.2B and 2C) revealed that the mRNAs from relatively few genes were upregulated at the transcriptional level, as the majority of the upregulated mRNAs were obtained for both conditions.

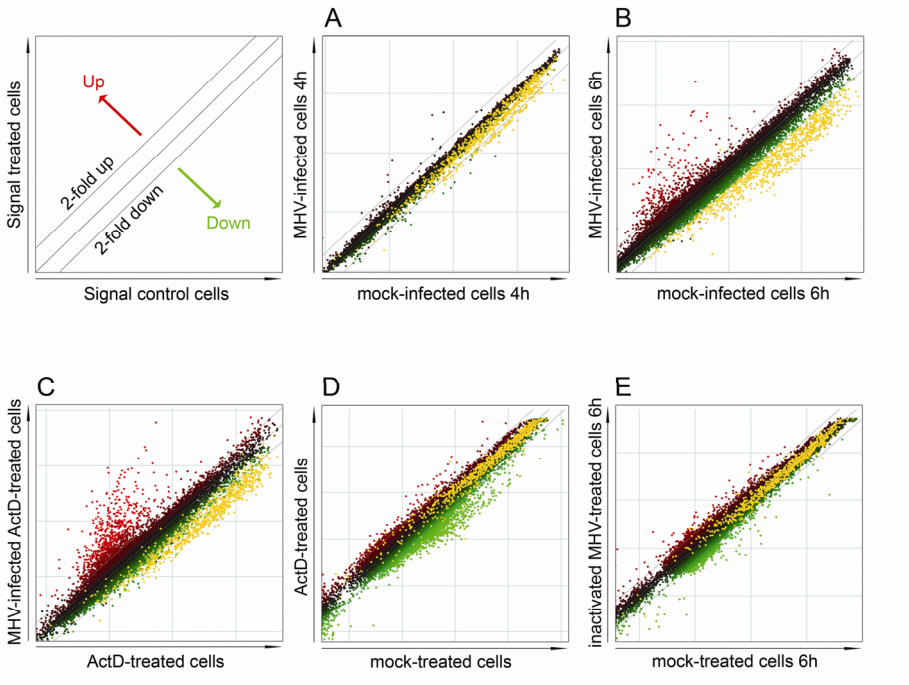

Fig.2. Replication-dependent mRNA decay in MHV-infected cells as determined by microarray analyses. LR7 cells were infected with MHV (MOI 10). Total RNA was isolated from MHV-infected and mock-infected cells and processed for microarray analysis as described in *Material & Methods*. The scatter plots display the average expression values from independent dye-swap hybridizations for each gene present on the arrays. Red spots represent upregulated gene transcripts while green spots represent downregulated transcripts. The dashed lines indicate the 2-fold change cut-off. Transcripts downregulated at 6 h p.i. (in panel B) are represented by the yellow dots throughout the Figure. Note that these transcripts are significantly changed at 6 h p.i. according to SAM, applying a false-discovery rate of 1% and a cut-off at a 2-fold change (described in *Material & Methods*). (A) The expression profile of MHV-infected cells compared to mock-infected cells at 4 h p.i. (average of 4 arrays; two independent dye-swaps; n = 4). (B) The expression profile of MHV-infected cells compared to mock-infected cells at 6 h p.i. (n = 6). (C) The expression profile of MHV-infected cells compared to mock-infected cells at 6 h p.i. (n = 4). Both MHV- and mock-infected cells were treated with ActD for 7 h (from –1 till 6 h p.i.) (D) The expression profile of ActD-treated cells compared to mock-treated cells. Non-infected cells were treated or mock treated with ActD for 7 h (n = 1). (E) The expression profile of cells treated with UV-inactivated viral particles compared to mock-treated cells at 6 h post inoculation (n = 1). By using Gene Ontology (GO) databases, 240 of the 678 mRNAs downregulated at 6 h p.i. could be annotated by their GO-terms for biological functions/processes (see Supplemental table S1). Strikingly, 50% of the mRNAs that could be annotated encode protein translation-related factors (ribosome biogenesis factors, translation initiation/elongation associated factors). In summary, the results show that, at the time of virus-induced host translational shutoff, significant downregulation of many mRNAs encoding largely translation-related factors was observed. This downregulation was found to be dependent on viral replication and to result from mRNA decay.

Since approximately 20% of the viral RNA present in the LR7 cells at 6 h p.i. was not removed by the oligo capture technique (unpublished results), a large number of the mRNAs upregulated in the presence of ActD are likely to result from cross hybridization of the remaining viral RNA. Indeed, this was confirmed for some hits using quantitative RT-PCR analysis (data not shown). However, we cannot exclude that some of these hits might also result from increased mRNA stability upon virus infection, a subject of further research. In order to exclude (potential) false-positive hits, the genelists of the experiments performed in the absence or presence of ActD were compared. As a result, 243 genes were excluded from the analysis since they were upregulated under both experimental conditions, leaving 40 genes that were specifically upregulated at the transcriptional level in MHV-infected LR7 cells at 6 h p.i. The genes identified were clustered according to their GO-terms for biological processes (see Supplemental table S2). Out of the 40 genes, we could annotate 29 genes. Examples of genes of which the expression was induced were those encoding inflammatory cytokines (*Cxcl1*, *Cxcl2*), a marker of the unfolded protein response (*Herpud1*), and dual specificity phosphatase 1 (*Dusp1*). In addition, several genes involved in regulation of transcription were differentially expressed. The expression of several genes at 4 and 6 h p.i. was confirmed by quantitative RT-PCR (see Supplemental table S3).

Phosporylation of eIF2α, and the Formation of Stress Granules and Processing Bodies

The observed downregulation of numerous mRNAs, many of which encode protein translation-related factors, is reminiscent of a cellular stress response. Recently, SGs have been associated with the initiation of host translational shutoff during stress. A key aspect in the formation of these cytoplasmic structures, which contain stalled translation preinitiation complexes, is the phosphorylation of the translation initiation factor eIF2α at serine 51, which results in the aggregation of the mRNA binding proteins TIA-1 and TIAR, both markers for SGs (29, 30). Phosphorylation of eIF2α was analyzed in MHV-infected LR7 cells at 4 and 6 h p.i., i.e. before and at the time of host translational shutoff, respectively (Fig.3A). Mock-infected cells and cells treated for 30 min with 0.5 mM sodium arsenite were taken along as controls. Sodium arsenite has been shown to induce phosphorylation of eIF2α at serine 51 (42). The expression levels and phosphorylation status of eIF2α in all samples were visualized by immunoblotting using antibodies against

total eIF2α and phosphorylated eIF2α (eIF2αP), respectively. Quantitative analysis revealed that the levels of phosphorylated eIF2α, corrected for the total amount of eIF2α, in MHV-infected cells were reproducibly ~2.5-fold higher at 6 h p.i. compared to mock-infected cells, while at 4 h p.i. no increase could be observed.

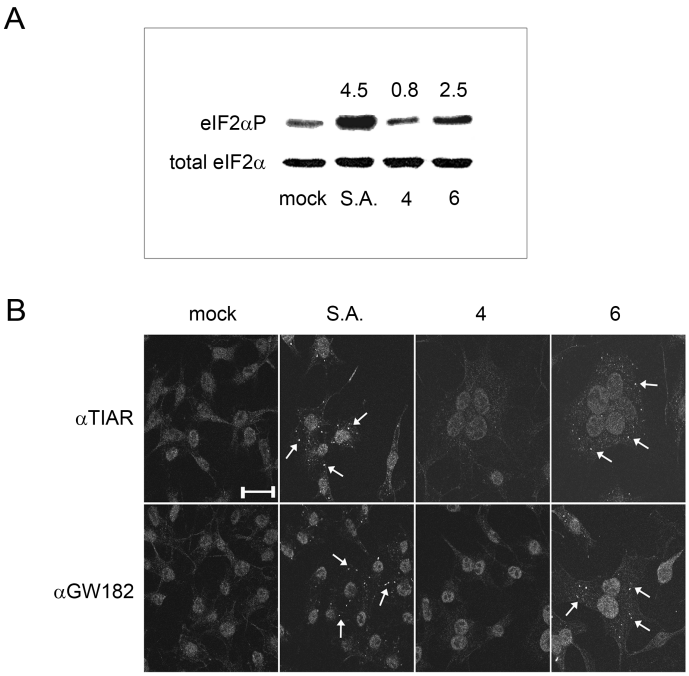

Fig.3. MHV induces phosphorylation of eIF2α at Ser51, and the subsequent formation of SGs and P bodies. (A) The phosphorylation state of eIF2α in MHV-infected LR7 cells at 4 and 6 h p.i. (indicated by 4 and 6) or after mock infection was determined by Western blotting using eIF2αP-specific antibodies (top) and related to total eIF2α levels by stripping and reprobing of the membrane (bottom). The fold change differences between MHV-infected and mock-infected cells are indicated above each lane. As a positive control, LR7 cells were treated with 0.5 mM sodium arsenite (indicated as S.A.) for 30 min. This experiment was repeated twice with similar results. (B) LR7 cells were mock-infected, treated with S.A. for 30 min, or infected with MHV. Cells were fixed and processed for immunofluorescence using TIAR (αTIAR) and GW182 (αGW182) antibodies according to *Material & Methods*. MHV-infected cells were fixed at 4 and 6 h p.i. (indicated by 4 and 6). Representative images are shown for each condition. The scaled bar corresponds to 20 μM.

Subsequently, we investigated whether SGs were formed in LR7 cells upon MHV infection. As a positive control, LR7 cells were incubated with sodium arsenite as described above. The cells were fixed at the indicated time-points p.i., and processed for

immunofluorescence using anti-TIAR antibodies. Indeed, cytoplasmic foci containing TIAR, representing SGs, could be detected at the time of increased eIF2α phosphorylation and host translational shutoff (at 6 h p.i.), but hardly or not at 4 h p.i. (Fig.3B). SGs were observed both in single cells and in syncytia. Next, we analyzed the formation of other cytoplasmic structures, P bodies, which are sites of mRNA degradation. P bodies are related to SGs, although their formation does not require the phosphorylation of eIF2α. The GW182 antigen has recently been described as a marker for P bodies (19, 20). Consistent with the results described above, P bodies could be detected by immunofluorescence assays using antibodies against GW182 at 6 h p.i., when mRNA decay could be observed, but hardly or not at 4 h p.i. (Fig.3B). Altogether, the results show that MHV infection of LR7 cells induces the phosphorylation of eIF2α at serine 51, and the formation of SGs and P bodies, concomitant with the observed host translational shutoff and mRNA decay.

MHV Replication is Not Negatively Affected in Cells with Impaired Host Translational Shutoff

To investigate to what extent the cellular stress response and the host translational shutoff affects MHV infection, we studied replication in MEFs expressing a mutant form of eIF2α (eIF2α^{S51A}) that cannot be phosphorylated at serine 51 (49). Host translational shutoff is not observed in these cells during stress or alphavirus infection (43, 49). In addition, replication was monitored in TIA-1$^{-/-}$ and TIAR$^{-/-}$ MEFs. These MEFs have been demonstrated to exhibit impaired SG assembly, as well as delayed host translational shutoff after viral infections (22, 43).

Unfortunately, host translational shutoff could not be studied by metabolic labeling of the cells upon infection with MHV, as only 10-20% of the MEF cells in a dish could be infected after a high multiplicity infection with MHV (data not shown). Nevertheless, viral replication in the MEF cells was monitored, not by determining the production of infectious virions, but by following the expression of a reporter gene after infection with MHV-EFLM, which carries the firefly luciferase (FL) in an MHV-A59 background. FL expressed by MHV has been shown to be a reliable measure for virus replication (12). The intracellular FL levels were determined at different time-points p.i. and normalized for the number of infected cells, which differed slightly between the different MEF cell lines.

Clearly, MHV replication was enhanced in the eIF2α^{S51A}-expressing cells as compared to the wild-type eIF2α-expressing cells (Fig.4A). Similarly, replication was also enhanced in the TIAR$^{-/-}$ cells, while MHV replicated to approximately the same extent in the TIA-1$^{-/-}$ and wild-type MEF cells (Fig.4B). Overall, the results show that replication of MHV is not negatively affected but rather enhanced in cells with impaired host translational shutoff.

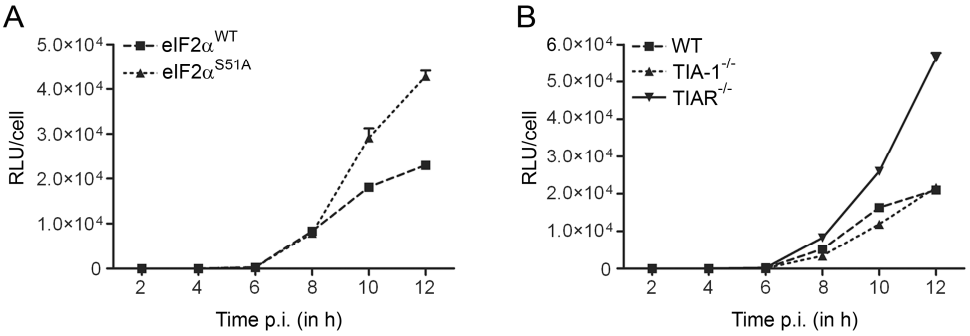

Fig.4. MHV replication is not negatively affected in MEF cells with impaired host translational shutoff and reduced SG assembly. Confluent monolayers of MEF cells were infected with MHV-EFLM. Cells were lysed at the indicated time-points p.i. and the intracellular luciferase levels were determined (in RLU). Since the number of infected cells differed to some extent between the different MEFs, the obtained RLU values for each cell line were normalized for the number of infected cells as determined by immunocytochemistry using a polyclonal anti-MHV serum (47). Error bars indicate the standard deviations in all graphs (n = 3). (A) Luciferase expression in MEF cells expressing wild-type eIF2α (eIF2α^{WT}) or mutant eIF2α (eIF2α^{S51A}). (B) Luciferase expression in wild-type (WT), TIA-1 knock-out (TIA-1$^{-/-}$), and TIAR knock-out (TIAR$^{-/-}$) cells.

Discussion

A variety of strategies has been described by which viruses dominate the host-cell protein synthetic machinery, optimize viral mRNA translation and evade the host-cell antiviral responses that act at the translational level (50). For MHV it was shown already in the eighties that infection induces host translational shutoff, while maintaining its own protein synthesis (25, 47, 52). However, the cellular processes underlying MHV-induced inhibition of host protein synthesis remained largely unknown. We now show that this inhibition coincides with degradation of numerous mRNAs, many of which encode protein translation-related factors. In addition, infection with MHV results in increased phosphorylation of eIF2α and in the formation of SGs and P bodies, which are sites of

mRNA stalling and degradation, respectively. Altogether these results indicate that MHV infection induces an integrated stress response, which results in increased phosphorylation of eIF2α and in the formation of SGs and P bodies, leading to shutdown of host mRNA translation and to mRNA decay (Fig.5).

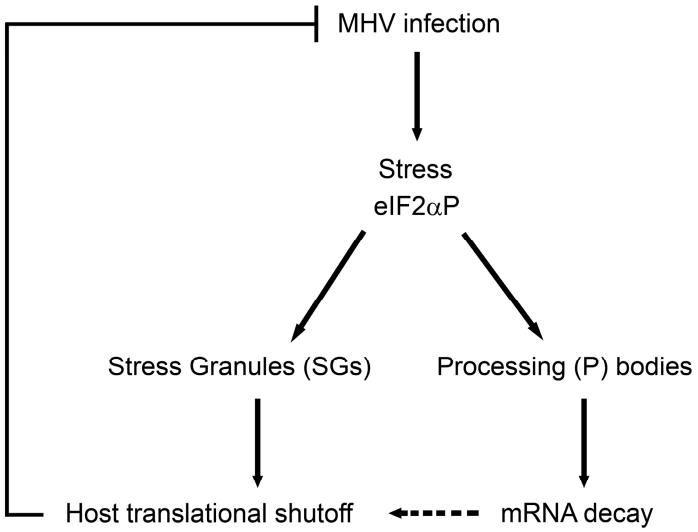

Fig.5. Model for MHV-induced host translational shutoff. A cellular stress response is elicited upon infection with MHV, which results in increased phosphorylation of eIF2α (eIF2αP). Subsequently, SGs containing stalled translational preinitiation complexes are formed and host translational shutoff is induced. In addition, the stress response also induces the formation of P bodies, which are cytoplasmic sites of mRNA decay. Degradation of many mRNAs encoding protein translation-related factors is observed, which may contribute to the MHV-induced host translational shutoff. Overall, the initiated stress response appears to inhibit MHV replication.

Our application of microarray analysis to assess changes in cellular mRNA profiles in MHV-infected cells revealed that mRNA levels were regulated both by transcriptional and by post-transcriptional mechanisms. Relatively few genes (n = 40) were identified, of which transcription was enhanced (see Supplementary data). Among these were genes encoding inflammatory cytokines (*Cxcl1* and *Cxcl2*) and proteins associated with cellular transcription. The induction of *Dusp1*, which plays an important role as a protein phosphatase in the cellular response to stress (31, 41) and of *Herpud1*, which is a marker of the unfolded protein response (31, 41), suggests that cells infected with MHV elicit a stress response. Several of these upregulated gene transcripts have also been identified in a gene

expression profiling study of MHV-infected cells using a different microarray platform (62).

Perhaps more striking is the decline of a large number of mRNAs at the time of host translational shutoff (see Supplementary data). This reduction was shown to be dependent on viral replication and to be caused by mRNA degradation, since it was also observed in the presence of the cellular transcription inhibitor ActD. Transcriptional inhibition results in a fast degradation of short-lived mRNAs, especially those containing AU-rich elements (AREs) in their 3' UTRs (57). However, ActD treatment itself resulted in a different expression profile as compared to MHV infection, indicating that MHV infection does not simply result in increased instability of short-lived mRNAs. Interestingly, MHV infection induced the degradation of transcripts encoding the chemokines Cxcl1 and Cxcl2 in the presence of ActD (data not shown), whereas higher levels of these transcripts were observed during infection in the absence of ActD, indicating that the expression of individual genes can be regulated both at the transcriptional and post-transcriptional level.

Downregulation of many transcripts encoding ribosome biogenesis factors during CoV infection has also been observed after infection of Vero cells with SARS-CoV (36). These reduced mRNA levels are reminiscent of the decline of ribosome biogenesis factor encoding mRNAs observed in yeast in response to different stress stimuli such as heat and nutrient deprivation (7, 21). In agreement with our results, mRNA decay was demonstrated to be the main cause of the observed downregulation of these mRNA levels (23). These results indicate that CoV infection elicits a cellular response, which resembles the reaction of yeast cells upon environmental stress. Recently, expression of the SARS-CoV nsp1 has been shown to result in degradation of several host mRNAs and in translational shutoff (27). A direct role for nsp1 in mRNA degradation might explain the observed effects, even though nsp1 has no sequence similarities with any known RNases, and is only poorly conserved among CoVs. Alternatively, expression of the SARS-CoV nsp1 might induce a cellular stress response resulting in mRNA decay and in inhibition of protein synthesis. In agreement herewith, others showed that expression of SARS-CoV nsp1 induced activation of the stress-related transcription factor NF-kappaB and chemokine upregulation (35).

Phosphorylation of eIF2α is induced in response to several stress stimuli (10). Indeed, a modestly increased level (~2.5-fold) of phosphorylated eIF2α was detected after infection with MHV. A similar increase in eIF2α phosphorylation has also been reported for some reoviruses (53). The kinase responsible for the phosphorylation of eIF2α after infection with MHV is not known. PERK, which is activated by endoplasmic reticulum stress, might be a good candidate as infection of cultured cells with SARS-CoV (8) or MHV (62) appears to lead to the induction of the unfolded protein response.

The recent discovery of cellular structures involved in translational arrest (SGs) and turnover of mRNA pools (P bodies) during stress prompted us to investigate the formation of these cytoplasmic structures in MHV-infected cells. In general, phosphorylation of eIF2α is required for the formation of SGs. Indeed, SGs were detected concomitant with increased phosphorylation of eIF2α and host translational shutoff. Similarly, the induction of SGs has recently also been demonstrated after infection with reovirus (53), Semliki Forest virus (43) and herpes simplex virus type 1 (18), all of which are able to induce host translational shutoff.

To the best of our knowledge, this is the first report that describes the induction of P bodies by virus infection. P bodies were formed at the time of mRNA decay, suggesting that these structures play a role in the degradation of the host transcripts. Whether also viral mRNAs localize to P bodies and are subsequently degraded remains to be established. We cannot exclude that other RNA decay pathways may be induced upon infection with MHV as well. However, the interferon-depended 2',5'-oligoadenylate synthetase pathway (10) is not likely to play a major role in MHV-infected cells, since no prominent upregulation of interferon-mediated gene transcription was observed, which is consistent with the results of others (3, 62). Whether the mRNA decay contributes to MHV-induced host translational shutoff remains to be established.

The CoV-induced cellular stress response, resulting in the inhibition of host protein synthesis, might be beneficial for the virus by downregulating cellular components of the antiviral response. On the other hand, as the coronaviral mRNAs are structurally equivalent

to the host mRNAs, viral protein synthesis might also be impaired, even though viral protein synthesis is still robust after host translational shutoff. The results obtained with the host translational shutoff-deficient (eIF2α^{S51A}) MEF cells show that in the absence of phosphorylatable eIF2α MHV replication is not negatively affected. Thus, the stress response induced upon infection with MHV, which results in the phosphorylation of eIF2α and the subsequent inhibition of protein synthesis, does not appear to be beneficial for MHV replication *in vitro*. This is in contrast to reoviruses, replication of which has been demonstrated to be facilitated by the induced cellular stress response and eIF2α phosphorylation (53). Our conclusions are corroborated by the results obtained with the TIA-1$^{-/-}$ and TIAR$^{-/-}$ MEFs, which exhibit impaired SG assembly and host translational shutoff, and in which also MHV replication was not negatively affected but, rather, enhanced. Similar results, using the same TIA-1$^{-/-}$ and TIAR$^{-/-}$ MEFs, were previously obtained for the replication of vesicular stomatitis virus, Sindbis virus, and herpes simplex virus type 1, but not for West Nile virus (37). The latter virus was found to require TIA-1 and TIAR binding to viral RNA for efficient replication. The importance of the CoV-induced cellular stress response and the host translational shutoff for virus replication *in vivo* remains to be established.

Even though it appears that infection with MHV induced an integrated stress response resulting in host translational shutoff, the viral proteins are still efficiently made in comparison with the host proteins. Several factors are likely to play a role in the CoV "escape" from translational inhibition. Previously it has been reported that the leader sequence present at the 5'end of all MHV encoded mRNAs mediates their preferential translation (55, 56). However, the precise mechanism by which this is established is still unknown. The exponential increase in the abundance of viral mRNAs during infection is also likely to contribute to a preferential translation of these mRNAs, simply as a result of increasing abundance in the competition for the limited translational machinery. We have calculated that at 6 h p.i. up to 40% of all mRNAs in the cell is virus-encoded (data not shown). Furthermore, the downregulation of many mRNAs encoding protein translation-related factors, probably via the induction of P bodies, is also likely to increase the success of the viral mRNAs in their competition with the host-encoded mRNAs.

Material & Methods

Cells and viruses

LR7 mouse fibroblast cells (32), were maintained in Dulbecco's Modified Eagle's Medium (DMEM) (Cambrex Bio Science) containing 10% (v/v) fetal calf serum (Bodinco B.V.), 100 U/ml Penicillin, and 100 μg/ml Streptomycin (referred to as complete DMEM), supplemented with Geneticin G418 (250 μg/ml). The MEFs expressing wild-type or mutant (S51A) eIF2α (49) as well as the MEF cell lines from wild-type, TIAR knock-out ($TIAR^{-/-}$) and TIA-1 knock-out ($TIA^{-/-}$) embryo mice (37) were also maintained in complete DMEM. MHV strain A59 and MHV-EFLM, the latter containing the firefly luciferase reporter gene (12), were grown on LR7 cells. Inactivation of MHV-A59 was performed by UV light (366 nm), using a Chromato-Vue transilluminator (1 min, 6000 μW/cm^2) from Ultraviolet products Inc. The inactivated particles retained their fusion activity, as was demonstrated using a fusion-from-without assay on LR7 cells.

Metabolic labeling of MHV-infected cells

LR7 cells were inoculated with MHV-A59 at a multiplicity of infection (MOI) of 10 $TCID_{50}$ (50% tissue culture infectious doses) per cell, in phosphate buffered saline (PBS) containing 50 μg/ml diethylaminoethyl-dextran (PBS-DEAE). After 1 h, the cells were washed with and the culture medium was replaced by complete DMEM. At 2 h p.i. the fusion inhibitory mHR2 peptide (1 μM) (5) was added to the culture medium. At the indicated time-points, the cells were labeled with ^{35}S labeled amino acids (Amersham) for 15 min, after which cells were lysed and lysates were prepared for sodium dodecylsulfate-polyacrylamide gel electrophoresis (SDS-PAGE) and subsequent fluorography as previously described (14). Radioactivity in protein bands was quantitated in dried gels using a PhosphorImager (Molecular Dynamics).

Luciferase assay

Cell monolayers were infected with MHV-EFLM as described above. At the indicated times, the cells were lysed using the appropriate buffer provided with the steadylite HTS reporter gene assay system (PerkinElmer). Intracellular luciferase expression was measured according to the manufacturer's instructions, and the relative light units (RLU) were determined with a Berthold Centro LB 960 plate luminometer.

Total RNA isolation

LR7 cells were either mock-infected or infected with MHV-A59 as described above. When indicated, the cells were incubated with ActD (20 μg/ml) 1 h prior to infection, and maintained in the presence of this drug throughout the experiment. Total RNA was isolated from mock or MHV-A59 infected cells at the indicated time p.i. using the TRIzol reagent (Invitrogen). RNA was further purified using the RNeasy mini-kit with subsequent DNaseI treatment on the column (Qiagen). Viral RNA was removed from the total RNA samples using the GlobinClear kit (Ambion) with the use of an alternative oligo capture mix, containing three 5' biotinylated oligo's that anneal to either the 5' leader, the nucleocapsid gene, and the 3'untranslated region of the MHV-A59 genome, as will be reported in more detail elsewhere. All subsequent steps were performed according to the manufacturer's protocol. RNA integrity was determined by spectrometry and by a microfluidics-based platform using a UV-mini1240 device (Shimadzu) and a 2100 Bioanalyzer (Agilent Technologies), respectively.

cRNA synthesis, labeling, and hybridization onto microarrays

mRNA was amplified from 1 μg of total RNA by cDNA synthesis with oligo(dT) double-anchored primers, followed by *in vitro* transcription using a T7 RNA polymerase kit (Ambion) as described previously (46). During transcription, 5-(3-aminoallyl)-UTP was incorporated into the single stranded cRNA. Cy3 and Cy5 NHS-esters (Amersham Biosciences) were coupled to 2 μg cRNA. RNA quality was monitored after each successive step using the methods described above. A Mouse Array-Ready Oligo set (version 3.0) was purchased (Operon) and printed on Corning UltraGAPS slides. Mouse slides containing 35,000 spots (32,101 70-mer oligonucleotides, and 2,891 control spots) were hybridized with 1 μg of each alternatively labeled cRNA target at 42°C for 16-20 h using LifterSlips (Erie Scientific) and Corning Hybridization Chambers (60). After hybridization the slides were washed extensively and scanned using the Agilent G2565AA DNA Microarray Scanner.

Microarray data analysis

Images were quantified and background corrected using Imagene 5.6 software. The data was normalized using Lowess print-tip normalization as described previously (64). To identify the genes that were significantly different within each experiment, a one-class Significance Analysis of Microrarrays (SAM) (59) was performed on the average of independent dye-swap hybridizations (unless indicated otherwise), using a false discovery rate of 1%. To increase the confidence level, a cut-off at a 2-fold change in expression was applied. The resulting genelists were subjected to Genespring 7.2 software for further analysis.

ArrayExpress accession numbers

MIAME-compliant data in MAGE-ML format as well as complete descriptions of protocols have been submitted to the public microarray database ArrayExpress (http://www.ebi.ac.uk/arrayexpress/) with the following accession numbers: microarray layout, P-UMCU-8; gene expression data of MHV-infected LR7 cells, E-MEXP-895; protocols for total RNA isolation and mRNA amplification, P-MEXP-34397; cRNA labeling, P-MEXP-34400 and P-MEXP-35534; hybridization and washing of slides, P-MEXP-34401; scanning of slides, P-MEXP-34430; data normalization, P-MEXP-34431.

Quantitative RT-PCR

Altered gene expression levels of some genes, identified by microarray analysis, were verified by quantitative reverse transcription (RT)-PCR using Assay-On-Demand reagents (PE Applied Biosystems), according to the manufacturer's instructions, on cDNA generated as decribed above. Reactions were performed using an ABI Prism 7000 sequence detection system. The comparative Ct-method was used to determine the fold change for each individual gene. The housekeeping gene GAPDH was used as a reference in all experiments. The amounts of viral genomic RNA were determined by quantitative RT-PCR as described before (13).

Immunoblotting

Cells were lysed in ice-cold lysis buffer (20 mM MOPS [pH 7.2], 5 mM EDTA, 2 mM EGTA, and 0.5% (w/v) Nonidet-P40, containing 30 mM NaF, 40 mM β-Glycerophosphate, 20 mM Na-Pyrophosphate, 1 mM Na-Orthovanadate, 1 mM PMSF, 3 mM Benzamidine, 1.5 μM Pepstatin A, and 10 μM Leupeptin). Cell lysates were cleared by centrifugation at 100,000x g at 4°C for 30 min. Proteins present in the cell lysates were separated by

SDS-PAGE and transferred to Nitrocellulose membranes (0.1 μM, Schleicher Schuell). Subsequently, the membranes were incubated over night in block buffer (PBS containing 0.05% Tween-20, 5% (w/v) Protifar, and 5% (v/v) normal goat serum). Next, the membranes were washed three times with PBS (containing 0.05% Tween-20) and incubated for 16 h at 4°C with a rabbit polyclonal antibody specifically recognizing eIF2α phosphorylated on serine 51 (16). Following extensive washing, the membranes were incubated with peroxidase labeled goat-anti-rabbit IgG (Bio-Rad Laboratories), after which the amount of protein was visualized and quantitated using the Enhanced ChemoLuminescence (ECL) plus kit, a Typhoon imager, and ImageQuant TL software (Amersham Biosciences). For the detection of the total amount of eIF2α, membranes were stripped by incubating the blot in stripping buffer (62.5 mM Tris-HCl [pH 6.7], 100 mM β-mercaptoethanol, and 2% SDS) at 50°C for 30 min, after which the membranes were incubated with a monoclonal mouse-anti-eIF2α antibody (51) and peroxidase labeled goat-anti-mouse IgG (Cappel), and the protein bands were quantified as described above.

Indirect immunofluorescence

LR7 cells grown on 10-mm cover slips were infected with MHV-A59 as described above. At the indicated time-points, cells were fixed with 1% (w/v) paraformaldehyde in phosphate buffer (48 mg/L KH_2PO_4, 3 g/L NaCl, and 265 mg/L $Na_{2\ h}PO_4$) for 20 min, after which the cells were permeabilized using 0.1% Triton-X-100 in PBS for 10 min. After blocking with PBS containing 5% FCS, TIAR or GW182 were detected using a rabbit polyclonal antibody (Santa Cruz Biotechnologies) or a monoclonal antibody (Abcam), respectively. Subsequently, affinity-purified goat-anti-rabbit or donkey-anti-mouse secondary antibodies conjugated to Cy3 were used for visualisation. The cells were mounted with FluorSave Reagent (Calbiochem) and fluorescence was viewed with a Leica TCS SP confocal microscope.

Acknowledgements

We would like to thank the people at the Microarray Facility (UMC Utrecht, The Netherlands) for technical support, Adri Thomas (Dept. of Developmental Biology, Utrecht University, Utrecht, The Netherlands) and Gary Krause (Wayne State University School of Medicine, MI 48201, USA) for providing us the antibodies against total and phosphorylated eIF2α, Berend Jan Bosch for supplying us with the mHR2 peptide, Paul Anderson (Division of Rheumatology and Immunology, Brigham and Women's Hospital, Boston, Massachusetts 02115, USA), Randall Kaufman (Howard Hughes Medical Institute, University of Michigan, Ann Arbor, MI 48109, USA) and Costas Koumenis (Radiation Oncology, University of Pennsylvania, Philadelphia, USA) for providing the different MEF cell lines, and Monique Oostra for stimulating discussions. This work was supported by a grant from The Netherlands Organization for Scientific Research (NWO-VIDI-700.54.421) to C.A.M. de Haan.

Supplementary Data

Supplemental table S1. Downregulated gene transcripts in MHV-infected cells at 6 h p.i.

Gene ID	Name	Description	#
Protein biosynthesis			**120**
NM_001005859	1100001I22Rik	RIKEN cDNA 1100001I22 gene	
NM_001001987	1700073E17Rik	RIKEN cDNA 1700073E17 gene	
NM_026594	4930517K11Rik	RIKEN cDNA 4930517K11gene	
NM_013715	Cops5	COP9 (constitutive photomorphogenic) homolog, subunit 5	
NM_010106	Eef1a1	Eukaryotic translation elongation factor 1 alpha 1	
NM_018796	Eef1b2	Eukaryotic translation elongation factor 1 beta 2	
NM_026007	Eef1g	Eukaryotic translation elongation factor 1 gamma	
NM_011508	EIF1	Eukaryotic translation initiation factor 1	
NM_080635	EIF3s3	Eukaryotic translation initiation factor 3, subunit 3 (gamma)	
NM_025344	EIF3s5	Eukaryotic translation initiation factor 3, subunit 5 (epsilon)	
NM_008388	EIF3s6	Eukaryotic translation initiation factor 3, subunit 6	
NM_146200	EIF3s8	Eukaryotic translation initiation factor 3, subunit 8	
NM_007990	Fau	Finkel-Biskis-Reilly murine sarcoma virus (FBR-MuSV) ubiquitously expressed (fox derived)	
NM_025553	Mrpl11	39S ribosomal protein L11, mitochondrial precursor	
NM_025796	Mrpl32	39S ribosomal protein L33, mitochondrial precursor	
NM_080452	Mrps2	Mitochondrial 28S ribosomal protein S2	
NM_080456	Mrps6	Mitochondrial ribosomal protein S6	
NM_133794	Qars	Glutaminyl-tRNA synthetase	
NM_024212	Rpl4	Ribosomal protein L4	
NM_016980	Rpl5	Ribosomal protein L15	
NM_011290	Rpl6	Ribosomal protein L16	
NM_011291	Rpl7	Ribosomal protein L17	
NM_013721	Rpl7a	Ribosomal protein L17a	
NM_012053	Rpl8	Ribosomal protein L8	
NM_052835	Rpl10	Ribosomal protein L10	
NM_011287	Rpl10a	Rbosomal protein L10A	
NM_009438	Rpl13a	Ribosomal protein L13A	
NM_025974	Rpl14	Ribosomal protein L14	
NM_025586	Rpl15	Ribosomal protein L15	
NM_009077	Rpl18	Ribosomal protein L18	
NM_009078	Rpl19	Ribosomal protein L19	
NM_026517	Rpl22l1	Ribosomal protein L22 like 1	
NM_001045516	Rpl23a	Ribosomal protein L23a	
NM_009080	Rpl26	Ribosomal protein L26	
NM_011289	Rpl27	Ribosomal protein L27	
NM_011975	Rpl27a	Ribosomal protein L27a	
NM_009081	Rpl28	Ribosomal protein L28	
NM_009082	Rpl29	Ribosomal protein L29	
NM_172086	Rpl32	Ribosomal protein L32	
NM_021338	Rpl35a	Ribosomal protein L35	

NM_018730	Rpl36	Ribosomal protein L36	
NM_023372	Rpl38	Ribosomal protein L38	
NM_026055	Rpl39	Ribosomal protein L39	
NM_018853	Rplp1	Ribosomal protein, large, P1	
NM_026020	Rplp2	Ribosomal protein, large, P2	
NM_012052	Rps3	Ribosomal protein S3	
NM_009094	Rps4x	Ribosomal protein S4, X-linked	
NM_009096	Rps6	Ribosomal protein S6	
NM_029767	Rps9	Ribosomal protein S9	
NM_011295	Rps12	Ribosomal protein S12	
NM_009091	Rps15	Ribosomal protein S15	
NM_013647	Rps16	Ribosomal protein S16	
NM_009092	Rps17	Ribosomal protein S17	
NM_025587	Rps21	Ribosomal protein S21	
NM_024175	Rps23	Ribosomal protein S23	
NM_009093	Rps29	Ribosomal protein S29	
XM_112297	predicted protein	Similar to 60S acidic ribosomal protein P1	
XM_112465	predicted protein	Similar to 60S ribosomal protein L7a	
XM_122526	predicted protein	Similar to 60S ribosomal protein L7a	
XM_125109	predicted protein	Similar to 40S ribosomal protein S6	
XM_125178	predicted protein	Similar to 60S ribosomal protein L11, transcript variant 1	
XM_134291	predicted protein	Similar to ribosomal protein L10	
XM_138109	predicted protein	Similar to 60S ribosomal protein L26	
XM_139220	predicted protein	Similar to 40S ribosomal protein S15 (RIG protein)	
XM_139232	predicted protein	Similar to ribosomal protein L27a	
XM_139574	predicted protein	Similar to ribosomal protein L36	
XM_140042	predicted protein	Similar to 60S ribosomal protein L29	
XM_140295	predicted protein	Similar to 40S ribosomal protein S19	
XM_141310	predicted protein	Similar to ribosomal protein L27a	
XM_141727	predicted protein	Similar to 60S ribosomal protein L32	
XM_141816	predicted protein	Similar to ribosomal protein L22 like 1	
XM_144987	predicted protein	Similar to ribosomal protein L27a	
XM_145287	predicted protein	Similar to 60S ribosomal protein L7a	
XM_146296	predicted protein	Similar to 60S ribosomal protein L29 (P23)	
XM_357236	predicted protein	Similar to 60S ribosomal protein L29	
XM_207492	predicted protein	Similar to ribosomal protein P1 isoform 2, transcript variant 1	
XM_285386	predicted protein	Similar to 60S ribosomal protein L26	
XM_286185	predicted protein	Similar to 60S ribosomal protein L11	
XM_355309	predicted protein	Similar to large subunit ribosomal protein L36a	
XM_356455	predicted protein	Similar to ribosomal protein L35a	
XM_356532	predicted protein	Similar to 40S ribosomal protein S17	
XM_356705	predicted protein	Similar to ribosomal protein L19	
XM_356811	predicted protein	Similar to 40S ribosomal protein S17	
XM_356848	predicted protein	Similar to 60S ribosomal protein L29	
XM_356977	predicted protein	Similar to 60S ribosomal protein L29	
XM_357137	predicted protein	Similar to 60S ribosomal protein L23a	

XM_357154	predicted protein	Similar to suppressor of initiator codon mutations, related sequence 1	
XM_357958	predicted protein	Similar to ribosomal protein L36	
XM_483949	predicted protein	Similar to 60S ribosomal protein L6	
XM_484210	predicted protein	Similar to 60S ribosomal protein L29	
XM_484271	predicted protein	Similar to suppressor of initiator codon mutations, related sequence 1	
XM_484358	predicted protein	Similar to 60S ribosomal protein L7a	
XM_484385	predicted protein	Similar to ribosomal protein S12	
XM_484464	predicted protein	Similar to suppressor of initiator codon mutations, related sequence 1	
XM_484573	predicted protein	Similar to 60S ribosomal protein L26-like 1	
XM_484811	predicted protein	Similar to 60S ribosomal protein L13a	
XM_484866	predicted protein	Similar to ribosomal protein L15	
XM_484945	predicted protein	Similar to 60S ribosomal protein L29, transcript variant 1	
XM_485216	predicted protein	Similar to ribosomal protein L27a	
XM_485637	predicted protein	Similar to 60S ribosomal protein L7	
XM_486168	predicted protein	Similar to suppressor of initiator codon mutations, related sequence 1	
XM_486245	predicted protein	Similar to 60S ribosomal protein L7a	
XM_487835	predicted protein	Similar to ribosomal protein P1 isoform 2	
XM_488179	predicted protein	Similar to ribosomal protein L36	
XM_489579	predicted protein	Similar to 60S ribosomal protein L29	
XM_619285	predicted protein	Similar to 60S ribosomal protein L7a	
XM_619852	predicted protein	Similar to ribosomal protein L27a	
XM_619886	predicted protein	Similar to 60S ribosomal protein L7a	
XM_619992	predicted protein	Similar to ribosomal protein L35a	
XM_620142	predicted protein	Similar to 60S ribosomal protein L29	
XM_621432	predicted protein	Similar to ribosomal protein S21	
XM_621866	predicted protein	Similar to suppressor of initiator codon mutations, related sequence 1	
XM_622608	predicted protein	Similar to ribosomal protein L30	
XM_622701	predicted protein	Similar to ribosomal protein L21	
XM_622966	predicted protein	Ubiquitin A-52 residue ribosomal protein fusion product 1	
Q8CDE3	predicted protein	Similar to ribosomal protein L7a	
Q6DI58	predicted protein	Similar to ribosomal protein L11	
Q5RJ56	predicted protein	Similar to ribosomal protein L29e	
Q497F4	predicted protein	Similar to ribosomal protein S12	
Antigen presentation			**5**
NM_009735	B2m	Beta-2 microglobulin	
NM_010380	H2-L	Histocompatibility 2, D region locus 1	
NM_019909	H2-K1	MHC (A.CA/J(H-2K-f) class I antigen	
NM_010391	H2-Q10	Histocompatibility 2, Q region locus 10	
NM_010392	H2-Q2	Histocompatibility 2, Q region locus 2	
Transport			**18**
NM_030052	4930503B16Rik	RIKEN cDNA 4930503B16 gene	
NM_011076	Abcb1b	ATP-binding cassette, sub-family B (MDR/TAP), member 1A	

NM_007502	Atp1b3	ATPase, Na+/K+ transporting, beta 3 polypeptide	
NM_025983	Atp5e	ATP synthase, H+ transporting, mitochondrial F1 complex, epsilon subunit	
NM_026468	Atp5g2	ATP synthase, H+ transporting, mitochondrial F0 complex, subunit c (subunit 9), isoform 2	
NM_009945	Cox7a2	Cytochrome c oxidase, subunit VIIa 2	
NM_010288	Gja1	Gap junction membrane channel protein alpha 1	
NM_008171	Grin2b	Glutamate receptor, ionotropic, NMDA2B (epsilon 2)	
NM_010604	Kcnj16	Potassium inwardly-rectifying channel, subfamily J, member 16	
NM_026936	Oxa1l	Oxidase assembly 1-like	
NM_027491	Rragd	Ras-related GTP binding D	
NM_025321	Sdhc	Succinate dehydrogenase complex, subunit C, integral membrane protein	
NM_011404	Slc7a5	Solute carrier family 7 (cationic amino acid transporter, y+ system), member 5	
NM_009447	Tuba4	Tubulin, alpha 4	
NM_025641	Uqcrh	Ubiquinol-cytochrome c reductase hinge protein	
NM_009931	Col4a1	Procollagen, type IV, alpha 1	
NM_009437	Tst	Thiosulfate sulfurtransferase, mitochondrial	
Signal transduction			**16**
NM_009627	Adm	Adrenomedullin	
NM_170687	Ank3	Ankyrin 3, epithelial, transcript variant 6	
NM_007589	Calm2	Calmodulin 2	
NM_145470	Depdc6	DEP domain containing 6, transcript variant 1	
NM_008143	Gnb2l1	Guanine nucleotide binding protein (G protein), beta polypeptide 2 like 1	
NM_198192	Gpr103	G protein-coupled receptor 103	
NM_175271	Gpr23	G protein-coupled receptor 23	
NM_019391	Lsp1	Lymphocyte specific 1	
NM_207142	Olfr1036	Olfactory receptor 1036	
AY318490	Olfr1285	Olfactory receptor Olfr1285	
NM_146597	Olfr702	Olfactory receptor 702	
AY317954	Olfr779	Olfactory receptor Olfr779	
NM_007952	Pdia3	Protein disulfide isomerase associated 3	
NM_011309	S100a1	S100 calcium binding protein A1	
NM_013650	S100a8	S100 calcium binding protein A8 (calgranulin A)	
NM_021407	Trem3	Triggering receptor expressed on myeloid cells 3	
Regulation of transcription			**9**
NM_009687	Apex1	Apurinic/apyrimidinic endonuclease 1	
NM_139149	Fus	Fusion, derived from t(12;16) malignant liposarcoma	
NM_008986	Ptrf	Polymerase I and transcript release factor	
NM_183208	Rai17	Retinoic acid induced 17	
NM_009087	Rpo1-3	RNA polymerase 1-3, transcript variant 1	
NM_026456	Tceb1	Transcription elongation factor B (SIII), polypeptide 1	
NM_026776	Vps25	Vacuolar protein sorting 25	
NM_011751	Zfp207	Zinc finger protein 207	

NM_023162	Znrd1	Zinc ribbon domain containing, 1	
Ubiquitin cycle			**5**
NM_008944	Psma2	Proteasome (prosome, macropain) subunit, alpha type 2	
NM_011966	Psma4	Proteasome (prosome, macropain) subunit, alpha type 4	
NM_008945	Psmb4	Proteasome (prosome, macropain) subunit, beta type 4	
NM_011187	Psmb7	Proteasome (prosome, macropain) subunit, beta type 7	
NM_011543	Skp1a	S-phase kinase-associated protein 1A	
Protein modifications			**12**
NM_009984	Ctsl	Cathepsin L	
NM_010480	Hspca	Heat shock protein 90kDa alpha (cytosolic), class A member 1	
NM_010477	Hspd1	Heat shock protein 1 (chaperonin)	
NM_008303	Hspe1	Heat shock protein 1 (chaperonin 10)	
NM_008746	Ntrk3	Neurotrophic tyrosine kinase, receptor, type 3, transcript variant 1	
NM_153565	Pcsk9	Proprotein convertase subtilisin/kexin type 9	
NM_008971	Ptk9	Protein tyrosine kinase 9	
NM_009143	Sdf2	Stromal cell derived factor 2	
NM_023476	Tinagl	Tubulointerstitial nephritis antigen-like	
NM_019639	Ubc	Ubiquitin C	
NM_013771	Yme1l1	YME1-like 1 (S. cerevisiae)	
XM_485424	predicted protein	Similar to heat shock protein 1 (chaperonin)	
Nucleosome assembly			**5**
NM_016750	H2afz	H2A histone family, member Z	
NM_008210	H3f3a	H3 histone, family 3A	
XM_484352	predicted protein	Similar to Histone H3.3	
XM_138832	predicted protein	Similar to H3 histone, family 3B	
NM_133786	Smc4l1	Structural maintenance of chromosomes 4	
Cytoskeleton			**5**
NM_009608	Actc1	Actin, alpha, cardiac	
NM_009610	Actg2	Actin, gamma 2, smooth muscle, enteric	
NM_007393	Actb	Actin, beta, cytoplasmic	
NM_009635	Avil	Advillin	
NM_010043	Des	Desmin	
Endocytosis			**5**
NM_007616	Cav1	Caveolin, caveolae protein 1	
NM_026972	Cd209b	CD209b antigen, transcript variant 1	
NM_016760	Clta	Clathrin, light polypeptide (Lca)	
NM_031195	Msr1	Macrophage scavenger receptor 1	
NM_009007	Rac1	RAS-related C3 botulinum substrate 1	
Cell death			**6**
NM_026121	Bag4	BCL2-associated athanogene 4	
NM_013492	Clu	Clusterin	
NM_146057	Dap	Death-associated protein	
NM_008495	Lgals1	Lectin, galactose binding, soluble 1	
NM_026669	Tegt	Testis enhanced gene transcript	

NM_009503	Vcp	Valosin containing protein	
DNA replication			**3**
NM_023144	Nono	Non-POU-domain-containing, octamer binding protein	
NM_026632	Rpa3	Replication protein A3	
NM_009354	Tert	Telomerase reverse transcriptase	
RNA processing			**8**
NM_025323	0610009D07Rik	RIKEN cDNA 0610009D07 gene	
NM_138669	Ddx48	DEAD (Asp-Glu-Ala-Asp) box polypeptide 48	
NM_007991	Fbl	Fibrillarin	
NM_133976	Imp3	U3 small nucleolar ribonucleoprotein, homolog (yeast)	
NM_016809	Rbm3	RNA binding motif protein 3	
NM_021525	Rcl1	RNA terminal phosphate cyclase-like 1	
NM_013663	Sfrs3	Splicing factor, arginine/serine-rich 3 (SRp20)	
XM_975802	predicted protein	Small nuclear ribonucleoprotein polypeptide F (Snrpf)	
Cell cycle, Differentiation, Proliferation			**9**
NM_027955	1700017G21Rik	RIKEN cDNA 1700017G21 gene	
NM_008864	Csh1	Chorionic somatomammotropin hormone 1	
NM_010239	Fth1	Ferritin heavy chain 1	
NM_139269	Hrasls3	HRAS like suppressor 3	
NM_033620	Pard3	Par-3 (partitioning defective 3) homolog (C. elegans), transcript variant 3	
NM_011045	Pcna	Proliferating cell nuclear antigen	
NM_016891	Ppp2r1a	Protein phosphatase 2 (formerly 2A), regulatory subunit A (PR 65), alpha isoform	
NM_016740	S100a11	S100 calcium binding protein A11 (calizzarin)	
NM_009388	Tkt	Transketolase	
Metabolism			**4**
NM_007608	Car5a	Carbonic anhydrase 5a, mitochondrial (Car5a), nuclear gene encoding mitochondrial protein	
NM_009940	Coq7	Demethyl-Q 7’	
NM_175154	Galk2	Galactokinase 2	
NM_013632	Pnp	Purine-nucleoside phosphorylase	
Others			**9**
NM_026790	D12Ertd647e	DNA segment, Chr 12, ERATO Doi 647, expressed (D12Ertd647e)	
NM_172120	Vps41	Vacuolar protein sorting 41	
NM_011340	Serpinf1	Serine (or cysteine) peptidase inhibitor, clade F, member 1	
NM_008536	Tm4sf1	Transmembrane 4 superfamily member 1	
NM_008102	Gch1	GTP cyclohydrolase 1	
NM_008925	Prkcsh	Protein kinase C substrate 80K-H	
NM_145506	Epb4.1l5	Erythrocyte protein band 4.1-like 5	
NM_177879	Sdk1	Sidekick homolog 1 (chicken)	
NM_172683	Pogz	Pogo transposable element with ZNF domain	

Genes were annotated according to their GO-terms for biological function/process.

Supplemental table S2. Upregulated gene transcripts in MHV-infected cells at 6 h p.i.

Gene ID	Name	Description	Fold induction	#
Regulation of transcription				**7**
NM_008235	Hes1	Hairy and enhancer of split 1	2.0	
NM_008321	Idb3	Inhibitor of DNA binding 3	2.8	
NM_008390	Irf1	Interferon regulatory factor 1	2.4	
NM_011498	Bhlhb2	Basic helix-loop-helix domain containing, class B2	2.1	
NM_011803	Klf6	Kruppel-like factor 6	2.7	
NM_013692	Tieg1	TGFbeta-inducible early gene 1	6.0	
NM_178392	Snapc1	Small nuclear RNA activating complex, polypeptide 1	2.1	
Nucleosome assembly				**4**
NM_008211	H3f3b	H3 histone, family 3B	2,2	
NM_015786	Hist1h1c	Histone 1, H1c	4,4	
NM_178192	Hist1h4a	Histone 1, H4a	2,3	
NM_178203	Hist1h3b	Histone 1, H3b	2,3	
Protein biosynthesis, tRNA processing				**3**
NM_013506	EIF4a2	Eukaryotic translation initiation factor 4A2	2,0	
NM_013647	Rps16	Ribosomal protein S16	2,2	
NM_029092	Rg9mtd1	RNA (guanine-9-) methyltransferase domain containing 1	2,0	
Apoptosis				**4**
NM_178655	Ank2	Ankyrin 2	2,1	
NM_008562	Mcl1	Myeloid cell leukemia sequence 1	2,3	
NM_133662	Ier3	Immediate early response 3	3,4	
NM_010907	Nfkbia	Nuclear factor of kappa light chain gene enhancer in B-cells inhibitor, alpha	2.6	
Chemotaxis				**2**
NM_008176	Cxcl1	Chemokine (C-X-C motif) ligand 1	7.3	
NM_009140	Cxcl2	Chemokine (C-X-C motif) ligand 2	6.3	
Antigen presentation, FasL biosynthesis				**2**
NM_181075	2610524H06Rik	RIKEN cDNA 2610524H06 gene	3.6	
NM_009344	Phlda1	Pleckstrin homology-like domain, family A, member 1	2.5	
Response to unfolded protein				**1**
NM_022331	Herpud1	Homocysteine-inducible, endoplasmic reticulum stress-inducible, ubiquitin-like domain member 1	2.6	
Ubiquitin cycle				**1**
NM_180600	Ube2q2	Ubiquitin-conjugating enzyme E2Q (putative) 2	2.6	

Nitric Oxide mediated signal transduction				**1**
NM_013602	Mt1	Metallothionein 1	3.1	
Cell cycle				**1**
NM_013642	Dusp1	Dual specificity phosphatase 1	2.4	
Blood coagulation				**1**
NM_008871	Serpine1	Serine (or cysteine) peptidase inhibitor, clade E, member 1	2.3	
Development				**1**
NM_011427	Snai1	Snail homolog 1	2.0	
G-coupled signaling				**1**
NM_020289	Olfr544	Olfactory receptor 544	2.0	
Unknown				**11**

Genes were annotated according to their GO-terms for biological function/process.

Supplemental table S3. Validation of microarray data by quantitative RT-PCR.

		Fold induction			
		Microarray		**RT-PCR**	
Gene ID	**Name**	**4 h**	**6 h**	**4 h**	**6 h**
NM_008176	Cxcl1	1,3	7,3	0,9	9,9
NM_009140	Cxcl2	1,4	6,3	1,0	5,5
NM_010907	Nfkbia	1,0	2,6	1,4	3,7
NM_008390	Irf1	1,0	2,4	1,4	3,2
NM_022331	Herpud1	1,0	2,6	0,6	2,4
NM_026055	Rpl39	-1,7	-7,1	-2,1	-3,0
NM_013492	Clusterin	-1,9	-5,0	-3,8	-8,5

References

1. **Anderson, P., and N. Kedersha.** 2006. RNA granules. J Cell Biol 172:803-8.

2. **Anderson, P., and N. Kedersha.** 2002. Stressful initiations. J Cell Sci 115:3227-34.

3. **Banerjee, S., S. An, A. Zhou, R. H. Silverman, and S. Makino.** 2000. RNase L-independent specific 28S rRNA cleavage in murine coronavirus-infected cells. J Virol 74:8793-802.

4. **Berlanga, J. J., J. Santoyo, and C. De Haro.** 1999. Characterization of a mammalian homolog of the GCN2 eukaryotic initiation factor 2alpha kinase. Eur J Biochem 265:754-62.

5. **Bosch, B. J., R. van der Zee, C. A. de Haan, and P. J. Rottier.** 2003. The coronavirus spike protein is a class I virus fusion protein: structural and functional characterization of the fusion core complex. J Virol 77:8801-11.

6. **Brostrom, C. O., and M. A. Brostrom.** 1998. Regulation of translational initiation during cellular responses to stress. Prog Nucleic Acid Res Mol Biol 58:79-125.

7. **Causton, H. C., B. Ren, S. S. Koh, C. T. Harbison, E. Kanin, E. G. Jennings, T. I. Lee, H. L. True, E. S. Lander, and R. A. Young.** 2001. Remodeling of yeast genome expression in response to environmental changes. Mol Biol Cell 12:323-37.

8. **Chan, C. P., K. L. Siu, K. T. Chin, K. Y. Yuen, B. Zheng, and D. Y. Jin.** 2006. Modulation of the unfolded protein response by the severe acute respiratory syndrome coronavirus spike protein. J Virol 80:9279-87.

9. **Cheadle, C., J. Fan, Y. S. Cho-Chung, T. Werner, J. Ray, L. Do, M. Gorospe, and K. G. Becker.** 2005. Stability regulation of mRNA and the control of gene expression. Ann N Y Acad Sci 1058:196-204.

10. **Clemens, M. J.** 2005. Translational control in virus-infected cells: models for cellular stress responses. Semin Cell Dev Biol 16:13-20.

11. **Cougot, N., S. Babajko, and B. Seraphin.** 2004. Cytoplasmic foci are sites of mRNA decay in human cells. J Cell Biol 165:31-40.

12. **de Haan, C. A., B. J. Haijema, D. Boss, F. W. Heuts, and P. J. Rottier.** 2005. Coronaviruses as vectors: stability of foreign gene expression. J Virol 79:12742-51.

13. **de Haan, C. A., K. Stadler, G. J. Godeke, B. J. Bosch, and P. J. Rottier.** 2004. Cleavage inhibition of the murine coronavirus spike protein by a furin-like enzyme affects cell-cell but not virus-cell fusion. J Virol 78:6048-54.

14. **de Haan, C. A., H. Vennema, and P. J. Rottier.** 2000. Assembly of the coronavirus envelope: homotypic interactions between the M proteins. J Virol 74:4967-78.

15. **de Haro, C., R. Mendez, and J. Santoyo.** 1996. The eIF-2alpha kinases and the control of protein synthesis. Faseb J 10:1378-87.

16. **DeGracia, D. J., J. M. Sullivan, R. W. Neumar, S. S. Alousi, K. R. Hikade, J. E. Pittman, B. C. White, J. A. Rafols, and G. S. Krause.** 1997. Effect of brain ischemia and reperfusion on the localization of phosphorylated eukaryotic initiation factor 2 alpha. J Cereb Blood Flow Metab 17:1291-302.

17. **Drosten, C., S. Gunther, W. Preiser, S. van der Werf, H. R. Brodt, S. Becker, H. Rabenau, M. Panning, L. Kolesnikova, R. A. Fouchier, A. Berger, A. M. Burguiere, J. Cinatl, M. Eickmann, N. Escriou, K. Grywna, S. Kramme, J. C. Manuguerra, S. Muller, V. Rickerts, M. Sturmer, S. Vieth, H. D. Klenk, A. D. Osterhaus, H. Schmitz, and H. W. Doerr.** 2003. Identification of a novel coronavirus in patients with severe acute respiratory syndrome. N Engl J Med 348:1967-76.

18. **Esclatine, A., B. Taddeo, and B. Roizman.** 2004. Herpes simplex virus 1 induces cytoplasmic accumulation of TIA-1/TIAR and both synthesis and cytoplasmic accumulation of tristetraprolin, two cellular proteins that bind and destabilize AU-rich RNAs. J Virol 78:8582-92.

19. **Eystathioy, T., E. K. Chan, S. A. Tenenbaum, J. D. Keene, K. Griffith, and M. J. Fritzler.** 2002. A phosphorylated cytoplasmic autoantigen, GW182, associates with a unique population of human mRNAs within novel cytoplasmic speckles. Mol Biol Cell 13:1338-51.

20. **Eystathioy, T., A. Jakymiw, E. K. Chan, B. Seraphin, N. Cougot, and M. J. Fritzler.** 2003. The GW182 protein colocalizes with mRNA degradation associated proteins hDcp1 and hLSm4 in cytoplasmic GW bodies. Rna 9:1171-3.

21. **Gasch, A. P., P. T. Spellman, C. M. Kao, O. Carmel-Harel, M. B. Eisen, G. Storz, D. Botstein, and P. O. Brown.** 2000. Genomic expression programs in the response of yeast cells to environmental changes. Mol Biol Cell 11:4241-57.

22. **Gilks, N., N. Kedersha, M. Ayodele, L. Shen, G. Stoecklin, L. M. Dember, and P. Anderson.** 2004. Stress granule assembly is mediated by prion-like aggregation of TIA-1. Mol Biol Cell 15:5383-98.

23. **Grigull, J., S. Mnaimneh, J. Pootoolal, M. D. Robinson, and T. R. Hughes.** 2004. Genome-wide analysis of mRNA stability using transcription inhibitors and microarrays reveals posttranscriptional control of ribosome biogenesis factors. Mol Cell Biol 24:5534-47.

24. **Harding, H. P., Y. Zhang, and D. Ron.** 1999. Protein translation and folding are coupled by an endoplasmic-reticulum-resident kinase. Nature 397:271-4.

25. **Hilton, A., L. Mizzen, G. MacIntyre, S. Cheley, and R. Anderson.** 1986. Translational control in murine hepatitis virus infection. J Gen Virol 67 (Pt 5):923-32.

26. **Ingelfinger, D., D. J. Arndt-Jovin, R. Luhrmann, and T. Achsel.** 2002. The human LSm1-7 proteins colocalize with the mRNA-degrading enzymes Dcp1/2 and Xrnl in distinct cytoplasmic foci. Rna 8:1489-501.

27. **Kamitani, W., K. Narayanan, C. Huang, K. Lokugamage, T. Ikegami, N. Ito, H. Kubo, and S. Makino.** 2006. Severe acute respiratory syndrome coronavirus nsp1 protein suppresses host gene expression by promoting host mRNA degradation. Proc Natl Acad Sci U S A 103:12885-90.

28. **Kaufman, R. J.** 2000. The double-stranded RNA-activated protein kinase PKR. In *Translational Control of Gene Expression*, Sonenberg, N., Hershey, J.W.B., Mathews, M.B. (eds), pp 503-527. Cold Spring Harbor, NY: Cold Spring Harbor Laboratory Press.

29. **Kedersha, N., G. Stoecklin, M. Ayodele, P. Yacono, J. Lykke-Andersen, M. J. Fitzler, D. Scheuner, R. J. Kaufman, D. E. Golan, and P. Anderson.** 2005. Stress granules and processing bodies are dynamically linked sites of mRNP remodeling. J Cell Biol 169:871-84.

30. **Kedersha, N. L., M. Gupta, W. Li, I. Miller, and P. Anderson.** 1999. RNA-binding proteins TIA-1 and TIAR link the phosphorylation of eIF-2 alpha to the assembly of mammalian stress granules. J Cell Biol 147:1431-42.

31. **Keyse, S. M., and E. A. Emslie.** 1992. Oxidative stress and heat shock induce a human gene encoding a protein-tyrosine phosphatase. Nature 359:644-7.

32. **Kuo, L., G. J. Godeke, M. J. Raamsman, P. S. Masters, and P. J. Rottier.** 2000. Retargeting of coronavirus by substitution of the spike glycoprotein ectodomain: crossing the host cell species barrier. J Virol 74:1393-406.

33. **Kyuwa, S., M. Cohen, G. Nelson, S. M. Tahara, and S. A. Stohlman.** 1994. Modulation of cellular macromolecular synthesis by coronavirus: implication for pathogenesis. J Virol 68:6815-9.

34. **Lai, M. M., P. R. Brayton, R. C. Armen, C. D. Patton, C. Pugh, and S. A. Stohlman.** 1981. Mouse hepatitis virus A59: mRNA structure and genetic localization of the sequence divergence from hepatotropic strain MHV-3. J Virol 39:823-34.

35. **Law, A. H., D. C. Lee, B. K. Cheung, H. C. Yim, and A. S. Lau.** 2007. Role for non-structuralprotein 1 of severe acute respiratory syndrome coronavirus in chemokine dysregulation. J Virol 81:416-22.

36. **Leong, W. F., H. C. Tan, E. E. Ooi, D. R. Koh, and V. T. Chow.** 2005. Microarray and real-time RT-PCR analyses of differential human gene expression patterns induced by severe acute respiratory syndrome (SARS) coronavirus infection of Vero cells. Microbes Infect 7:248-59.

37. **Li, W., Y. Li, N. Kedersha, P. Anderson, M. Emara, K. M. Swiderek, G. T. Moreno, and M. A. Brinton.** 2002. Cell proteins TIA-1 and TIAR interact with the 3' stem-loop of the West Nile virus complementary minus-strand RNA and facilitate virus replication. J Virol 76:11989-2000.

38. **Liu, J., F. V. Rivas, J. Wohlschlegel, J. R. Yates, 3rd, R. Parker, and G. J. Hannon.** 2005. A role for the P-body component GW182 in microRNA function. Nat Cell Biol 7:1261-6.

39. **Lu, L., A. P. Han, and J. J. Chen.** 2001. Translation initiation control by heme-regulated eukaryotic initiation factor 2alpha kinase in erythroid cells under cytoplasmic stresses. Mol Cell Biol 21:7971-80.

40. **Lyles, D. S.** 2000. Cytopathogenesis and inhibition of host gene expression by RNA viruses. Microbiol Mol Biol Rev 64:709-24.

41. **Ma, Y., and L. M. Hendershot.** 2004. Herp is dually regulated by both the endoplasmic reticulum stress-specific branch of the unfolded protein response and a branch that is shared with other cellular stress pathways. J Biol Chem 279:13792-9.

42. **McEwen, E., N. Kedersha, B. Song, D. Scheuner, N. Gilks, A. Han, J. J. Chen, P. Anderson, and R. J. Kaufman.** 2005. Heme-regulated inhibitor kinase-mediated phosphorylation of eukaryotic translation initiation factor 2 inhibits translation, induces stress granule formation, and mediates survival upon arsenite exposure. J Biol Chem 280:16925-33.

43. **McInerney, G. M., N. L. Kedersha, R. J. Kaufman, P. Anderson, and P. Liljestrom.** 2005. Importance of eIF2alpha phosphorylation and stress granule assembly in alphavirus translation regulation. Mol Biol Cell 16:3753-63.

44. **Pasternak, A. O., W. J. Spaan, and E. J. Snijder.** 2006. Nidovirus transcription: how to make sense...? J Gen Virol 87:1403-21.

45. **Robb, J. A., and C. W. Bond.** 1979. Pathogenic murine coronaviruses. I. Characterization of biological behavior *in vitro* and virus-specific intracellular RNA of strongly neurotropic JHMV and weakly neurotropic A59V viruses. Virology 94:352-70.

46. **Roepman, P., L. F. Wessels, N. Kettelarij, P. Kemmeren, A. J. Miles, P. Lijnzaad, M. G. Tilanus, R. Koole, G. J. Hordijk, P. C. van der Vliet, M. J. Reinders, P. J. Slootweg, and F. C. Holstege.** 2005. An expression profile for diagnosis of lymph node metastases from primary head and neck squamous cell carcinomas. Nat Genet 37:182-6.

47. **Rottier, P. J., M. C. Horzinek, and B. A. van der Zeijst.** 1981. Viral protein synthesis in mouse hepatitis virus strain A59-infected cells: effect of tunicamycin. J Virol 40:350-7.

48. **Sawicki, S. G., and D. L. Sawicki.** 2005. Coronavirus transcription: a perspective. Curr Top Microbiol Immunol 287:31-55.

49. **Scheuner, D., B. Song, E. McEwen, C. Liu, R. Laybutt, P. Gillespie, T. Saunders, S. Bonner-Weir, and R. J. Kaufman.** 2001. Translational control is required for the unfolded protein response and *in vivo* glucose homeostasis. Mol Cell 7:1165-76.

50. **Schneider, R. J., and I. Mohr.** 2003. Translation initiation and viral tricks. Trends Biochem Sci 28:130-6.

51. **Scorsone, K. A., R. Panniers, A. G. Rowlands, and E. C. Henshaw.** 1987. Phosphorylation of eukaryotic initiation factor 2 during physiological stresses which affect protein synthesis. J Biol Chem 262:14538-43.

52. **Siddell, S., H. Wege, A. Barthel, and V. ter Meulen.** 1981. Intracellular protein synthesis and the *in vitro* translation of coronavirus JHM mRNA. Adv Exp Med Biol 142:193-207.

53. **Smith, J. A., S. C. Schmechel, A. Raghavan, M. Abelson, C. Reilly, M. G. Katze, R. J. Kaufman, P. R. Bohjanen, and L. A. Schiff.** 2006. Reovirus induces and benefits from an integrated cellular stress response. J Virol 80:2019-33.

54. **Snijder, E. J., P. J. Bredenbeek, J. C. Dobbe, V. Thiel, J. Ziebuhr, L. L. Poon, Y. Guan, M. Rozanov, W. J. Spaan, and A. E. Gorbalenya.** 2003. Unique and conserved features of genome and proteome of SARS-coronavirus, an early split-off from the coronavirus group 2 lineage. J Mol Biol 331:991-1004.

55. **Tahara, S., C. Bergmann, G. Nelson, R. Anthony, T. Dietlin, S. Kyuwa, and S. Stohlman.** 1993. Effects of mouse hepatitis virus infection on host cell metabolism. Adv Exp Med Biol 342:111-6.

56. **Tahara, S. M., T. A. Dietlin, C. C. Bergmann, G. W. Nelson, S. Kyuwa, R. P. Anthony, and S. A. Stohlman.** 1994. Coronavirus translational regulation: leader affects mRNA efficiency. Virology 202:621-30.

57. **Tebo, J., S. Der, M. Frevel, K. S. Khabar, B. R. Williams, and T. A. Hamilton.** 2003. Heterogeneity in control of mRNA stability by AU-rich elements. J Biol Chem 278:12085-93.

58. **Teixeira, D., U. Sheth, M. A. Valencia-Sanchez, M. Brengues, and R. Parker.** 2005. Processing bodies require RNA for assembly and contain nontranslating mRNAs. Rna 11:371-82.

59. **Tusher, V. G., R. Tibshirani, and G. Chu.** 2001. Significance analysis of microarrays applied to the ionizing radiation response. Proc Natl Acad Sci U S A 98:5116-21.

60. **van de Peppel, J., P. Kemmeren, H. van Bakel, M. Radonjic, D. van Leenen, and F. C. Holstege.** 2003. Monitoring global messenger RNA changes in externally controlled microarray experiments. EMBO Rep 4:387-93.

61. **van der Hoek, L., K. Pyrc, M. F. Jebbink, W. Vermeulen-Oost, R. J. Berkhout, K. C. Wolthers, P. M. Wertheim-van Dillen, J. Kaandorp, J. Spaargaren, and B. Berkhout.** 2004. Identification of a new human coronavirus. Nat Med 10:368-73.

62. **Versteeg, G. A., O. Slobodskaya, and W. J. Spaan.** 2006. Transcriptional profiling of acute cytopathic murine hepatitis virus infection in fibroblast-like cells. J Gen Virol 87:1961-75.

63. Woo**, P. C., S. K. Lau, C. M. Chu, K. H. Chan, H. W. Tsoi, Y. Huang, B. H. Wong, R. W. Poon, J. J. Cai, W. K. Luk, L. L. Poon, S. S. Wong, Y. Guan, J. S. Peiris, and K. Y. Yuen.** 2005. Characterization and complete genome sequence of a novel coronavirus, coronavirus HKU1, from patients with pneumonia. J Virol 79:884-95.

64. **Yang, Y. H., S. Dudoit, P. Luu, D. M. Lin, V. Peng, J. Ngai, and T. P. Speed.** 2002. Normalization for cDNA microarray data: a robust composite method addressing single and multiple slide systematic variation. Nucleic Acids Res 30:e15.

Chapter 4

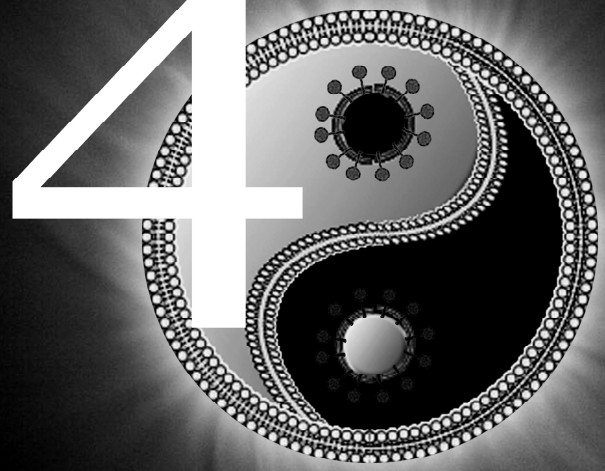

Mouse Hepatitis Coronavirus RNA Replication Depends on GBF1-Mediated ARF1 Activation

Monique H. Verheije
Matthijs Raaben
Muriel Mari
Eddie G. te Lintelo
Fulvio Reggiori
Frank J.M. van Kuppeveld
Peter J.M. Rottier
Cornelis A.M. de Haan

PLoS Pathogens; 2008 June; 4:e1000088.

Abstract

Coronaviruses induce in infected cells the formation of double membrane vesicles, which are the sites of RNA replication. Not much is known about the formation of these vesicles although recent observations indicate an important role for the endoplasmic reticulum in the formation of the mouse hepatitis coronavirus (MHV) replication complexes. We now show that MHV replication is sensitive to brefeldin A (BFA). Consistently, expression of a dominant-negative mutant of ARF1, known to mimic the action of the drug, inhibited MHV infection profoundly. Immunofluorescence analysis and quantitative electron microscopy demonstrated that BFA did not block the formation of RCs per se, but rather reduced their number. MHV RNA replication was not sensitive to BFA in MDCK cells, which are known to express a BFA-resistant guanine nucleotide exchange factor GBF1. Accordingly, individual knockdown of the Golgi-resident targets of BFA by transfection of small interfering RNAs (siRNAs) showed that GBF1, but not BIG1 or BIG2, was critically involved in MHV RNA replication. ARF1, the cellular effector of GBF1, also appeared to be involved in MHV replication, as siRNAs targeting this small GTPase inhibited MHV infection significantly. Collectively, our results demonstrate that GBF1-mediated ARF1 activation is required for efficient MHV RNA replication and reveal that the early secretory pathway and MHV replication complex formation are closely connected.

Introduction

Viruses rely on cellular host factors for virtually all steps of their infection cycle. However, the cellular proteins required and the cellular pathways hijacked by viruses have hardly been elucidated. All positive-strand RNA viruses assemble in infected cells their replication complexes (RCs) in association with intracellular membranes (1, 8, 44, 55, 69). The induction of such local micro-environments is likely advantageous for the virus, as membrane association may facilitate the recruitment of both the viral and cellular components involved in RNA replication. Alternatively, membrane association may provide a shielded environment that prevents the activation of, or protects against, antiviral host cell responses like those mediated by interferon.

Coronaviruses (CoVs) belong to a family of enveloped positive-strand RNA viruses in the order Nidovirales. Upon translation of the viral genomic RNA, two very large polyproteins (approximately 4,000 and 7,000 amino acids) are synthesized, the autoproteolytic cleavage products of which collectively form the RCs. These RCs are associated with double membrane vesicles (DMVs (4, 22, 71)), which appear as cytoplasmic foci when analyzed by fluorescence light microscopy and increase in number during the course of the infection (4, 16, 71, 73). It is plausible that the non-structural viral proteins (nsp's) mediate the formation of DMVs by modifying intracellular membranes and by recruiting cellular components to their need. Recent studies suggest the endoplasmic reticulum (ER) to be the lipid donor compartment of the membrane-bound CoV RCs (56, 59, 73, 74), although co-localization of nsp's with markers for endosomes, Golgi and autophagosomes has also been described (22, 64, 72, 73, 79).

Brefeldin A (BFA) is a well known fungal metabolite that induces the redistribution of Golgi proteins into the ER (42, 50), effectively resulting in the block of transport through the secretory pathway (20, 33). This drug inhibits the activation of ADP-ribosylation factor (ARF) small GTPases by targeting the large guanine nucleotide exchange factors (GEFs) GBF1 (Golgi-specific resistance factor 1), and BIG (BFA-inhibited GEF) 1 and 2 (29, 30, 48). More specifically, BFA locks ARF*GDP when bound to GEF, thereby blocking the GEF activity at an early stage of the reaction, prior to guanine nucleotide release (17, 24). The large GEFs function in the ER to Golgi transport pathway (18) and localize to the cis-

(GBF1) and trans-sides (BIG1 and BIG2) of the Golgi complex (86). The cellular effectors of these GEFs, ARFs, are divided into three classes: Class I (ARF1-3), Class II (ARF 4 and 5), and Class III (ARF6) (38). Class I ARFs regulate the assembly of coat complexes onto vesicles budding from compartments along the secretory pathway and activate lipid-modifying enzymes [reviewed in (5, 39)]. While the function of Class II ARFs remains largely unclear, the Class III ARF6 is thought to regulate endosomal membrane traffic (10, 62). GBF1 and the BIGs are likely to activate distinct subclasses of ARFs at specific locations in order to regulate different types of transport routes (86).

In the field of virology, BFA has been used, besides for studying viral protein transport and virus assembly (12, 27, 46, 49, 57, 75), to investigate the formation of RCs and RNA replication of several positive-strand RNA viruses (36, 45, 47, 65). For example, poliovirus RNA replication was shown to be sensitive to BFA. In the presence of this drug, poliovirus replication sites were not formed and RNA replication was completely blocked (28, 47). Remarkably, other members of the picornavirus family appeared to differ in their sensitivity to BFA. Whereas echovirus 11 RNA replication was strongly inhibited by BFA, RNA replication of encephalomyocarditis virus was not affected at all, while parechovirus 1 exhibited an intermediate sensitivity to BFA (21).

Relatively little is known about the host pathways involved in coronavirus RNA replication and in RC formation. Recently, we demonstrated the important role of the ER in the generation of the RCs. While MHV nsp4 was localized to this organelle when expressed alone, it was recruited to the RCs in infected cells (56). Furthermore, coronaviral replication was inhibited when the ER export machinery was blocked by use of the kinase inhibitor H89 or by expression of a dominant active mutant of Sar1 (56). Other cellular proteins and pathways are likely to contribute to the formation of the coronavirus RCs as well. Here, we studied the involvement of BFA-sensitive pathways in MHV replication and RC formation. Our results demonstrate that GBF1-mediated ARF1 activation is required for efficient MHV RNA replication. Moreover, together with our recent observation about the relevance of the ER in the same process, our data reveal that the early secretory pathway and MHV replication are intimately connected.

Results

MHV Genomic RNA Replication is Sensitive to BFA

BFA is known to disturb membrane traffic in most cell types, resulting in a redistribution of Golgi proteins into the ER (42, 50). We first confirmed the sensitivity of murine LR7 cells to BFA by immunofluorescence using antibodies directed against the Golgi protein marker GM130 (52). Indeed, after treatment of the cells with 5 μg/ml BFA for 1 h, the typical Golgi staining pattern of GM130 was lost, concomitant with a reticular redistribution of the protein marker (data not shown). Next, we tested whether MHV infection was sensitive to BFA. Therefore, LR7 cells were inoculated with a luciferase-expressing recombinant of MHV-A59 (MHV-EFLM) in presence or absence of 5 μg/ml BFA. After 1 h, the inoculum was removed and the cells were further incubated either in the presence or absence of BFA. At 7 h p.i., the intracellular luciferase expression level was determined relative to untreated cells. Luciferase expression was inhibited more than 95% when BFA was present from 1-7 h p.i., whereas BFA treatment during virus inoculation had only a minor effect on reporter gene expression (Fig.1A). Although this latter decrease might have resulted in part from a reduced entry, the negative effect of BFA on MHV replication and transcription is evident from the profoundly impaired MHV reporter gene expression when BFA was added post inoculation (1-7 h p.i.). In a control experiment, the effect of BFA on Sindbis virus replication in LR7 cells was assayed by using Sindbis pseudovirus particles containing luciferase-expressing replicons. As described previously (51), Sindbis virus replication was not affected by the BFA treatment (Fig.1A). This result indicates that the observed effect of BFA on MHV-driven luciferase expression was not due to non-specific drug-induced toxicity.

Although we demonstrated in previous studies that reporter gene expression by MHV is a reliable measure for coronavirus replication (15), we wanted to confirm that the reduction in luciferase expression resulted from a corresponding decrease in viral RNA synthesis rather than from inhibition of viral protein translation. To this end, a similar experiment as shown in Fig.1A was performed, in which the amount of intracellular genomic viral RNA was determined by real-time Taqman PCR. As for the luciferase expression levels, the amount of genomic RNA was found to be severely reduced when BFA was added directly after the virus inoculation (Fig.1B), whereas a less profound effect was observed when cells

were treated during virus inoculation. Very similar results were obtained when targeting the Taqman PCR to a different region of the viral genome (data not shown). To more directly check for an effect of BFA on the translation of viral mRNAs, we performed an additional experiment. LR7 cells were infected at high multiplicity with the recombinant virus MHV-2aFLS, which expresses the firefly luciferase, and subsequently transfected with a synthetic mRNA encoding Renilla luciferase. This synthetic mRNA mimics viral mRNAs as it contains 5' and 3' untranslated regions identical to those found in the viral genome. The cells were incubated in the presence or absence of BFA (2-6 h p.i.) after which the intracellular Renilla and firefly luciferase expression levels were determined. The results show that BFA treatment did not inhibit the synthesis of Renilla luciferase from the synthetic mRNA, while firefly luciferase expression driven by the recombinant virus was severely affected (Fig.1C). Renilla luciferase expression was also not affected in the absence of a viral infection (data not shown). All together, these results indicate that BFA inhibits MHV RNA replication while translation of viral mRNAs is not affected.

Next, we determined the post inoculation period during which MHV replication was most sensitive to BFA, by analyzing the luciferase expression levels as they are a reliable measure for RNA replication. Thus LR7 cells infected with MHV-EFLM were treated with BFA for overlapping 2 h periods. At the end of each incubation period the intracellular luciferase expression levels were determined and compared to those in mock-treated cells. The results showed that replication was affected throughout the course of the infection (Fig.1D); however, the effects were most pronounced during the early phases of infection.

ARF1-T31N Inhibits MHV Replication

To confirm our observation that BFA inhibits MHV replication, but also to prove that the effects of this drug are due to the inhibition of GEF activities, we next analyzed to what extent the expression of a dominant-negative mutant of ARF1 (T31N) would affect MHV infection. This ARF1 mutant has a decreased affinity for GTP and, following GDP displacement, it remains 'nucleotide-free' for a longer period than wild-type ARF1 (76). As a consequence, expression of ARF1-T31N mirrors the effects of BFA (11).

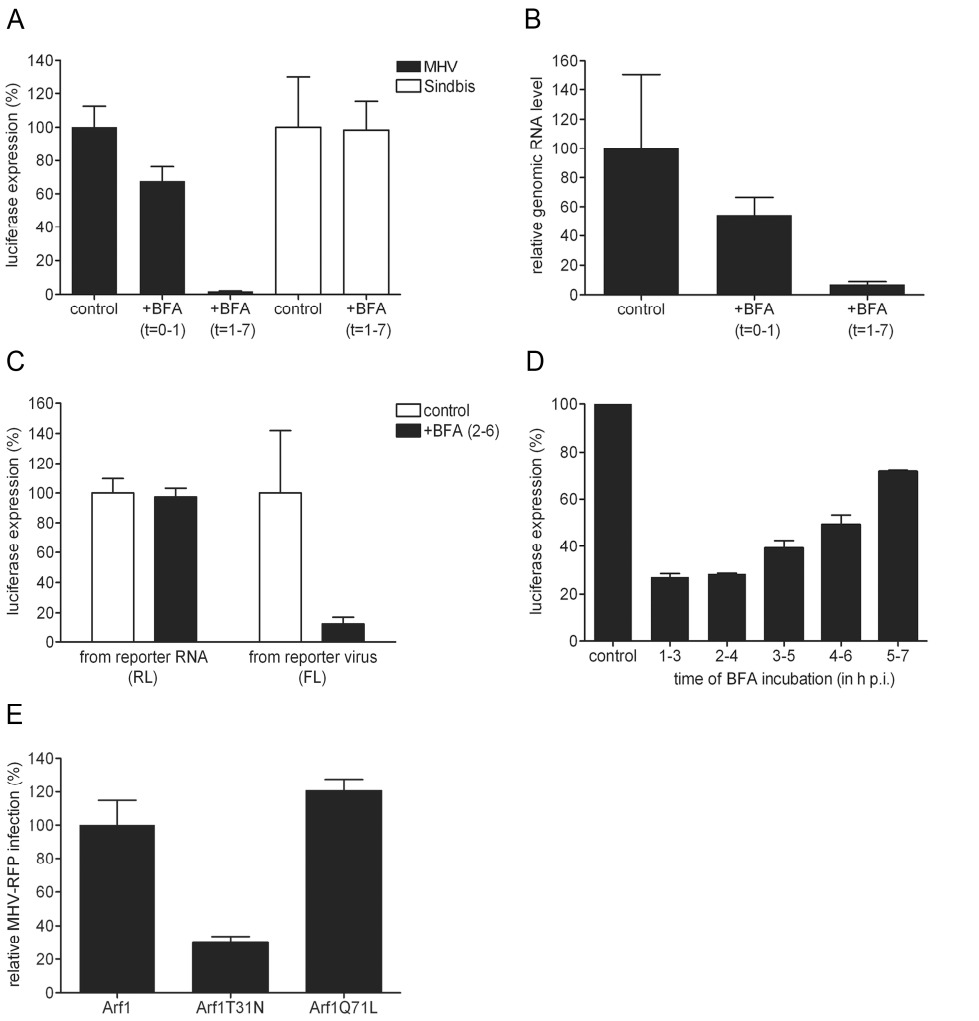

Fig.1. BFA inhibits MHV replication in mouse LR7 cells. (A, B, D) LR7 cells were inoculated with MHV-EFLM or with Sindbis pseudovirus particles containing a luciferase replicon and incubated with 5 µg/ml BFA during the indicated time periods. At the end of each incubation period, virus replication was analyzed by determining the luciferase expression level (A and D) or the amount of viral genomic RNA (B) as described in Material and Methods. (C) LR7 cells were inoculated with MHV-2aFLS, transfected with synthetic RNA transcribed from pM5f-RL-M3, and incubated from 2-6 h p.i. in presence or absence of 5 µg/ml BFA. Renilla (RL) and firefly (FL) luciferase expression levels were determined in cell lysates at 6 h p.i. and are depicted relative to untreated samples; (E) LR7 cells were transfected with pARF1-YFP, pARF1T31N-YFP, or pARF1Q71L-YFP and inoculated with MHV-RFP (MOI 1) 24 h later. At 18 h p.i. FACS analyses were performed as described in Materials and Methods. The percentages of GFP/YFP positive cells that were also RFP positive were determined relative to wild-type ARF1 expressing cells. Results of representative experiments performed in triplicate are shown. Error bars indicate standard deviations.

In addition to this protein, we included a constitutive-active ARF1 mutant (ARF1-Q71L), which persists in the GTP-bound state longer than wild-type ARF, resulting in a prolonged ARF1 activation. Expression of this latter mutant is known to inhibit transport at later steps in the secretory pathway, e.g. from vesicular tubular clusters (VTC) to the Golgi complex and between Golgi stacks (11). LR7 cells were transfected with plasmids expressing YFP fusions of wild-type ARF1, ARF1-T31N, or ARF1-Q71L. After transfection, cells were inoculated with an RFP-expressing MHV-A59 recombinant (MHV-RFP) that allows flow cytometric analysis of MHV replication (56). The percentage of RFP-positive cells in the YFP-expressing population was determined relative to that of the wild-type ARF1 expressing cells (Fig.1E). Overexpression of the wild-type ARF1 fusion protein did not significantly affect MHV infection when compared to non-transfected cells (data not shown). The results indicate that over-expression of the dominant-negative ARF1 mutant inhibited MHV infection profoundly, thereby confirming the results obtained with BFA. In contrast, expression of the constitutive-active mutant of ARF1 did not influence MHV replication.

BFA Inhibits but does Not Entirely Block the Formation of MHV RCs

As BFA is known to affect intracellular vesicle formation and transport, and because MHV replicates its genome in association with DMVs, we next investigated the effect of BFA on the assembly of the MHV RCs. First, we checked whether the morphological integrity of the RCs was affected in the presence of BFA. Therefore, LR7 cells infected with MHV-A59 were treated with BFA for 30 min starting 5.5 h p.i. Subsequently, the cells were fixed and processed for immunofluorescence using antibodies both against nsp8, which served as a protein marker for the MHV replication sites (7, 43), and against the viral structural protein M, known to reside in the Golgi (35). The nsp8 antibody revealed the typical perinuclear staining pattern in both treated and non treated infected cells (Fig.2A). In contrast, a dispersed distribution of M protein was observed in BFA-treated cells reflecting the collapse of the Golgi, whereas in non-treated cells the M protein showed a clear Golgi-like staining (Fig.2A). These results indicate that, once formed, the replication sites are not disrupted by BFA.

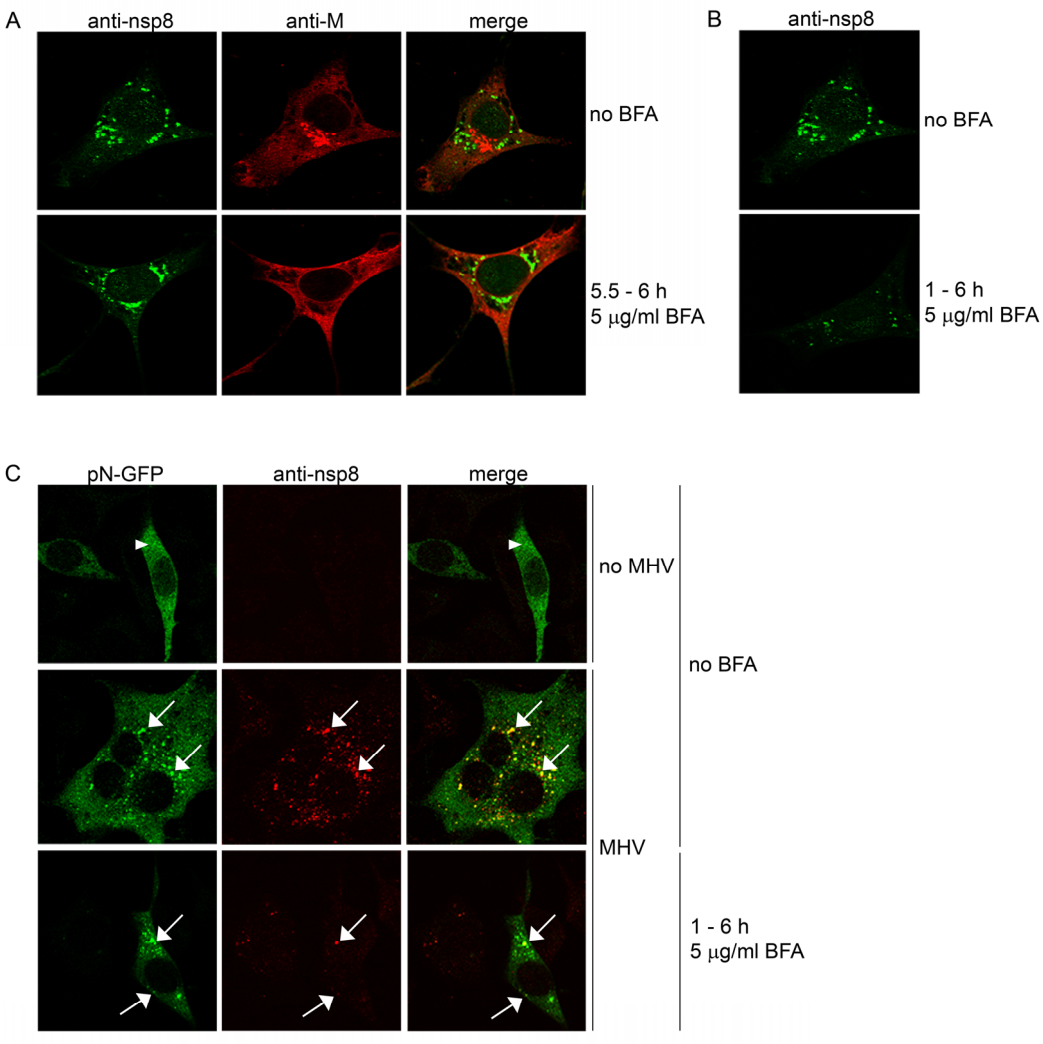

Fig.2. Immunofluorescence analysis of MHV RCs. LR7 cells were inoculated with MHV-A59 and subsequently mock-treated (panel A, upper row), treated with 5 μg/ml BFA from 5.5-6 h p.i. (panel A, lower row) or from 1-6 h p.i. (panel B). Immunostaining was performed using antibodies against nsp8 (anti-nsp8) and against the M protein (anti-M). LR7 cells were transfected with pN-EGFP and subsequently mock-infected (panel C, upper row), infected with MHV-A59 (panel C, middle row), or infected with MHV-A59 and treated with 5 μg/ml BFA from 1 to 7 h p.i. (panel C, bottom row). At 7 h p.i., cells were fixed and an immunostaining was performed using the nsp8 antibodies. Identical confocal microscopy settings were used for mock-treated and BFA-treated samples. Arrowheads in panel C indicate cytosolic staining; arrows indicate nsp8-positive foci.

Subsequently, we investigated whether BFA inhibited RC formation early in the infection. BFA was therefore added to LR7 cells directly after inoculation with MHV-A59 and staining was performed at 6 h p.i. using the nsp8 antibody. Although some perinuclear staining of nsp8 could be detected in BFA-treated cells, the number and intensity of nsp8 containing foci were clearly reduced when compared to non-treated cells (Fig.2B). Next we investigated whether these nsp8 puncta represented MHV replication sites. Therefore, we studied the ability of the nsp8 foci to recruit the nucleocapsid protein N, a protein previously shown to localize to the RCs (7, 16). Three parallel cultures of LR7 cells were transfected with a plasmid coding for a MHV N-GFP fusion protein and 24 h post transfection two of them were infected with MHV-A59. BFA (5 μg/ml) was added to one of these latter cultures directly after inoculation (t = 1 h p.i.). At 6 h p.i., the cells were fixed and subsequently processed for immunofluorescence using the anti-nsp8 antibody (Fig.2C). As expected, N-GFP was diffusely localized to the cytosol in non-infected cells (indicated by an arrowhead in Fig.2C). In contrast, when cells were infected with MHV, this fusion protein also appeared in foci that co-localized with nsp8 (indicated by arrows in Fig.2C). This co-localization was observed both in mock- and in BFA-treated cells, indicating that the nsp8 foci that had been formed in the presence of BFA, though decreased in number and intensity, correspond with the replication sites. In complete agreement with the luciferase expression data shown above, this result demonstrates that BFA inhibits, but does not completely block, the formation of RCs.

BFA Treatment Reduces the Number of DMVs

To study the effects of BFA on the DMVs at an ultrastructural level, MHV-infected LR7 cells were fixed at 6 h p.i. and embedded in Epon resin in order to be analyzed by electron microscopy. DMVs (indicated by the asterisks in Fig.3A) were always seen organized in clusters often located in the perinuclear area. The morphology and dimensions of these vesicles were similar to those as previously described for DMVs harboring the RCs (13, 22, 71, 73, 74, 79). Importantly, these vesicles were not observed in mock-infected cells (data not shown). Fig.3B shows a close view of these DMVs, in which the translucent interior is surrounded by a double membrane. The presence of an inner web-like structure is most likely artificial (73).

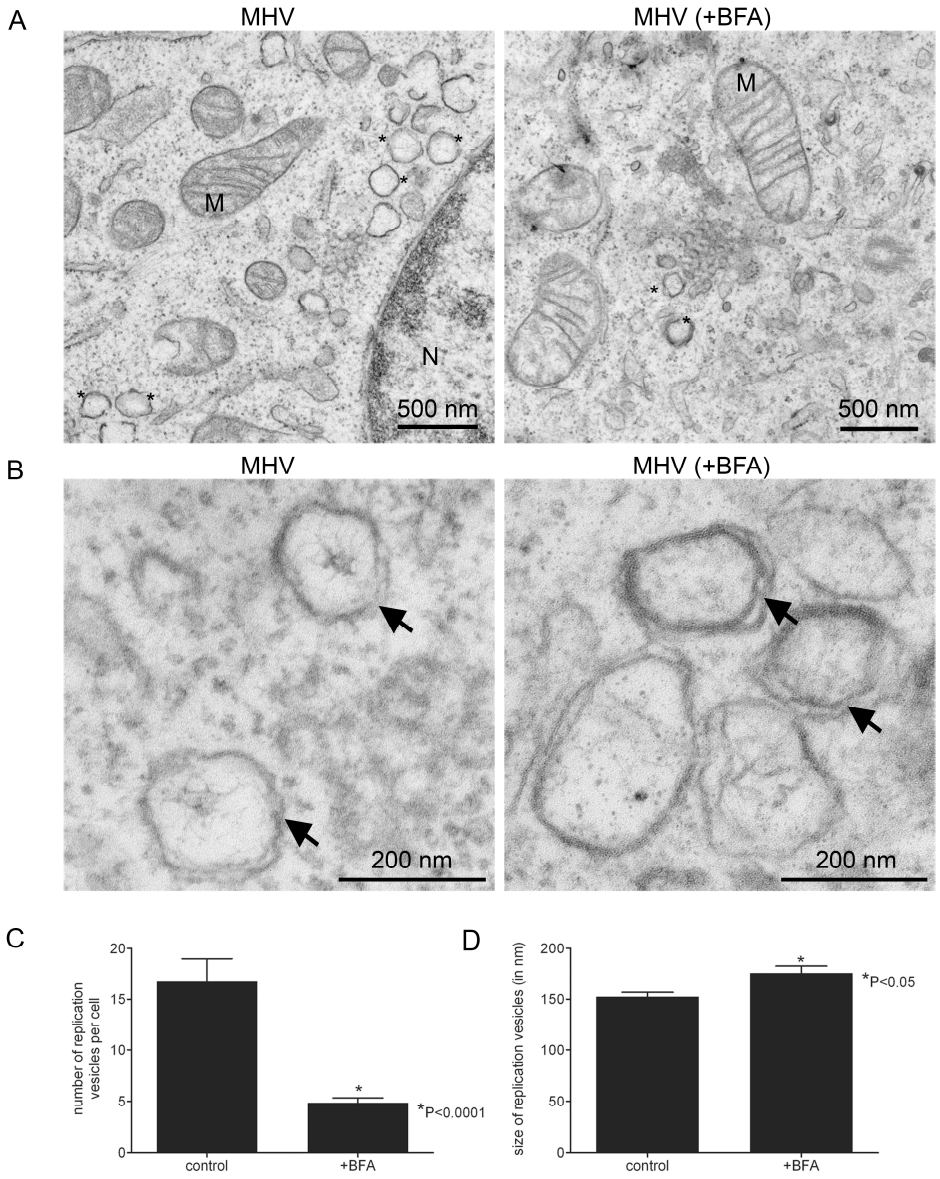

Fig.3. Ultrastructural analysis of MHV-infected LR7 cells. LR7 cells were inoculated with MHV-A59 and treated with or without 5 μg/ml BFA from 1-6 h p.i., chemically fixed and embedded with Epon resin. (A) Numerous clusters of virus-induced DMVs (indicated by *) were found in the perinuclear region of the cell (N-nucleus; M-mitochondrion); Panel B shows a close view of DMVs, clearly demonstrating the presence of double membranes (indicated by arrows); (C) The average number of DMVs per cell obtained by counting 20 infected cells; (D) Average DMV diameter obtained measuring 38 of them. Error bars indicate standard error of the mean (SEM).

Treatment of cells with BFA (1-6 h) led to the expected disappearance of an apparent Golgi complex with the concomitant expansion of the ER volume (not shown). In these cells, vesicles with a morphology almost identical to those present in non BFA-treated cells were observed (Fig.3A). However, the number of these DMVs was significantly decreased ($P < 0.005$) in BFA-treated cells as compared to non-treated cells (4.9 vs. 16.8 on average per section, Fig.3C). The reduction in the number of DMVs is likely to be an underestimation as only EM sections were included in the analyses in which at least one replication vesicle could be detected. Strikingly, the double membrane of the replication vesicles was visually more pronounced in BFA-treated cells than in untreated cells (Fig.3B), which might relate to the swelling of the ER observed after BFA addition. The DMVs were slightly bigger in the BFA-treated cells (175.4 nm +/- 7.1 compared to 152.4 nm +/- 4.5 in non-treated cells; $P < 0.05$; Fig.3D), although the significance of this latter observation is not clear at present. Overall, our ultrastructural analysis of MHV-infected cells confirms that treatment of cells with BFA decreased the number of replication vesicles, consistent with the reduced viral RNA replication in the presence of BFA.

The GEF GBF1 is Required for MHV Replication

To address which ARF GEFs contribute to MHV replication, we next focused on the BFA-sensitive GEFs localized in the secretory pathway, i.e. GBF1, BIG1 and BIG2. First, we studied whether coronavirus replication was affected by BFA in MDCK cells. These cells have a BFA-resistant Golgi-apparatus due to a point mutation in GBF1 (M832L; F. van Kuppeveld, unpublished results). However, the trans-Golgi network (TGN) and the endocytic organelles in MDCK cells are still sensitive to BFA (26, 82, 83). MDCK cells stably expressing the CEACAM1a receptor (MDCK-MHVR; [66]) were inoculated with MHV-EFLM and BFA was added either during (0-1 h p.i.) or after (1-7 h p.i.) the inoculation. The results show that MHV replication was not affected by BFA treatment of the cells during either time period (Fig.4A), pointing toward a possible involvement of the BFA-sensitive GBF1 protein in MHV replication.

To confirm that GBF1, rather than BIG1 or BIG2, is required for MHV replication, each one of these GEFs was specifically and singularly depleted by RNA interference before assaying MHV replication. For each target gene, three siRNA oligos were transfected into

HeLa-CEACAM1a cells. At 72 h post transfection, the cells were infected with luciferase-expressing MHV-2aFLS. Six h later, the number of viable cells and luciferase expression levels were determined (Fig.S1A and S1B) as described in the Materials and Methods. In Fig.4B the results are presented as relative luciferase expression (RII) levels, i.e. luciferase activity expressed relative to mock-treated cells after correction for the number of viable cells. Transfection of control siRNAs targeting the housekeeping protein glyceraldehyde 3-phosphate dehydrogenase (GAPDH) did not change the RII, whereas siRNAs targeting firefly luciferase reduced the RII up to 95% ($P < 0.05$) demonstrating the efficiency of the siRNA transfection. Importantly, down-regulation of GBF1 resulted in a drastic inhibition of RII ($P < 0.05$) whereas siRNAs targeting BIG1 and BIG2 did not have a significant effect (Fig.4B). Almost identical results were obtained when the three siRNA oligos for each gene were singly transfected (data not shown). In a parallel experiment, we demonstrated that down-regulation of the major target of GBF1, ARF1, had a similar phenotypic effect on MHV replication as seen for GBF1 (Fig.4B).

To prove the specificity of our results, we performed a series of controls. First, the specific knockdown of the respective mRNAs after siRNA transfection was confirmed by quantitative RT-PCR analysis. At 72 h after transfection of the siRNAs, the corresponding mRNA levels for BIG1, BIG2, GBF1 and ARF1 were found to be reduced by 73%, 74%, 75%, and 94%, respectively. The mRNA levels were not affected after transfection of non-corresponding siRNAs, demonstrating the specificity of the mRNA depletion (data not shown). Second, the functional knock-down of GBF1 and ARF1 at the protein level was demonstrated by co-transfection of plasmids encoding GBF1-YFP and ARF1-YFP together with either GBF1- or ARF1-specific siRNAs, respectively. This approach was chosen because of the unavailability of specific anti-antibodies. Twenty-four h after transfection, the cells were fixed and YFP-positive cells were counted. Fig.4C demonstrates that GBF1 and ARF1 expression are prohibited in the presence of their specific siRNAs.

Next, we analyzed whether inhibition of MHV replication after depletion of ARF1 coincided with a collapse of the Golgi complex as observed after BFA treatment. Again, HeLa-CEACAM1a cells were transfected with siRNAs targeting ARF1 and subsequently processed for immunofluorescence at 72 h post transfection using the GM130 antibody.

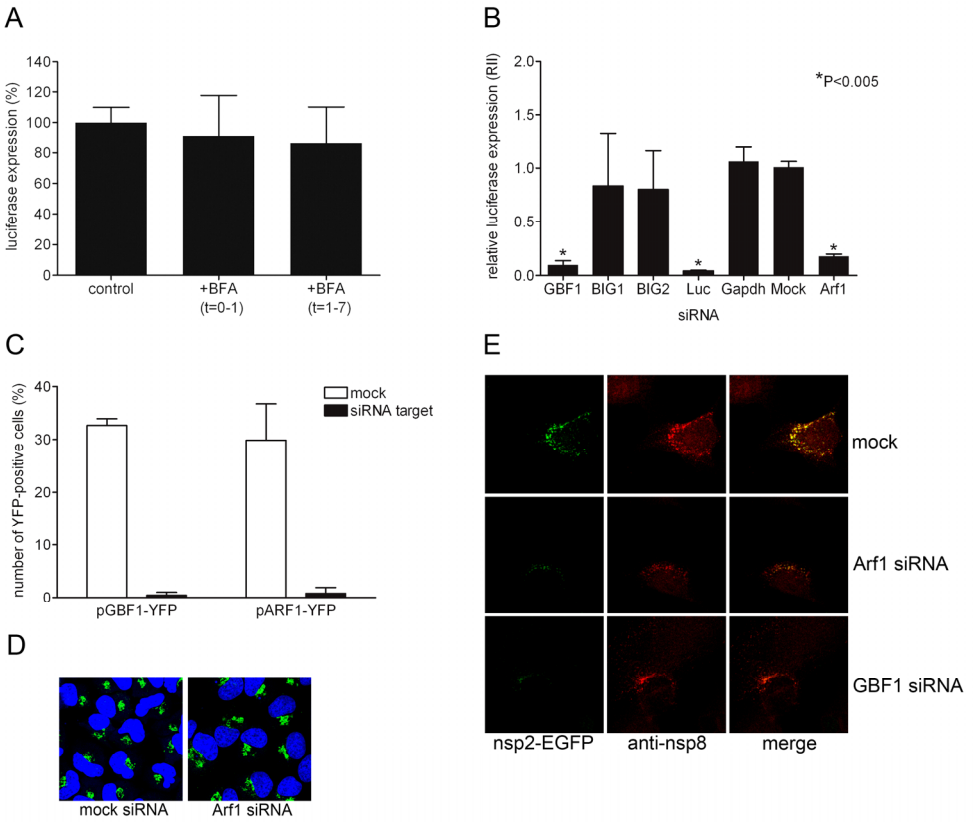

Fig.4. The role of Golgi-residing GEFs in MHV replication. (A) MDCK(MHVR) cells were inoculated with MHV-EFLM and incubated with 5 µg/ml BFA during the indicated time periods. At 7 h p.i. the luciferase expression levels were determined; (B) HeLa-CEACAM1a cells were transfected with three siRNAs directed against either GBF1, BIG1, BIG2, ARF1, firefly luciferase (luc), or GAPDH or were mock transfected (mock). 72 h post transfection, cells were inoculated with MHV-2aFLS. At 6 h p.i., cell viability and luciferase expression levels were measured as described in Materials and Methods. The graph depicts the relative luciferase expression (RII) compared to mock-treated cells after correction for cell viability; (C) HeLa-CEACAM1a cells were transfected with plasmids pGBF1-YFP and pARF1-YFP in the presence or absence of their corresponding siRNAs. At 24 h post transfection, cells were fixed and the percentage of YFP-positive cells was determined; (D) HeLa-CEACAM1a cells transfected with siRNAs targeting ARF1 and mock-transfected cells were fixed at 72 h post transfection and processed for immunostaining using antibodies against the Golgi marker GM130. (E) HeLa-CEACAM1a cells were transfected with siRNAs directed against GBF1 or ARF1, or were mock transfected. 72 h post transfection, the cells were inoculated with MHV-nsp2GFP and at 6 h p.i. they were fixed and processed for immunofluorescence using the nsp8 antibody. (A-C) The results of a representative experiment performed in triplicate are shown. Error bars indicate standard deviations. (D-E) Representative images are shown.

In ARF1 siRNA-transfected cells, GM130 staining was indistinguishable from that in mock-treated cells (Fig.4D) indicating that loss of ARF1 did not lead to the collapse of the Golgi into the ER. This is in complete accordance with the results of Volpicelli-Daley *et al.* (81), who demonstrated that ARF1 depletion alone is not sufficient to mimic the BFA effect on the Golgi complex, but rather requires a simultaneous depletion of ARF1 and ARF4 (81).

Having established that depletion of GBF1 or ARF1 affects MHV replication profoundly, we studied whether the formation of MHV RCs was similarly affected. To this end, we performed a similar knock down experiment in which we transfected siRNAs targeting either ARF1 or GBF1 and subsequently infected the cells with a recombinant MHV, which expressed an additional copy of nsp2, now fused to GFP. The nsp2-GFP fusion protein co-localizes with nsp8 and provides an additional marker for RCs (data not shown). 6 h after infection, cells were fixed and processed for immunofluorescence with the nsp8 antibody. In mock transfected cells, many GFP and nsp8 positive foci were observed, which largely co-localized (Fig.4E). In agreement with the relative luciferase expression values shown in Fig.4B, both in ARF1- and GBF1-depleted cells, the number and intensity of nsp8 positive foci was reduced, similar to what had been observed in BFA-treated cells (Fig 2B). Apparently, the number of MHV RCs is reduced in these cells. Strikingly, however, it appeared that nsp2-GFP expression was much more affected than that of nsp8 by the depletion of either ARF1 or GBF1, as hardly any GFP fluorescence could be detected. While nsp8 is expressed directly from the viral genome, the nsp2-GFP fusion protein is expressed from a subgenomic mRNA and hence replication and transcription is required for its expression. These results therefore indicate that not only fewer RCs are formed in the absence of either GBF1 or ARF1, but that these RCs are also impaired in their RNA synthesis.

In conclusion, our results demonstrate that depletion of GBF1 and ARF1 reduces MHV replication as well as the number of RCs. Furthermore, our results indicate that RCs formed in the absence of either GBF1 or Arf1 are less active. In addition, inhibition of MHV replication is not caused by collapse of the Golgi apparatus per se, as in ARF1-depleted

cells virus replication is severely affected whereas the overall morphology of the Golgi complex is unaltered.

ARF1, COPI and PLD are Not Recruited to the RCs

We next addressed the question whether ARF1 is recruited to the replication sites. To this end, LR7 cells expressing wild-type ARF1 fused to YFP were infected with MHV-A59 and either fixed at an early (4 h) or late (7 h) time point p.i. before identifying the replication sites by immunostaining the cells with nsp8 antibodies. Fig.5A shows that ARF1-YFP was predominantly localized to the Golgi apparatus (indicated by the arrowhead on the left panel of Fig.5A) both at 4 h p.i. and 7 h p.i. At 4 h p.i., only in a minority of cells co-localization between ARF1 and nsp8 was observed (indicated by the arrows in Fig.5A). No co-localization could be observed in infected cells at 7 h p.i. Similar results were obtained for GBF1 (data not shown).

Many downstream effectors of ARF1 have been described, and the list is still growing. One of the best known functions of ARF1 involves the regulation of COPI-mediated vesicular transport. For BFA-sensitive poliovirus, COPI has been found to localize at the replication vesicles (21). To study whether a similar recruitment of COPI to the replication vesicles occurs during MHV replication, we determined its localization in MHV-infected cells. Thus, HeLa-CEACAM1a cells were infected with MHV-nsp2GFP. This recombinant virus allowed us to directly visualize the replication vesicles without having to perform an immunostaining with anti-nsp8 antibodies. This was desirable as both the antibody against αγCOP (two subunits of the COPI coat) and the nsp8 antibody were raised in rabbits. At 7 h p.i., cells were fixed and processed for immunofluorescence analysis using the αγCOP antibody. The results show that, in addition to a diffuse staining throughout the cell, COPI was primarily localized in a Golgi-like pattern (Fig.5B). COPI did not co-localize with the nsp2-GFP positive sites, indicating that COPI was not recruited to the replication sites of MHV.

Another well known effector of ARF1 is phospholipase D (PLD), a lipid-metabolizing enzyme involved in membrane dynamics and vesicular transport (31, 67). To analyze whether RCs recruit PLD, LR7 cells were transfected with a construct expressing PLD1b

fused to GFP and subsequently infected with MHV-A59. The cells were fixed at 7 h p.i. before identifying the replication sites by immunostaining the cells with nsp8 antibodies. No co-localization between the RCs and PLD1b could be observed (Fig.S2A). Furthermore, specific inhibition of PLD by 1-butanol (25) did not affect MHV luciferase expression compared to controls (Fig.S2B). Further studies will be required to examine the role of other ARF1 effectors.

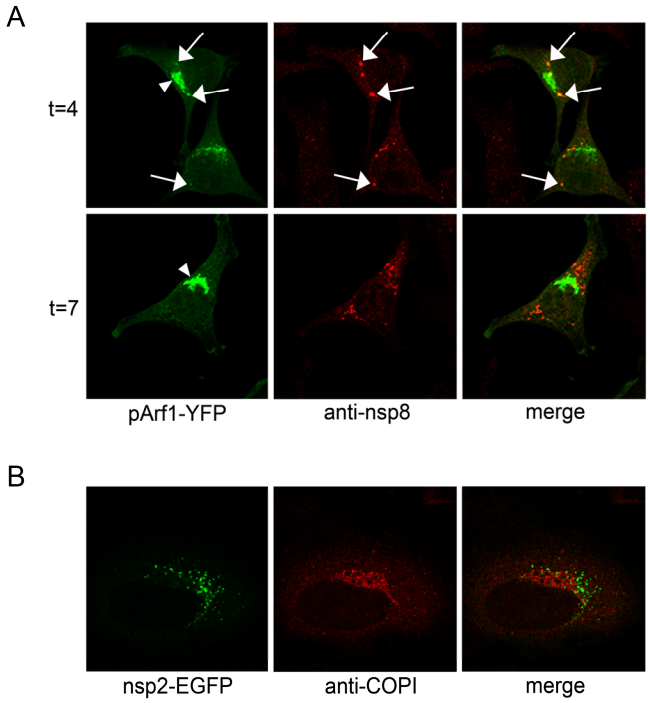

Fig.5. ARF1 and COPI do not co-localize with the RCs. (A) LR7 cells were transfected with pARF1-YFP, pARF1T31N-YFP, or pARF1Q71L-YFP and inoculated with MHV-A59 (MOI 1) 24 h later. At 4 h and 7 h p.i. cells were processed for immunofluorescence using antibodies against nsp8. Arrows indicate co-localization of nsp8 with ARF1; arrowheads indicate ARF1 localizing to the Golgi complex; (B) HeLa-CEACAM1a cells were inoculated with MHV-nsp2-GFP (MOI 1), fixed 7 h later and processed for immunofluorescence using antibodies against αγCOPI.

MHV Reduces but does Not Block Protein Secretion

Finally, we studied whether normal vesicular trafficking is affected in MHV-infected cells. To investigate this, we made use of a Gaussia reporter gene, the protein product of which is

secreted upon expression (2, 78). Cells were transfected with a plasmid encoding this gene under the control of a CMV promoter and subsequently infected with either MHV-A59, mock-infected, or treated with BFA. At 4.5 h p.i. the intracellular and extracellular levels of Gaussia luciferase were measured. Thus, the ratio of luciferase activity in the cell lysate and in culture supernatant was determined for each condition. While in mock-infected cells almost 60% of the total amount of Gaussia luciferase was found in the culture supernatant, in MHV-infected cells the amount of secreted Gaussia luciferase was decreased about 2-fold to 30% (Fig.6). BFA treatment inhibited, as expected, Gaussia protein secretion almost completely. From this we conclude that, although MHV RNA replication depends on GBF1-mediated ARF1 activation, MHV infection does not drastically impair the secretory pathway. This result was not unexpected, as coronaviruses require a functional secretory pathway for the release of their progeny virions.

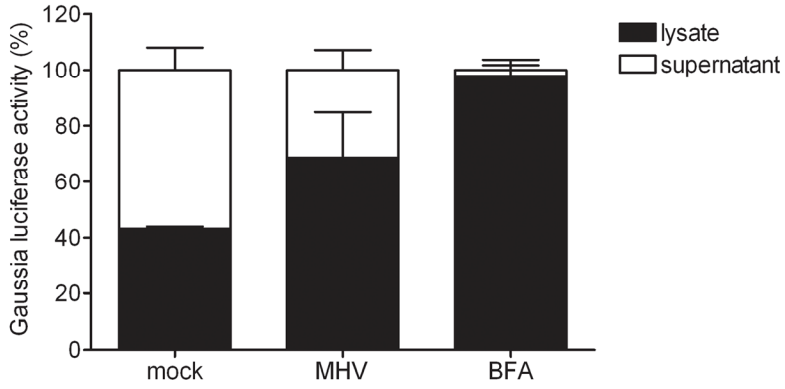

Fig.6. MHV reduces but does not block protein secretion. LR7 cells, transfected with a plasmid encoding the Gaussia gene, were at 1 h post transfection either infected with MHV-A59 or mock-infected or were treated with BFA. At 4.5 h p.i. Gaussia luciferase activity was determined both in the cell lysate and culture supernatant. The relative amount of luciferase present in the supernatant and cell lysate is depicted.

Discussion

RNA viruses use and manipulate cellular membranes for the assembly of their replication and transcription structures. We and others have shown that coronaviruses exploit the early secretory pathway, but the way in which they do so is not understood. In this report we have demonstrated, using several different approaches, that MHV requires a functional

GBF1-ARF1 pathway for efficient RNA replication. First, we showed that MHV, but not Sindbis virus replication is sensitive to BFA in murine LR7 cells. Second, we observed that MHV replication is not sensitive to BFA in MDCK cells, which contain a BFA-resistant GBF1. Third, we show that the specific siRNA-based knockdown of the BFA-sensitive GEF GBF1, but not BIG1 and BIG2, strongly affect MHV infection. Fourth, also ARF1, a downstream effector of GBF1, appeared to be required for efficient MHV replication, as shown by the inhibition of MHV-driven reporter gene expression during siRNA-mediated down regulation of ARF1 as well as during expression of an inactive ARF1 mutant.

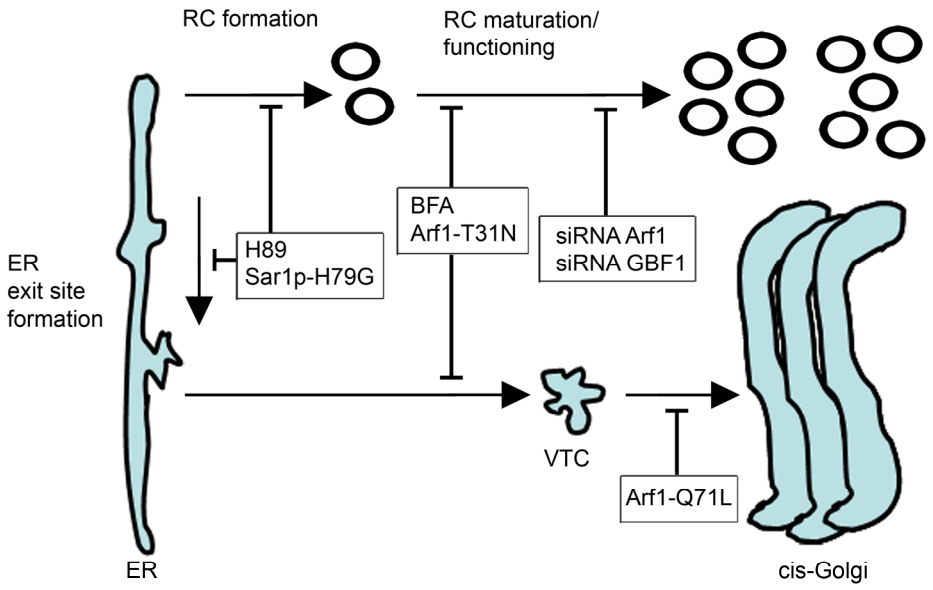

Fig.7. Model of MHV RCs and their links to the early secretory pathway. Two major steps in the anterograde protein secretion route (reviewed in [81]) are linked to MHV RC formation and/or RNA replication. First, transport of proteins out of the ER requires ER exit site formation controlled by Sar1p (82, 83, 84). Blocking this early step by using the drug H89 (85) or by expressing of a dominant mutant of Sar1p (86) blocks MHV replication profoundly (11). Next, ER exit sites develop into, or form de novo, vesicular-tubular clusters (VTCs) (also called ERGIC), for which GBF1 and ARF1 are required. This step, which can be blocked by BFA, by expressing a dominant-negative mutant of ARF1 or by down-regulating ARF1 using siRNAs (49), is also involved in MHV RC formation (this manuscript). However, a fully functional secretory pathway is not essential, as a dominant-active mutant of ARF1, which blocks transport between VTCs and cis-Golgi (49), does not impair MHV replication.

The inhibition of coronavirus RNA replication in the presence of BFA is either caused by direct inhibition of RC formation, resulting in reduced RNA replication, or by inhibition of RNA replication via another mechanism, resulting in reduced de novo formation of RCs. Though it is difficult to distinguish between these two scenarios, our results indicate the latter option to be most plausible. Although BFA reduced the number of RCs, their formation was not completely blocked as demonstrated by immunofluorescence staining of the RCs using the nsp8 antibody and by quantitative electron microscopy. Apparently, BFA did not prevent the formation of RCs after translation of the incoming genomic RNA. In addition, MHV replication was inhibited by BFA throughout the infection. Early in infection the inhibition was more profound than at later time-points, when many transcriptionally active RCs have already been formed. Furthermore, while the inhibition of reporter gene expression in the presence of BFA, or after depletion of either GBF1 or ARF1, is in complete agreement with the reduced numbers of RCs, our results also indicate that the few RCs that are formed in the absence of GBF1 or ARF1 are less active. Therefore, we hypothesize that BFA inhibits MHV RNA replication by affecting RC maturation or functioning rather than RC formation per se (Fig.7).

Replication of several viruses has now been shown to be sensitive to BFA. These viruses, which include poliovirus (28, 36, 47), grapevine fanleaf nepovirus (65) and MHV (this study), all appear to use ER-derived membranes for the formation of their RCs ([68)] [65] and [56, 73, 74], respectively). Strikingly, picornaviruses belonging to different genera were found to differ in their sensitivity to BFA, which was suggested to correspond with differences in the assembly of their RCs (21). Replication of equine arterivirus, a distant relative of coronaviruses, was observed not to be sensitive to BFA (59), while other nidoviruses have not been studied to date.

Unlike for poliovirus (3), ARF1 is hardly recruited to coronavirus RCs. We therefore hypothesize that downstream effectors of GBF1-ARF1 are involved in MHV replication. To date, more than 20 downstream effectors of ARF1 have been identified (9, 18, 34, 53), and each one of these might thus be somehow implicated in the functioning of the MHV RCs. The most well known effector of ARF1 is COPI. For picornaviruses, BFA sensitivity was suggested to correlate with the recruitment of COPI to these sites (21). However, no

co-localization between COPI and MHV RCs could be observed. This is in agreement with the almost complete absence of ARF1 at these sites. In addition, coronavirus RCs did not co-localize with PLD1 nor was coronavirus replication affected by inhibition of phospholipase D, a lipid-metabolizing enzyme involved in membrane dynamics and vesicular transport (31, 67). It might be that the GBF1-ARF1 pathway simply functions to deliver lipids to RCs. In agreement herewith, cerulenin, an inhibitor of phospholipid biosynthesis, severely inhibits MHV replication (C.A.M. de Haan, unpublished results). Nonetheless, the observed inhibition of MHV infection after BFA treatment is probably not an indirect consequence of the collapse of the Golgi complex as, unlike BFA treatment, ARF1 depletion did not affect the morphology of the Golgi complex (Fig.4D). Consistent herewith, another recent study showed that ARF1 depletion did not affect the Golgi morphology or protein transport (81).

Several studies have indicated that coronavirus replication and the ER are closely connected. Electron microscopical analyses of infected cells showed partial co-localization of coronavirus replicase proteins with the soluble ER resident protein disulfide isomerise (73), while DMVs were often found in close proximity to the ER and occasionally in continuous association with it (73, 74). Furthermore, when expressed in absence of a coronavirus infection, the nsp3 and nsp4 proteins were inserted into the ER and became modified by addition of N-linked sugars (23, 32, 56), whereas expression of tagged MHV nsp4 in MHV-infected cells resulted in recruitment of the protein to RCs (56). In addition, coronavirus replication was inhibited when the ER export machinery was blocked by the use of kinase inhibitor H89 or by expression of dominant-active mutant of the small GTPase Sar1 (56). We now show by using several approaches that MHV RNA replication also depends on GBF1-mediated ARF1 activation. Apparently, an intimate association exists between the early secretory pathway and MHV replication. Interestingly, whereas H89 blocked RC formation completely (56), this was not the case when GBF1-mediated activation of ARF1 was impaired by BFA. Rather it appears that RCs formed in absence of GBF1 or ARF1 are less active, suggesting a role for these proteins in RC maturation or functioning (Fig.7). Clearly, further investigations are needed to unravel the precise mechanism by which the secretory pathway contributes to the biogenesis of functional coronavirus RCs and to RNA replication.

Material & Methods

Cells and viruses

HeLa-CEACAM1a cells were generated by transfecting HeLa cells (obtained from the MPI-CBG High-Throughput Technology Development Studio (60)) with the expression plasmid pMHVR (19) as described before (85). Murine LR7 (37), HeLa-CEACAM1a, and Madin-Darby Canine Kidney-CEACAM1a [MDCK(MHVR); (66) cells, which all stably express the MHV receptor mCEACAM1a, were maintained as monolayer cultures in Dulbecco modified Eagle medium (DMEM; Cambrex) containing 10% fetal calf serum (FCS), 100 IU of penicillin/ml, 100 µg of streptomycin/ml (all from Life Technologies), and 0.5 mg/ml G418 (Life Technologies, Paisley, UK).

Split cells, i.e. BHK-21 cells stably expressing Sindbis virus structural proteins (63), were maintained in Glasgow MEM (Invitrogen) containing 10% FCS, 100 IU of penicillin/ml, 100 µg of streptomycin/ml, 250 µg/ml G418 and 125 µg/ml hygromycine B (Boehringer GmbH) and used to generate Sindbis pseudovirus particles containing a replicon expressing firefly luciferase. To this end, the firefly luciferase gene was cloned into the pSinRep5 vector (Invitrogen) using conventional cloning procedures. The resulting vector was subsequently processed further according to Polo *et al*. (63) to produce the pseudovirus particles.

LR7 cells were used to propagate the wild-type and recombinant MHVs (based on strain A59). The recombinant viruses expressing the firefly luciferase gene (MHV-EFLM and MHV-2aFLS) or the red fluorescent protein (RFP) gene have been described before (15, 56). The recombinant virus MHV-nsp2GFP, which expresses a nsp2-green fluorescent protein (GFP) fusion protein, was generated in a similar way as described previously for MHV-nsp4GFP (56). Briefly, an nsp2-GFP fusion construct was cloned behind an additional transcription regulation sequence into a derivative of the RNA transcription vector pMH54 (37). Targeted recombination to obtain the recombinant MHV-nsp2GFP was performed as described before (37).

Antibodies and plasmids

Antibodies directed against the MHV nsp8 (anti-p22, kindly provided by M. Denison, Vanderbilt University Medical Center, Nashville, USA (43)), the amino terminus of the MHV M protein (J1.3, kindly provided by J. Fleming, University of Wisconsin, Madison, USA (77)), against αγCOPI (anti-αγCOPI, kindly provided by F. Wieland, University of Heidelberg, Germany), against GBF1 (anti-GBF1) and against the Golgi marker GM130 (anti-GM130) (the latter two from BD Transduction Laboratories, San Jose, USA) were used. The conjugated secondary antibodies were purchased from Jackson Immunoresearch Laboratories.

Plasmids containing the different ARF1 and GBF1 genes in frame with either a GFP or a yellow fluorescent protein (YFP) tag were obtained from G. Romero (80) and C. Jackson (54), respectively. pGBF1-YFP and pARF1-YFP encode the wild-type proteins fused to YFP. pARF1T31N-YFP and pARF1Q71L-GFP encode a dominant-negative and a dominant-active mutant of ARF1 fused to YFP and GFP, respectively (11). The pN-EGFP plasmid, which encodes the MHV nucleocapsid (N) protein extended at its C-terminus with GFP was constructed by cloning a PCR fragment, specifying the N gene without its stop codon, into pEGFP-N3 (Clontech),

using conventional cloning procedures. The plasmid encoding the Gaussia reporter gene behind a CMV promoter was generated by replacing the EGFP gene in pEGFP-C1 (Clontech) with the Gaussia luciferase gene from pGLuc-Basic (New England Biolabs) using conventional cloning methods. The viral expression plasmid pM5f-RL-M3 was generated by cloning a synthetic DNA segment (Genscript©) corresponding to the extreme 5' 211 nt and the extreme 3' 401 nt of the MHV-A59 genome, separated by a NheI restriction site and flanked by a T7 promoter and a poly(A) sequence, upstream and downstream, respectively, into pUC57. Subsequently, the coding region for Renilla luciferase, obtained from pRLnull (Promega), was cloned into the NheI-digested vector.

DNA transfection

Subconfluent monolayers of LR7 cells grown on coverslips in 2-cm^2 tissue culture dishes were overlaid with transfection medium consisting of 0.2 ml of Optimem (Invitrogen) that contained 1 µl Lipofectamine 2000 (Invitrogen) and 1 µg of DNA. After 3 h, the medium was replaced with DMEM containing 10% FCS. At 24 h after transfection the cells were processed further as indicated.

RNA synthesis and transfection

The plasmid pM5f-RL-M3 was linearized using a PacI restriction site directly downstream of the poly(A) sequence, and subsequently RNA transcripts were produced using the T7 MessageMachine Kit (Ambion) according to the manufacturer's instructions. Of the transcripts, 0.5 pmol of RNA was transfected into mock- or MHV-2aFLS-inoculated LR7 cells at 1 h p.i. using Lipofectamine 2000 (Invitrogen). Next, the cells were treated with or without 5 µg/ml BFA from 2 h until 6 h p.i., after which the cells were lysed and intracellular Renilla and firefly luciferase activity was measured with the Dual-Luciferase Assay Kit (Promega) according to the manufacturer's protocol.

Confocal immunofluorescence microscopy

Cells were fixed using a 4% paraformaldehyde solution in phosphate buffered saline (PBS), and subsequently permeabilized with 0.1% Triton-X100 in PBS. Next, the cells were incubated for 1 h with the first antibody diluted in PBS containing 10% normal goat serum. After several washing steps, the cells were incubated with an appropriate dilution of secondary antibody in the same buffer for 1 h. After three subsequent washing steps, the coverslips were mounted in Fluosave (Calbiochem). The immunofluorescence staining was analyzed using a confocal laser-scanning microscope (Leica). GFP/YFP and FITC were excited at 488 nm and Cy5 at 633 nm.

Quantification of virus replication

Virus replication was quantified by determining either the virus-driven luciferase expression levels or the amount of genomic RNA. To this end, LR7 or MDCK(MHVR) cells were inoculated at a multiplicity of infection (MOI) of 1 with MHV-EFLM, MHV-2aFLS or Sindbis pseudovirus particles in the presence or absence of 5 µg/ml BFA in DMEM. After 1 h, the culture medium was replaced by DMEM containing 10% FCS and antibiotics, again in the presence or absence of 5 µg/ml BFA. At the indicated time-points, the luciferase expression in the cells was determined using the firefly luciferase assay system (Promega) according to manufacturer's instructions and using a single-tube luminometer (Turner Designs, TD-20/20). Alternatively, RNA was isolated from the cells using the Qiagen RNeasy kit (Qiagen) according to the manufacturer's protocol. TaqMan single-tube reverse transcription-

PCR (RT-PCR) assay (PE Biosystems, Foster City, California, USA) was performed essentially as described by de Haan *et al*. (14). The reactions were performed in triplicate according to the manufacturer's instructions by using the TaqMan RT-PCR kit (PE Biosystems) and an ABI Prism 7000 sequence detector.

Small interfering (si)RNA-mediated knockdown experiments

siRNA duplexes targeting different sites within the coding sequences of GBF1, BIG1, BIG2, and ARF1 were designed by and obtained from Ambion Inc. (three siRNAs per gene; nucleotide sequences available on request). siRNAs targeting GAPDH, luciferase GL2+GL3, and Kif11 (all from Ambion) were taken along as controls in each experiment. One day after seeding the HeLa-CEACAM1a cells, they were transfected with a final concentration of 10 nM siRNA using Oligofectamine (Invitrogen). 72 h after transfection, the cells were inoculated with MHV-2aFLS at such a MOI that approximately 10% of the mock-treated cells became infected. At 6 h post infection (p.i.), the cell number and viability was measured by Wst-1 assay according to the manufacturer's protocol (Roche Diagnostics GmbH). Subsequently, the medium was replaced by DMEM lacking phenol red (Cambrex) and Steadylite HTS firefly luciferase substrate (Perkin Elmer) was added. Luciferase expression was determined using a luminescence plate reader (Berthold Centro LB 960). Each siRNA experiment was performed in triplicate. For each well, luciferase values were corrected for the cell number and viability as determined by the Wst1 assay relative to the mock-treated cells. To validate the functional knockdown of the targeted genes, mRNA levels of each gene were determined after siRNA transfection using Taqman Gene Expression Assays (Applied Biosystems, CA, USA), according to the manufacturer's protocol.

ARF1/GBF1 expression assay

To determine whether siRNAs targeting the ARF1 and GBF1 genes effectively depleted HeLa-CEACAM1a cells from the corresponding proteins, a siRNA transfection experiment was performed in which 40 ng of the plasmids encoding either ARF1-YFP or GBF1-YFP were added to the transfection mixture containing the corresponding siRNAs. Twenty-four h after transfection, the cells were fixed and representative images were taken by an automated CellWorxTM microscope (Applied Precision) with a 10x objective.

Flow cytometry

LR7 cells transfected with pARF1-YFP, pARF1T31N-YFP, or pARF1Q71L-GFP were inoculated with MHV-RFP (MOI 5) at 24 h post transfection. 2 h p.i., 1 μM HR2 peptide (6) was added to inhibit syncytia formation. At 18 h p.i., the cells were collected and fixed using a 3% paraformaldehyde solution. After two washes with PBS, the samples were analyzed employing a FACScalibur™ flow cytometer (Becton Dickinson) gating for YFP/GFP-positive cells in the forward and side scatter, such that a limited cell population with similar ARF1 expression levels was selected. From the YFP/GFP-positive population, the fraction of cells expressing RFP was determined.

Fixation of cells and embedding in Epon resin for electron microscopy (EM) analysis

LR7 cells infected with MHV-A59 and treated from 1 to 6 h p.i. with or without 5 μg/ml BFA were resuspended in 2% glutaraldehyde in 0.1 M cacodylate buffer (pH 7.4) for at least 2 h at room temperature (RT). This buffer was then replaced with fresh one and the fixation was continued overnight. Cells were then centrifuged, washed 3 times with the 0.1 M cacodylate buffer before being post-fixed in 1% OsO4, 1.5% ferrocyanide at 4˚C for 60 min.

Next, the cell pellet was washed 5 times with distilled water and left sit in the last wash for 30 min before being centrifuged and resuspended in warm 2% low melting point agar (Roche, Basel, Switzerland) and immediately spun down. After solidification of the agar on ice, the tip containing the cells was cut into small 1 mm^3 blocks. These blocks were then dehydrated by immerging them into increasing amounts of ethanol (50%, 70%, 80%, 90%, 96% and 3 times 100%) by incubation on a rotatory wheel for at least 15 min at RT for each step. These amalgamations were followed by others in 1,2-propylene oxide (Merck, Haarlem, Netherlands)-Epon resin (3:1) for 30 min, 1,2-propylene oxide -Epon resin (1:1) for 30 min, 1,2-propylene oxide-Epon (3:1) for 60 min and Epon resin overnight. The Epon solution was prepared by mixing 12 g of glycid ether 100.8 g of 2-dodecenylsuccinic acid anhydride, 5 g of methylnadic anhydride and 560 ml of benzyldimethylamine (all from Serva, Heidelberg, Germany). The Epon resin was then replaced the following day with freshly made resin and the incubation continued for 4 h at RT. After centrifugation at 3000 rpm for 10 min, the Epon resin was polymerized by heating the sample at 63ºC for 3 days. 65-80 nm sections were then cut using an Ultracut E ultramicrotome (Leica Microsystems) and transferred on Formvar carbon-coated copper grids. Sections were stained first with 6% uranyl acetate for 30 min at RT and then with a lead-citrate solution (80 mM lead nitrate, 120 mM sodium citrate, pH 12) for 2 min before being viewed. Analysis of EM sections was performed by using a Jeol1010 electron microscope.

Counting and statistics of EM micrographs

DMVs were defined based on the two following morphological criteria: the typical double membrane and the presence of the previously described web-like structure in their proximity (73). The size and the number of the DMVs in control and BFA-treated cells were determined by analyzing 60 randomly selected cell profiles. The results were statistically analyzed with the Student's t-test.

Acknowledgements

We would like to thank D. Duijsings for helpful discussions, M. Denison and J. Fleming for providing us with the antibodies directed against the MHV nsp8 and M protein, respectively, and G. Romero and C. Jackson for providing the plasmids containing ARF1 and GBF1, respectively.

Supplementary Data

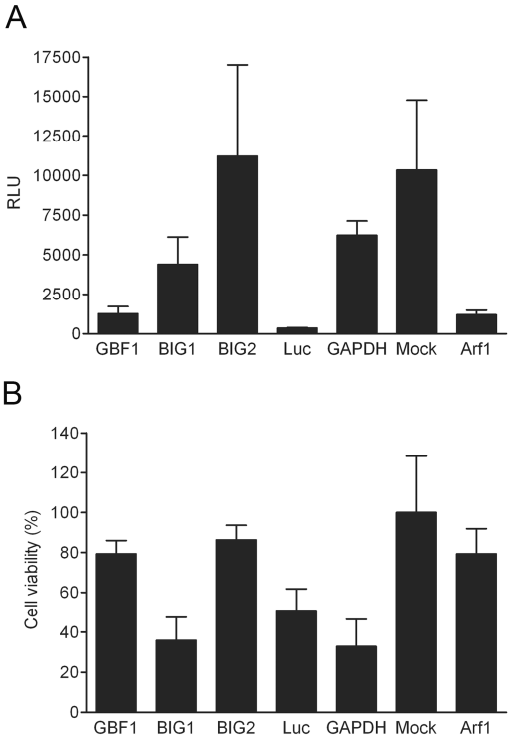

Supplemental Fig.S1. The effect of depletion of Golgi-residing GEFs on MHV replication. HeLa-CEACAM1a cells were transfected with three siRNAs directed against either GBF1, BIG1, BIG2, ARF1, firefly luciferase (luc) or GAPDH, or were mock-transfected (mock). 72 h post transfection, the cells were inoculated with MHV-2aFLS. At 6 h p.i., (A) the luciferase expression levels (RLU) and (B) the cell viability (relative to mock-treated cells) were measured.

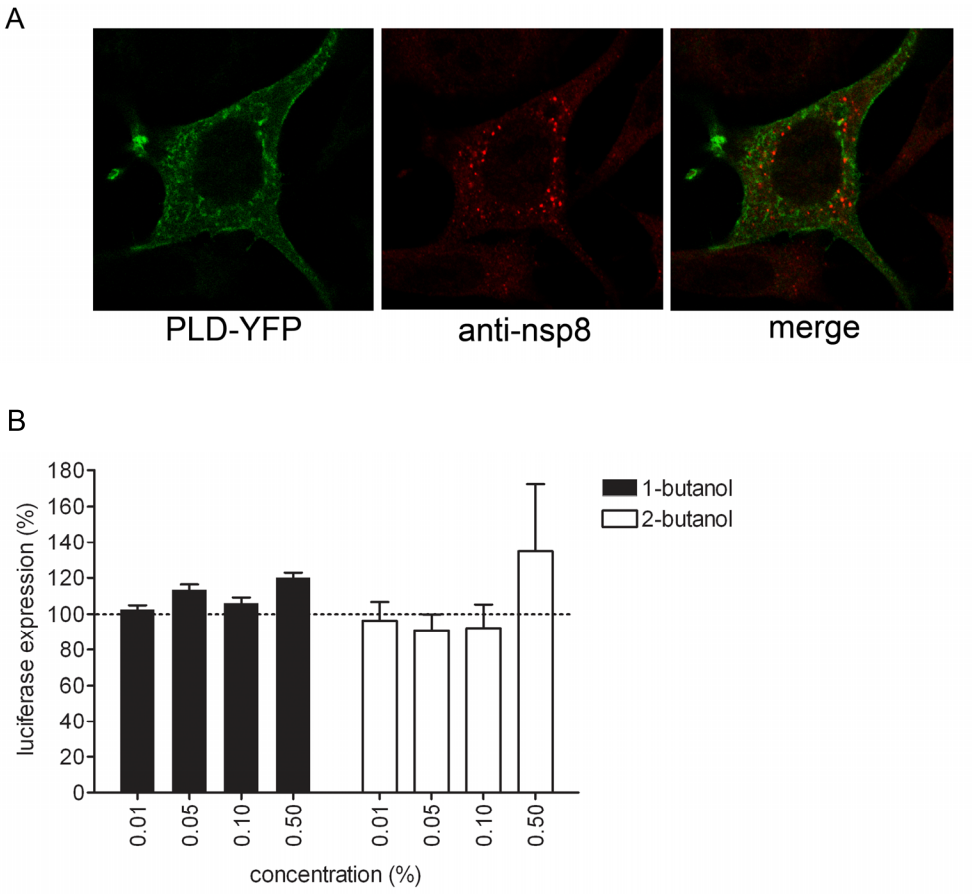

Supplemental Fig.S2. The role of PLD in MHV replication. (A) LR7 cells were transfected with pPLD1 and inoculated with MHV-A59 (MOI 1) 24 h later. At 7 h p.i. cells were processed for immunofluorescence using antibodies against nsp8. (B) LR7 cells were inoculated with MHV-2aFLS (MOI 1), and at 1 h p.i. they were either mock-treated or treated with different amounts of 1-butanol or 2-butanol, as indicated. At 6 h p.i. luciferase expression was measured.

References

1. **Ahlquist, P., A. O. Noueiry, W. M. Lee, D. B. Kushner, and B. T. Dye.** 2003. Host factors in positive-strand RNA virus genome replication. J Virol 77:8181-6.

2. **Badr, C. E., J. W. Hewett, X. O. Breakefield, and B. A. Tannous.** 2007. A highly sensitive assay for monitoring the secretory pathway and ER stress. PLoS ONE 2:e571.

3. **Belov, G. A., M. H. Fogg, and E. Ehrenfeld.** 2005. Poliovirus proteins induce membrane association of GTPase ADP-ribosylation factor. J Virol 79:7207-16.

4. **Bi, W., J. D. Pinon, S. Hughes, P. J. Bonilla, K. V. Holmes, S. R. Weiss, and J. L. Leibowitz.** 1998. Localization of mouse hepatitis virus open reading frame 1A derived proteins. J Neurovirol 4:594-605.

5. **Bonifacino, J. S., and B. S. Glick.** 2004. The mechanisms of vesicle budding and fusion. Cell 116:153-66.

6. **Bosch, B. J., R. van der Zee, C. A. de Haan, and P. J. Rottier.** 2003. The coronavirus spike protein is a class I virus fusion protein: structural and functional characterization of the fusion core complex. J Virol 77:8801-11.

7. **Bost, A. G., E. Prentice, and M. R. Denison.** 2001. Mouse hepatitis virus replicase protein complexes are translocated to sites of M protein accumulation in the ERGIC at late times of infection. Virology 285:21-9.

8. **Buck, K. W.** 1996. Comparison of the replication of positive-stranded RNA viruses of plants and animals. Adv Virus Res 47:159-251.

9. **D'Souza-Schorey, C., and P. Chavrier.** 2006. ARF proteins: roles in membrane traffic and beyond. Nat Rev Mol Cell Biol 7:347-58.

10. **D'Souza-Schorey, C., G. Li, M. I. Colombo, and P. D. Stahl.** 1995. A regulatory role for ARF6 in receptor-mediated endocytosis. Science 267:1175-8.

11. **Dascher, C., and W. E. Balch.** 1994. Dominant inhibitory mutants of ARF1 block endoplasmic reticulum to Golgi transport and trigger disassembly of the Golgi apparatus. J Biol Chem 269:1437-48.

12. **Dasgupta, A., and D. W. Wilson.** 2001. Evaluation of the primary effect of brefeldin A treatment upon herpes simplex virus assembly. J Gen Virol 82:1561-7.

13. **David-Ferreira, J. F., and R. A. Manaker.** 1965. An Electron Microscope Study of the Development of a Mouse Hepatitis Virus in Tissue Culture Cells. J Cell Biol 24:57-78.

14. **de Haan, C. A., K. Stadler, G. J. Godeke, B. J. Bosch, and P. J. Rottier.** 2004. Cleavage inhibition of the murine coronavirus spike protein by a furin-like enzyme affects cell-cell but not virus-cell fusion. J Virol 78:6048-54.

15. **de Haan, C. A., L. van Genne, J. N. Stoop, H. Volders, and P. J. Rottier.** 2003. Coronaviruses as vectors: position dependence of foreign gene expression. J Virol 77:11312-23.

16. **Denison, M. R., W. J. Spaan, Y. van der Meer, C. A. Gibson, A. C. Sims, E. Prentice, and X. T. Lu.** 1999. The putative helicase of the coronavirus mouse hepatitis virus is processed from the replicase gene polyprotein and localizes in complexes that are active in viral RNA synthesis. J Virol 73:6862-71.

17. **Donaldson, J. G., D. Finazzi, and R. D. Klausner.** 1992. Brefeldin A inhibits Golgi membrane-catalysed exchange of guanine nucleotide onto ARF protein. Nature 360:350-2.

18. **Donaldson, J. G., and C. L. Jackson.** 2000. Regulators and effectors of the ARF GTPases. Curr Opin Cell Biol 12:475-82.

19. **Dveksler, G. S., M. N. Pensiero, C. B. Cardellichio, R. K. Williams, G. S. Jiang, K. V. Holmes, and C. W. Dieffenbach.** 1991. Cloning of the mouse hepatitis virus (MHV) receptor: expression in human and hamster cell lines confers susceptibility to MHV. J Virol 65:6881-91.

20. **Garcia-Mata, R., T. Szul, C. Alvarez, and E. Sztul.** 2003. ADP-ribosylation factor/COPI-dependent events at the endoplasmic reticulum-Golgi interface are regulated by the guanine nucleotide exchange factor GBF1. Mol Biol Cell 14:2250-61.

21. **Gazina, E. V., J. M. Mackenzie, R. J. Gorrell, and D. A. Anderson.** 2002. Differential requirements for COPI coats in formation of replication complexes among three genera of Picornaviridae. J Virol 76:11113-22.

22. **Gosert, R., A. Kanjanahaluethai, D. Egger, K. Bienz, and S. C. Baker.** 2002. RNA replication of mouse hepatitis virus takes place at double-membrane vesicles. J Virol 76:3697-708.

23. **Harcourt, B. H., D. Jukneliene, A. Kanjanahaluethai, J. Bechill, K. M. Severson, C. M. Smith, P. A. Rota, and S. C. Baker.** 2004. Identification of severe acute respiratory syndrome coronavirus replicase products and characterization of papain-like protease activity. J Virol 78:13600-12.

24. **Helms, J. B., and J. E. Rothman.** 1992. Inhibition by brefeldin A of a Golgi membrane enzyme that catalyses exchange of guanine nucleotide bound to ARF. Nature 360:352-4.

25. **Hu, T., and J. H. Exton.** 2005. 1-Butanol interferes with phospholipase D1 and protein kinase Calpha association and inhibits phospholipase D1 basal activity. Biochem Biophys Res Commun 327:1047-51.

26. **Hunziker, W., J. A. Whitney, and I. Mellman.** 1991. Selective inhibition of transcytosis by brefeldin A in MDCK cells. Cell 67:617-27.

27. **Irurzun, A., L. Perez, and L. Carrasco.** 1993. Brefeldin A blocks protein glycosylation and RNA replication of vesicular stomatitis virus. FEBS Lett 336:496-500.

28. **Irurzun, A., L. Perez, and L. Carrasco.** 1992. Involvement of membrane traffic in the replication of poliovirus genomes: effects of brefeldin A. Virology 191:166-75.

29. **Jackson, C. L.** 2004. The Sec7 Family of Arf Guanine Nucleotide Exchange Factors p. 71-99, Proteins and Cell Regulation, vol. 1. Springer Netherlands.

30. **Jackson, C. L., and J. E. Casanova.** 2000. Turning on ARF: the Sec7 family of guanine-nucleotide-exchange factors. Trends Cell Biol 10:60-7.

31. **Jenkins, G. M., and M. A. Frohman.** 2005. Phospholipase D: a lipid centric review. Cell Mol Life Sci 62:2305-16.

32. **Kanjanahaluethai, A., Z. Chen, D. Jukneliene, and S. C. Baker.** 2007. Membrane topology of murine coronavirus replicase non-structuralprotein 3. Virology 361:391-401.

33. **Kawamoto, K., Y. Yoshida, H. Tamaki, S. Torii, C. Shinotsuka, S. Yamashina, and K. Nakayama.** 2002. GBF1, a guanine nucleotide exchange factor for ADP-ribosylation factors, is localized to the cis-Golgi and involved in membrane association of the COPI coat. Traffic 3:483-95.

34. **Kawasaki, M., K. Nakayama, and S. Wakatsuki.** 2005. Membrane recruitment of effector proteins by Arf and Rab GTPases. Curr Opin Struct Biol 15:681-9.

35. **Klumperman, J., J. K. Locker, A. Meijer, M. C. Horzinek, H. J. Geuze, and P. J. Rottier.** 1994. Coronavirus M proteins accumulate in the Golgi complex beyond the site of virion budding. J Virol 68:6523-34.

36. **Knox, C., K. Moffat, S. Ali, M. Ryan, and T. Wileman.** 2005. Foot-and-mouth disease virus replication sites form next to the nucleus and close to the Golgi apparatus, but exclude marker proteins associated with host membrane compartments. J Gen Virol 86:687-96.

37. **Kuo, L., G. J. Godeke, M. J. Raamsman, P. S. Masters, and P. J. Rottier.** 2000. Retargeting of coronavirus by substitution of the spike glycoprotein ectodomain: crossing the host cell species barrier. J Virol 74:1393-406.

38. **Lee, F. J., L. A. Stevens, L. M. Hall, J. J. Murtagh, Jr., Y. L. Kao, J. Moss, and M. Vaughan.** 1994. Characterization of class II and class III ADP-ribosylation factor genes and proteins in Drosophila melanogaster. J Biol Chem 269:21555-60.

39. **Lee, M. C., E. A. Miller, J. Goldberg, L. Orci, and R. Schekman.** 2004. Bi-directional protein transport between the ER and Golgi. Annu Rev Cell Dev Biol 20:87-123.

40. **Lee, T. H., and A. D. Linstedt.** 2000. Potential role for protein kinases in regulation of bidirectional endoplasmic reticulum-to-Golgi transport revealed by protein kinase inhibitor H89. Mol Biol Cell 11:2577-90.

41. **Lippincott-Schwartz, J., T. H. Roberts, and K. Hirschberg.** 2000. Secretory protein trafficking and organelle dynamics in living cells. Annu Rev Cell Dev Biol 16:557-89.

42. **Lippincott-Schwartz, J., L. C. Yuan, J. S. Bonifacino, and R. D. Klausner.** 1989. Rapid redistribution of Golgi proteins into the ER in cells treated with brefeldin A: evidence for membrane cycling from Golgi to ER. Cell 56:801-13.

43. **Lu, X. T., A. C. Sims, and M. R. Denison.** 1998. Mouse hepatitis virus 3C-like protease cleaves a 22-kilodalton protein from the open reading frame 1a polyprotein in virus-infected cells and *in vitro*. J Virol 72:2265-71.

44. **Mackenzie, J.** 2005. Wrapping things up about virus RNA replication. Traffic 6:967-77.

45. **Mackenzie, J. M., M. K. Jones, and E. G. Westaway.** 1999. Markers for trans-Golgi membranes and the intermediate compartment localize to induced membranes with distinct replication functions in flavivirus-infected cells. J Virol 73:9555-67.

46. **Madan, V., M. A. Sanz, and L. Carrasco.** 2005. Requirement of the vesicular system for membrane permeabilization by Sindbis virus. Virology 332:307-15.

47. **Maynell, L. A., K. Kirkegaard, and M. W. Klymkowsky.** 1992. Inhibition of poliovirus RNA synthesis by brefeldin A. J Virol 66:1985-94.

48. **Melancon, P., X. Zhao, and T. K. R. Lasell.** 2004. Large ARF GEFs of the Golgi complex, p. 101-119, Proteins and Cell Regulation, vol. 1. Springer Netherlands.

49. **Mirazimi, A., C. H. von Bonsdorff, and L. Svensson.** 1996. Effect of brefeldin A on rotavirus assembly and oligosaccharide processing. Virology 217:554-63.

50. **Misumi, Y., Y. Misumi, K. Miki, A. Takatsuki, G. Tamura, and Y. Ikehara.** 1986. Novel blockade by brefeldin A of intracellular transport of secretory proteins in cultured rat hepatocytes. J Biol Chem 261:11398-403.

51. **Molina, S., M. A. Sanz, V. Madan, I. Ventoso, A. Castello, and L. Carrasco.** 2007. Differential inhibition of cellular and Sindbis virus translation by brefeldin A. Virology 363:430-6.

52. **Nakamura, N., M. Lowe, T. P. Levine, C. Rabouille, and G. Warren.** 1997. The vesicle docking protein p115 binds GM130, a cis-Golgi matrix protein, in a mitotically regulated manner. Cell 89:445-55.

53. **Nie, Z., D. S. Hirsch, and P. A. Randazzo.** 2003. Arf and its many interactors. Curr Opin Cell Biol 15:396-404.

54. **Niu, T. K., A. C. PfeIFer, J. Lippincott-Schwartz, and C. L. Jackson.** 2005. Dynamics of GBF1, a Brefeldin A-sensitive Arf1 exchange factor at the Golgi. Mol Biol Cell 16:1213-22.

55. **Novoa, R. R., G. Calderita, R. Arranz, J. Fontana, H. Granzow, and C. Risco.** 2005. Virus factories: associations of cell organelles for viral replication and morphogenesis. Biol Cell 97:147-72.

56. **Oostra, M., E. G. te Lintelo, M. Deijs, M. H. Verheije, P. J. M. Rottier, and C. A. M. de Haan.** 2007. Localization and membrane topology of the coronavirus non-structuralprotein 4: involvement of the early secretory pathway in replication. J.Virol.

57. **Opstelten, D. J., M. J. Raamsman, K. Wolfs, M. C. Horzinek, and P. J. Rottier.** 1995. Envelope glycoprotein interactions in coronavirus assembly. J Cell Biol 131:339-49.

58. **Orci, L., A. Perrelet, M. Ravazzola, F. T. Wieland, R. Schekman, and J. E. Rothman.** 1993. "BFA bodies": a subcompartment of the endoplasmic reticulum. Proc Natl Acad Sci U S A 90:11089-93.

59. **Pedersen, K. W., Y. van der Meer, N. Roos, and E. J. Snijder.** 1999. Open reading frame 1a-encoded subunits of the arterivirus replicase induce endoplasmic reticulum-derived double-membrane vesicles which carry the viral replication complex. J Virol 73:2016-26.

60. **Pelkmans, L., E. Fava, H. Grabner, M. Hannus, B. Habermann, E. Krausz, and M. Zerial.** 2005. Genome-wide analysis of human kinases in clathrin- and caveolae/raft-mediated endocytosis. Nature 436:78-86.

61. **Pepperkok, R., M. Lowe, B. Burke, and T. E. Kreis.** 1998. Three distinct steps in transport of vesicular stomatitis virus glycoprotein from the ER to the cell surface *in vivo* with differential sensitivities to GTP gamma S. J Cell Sci 111 (Pt 13):1877-88.

62. **Peters, P. J., V. W. Hsu, C. E. Ooi, D. Finazzi, S. B. Teal, V. Oorschot, J. G. Donaldson, and R. D. Klausner.** 1995. Overexpression of wild-type and mutant ARF1 and ARF6: distinct perturbations of nonoverlapping membrane compartments. J Cell Biol 128:1003-17.

63. **Polo, J. M., B. A. Belli, D. A. Driver, I. Frolov, S. Sherrill, M. J. Hariharan, K. Townsend, S. Perri, S. J. Mento, D. J. Jolly, S. M. Chang, S. Schlesinger, and T. W. Dubensky, Jr.** 1999. Stable alphavirus packaging cell lines for Sindbis virus and Semliki Forest virus-derived vectors. Proc Natl Acad Sci U S A 96:4598-603.

64. **Prentice, E., W. G. Jerome, T. Yoshimori, N. Mizushima, and M. R. Denison.** 2004. Coronavirus replication complex formation utilizes components of cellular autophagy. J Biol Chem 279:10136-41.

65. **Ritzenthaler, C., C. Laporte, F. Gaire, P. Dunoyer, C. Schmitt, S. Duval, A. Piequet, A. M. Loudes, O. Rohfritsch, C. Stussi-Garaud, and P. PfeIFfer.** 2002. Grapevine fanleaf virus replication occurs on endoplasmic reticulum-derived membranes. J Virol 76:8808-19.

66. **Rossen, J. W., G. J. Strous, M. C. Horzinek, and P. J. Rottier.** 1997. Mouse hepatitis virus strain A59 is released from opposite sides of different epithelial cell types. J Gen Virol 78 (Pt 1):61-9.

67. **Roth, M. G., K. Bi, N. T. Ktistakis, and S. Yu.** 1999. Phospholipase D as an effector for ADP-ribosylation factor in the regulation of vesicular traffic. Chem Phys Lipids 98:141-52.

68. **Rust, R. C., L. Landmann, R. Gosert, B. L. Tang, W. Hong, H. P. Hauri, D. Egger, and K. Bienz.** 2001. Cellular COPII proteins are involved in production of the vesicles that form the poliovirus replication complex. J Virol 75:9808-18.

69. **Salonen, A., T. Ahola, and L. Kaariainen.** 2005. Viral RNA replication in association with cellular membranes. Curr Top Microbiol Immunol 285:139-73.

70. **Schekman, R., and L. Orci.** 1996. Coat proteins and vesicle budding. Science 271:1526-33.

71. **Shi, S. T., J. J. Schiller, A. Kanjanahaluethai, S. C. Baker, J. W. Oh, and M. M. Lai.** 1999. Colocalization and membrane association of murine hepatitis virus gene 1 products and De novo-synthesized viral RNA in infected cells. J Virol 73:5957-69.

72. **Sims, A. C., J. Ostermann, and M. R. Denison.** 2000. Mouse hepatitis virus replicase proteins associate with two distinct populations of intracellular membranes. J Virol 74:5647-54.

73. **Snijder, E. J., Y. van der Meer, J. Zevenhoven-Dobbe, J. J. Onderwater, J. van der Meulen, H. K. Koerten, and A. M. Mommaas.** 2006. Ultrastructure and origin of membrane vesicles associated with the severe acute respiratory syndrome coronavirus replication complex. J Virol 80:5927-40.

74. **Stertz, S., M. Reichelt, M. Spiegel, T. Kuri, L. Martinez-Sobrido, A. Garcia-Sastre, F. Weber, and G. Kochs.** 2007. The intracellular sites of early replication and budding of SARS-coronavirus. Virology 361:304-15.

75. **Suikkanen, S., M. Antila, A. Jaatinen, M. Vihinen-Ranta, and M. Vuento.** 2003. Release of canine parvovirus from endocytic vesicles. Virology 316:267-80.

76. **Szul, T., R. Garcia-Mata, E. Brandon, S. Shestopal, C. Alvarez, and E. Sztul.** 2005. Dissection of membrane dynamics of the ARF-guanine nucleotide exchange factor GBF1. Traffic 6:374-85.

77. **Taguchi, F., and J. O. Fleming.** 1989. Comparison of six different murine coronavirus JHM variants by monoclonal antibodies against the E2 glycoprotein. Virology 169:233-5.

78. **Tannous, B. A., D. E. Kim, J. L. Fernandez, R. Weissleder, and X. O. Breakefield.** 2005. Codon-optimized Gaussia luciferase cDNA for mammalian gene expression in culture and *in vivo*. Mol Ther 11:435-43.

79. **van der Meer, Y., E. J. Snijder, J. C. Dobbe, S. Schleich, M. R. Denison, W. J. Spaan, and J. K. Locker.** 1999. Localization of mouse hepatitis virus non-structuralproteins and RNA synthesis indicates a role for late endosomes in viral replication. J Virol 73:7641-57.

80. **Vasudevan, C., W. Han, Y. Tan, Y. Nie, D. Li, K. Shome, S. C. Watkins, E. S. Levitan, and G. Romero.** 1998. The distribution and translocation of the G protein ADP-ribosylation factor 1 in live cells is determined by its GTPase activity. J Cell Sci 111 (Pt 9):1277-85.

81. **Volpicelli-Daley, L. A., Y. Li, C. J. Zhang, and R. A. Kahn.** 2005. Isoform-selective effects of the depletion of ADP-ribosylation factors 1-5 on membrane traffic. Mol Biol Cell 16:4495-508.

82. **Wagner, M., A. K. Rajasekaran, D. K. Hanzel, S. Mayor, and E. Rodriguez-Boulan.** 1994. Brefeldin A causes structural and functional alterations of the trans-Golgi network of MDCK cells. J Cell Sci 107 (Pt 4):933-43.

83. **Wang, E., J. G. Pennington, J. R. Goldenring, W. Hunziker, and K. W. Dunn.** 2001. Brefeldin A rapidly disrupts plasma membrane polarity by blocking polar sorting in common endosomes of MDCK cells. J Cell Sci 114:3309-21.

84. **Ward, T. H., R. S. Polishchuk, S. Caplan, K. Hirschberg, and J. Lippincott-Schwartz.** 2001. Maintenance of Golgi structure and function depends on the integrity of ER export. J Cell Biol 155:557-70.

85. **Wurdinger, T., M. H. Verheije, M. Raaben, B. J. Bosch, C. A. de Haan, V. W. van Beusechem, P. J. Rottier, and W. R. Gerritsen.** 2005. Targeting non-human coronaviruses to human cancer cells using a bispecific single-chain antibody. Gene Ther 12:1394-404.

86. **Zhao, X., T. K. Lasell, and P. Melancon.** 2002. Localization of large ADP-ribosylation factor-guanine nucleotide exchange factors to different Golgi compartments: evidence for distinct functions in protein traffic. Mol Biol Cell 13:119-33.

Chapter 5

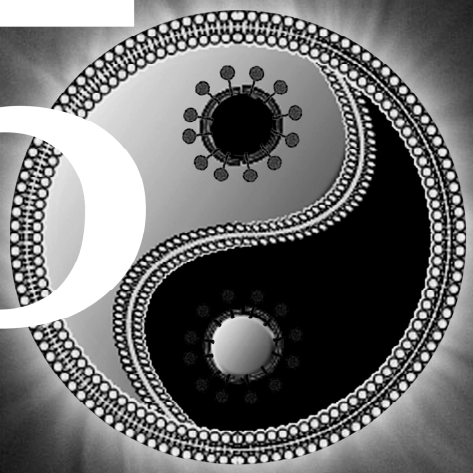

The Ubiquitin-Proteasome System Plays an Important Role in Coronavirus Cell Entry and Replication

Matthijs Raaben
Monique H. Verheije
Eddie te Lintelo
Clara C. Posthuma
Eric J. Snijder
Peter J.M. Rottier
Cornelis A.M. de Haan

Manuscript in preparation.

Abstract

The ubiquitin-proteasome system (UPS) is a key player in regulating the intracellular sorting and degradation of proteins. Viruses from diverse families are known to require the UPS for efficient replication. In this study we analyzed its role during coronavirus (CoV) infection. We interfered with the functioning of the UPS either by treating cells with chemical inhibitors of the proteasome, or by using cells which contain a temperature-sensitive ubiquitin-activating enzyme E1, or by depletion of ubiquitin with small interfering RNAs. Inhibition of the proteasome by different chemical compounds (i.e. MG132, Epoxomicin and Velcade) appeared to not only impair virus entry, but also RNA replication of different CoVs (i.e. mouse hepatitis virus [MHV], feline infectious peritonitis virus, and severe acute respiratory syndrome CoV). MHV assembly and release were, however, not appreciably affected by these compounds. The inhibitory effect on CoV replication did not result from an induced cellular stress response, as replication was equally sensitive to the compounds in cells lacking the stress kinase GCN2. MHV RNA replication was not only affected by inhibition of the proteasome, but also when we interfered with protein ubiquitination. Replication was reduced in cells expressing a temperature-sensitive ubiquitin-activating enzyme E1 at the restrictive temperature, as well as in cells, in which ubiquitin was depleted by using small interfering RNAs. However, the number of infected cells was not affected under these conditions, excluding an important role of ubiquitination in virus entry. These results offer new insights into the role of the UPS in CoV entry and replication and identify the UPS as an attractive anti-CoV drug target.

Introduction

The cellular ubiquitin-proteasome system (UPS), which is the most important pathway of intracellular protein degradation in eukaryotic cells, plays a central role in cellular protein homeostasis (55, 59). All viruses exploit and manipulate the machinery of the host cell for their own advantage. Also the cellular UPS has been shown to be important in several stages of the infection cycle of different viruses (7, 13, 46, 50, 65).

Proteins destined for proteasomal degradation are conjugated with chains of the small protein ubiquitin, which constitute the recognition motif for the proteasome (21). Besides targeting proteins for degradation, conjugation with ubiquitin can also regulate intracellular protein sorting, as has been described for numerous membrane proteins (22). Attachment of ubiquitin moieties to protein substrates occurs by the sequential action of three enzymes. First, the ubiquitin-activating enzyme E1 forms a high-energy thiolester bond with ubiquitin, after which ubiquitin is transferred to the ubiquitin-conjugating enzyme E2. Subsequently, the ubiquitin is conjugated to a lysine side chain of the substrate by the corporate action of E2 and an ubiquitin ligase E3. Conjugated ubiquitin can be removed or trimmed by so-called deubiquitinating enzymes. Poly-ubiquitinated substrates can enter the catalytic 20S core complex of the proteasome, which subsequently cleaves the proteins into smaller peptides. The proteasome can control direct hydrolysis of functionally active protein, but also the degradation of misfolded polypeptides. Altogether, the cellular UPS controls many different processes, which include regulation of cell cycle progression, apoptosis, and antigen presentation (18).

Coronaviruses (CoVs) are enveloped, positive-stranded RNA viruses and are common pathogens in many animal species. With a genome of 28 to 32 kb, CoVs are the largest enveloped RNA viruses known to date. Several of these viruses cause severe disease in animals, including porcine transmissible gastroenteritis virus (TGEV), bovine coronavirus (BCoV), avian infectious bronchitis viruses (IBV), and feline infectious peritonitis virus (FIPV). With the emergence of new human CoVs (HCoVs), such as the severe acute respiratory syndrome (SARS)-CoV) (14), HCoV-NL63 (57), and HCoV-HKU1 (62), the interest in CoV research has significantly increased. The well studied mouse hepatitis virus (MHV) is often used as model CoV.

Also CoVs depend on the cellular machinery for efficient replication at virtually every step of their life cycle. The CoV replication cycle starts with attachment of the virus to specific cellular receptors. The spike (S) class I fusion protein is responsible for virus entry, mediating both binding to a specific receptor on the target cell and subsequent fusion of the viral envelope with a cellular limiting membrane (6). Following virus entry, the viral genome is released into the cytoplasm of the cell where replication takes place. Upon translation of the genomic RNA, two large polyproteins are synthesized and autoproteolytically processed, the products of which cooperatively form the replication-transcription complexes that are associated with double membrane vesicles (4, 19, 49). Subsequently, a nested set of (sub)genomic mRNAs is being produced (39), which encode among others the viral structural proteins. These proteins, together with the newly synthesized genomic RNA, assemble the progeny virions via budding through the membranes at the ER-to-Golgi intermediate compartment (ERGIC) (30). The newly synthesized virions are subsequently released by exocytosis.

In this study we have analyzed the role of the UPS during CoV infection. While a previous study has reported that inhibition of the proteasome affected entry of MHV (63), no in depth analysis of the role of the UPS in the CoV infectious cycle has been performed. Here, we interfered with the UPS either by treating cells with chemical inhibitors of the proteasome, by using cells that express a temperature-sensitive ubiquitin-activating enzyme E1, or by depletion of ubiquitin with small interfering (si)RNAs. While MHV replication was severely reduced under all three experimental conditions, virus entry was only affected by the chemical inhibitors of the proteasome.

Results

MG132 Inhibits MHV Entry and Replication

We started our analysis of the role of the UPS in the CoV infection cycle, by studying the one-step growth of MHV strain A59 (MHV-A59) in absence or presence of the well-known proteasome inhibitor MG132. In this assay the effect of proteasome inhibition on any step of the infection cycle is investigated. To this end, LR7 cells were inoculated with MHV-EFLM in the presence or absence of 10 μM MG132. MHV-EFLM is a recombinant virus that expresses the firefly luciferase (FL) reporter gene (12). Virus RNA replication, which

was measured by determining the intracellular FL activity at different time-points post infection (p.i.), was significantly reduced in the presence of MG132 (Fig.1A). The extracellular accumulation of progeny virions also appeared to be affected, although this reduction may also be a reflection of reduced synthesis of viral proteins (Fig.1A).

To determine which specific step(s) of the MHV replication cycle was/were affected by proteasome inhibition, we evaluated the effects of adding MG132 to the culture media at different time-points. First we determined the dose-response curves when the drug was applied either already during (i.e. from 0 till 6 h post inoculation) or after the virus inoculation period (i.e. from 2-6 h or from 2-8 h post inoculation). As shown in Fig.1B, virus replication was much more affected when the drug was already present during virus inoculation (IC_{50} = 0.17 μM) than upon addition of the drug at 2 h p.i. (IC_{50} ~ 0.5 μM). The length of the MG132 post-incubation period did not affect the IC_{50} values strongly (compare the 2-6 and 2-8 h periods). These results indicate that both virus replication and entry are affected by proteasome inhibition.

The inhibition of MHV entry by MG132 is in agreement with a previous study (63). In this report, however, MHV strain 4 (MHV-4, also known as MHV-JHM) was found to be affected by inhibition of the proteasome more severely than MHV-A59. Since the route of entry into cells is dependent both on the virus strain and on the cell type used (15, 35), and the S protein of MHV is the sole viral determinant of cellular entry, we next investigated the effect of proteasome inhibition on the entry of two recombinant viruses only differing in their S protein. To this end, we constructed a virus that contained the S gene of MHV-4 (16) in the MHV-EFLM background (strain A59). Replication of this virus (i.e. MHV-S_4-EFLM) was monitored in the presence and absence of MG132. As shown in Fig.1C, very similar results were obtained for both viruses, regardless of their spike protein. A similar antiviral effect of MG132 was also observed for both viruses upon infection of HeLa cells expressing the MHV receptor (data not shown).

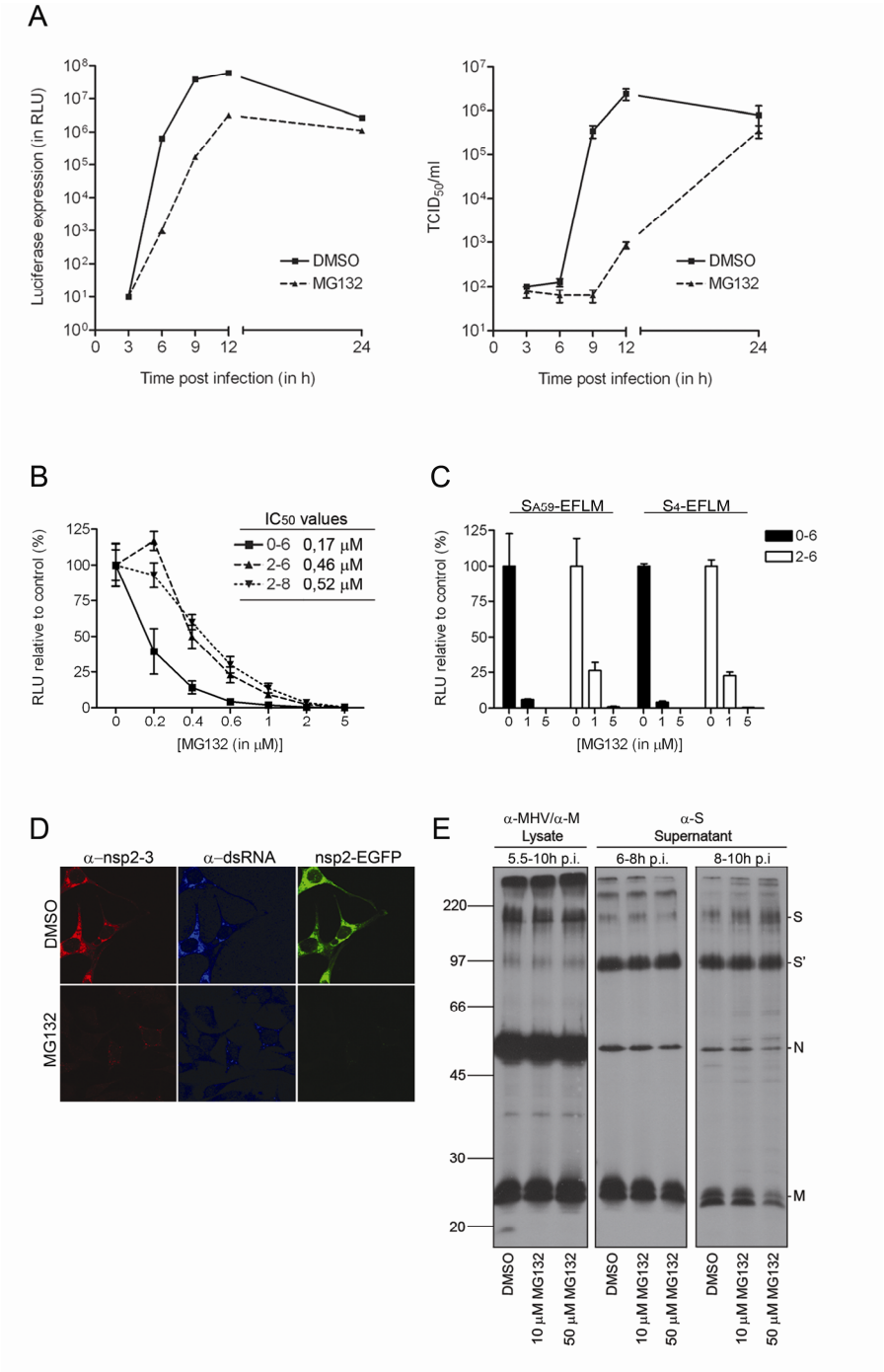
A
Luciferase expression (in RLU)
DMSO
MG132
Time post infection (in h)
TCID50/ml
DMSO
MG132
Time post infection (in h)
B
RLU relative to control (%)
IC50 values
0-6 0,17 µM
2-6 0,46 µM
2-8 0,52 µM
[MG132 (in µM)]
C
SA59-EFLM
S4-EFLM
0-6
2-6
RLU relative to control (%)
[MG132 (in µM)]
D
α–nsp2-3
α–dsRNA
nsp2-EGFP
DMSO
MG132
E
α-MHV/α-M
Lysate
α-S
Supernatant
5.5-10h p.i.
6-8h p.i.
8-10h p.i
220
97
66
45
30
20
S
S'
N
M
DMSO
10 µM MG132
50 µM MG132

Fig.1 MHV infection is reduced by treatment with MG132. (A) LR7 cells were infected with MHV-EFLM (MOI 1) in the presence of 10 μM MG132. As a control, the cells were treated with an equal volume of vehicle (DMSO). The intracellular luciferase expression levels, at the indicated time-points p.i., were determined in relative light units (RLU). Standard deviations (n = 3) are indicated. In parallel, culture media were collected at the different times p.i. after which the viral infectivity was determined by a quantal assay on LR7 cells. The 50% tissue culture infectious dose ($TCID_{50}$) values are indicated. (B) LR7 cells were infected with MHV-EFLM in the absence (DMSO control) or presence of different concentrations of MG132. The drug was added from 0-6, 2-6, or 2-8 h p.i., after which the intracellular luciferase expression levels were determined. Luciferase expression is indicated as a percentage relative to the DMSO control. The 50% inhibitory concentrations (IC_{50}) values for each condition are indicated in the graph. (C) LR7 cells were infected with MHV-EFLM containing either the A59 spike (S_{A59}-EFLM) or the JHM spike (S_4-EFLM), in the absence or presence of different concentration of MG132. The drug was present from 0-6 or from 2-6 h p.i. The luciferase expression levels were determined and are indicated relative to the DMSO control. (D) MHV-nsp2EGFP infected LR7 cells were mock treated or treated with 10 μM MG132 from 2-7 h p.i. At 7 h post inoculation, cells were fixed and processed for immunofluorescence as described in the *Material & Methods*. (E) MHV-infected cells were labeled for 30 min at 5 h p.i. with [^{35}S] labeled amino acids and subsequently chased from 5.5-10 h p.i. Progeny virions released into the culture medium from 6-8 and from 8-10 h p.i. were affinity purified using antibodies against the S protein. At 10 h p.i., the cells were lysed and processed for immunoprecipitation with anti-MHV serum. Immunoprecipitates were analyzed by SDS-PAGE. Cells were mock-treated or treated with 10 or 50 μM MG132 from 5.5 h p.i. onwards. The molecular weight markers are indicated at the left, while the positions of the MHV structural proteins (i.e. M, N, and S) in the gel are depicted at the right (S' represents the furin-cleaved forms of the S proteins).

Confocal microscopy was used to confirm the inhibition of MHV replication by MG132. To this end, an infection experiment was performed using a recombinant virus that expressed a nsp2-GFP fusion protein. In this experiment, LR7 cells infected with MHV-nsp2EGFP were mock-treated or treated with MG132 from 2-7 h p.i. Subsequently, the cells were stained for two markers of the replication sites (i.e. non-structural protein [nsp]2-3 and dsRNA). In agreement with our previous results, in the presence of MG132 much less nsp2-3, dsRNA, and nsp2EGFP was produced than in the control cells. (Fig.1D).

The UPS has been demonstrated to play an important role in the assembly and release of several viruses (20, 53, 56, 60). The impaired appearance of extracellular infectivity shown in Fig.1A may indicate a similar effect of MG132 on assembly of MHV. Therefore we studied the effect of the drug on the synthesis and release of MHV particles using an assembly assay. In this assay, cells infected with MHV were metabolically labeled from 5-5.5 h p.i. in the absence of MG132. Subsequently, the cells were chased in the presence of

cycloheximide to inhibit protein synthesis and, in addition, were mock-treated or treated with MG132. After 30 min (i.e. at 6 h p.i.), the chase medium was refreshed and the release of newly assembled viral particles was monitored from 6-8 and from 8-10 h p.i. Virus particles were affinity-isolated from the culture media harvested at 8 or 10 h p.i. using antibodies to the S protein. At 10 h p.i., cells were lysed, and cell lysates were monitored for viral protein production. As shown in Fig.1E, no appreciable effect of MG132 on virus assembly could be observed. Only in the presence of 50 μM MG132, a slight decrease in the amount of immunoprecipitated M protein was detected. From these results we conclude that the proteasome inhibitor MG132 affects MHV entry and replication. Assembly of MHV was not affected by the drug.

The Inhibitory Effect of MG132 does Not Result From Induction of a Cellular Stress Response

Previously, Neznanov and co-workers showed that the inhibitory effect of proteasome inhibition on vesicular stomatitis virus (VSV) infection was partially caused by the induction of a cellular stress response, the initiation of which required the protein kinase GCN2 (36). Upon activation, this kinase phosphorylates serine 51 of eukaryotic initiation factor 2α (eIF2α), which results in global translational repression (2, 3). To test whether the inhibition of the proteasome affected MHV replication via the induction of a stress response, we infected wild-type and GCN2 knock-out ($GCN2^{-/-}$) as well as $eIF2\alpha^{S51S}$ wild-type and $eIF2\alpha^{S51A}$ mutant mouse embryonic fibroblasts with MHV-EFLM. The cells were subsequently treated with MG132 or mock-treated from 2-6 h p.i. In all different cells, MHV replication was severely affected by treatment with MG132 (Fig.2A). As a control, we performed the same experiment with a recombinant VSV expressing FL (VSV-FL). Consistent with previous results (3, 9), replication of VSV was markedly increased in the $GCN2^{-/-}$ and $eIF2\alpha^{S51A}$ cells when compared to the parental cells (data not shown). However replication of VSV was only modestly affected by the addition of MG132 in all cells tested (Fig.2A). Next, the effect of proteasome inhibition on mRNA translation was investigated by transfection of synthetic luciferase reporter mRNAs in cells, after which they were treated for 4 h with 10 μM MG132. Subsequently, cells were lysed and intracellular luciferase levels were determined. As shown in Fig.2B, treatment with MG132

did not inhibit mRNA translation. In addition, we performed metabolic labeling of LR7 cells treated for 4 h with MG132. Also here, no significant differences in the amount of protein synthesis could be detected (Fig.2C). From these results, we conclude that the inhibitory effect of MG132 on virus replication is specific for MHV, as it is not observed for VSV, and not caused by the induction of a stress response.

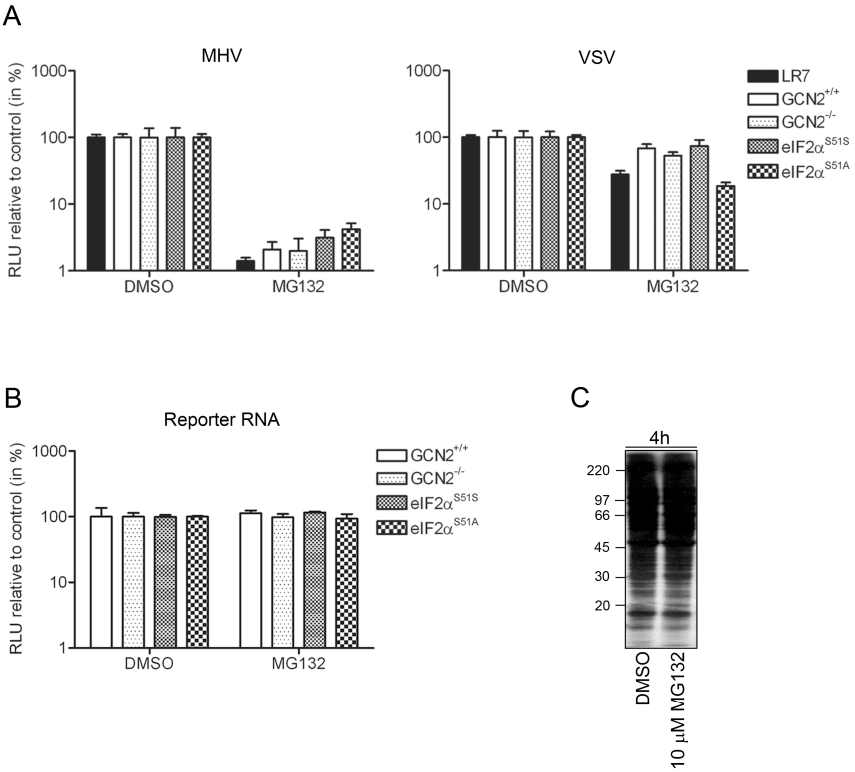

Fig.2. The inhibitory effect of MG132 on MHV replication does not result from induction of a cellular stress response. (A) The different cells (i.e. LR7, $GCN2^{+/+}$, $GCN2^{-/-}$, $eIF2^{S51S}$, and $eIF2^{S51A}$) were infected with MHV-EFLM or with VSV-FL and subsequently cultured in the absence or presence of 10 μM MG132 (from 2-6 h p.i.). The intracellular luciferase expression levels at 6 h p.i. are indicated as a percentage relative to the DMSO control of each individual cell line. Standard deviations (n = 6) are indicated. (B) The cells were transfected with the reporter RNA and subsequently cultured in the absence or presence of 10 μM MG132 (from 2-6 h post transfection). The luciferase levels at 6 h post transfection are indicated as a percentage relative to the DMSO control. (C) Metabolic labeling of LR7 cells that were treated for 4 h with 10 μM MG132 or mock-treated. Cell lysates were analyzed by SDS-PAGE. The molecular weight markers are indicated at the left.

Coronavirus Replication is Affected by Different Proteasome Inhibitors

Next, we studied whether the inhibition of virus replication caused by MG132 is specific for this proteasome inhibitor or whether it is also observed when other inhibitors of the proteasome are used. While MG132 has been shown to also inhibit other proteases than the proteasome (i.e. cathepsin A and tripeptidyl peptidase II) (29), epoxomycin and lactacystin target the proteasome more specifically (33, 38). Epoxomicin reduced MHV replication in LR7 cells approximately to the same extent as MG132, both when added during virus inoculation and directly thereafter (Fig.3A). Lactacystin, however, was not very potent in its antiviral activity under these experimental conditions. In agreement with the results obtained for MG132, both drugs affected MHV replication more extensively when already applied during the inoculation period than thereafter.

To confirm that these drugs indeed block proteasome activity we applied them to LR7 cells expressing a GFP protein containing a degron sequence. Under normal conditions this protein is not stable and thus not detected (23). However, when MG132 or epoxomicin were applied to these cells, GFP expression was stabilized in a concentration-dependent manner, which correlated with the inhibitory effect of the drugs on MHV replication (Fig.3B). Consistently, lactacystin was much less effective in this assay, in agreement with its limited antiviral activity.

Subsequently, we evaluated whether the antiviral activity of the proteasome inhibitors also holds true for other CoV family members. In these experiments we used the dipeptide boronic acid proteasome inhibitor bortezomib (Velcade), which is a drug approved for clinical use against multiple myeloma (44), and applied it to cells infected with either MHV, FIPV, or SARS-CoV. Velcade demonstrated a dose-dependent antiviral effect for all three CoVs (Fig.3C), with the strongest effect being observed when the drug was applied 1 h prior to the infection. Velcade exhibited a similar potency as MG132 and epoxomycin with respect to its antiviral activity and its ability to stabilize GFP-degron expression (data not shown). Overall, these results demonstrate that inhibition of virus entry and replication by proteasome inhibitors is a general feature of CoVs. Furthermore, the antiviral activity of these inhibitors correlates with their ability to inhibit the proteasome.

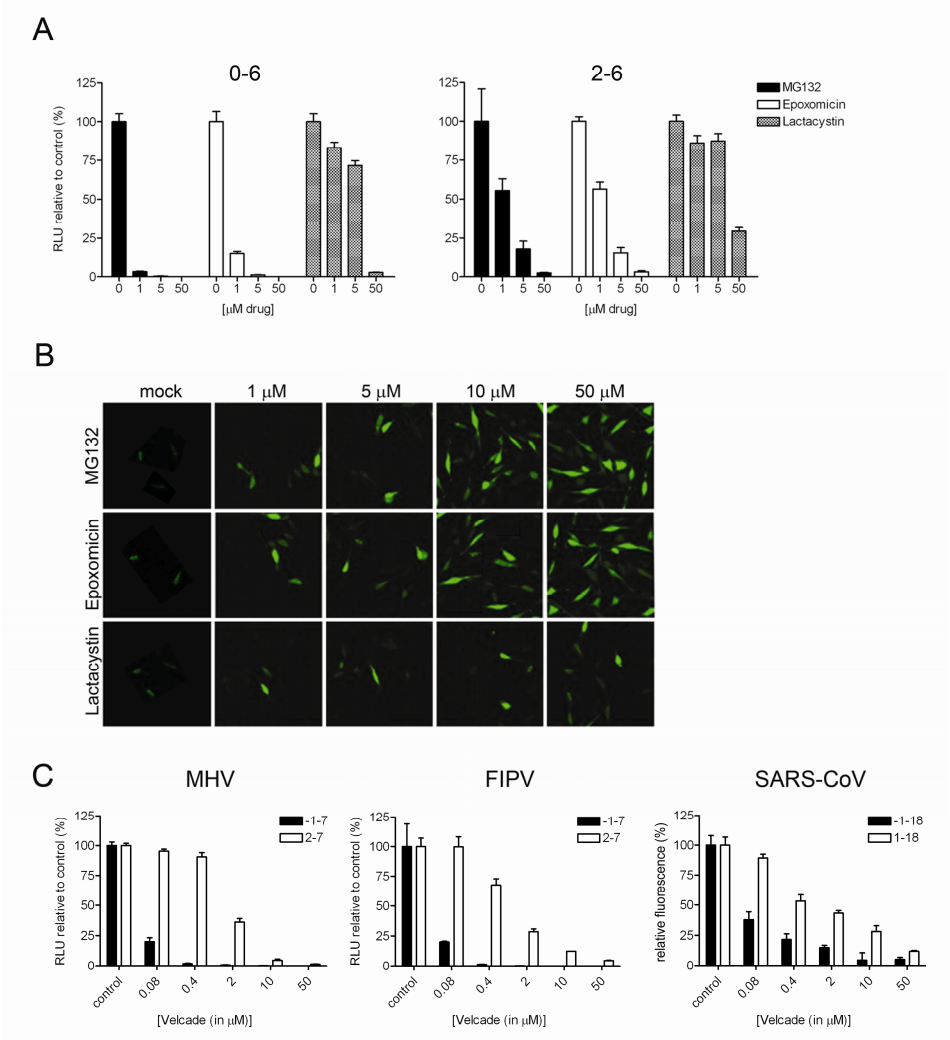

Fig.3. MHV infection is reduced by treatment with multiple proteasome inhibitors. (A) LR7 cells were infected with MHV-EFLM in the absence or presence of different concentrations of the inhibitors MG132, epoxomicin, and lactacystin. The compounds were added either from 0-6 or from 2-6 h post virus inoculation. The intracellular luciferase expression levels at 6 h p.i. are indicated as a percentage relative to the DMSO control. (B) LR7 cells transfected with the pEGFP-degron plasmid were treated with the indicated concentrations of the inhibitors for 6 h. Subsequently, the cells were fixed and processed for microscopical analysis. Representative images for each condition are shown. (C) LR7 cells infected with MHV-EFLM, FCWF cells infected with FIPV-Δ3abcFL, and Vero cells infected with SARS-GFP were treated with different concentrations of Velcade for the indicated times p.i. The reporter gene expression levels (i.e. FL for MHV and FIPV, and GFP for SARS) were quantified and are indicated as a percentage relative to the PBS control. Standard deviations are indicated (n = 3).

Replication but Not Entry of MHV is Affected in Cells Deficient for Ubiquitin Conjugation

We subsequently determined the role of the host ubiquitination machinery in virus entry and replication, as proteins destined for proteasomal degradation are often, but not always, modified with ubiquitin. To investigate the effect of ubiquitination on MHV infection we first made use of cells (CHO-ts20) that exhibit a temperature-sensitive defect in ubiquitin conjugation, resulting from their expressing a thermo-labile ubiquitin activating enzyme E1. Wild-type cells (CHO-E36) were taken along as controls.

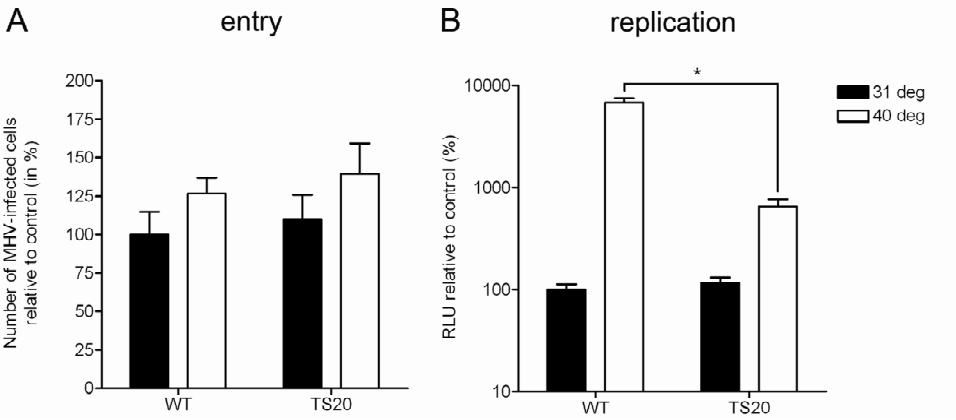

Fig.4. Replication but not entry of MHV is affected in cells deficient for ubiquitin conjugation. CHO-E36 (indicated as wild-type [WT]) or CHO-ts20 (indicated as TS20) cells grown in 24-wells clusters were infected with MHV-EFLM at the indicated temperatures (i.e. 31 and 40°C). Incubation was continued at the same temperatures for 8 h. (A) The total number of virus-infected cells per well for each condition was determined by staining for viral antigen using a polyclonal anti-MHV serum and are indicated as a percentage relative to the control. (B) In parallel, the intracellular luciferase expression levels at 8 h p.i. were determined, which are shown as a percentage relative to the expression levels at 31°C in the wild-type cells. Standard deviations are indicated (n = 6).

Both cell lines were transfected with a plasmid encoding the MHV receptor (i.e. Ceacam1a [12]) to render them susceptible to MHV infection and grown for 24 h at the permissive temperature. Subsequently, 1 h prior to inoculation with MHV-EFLM, the cells were placed at either the permissive (31°C) or the non-permissive (40°C) temperature. At 8 h p.i., cells were fixed and stained for viral antigen after which the virus positive cells were counted. In parallel, cells were lysed and FL activity was measured. At both 31°C and 40°C, an equal number of MHV-positive cells could be detected for both cell types (Fig.4A).

Replication, however, was severely reduced in the CHO-ts20 as compared to the parental cells when kept at 40°C (Fig.4B). While virus replication was significantly enhanced at 40°C in the wild-type cells, this was not observed to the same extent for the mutant cells. Overall, these results show that replication but not entry of MHV is significantly affected in cells that are deficient in ubiquitin conjugation.

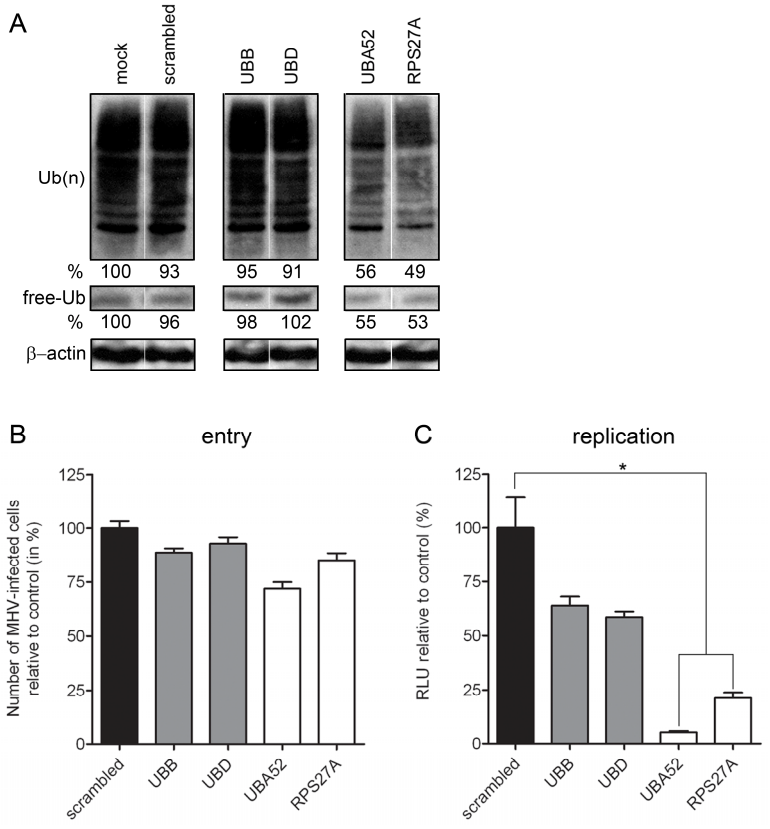

Fig.5. MHV replication is reduced in cells depleted for ubiquitin. HeLa-CEACAM1a cells grown in 96-wells clusters were transfected with 10 nM of siRNAs targeting the indicated ubiquitin genes. Mock- and scrambled siRNA-transfected cells were taken along as controls. (A) 72 h after transfection, cells were lysed and processed for Western blotting using antibodies against ubiquitin and β-actin (loading control). The levels of free ubiquitin and ubiquitin conjugates were quantified as described in *Material & Methods* and are expressed as a percentage relative to mock-transfected cells. Note that the values were corrected for the loading control. (B) The siRNA-transfected cells were inoculated with MHV-EFLM. Cells were fixed and stained for viral antigen using the polyclonal anti-MHV-serum. The total numbers of MHV-infected cells per well are indicated as a percentage relative to the control. Standard deviations are indicated (n = 3). (C) In parallel, the intracellular luciferase expression levels at 6 h p.i. are shown as a percentage relative to the control (scrambled siRNA-transfected cells). Note that the RLU values are corrected for cell viability.

Replication but Not Entry of MHV is Affected after Ubiquitin Depletion

To confirm the results obtained with the cells expressing a thermo-labile ubiquitin activating enzyme E1, we studied MHV entry and replication after ubiquitin depletion. Ubiquitin is synthesized in cells either in the form of polyubiquitin polypeptide chains or as ubiquitin-ribosomal protein fusions. Therefore, MHV infection was monitored after siRNA-mediated silencing of different ubiquitin-encoding genes (i.e. *UBA52*, *Rps27A*, *UBB*, and *UBD*). As depicted in Fig.5A, both the amount of poly-ubiquitinated proteins and free ubiquitin levels were clearly reduced when cells were treated with siRNAs targeting either *UBA52* or *Rps27A*, but not with siRNAs targeting *UBB* and *UBD*. Next, siRNA-treated cells were infected with MHV-EFLM, after which the number of MHV-positive cells was determined by immunocytochemistry. As shown in Fig.5B, entry of MHV was hardly affected by depletion of ubiquitin. In a parallel experiment, the luciferase expression levels were determined. The results show that MHV replication was significantly reduced in the *UBA52*- and *Rps27A*-depleted cells as compared to the siRNA control (Fig.5C), which correlated with the observed effects of ubiquitin depletion. These results, which are in agreement with those obtained with the CHO-ts20 cells, indicate that protein ubiquitination facilitates MHV replication, but is not important for entry into host cells.

Discussion

In the present study we have shown that a properly functioning UPS is required for optimal CoV entry and replication. Interfering with the UPS either by treating cells with chemical inhibitors of the proteasome, by using cells expressing a temperature sensitive ubiquitin-activating enzyme E1, or by depletion of ubiquitin with siRNAs, severely affected MHV replication. However, virus entry was only reduced after treatment with the proteasome inhibitors, not after interference with protein ubiquitination. Replication of other CoVs, besides MHV, was also affected by proteasome inhibition. Inhibition of CoV replication was specific as it was not observed for VSV. Moreover, it did not result from an induced stress response as it still occured in cells lacking the stress kinase GCN2.

Entry of CoVs appeared to be affected by different inhibitors of the proteasome. This is in agreement with a previous study that reported an inhibitory effect of MG132 on the entry of MHV (63). While in this study, MHV strain JHM was found to be more sensitive to

MG132 than MHV strain A59, we could not confirm that result when comparing the antiviral potency of MG132 against viruses carrying either an A59 or a JHM spike. For several other viruses, including influenza virus, herpes simplex virus, and minute virus of mice, proteasome inhibition has also been shown to affect virus entry (13, 27, 45).

What could be the mechanism of CoV entry inhibition? Proteasome inhibitors are known to reduce the levels of free ubiquitin in the cell (34). This effect is, however, unlikely to explain the inhibitory action of the proteasome inhibitors on coronavirus entry. Depletion of free ubiquitin by using RNA interference did not affect virus entry, nor was entry reduced in cells expressing a thermo-labile ubiquitin activating enzyme E1 at the restrictive temperature. Consistently, the MHV receptor appeared not to be ubiquitinated (63). We speculate that the proteasome is somehow directly involved in the coronavirus entry process, possibly during particle disassembly. In agreement herewith, Yu and coworkers found MHV particles to be trapped within endosomes upon treatment with MG132, which may indicate that proteasome activity is somehow important for the release of virus from the endosome into the cytosol (63). Like for MHV, cell entry of herpes simplex which was also facilitated by the proteasome, similarly appeared independent of protein ubiquitination (13). The authors hypothesized that proteasomal degradation independently of ubiquitin conjugation (25, 26) may play a role in herpes simplex virus entry. The same explanation may hold true for CoVs.

In contrast to virus entry, ubiquitination was found to be vital for efficient replication of MHV. Similar results were recently obtained for coxsackievirus and vaccinia virus (46, 50). Yet, the mechanism(s) by which ubiquitination facilitates virus replication remains unclear. For coxsackievirus, the viral RNA polymerase was found to be modified by ubiquitin moieties, which might be critical for its functioning. Infection with this virus was shown to induce the accumulation of protein-ubiquitin conjugates, with a concomitant decrease in the levels of free ubiquitin (50). During MHV infection, however, such an increase in protein-ubiquitin conjugates was not observed (data not shown). Interestingly, several studies have recently shown that the papain-like protease (PLpro) domain of CoVs mimics the folding of cellular deubiquitinating enzymes and contains deubiquitinating activity (1, 8, 43, 54). The requirement of ubiquitination for efficient CoV replication and the deubiquitinating activity

of a non-structural protein that is localized to the replication-transcription complexes may somehow be connected.

Unlike MHV entry and replication, its assembly appeared to be independent on proteasome functioning. That the UPS can be important for assembly and release has been shown for several other enveloped viruses (5, 10, 28). This dependence appears to relate to these viruses exploiting the cellular vacuolar protein sorting (VPS) machinery for their budding. This machinery is involved in the formation of multivesicular bodies (MVBs), which depends on mono-ubiquitinated cargo proteins (42). Viruses shown to be dependent for their assembly on the VPS4 protein, an essential cellular component of the MVB sorting pathway, were also sensitive to proteasome inhibition in their assembly. The insensitivity of MHV assembly to proteasome inhibition suggests that this process is not dependent of the VPS machinery. Indeed, the production of new virus particles appeared not to be affected in cells expressing a non-functional VPS4 (our unpublished results).

This study has demonstrated important roles for the UPS in CoV entry and replication. Although further studies are needed to elucidate the precise mechanism(s) by which the UPS facilitates CoV infection, it is already becoming clear that proteasome inhibitors could present a new class of anti-coronaviral drugs. Actually, proteasome inhibitors have already been shown to protect against coxsackievirus-induced myocarditis in a mouse model (17). Of note, some proteasome inhibitors, including the drug Velcade used in this study, are in use for the treatment of certain cancers (44, 52, 64). The major advantage of drugs targeting host, rather than viral, components may be the lower probability of generating viral drug-resistant variants as the evolutionary escape possibilities for the virus will be limited due to direct mutation of the drug target not being possible. Therefore, the appearance of drug resistant variants will be restricted compared to conventional antiviral drug approaches. The feasibility of proteasome inhibition as an effective means to treat CoV infections *in vivo*, however, remains to be established.

Material & Methods

Cells

Murine LR7 (31), feline FCWF, Vero-E6, and BHK-21 cells were used to propagate the viruses and for the infection experiments. CHO-E36 and -ts20 cells were maintained at 31°C in α-Minimal Essential Medium supplemented with 10% (v/v) fetal calf serum (Bodinco B.V.), 100 U/ml Penicillin, and 100 µg/ml Streptomycin. The mouse embryonic fibroblasts (MEFs) expressing wild-type (S51S) or mutant (S51A) eIF2α (47) as well as the MEF cell lines from wild-type ($GCN2^{+/+}$) and GCN2 knock-out ($GCN2^{-/-}$) embryo mice, and HeLa-CEACAM1a cells (58), were maintained in complete Dulbecco's Modified Eagle's Medium (DMEM) (Cambrex Bio Science) containing 10% (v/v) fetal calf serum (Bodinco B.V.), 100 U/ml Penicillin, and 100 µg/ml Streptomycin, supplemented with 1x Non-Essential Amino Acids (Invitrogen).

Viruses

MHV-EFLM (12) and MHV-nsp2GFP (58), FIPV-Δ3abcFL (12), SARS-CoV-GFP (51), and VSV-FL (41) were used for the infection experiments. MHV-S_4-EFLM (containing the firefly luciferase (64) gene between the E and M gene, and the S gene of MHV strain JHM in a MHV-A59 background) was generated by targeted RNA recombination as described previously (31). The RNA transcription vector pMH54-S_4-EFLM required for the generation of this virus was constructed by cloning the DNA fragment resulting from digestion of plasmid pXHEFLM (12) with *EcoR*V and *Nhe*I, which contains the FL expression cassette, into vector pMH54-S_4 (40) (kindly provided by Susan Weiss) treated with the same enzymes.

Chemicals

Stocks of 10 mM MG132, 1 mM epoxomicin, and 5 mM lactacystin (all obtained from Sigma-Aldrich) were prepared in dimethylsulfoxide (DMSO). A stock of 1 mM Velcade (Millennium Pharmaceuticals Inc.) was prepared in phosphate buffered saline (PBS). All stocks were stored at –20°C.

Luciferase Assays

Cell monolayers infected with the FL-expressing viruses were lysed at the indicated times p.i. using the appropriate buffer provided with the Firefly Luciferase Assay system (Promega). Intracellular luciferase expression was measured according to the manufacturer's instructions, and the relative light units (RLU) were determined with a Berthold Centro LB 960 plate luminometer.

Confocal immunofluorescence microscopy

Cells were fixed with a 4% paraformaldehyde solution (in PBS), and subsequently permeabilized with 0.1% Triton-X-100 in PBS. When indicated, the cells were incubated for 1 h with the first antibody directed against nsp2-3 (kindly provided by Susan Baker) (24) or against dsRNA (English and Scientific Consulting Bt. [K1]) (48) diluted in PBS containing 10% normal goat serum. After several washing steps, the cells were incubated with an appropriate dilution of secondary antibody in the same buffer for 1 h. After three subsequent washing steps, the coverslips were mounted in FluorSave (Calbiochem). The immunofluorescence staining was analyzed using a confocal laser-scanning microscope (Leica). GFP was excited at 488 nm, Cy3 at 568 nm, and Cy5 at 633 nm.

Metabolic labeling and immunoprecipitation

At the indicated times, the cells were starved for 30 min in cysteine- and methionine-free modified Eagle's medium containing 10 mM HEPES (pH 7.2) and 5% dialyzed fetal calf serum. The medium was then replaced by similar medium containing 100 μCi of ^{35}S *in vitro* cell-labeling mixture (Amersham Biosciences), after which the cells were further incubated for 15-30 min. Subsequently, the cells were either lysed or incubation was continued with culture medium (chase). Cells were lysed and cell lysates were subjected to immunoprecipitation as described before (37), using polyclonal antisera directed against MHV (k135) and M (anti-M_c) (32). Culture media were subjected to immunoprecipitation in the absence of detergents using the A3.10 monoclonal antibody directed against S (61). The immunoprecipitates were analyzed by sodium dodecyl sulfate-polyacrylamide gel electrophoresis (SDS-PAGE).

Reporter RNA synthesis and transfection

The reporter plasmid pM5f-RL-M3 (58) was linearized using a *Pac*I restriction site directly downstream of the poly(A) sequence. Subsequently, RNA transcripts were produced using the T7 MessageMachine Kit (Ambion) according to the manufacturer's instructions. Next, 0.5 pmol of RNA was transfected into cells using Lipofectamine 2000 (Invitrogen). Cells were treated with 10 μg/ml MG132 or mock-treated for 4 h, after which the cells were lysed and intracellular Renilla luciferase activity was measured with the Renilla Luciferase Assay Kit (Promega) according to the manufacturer's protocol.

Immunocytochemistry

Cell monolayers were fixed, permeabilized, and processed for immunocytochemistry as described previously (11). Peroxidase was visualized using an AEC substrate kit from Vector Laboratories. MHV-positive cells were detected and counted by using bright-field light microscopy.

Ubiquitin knock-down

siRNA duplexes targeting different sites within the coding sequences of *UBB*, *UBD*, *UBS52*, and *RPS27A* were designed by and obtained from Ambion Inc. (three siRNAs per gene). Scrambled siRNAs or siRNAs targeting FL (GL2+GL3) and *Eg5* (all from Ambion) were taken along as controls in each experiment. One day after seeding the HeLa-CEACAM1a cells, they were transfected with a final concentration of 10 nM siRNA using Oligofectamine (Invitrogen). 72 h after transfection, the cells were inoculated with MHV-EFLM. At 6 h p.i., the cell number and viability was measured by Wst-1 assay according to the manufacturer's protocol (Roche Diagnostics GmbH). Subsequently, intracellular luciferase expression was determined as described above. Each siRNA experiment was performed in triplicate. For each well, luciferase values were corrected for cell number and viability as determined by the Wst1 assay.

Western blotting

Depletion of ubiquitin after siRNA transfection was confirmed by western blotting. To this end, cells were lysed in ice-cold lysis buffer (20 mM MOPS [pH 7.2], 5 mM EDTA, 2 mM EGTA, and 0.5% (w/v) Nonidet-P40, containing 30 mM NaF, 40 mM β-Glycerophosphate, 20 mM Na-Pyrophosphate, 1 mM Na-Orthovanadate, 1 mM PMSF, 3 mM Benzamidine, 1.5 μM Pepstatin A, and 10 μM Leupeptin). Cell lysates were cleared by

centrifugation at 100,000 x g at 4°C for 30 min. Proteins present in the cell lysates were separated by SDS-PAGE and transferred to a Nitrocellulose membrane (0.1 μM, Schleicher Schuell). Subsequently, the membrane was incubated over night in block buffer (PBS containing 0.05% Tween-20 and 0.5% cold fish skin gelatin (Sigma-Aldrich). Next, the membrane was washed three times with PBS (containing 0.05% Tween-20) and incubated for 16 h at 4ºC with a peroxidase-labelled mouse polyclonal antibody against ubiquitin (P4D1; Santa Cruz Biotechnology, Inc.). Following extensive washing of the membrane, the amount of protein was visualized and quantitated using the Enhanced ChemoLuminescence (ECL) plus kit, a Typhoon imager, and ImageQuant TL software (all from Amersham Biosciences).

Acknowledgements

This work was supported by grants from the M.W. Beijerinck Virology Fund (Royal Netherlands Academy of Arts and Sciences), and The Netherlands Organization for Scientific Research (NWO-VIDI-700.54.421) to C.A.M. de Haan. We thank Mikihiko Naito (Institute of Molecular and Cellular Biosciences, The University of Tokyo, Tokyo, Japan) for providing the pEGFP-degron plasmid, Costas Koumenis (Radiation Oncology, University of Pennsylvania, Philadelphia, USA) and David Ron (Skirball Institute of Biomolecular Medicine, New York University School of Medicine, New York, USA) for providing the eIF2$\alpha^{S51S/A}$ and GCN2 wild-type and knock-out MEFs, respectively, John Bell (Ottawa Health Research Institute, University of Ottawa, Ottawa, ON, Canada) for providing the VSV-FL virus, Susan Baker (Department of Microbiology and Immunology, Loyola University, Maywood, IL, USA) for the nsp2-3 antibody, and Susan Weiss (Department of Microbiology, University of Pennsylvania School of Medicine, Philadelphia, Pennsylvania, USA) for transcription vector pMH54-S_4. We also thank Marne Hagemeijer and Mijke Vogels for stimulating discussions.

References

1. **Barretto, N., D. Jukneliene, K. Ratia, Z. Chen, A. D. Mesecar, and S. C. Baker.** 2005. The papain-like protease of severe acute respiratory syndrome coronavirus has deubiquitinating activity. J Virol 79:15189-98.

2. **Berlanga, J. J., J. Santoyo, and C. De Haro.** 1999. Characterization of a mammalian homolog of the GCN2 eukaryotic initiation factor 2alpha kinase. Eur J Biochem 265:754-62.

3. **Berlanga, J. J., I. Ventoso, H. P. Harding, J. Deng, D. Ron, N. Sonenberg, L. Carrasco, and C. de Haro.** 2006. Antiviral effect of the mammalian translation initiation factor 2alpha kinase GCN2 against RNA viruses. Embo J 25:1730-40.

4. **Bi, W., J. D. Pinon, S. Hughes, P. J. Bonilla, K. V. Holmes, S. R. Weiss, and J. L. Leibowitz.** 1998. Localization of mouse hepatitis virus open reading frame 1A derived proteins. J Neurovirol 4:594-605.

5. **Bieniasz, P. D.** 2006. Late budding domains and host proteins in enveloped virus release. Virology 344:55-63.

6. **Bosch, B. J., R. van der Zee, C. A. de Haan, and P. J. Rottier.** 2003. The coronavirus spike protein is a class I virus fusion protein: structural and functional characterization of the fusion core complex. J Virol 77:8801-11.

7. **Burch, A. D., and S. K. Weller.** 2004. Nuclear sequestration of cellular chaperone and proteasomal machinery during herpes simplex virus type 1 infection. J Virol 78:7175-85.

8. **Chen, Z., Y. Wang, K. Ratia, A. D. Mesecar, K. D. Wilkinson, and S. C. Baker.** 2007. Proteolytic processing and deubiquitinating activity of papain-like proteases of human coronavirus NL63. J Virol 81:6007-18.

9. **Connor, J. H., and D. S. Lyles.** 2005. Inhibition of host and viral translation during vesicular stomatitis virus infection. eIF2 is responsible for the inhibition of viral but not host translation. J Biol Chem 280:13512-9.

10. **Crump, C. M., C. Yates, and T. Minson.** 2007. Herpes simplex virus type 1 cytoplasmic envelopment requires functional Vps4. J Virol 81:7380-7.

11. **de Haan, C. A., Z. Li, E. te Lintelo, B. J. Bosch, B. J. Haijema, and P. J. Rottier.** 2005. Murine coronavirus with an extended host range uses heparan sulfate as an entry receptor. J Virol 79:14451-6.

12. **de Haan, C. A., L. van Genne, J. N. Stoop, H. Volders, and P. J. Rottier.** 2003. Coronaviruses as vectors: position dependence of foreign gene expression. J Virol 77:11312-23.

13. **Delboy, M. G., D. G. Roller, and A. V. Nicola.** 2008. Cellular proteasome activity facilitates herpes simplex virus entry at a postpenetration step. J Virol 82:3381-90.

14. **Drosten, C., S. Gunther, W. Preiser, S. van der Werf, H. R. Brodt, S. Becker, H. Rabenau, M. Panning, L. Kolesnikova, R. A. Fouchier, A. Berger, A. M. Burguiere, J. Cinatl, M. Eickmann, N. Escriou, K. Grywna, S. Kramme, J. C. Manuguerra, S. Muller, V. Rickerts, M. Sturmer, S. Vieth, H. D. Klenk, A. D. Osterhaus, H. Schmitz, and H. W. Doerr.** 2003. Identification of a novel coronavirus in patients with severe acute respiratory syndrome. N Engl J Med 348:1967-76.

15. **EIFart, P., K. Ludwig, C. Bottcher, C. A. de Haan, P. J. Rottier, T. Korte, and A. Herrmann.** 2007. Role of endocytosis and low pH in murine hepatitis virus strain A59 cell entry. J Virol 81:10758-68.

16. **Gallagher, T. M., and M. J. Buchmeier.** 2001. Coronavirus spike proteins in viral entry and pathogenesis. Virology 279:371-4.

17. **Gao, G., J. Zhang, X. Si, J. Wong, C. Cheung, B. McManus, and H. Luo.** 2008. Proteasome inhibition attenuates coxsackievirus-induced myocardial damage in mice. Am J Physiol Heart Circ Physiol 295:H401-8.

18. **Goldberg, A. L.** 2007. Functions of the proteasome: from protein degradation and immune surveillance to cancer therapy. Biochem Soc Trans 35:12-7.

19. **Gosert, R., A. Kanjanahaluethai, D. Egger, K. Bienz, and S. C. Baker.** 2002. RNA replication of mouse hepatitis virus takes place at double-membrane vesicles. J Virol 76:3697-708.

20. **Harty, R. N., M. E. Brown, J. P. McGettigan, G. Wang, H. R. Jayakar, J. M. Huibregtse, M. A. Whitt, and M. J. Schnell.** 2001. Rhabdoviruses and the cellular ubiquitin-proteasome system: a budding interaction. J Virol 75:10623-9.

21. **Hershko, A., and A. Ciechanover.** 1998. The ubiquitin system. Annu Rev Biochem 67:425-79.

22. **Hicke, L., and R. Dunn.** 2003. Regulation of membrane protein transport by ubiquitin and ubiquitin-binding proteins. Annu Rev Cell Dev Biol 19:141-72.

23. **Ishioka, T., R. Katayama, R. Kikuchi, M. Nishimoto, S. Takada, R. Takada, S. Matsuzawa, J. C. Reed, T. Tsuruo, and M. Naito.** 2007. Impairment of the ubiquitin-proteasome system by cellular FLIP. Genes Cells 12:735-44.

24. **Kanjanahaluethai, A., and S. C. Baker.** 2000. Identification of mouse hepatitis virus papain-like proteinase 2 activity. J Virol 74:7911-21.

25. **Kerscher, O.** 2007. SUMO junction-what's your function? New insights through SUMO-interacting motifs. EMBO Rep 8:550-5.

26. **Kerscher, O., R. Felberbaum, and M. Hochstrasser.** 2006. Modification of proteins by ubiquitin and ubiquitin-like proteins. Annu Rev Cell Dev Biol 22:159-80.

27. **Khor, R., L. J. McElroy, and G. R. Whittaker.** 2003. The ubiquitin-vacuolar protein sorting system is selectively required during entry of influenza virus into host cells. Traffic 4:857-68.

28. **Kian Chua, P., M. H. Lin, and C. Shih.** 2006. Potent inhibition of human Hepatitis B virus replication by a host factor Vps4. Virology 354:1-6.

29. **Kisselev, A. F., and A. L. Goldberg.** 2001. Proteasome inhibitors: from research tools to drug candidates. Chem Biol 8:739-58.

30. **Krijnse-Locker, J., M. Ericsson, P. J. Rottier, and G. Griffiths.** 1994. Characterization of the budding compartment of mouse hepatitis virus: evidence that transport from the RER to the Golgi complex requires only one vesicular transport step. J Cell Biol 124:55-70.

31. **Kuo, L., G. J. Godeke, M. J. Raamsman, P. S. Masters, and P. J. Rottier.** 2000. Retargeting of coronavirus by substitution of the spike glycoprotein ectodomain: crossing the host cell species barrier. J Virol 74:1393-406.

32. **Locker, J. K., J. K. Rose, M. C. Horzinek, and P. J. Rottier.** 1992. Membrane assembly of the triple-spanning coronavirus M protein. Individual transmembrane domains show preferred orientation. J Biol Chem 267:21911-8.

33. **Meng, L., R. Mohan, B. H. Kwok, M. Elofsson, N. Sin, and C. M. Crews.** 1999. Epoxomicin, a potent and selective proteasome inhibitor, exhibits *in vivo* antiinflammatory activity. Proc Natl Acad Sci U S A 96:10403-8.

34. **Mimnaugh, E. G., H. Y. Chen, J. R. Davie, J. E. Celis, and L. Neckers.** 1997. Rapid deubiquitination of nucleosomal histones in human tumor cells caused by proteasome inhibitors and stress response inducers: effects on replication, transcription, translation, and the cellular stress response. Biochemistry 36:14418-29.

35. **Nash, T. C., and M. J. Buchmeier.** 1997. Entry of mouse hepatitis virus into cells by endosomal and nonendosomal pathways. Virology 233:1-8.

36. **Neznanov, N., E. M. Dragunsky, K. M. Chumakov, L. Neznanova, R. C. Wek, A. V. Gudkov, and A. K. Banerjee.** 2008. Different effect of proteasome inhibition on vesicular stomatitis virus and poliovirus replication. PLoS ONE 3:e1887.

37. **Oostra, M., C. A. de Haan, R. J. de Groot, and P. J. Rottier.** 2006. Glycosylation of the severe acute respiratory syndrome coronavirus triple-spanning membrane proteins 3a and M. J Virol 80:2326-36.

38. **Ostrowska, H., C. Wojcik, S. Omura, and K. Worowski.** 1997. Lactacystin, a specific inhibitor of the proteasome, inhibits human platelet lysosomal cathepsin A-like enzyme. Biochem Biophys Res Commun 234:729-32.

39. **Pasternak, A. O., W. J. Spaan, and E. J. Snijder.** 2006. Nidovirus transcription: how to make sense...? J Gen Virol 87:1403-21.

40. **Phillips, J. J., M. M. Chua, E. Lavi, and S. R. Weiss.** 1999. Pathogenesis of chimeric MHV4/MHV-A59 recombinant viruses: the murine coronavirus spike protein is a major determinant of neurovirulence. J Virol 73:7752-60.

41. **Power, A. T., J. Wang, T. J. Falls, J. M. Paterson, K. A. Parato, B. D. Lichty, D. F. Stojdl, P. A. Forsyth, H. Atkins, and J. C. Bell.** 2007. Carrier cell-based delivery of an oncolytic virus circumvents antiviral immunity. Mol Ther 15:123-30.

42. **Raiborg, C., T. E. Rusten, and H. Stenmark.** 2003. Protein sorting into multivesicular endosomes. Curr Opin Cell Biol 15:446-55.

43. **Ratia, K., K. S. Saikatendu, B. D. Santarsiero, N. Barretto, S. C. Baker, R. C. Stevens, and A. D. Mesecar.** 2006. Severe acute respiratory syndrome coronavirus papain-like protease: structure of a viral deubiquitinating enzyme. Proc Natl Acad Sci U S A 103:5717-22.

44. **Richardson, P. G., C. Mitsiades, T. Hideshima, and K. C. Anderson.** 2006. Bortezomib: proteasome inhibition as an effective anticancer therapy. Annu Rev Med 57:33-47.

45. **Ros, C., C. J. Burckhardt, and C. Kempf.** 2002. Cytoplasmic trafficking of minute virus of mice: low-pH requirement, routing to late endosomes, and proteasome interaction. J Virol 76:12634-45.

46. **Satheshkumar, P. S., L. C. Anton, P. Sanz, and B. Moss.** 2009. Inhibition of the Ubiquitin-Proteasome System Prevents Vaccinia Virus DNA Replication and Expression of Intermediate and Late Genes. J Virol.

47. **Scheuner, D., B. Song, E. McEwen, C. Liu, R. Laybutt, P. Gillespie, T. Saunders, S. Bonner-Weir, and R. J. Kaufman.** 2001. Translational control is required for the unfolded protein response and *in vivo* glucose homeostasis. Mol Cell 7:1165-76.

48. **Schonborn, J., J. Oberstrass, E. Breyel, J. Tittgen, J. Schumacher, and N. Lukacs.** 1991. Monoclonal antibodies to double-stranded RNA as probes of RNA structure in crude nucleic acid extracts. Nucleic Acids Res 19:2993-3000.

49. **Shi, S. T., J. J. Schiller, A. Kanjanahaluethai, S. C. Baker, J. W. Oh, and M. M. Lai.** 1999. Colocalization and membrane association of murine hepatitis virus gene 1 products and *De novo*-synthesized viral RNA in infected cells. J Virol 73:5957-69.

50. **Si, X., G. Gao, J. Wong, Y. Wang, J. Zhang, and H. Luo.** 2008. Ubiquitination is required for effective replication of coxsackievirus B3. PLoS ONE 3:e2585.

51. **Sims, A. C., S. E. Burkett, B. Yount, and R. J. Pickles.** 2008. SARS-CoV replication and pathogenesis in an *in vitro* model of the human conducting airway epithelium. Virus Res 133:33-44.

52. **Sterz, J., I. von Metzler, J. C. Hahne, B. Lamottke, J. Rademacher, U. Heider, E. Terpos, and O. Sezer.** 2008. The potential of proteasome inhibitors in cancer therapy. Expert Opin Investig Drugs 17:879-95.

53. **Strack, B., A. Calistri, M. A. Accola, G. Palu, and H. G. Gottlinger.** 2000. A role for ubiquitin ligase recruitment in retrovirus release. Proc Natl Acad Sci U S A 97:13063-8.

54. **Sulea, T., H. A. Lindner, E. O. Purisima, and R. Menard.** 2005. Deubiquitination, a new function of the severe acute respiratory syndrome coronavirus papain-like protease? J Virol 79:4550-1.

55. **Tanahashi, N., H. Kawahara, Y. Murakami, and K. Tanaka.** 1999. The proteasome-dependent proteolytic system. Mol Biol Rep 26:3-9.

56. **Taylor, G. M., P. I. Hanson, and M. Kielian.** 2007. Ubiquitin depletion and dominant-negative VPS4 inhibit rhabdovirus budding without affecting alphavirus budding. J Virol 81:13631-9.

57. **van der Hoek, L., K. Pyrc, M. F. Jebbink, W. Vermeulen-Oost, R. J. Berkhout, K. C. Wolthers, P. M. Wertheim-van Dillen, J. Kaandorp, J. Spaargaren, and B. Berkhout.** 2004. Identification of a new human coronavirus. Nat Med 10:368-73.

58. **Verheije, M. H., M. Raaben, M. Mari, E. G. Te Lintelo, F. Reggiori, F. J. van Kuppeveld, P. J. Rottier, and C. A. de Haan.** 2008. Mouse hepatitis coronavirus RNA replication depends on GBF1-mediated ARF1 activation. PLoS Pathog 4:e1000088.

59. **Voges, D., P. Zwickl, and W. Baumeister.** 1999. The 26S proteasome: a molecular machine designed for controlled proteolysis. Annu Rev Biochem 68:1015-68.

60. **Watanabe, H., Y. Tanaka, Y. Shimazu, F. Sugahara, M. Kuwayama, A. Hiramatsu, K. Kiyotani, T. Yoshida, and T. Sakaguchi.** 2005. Cell-specific inhibition of paramyxovirus maturation by proteasome inhibitors. Microbiol Immunol 49:835-44.

61. **Weismiller, D. G., L. S. Sturman, M. J. Buchmeier, J. O. Fleming, and K. V. Holmes.** 1990. Monoclonal antibodies to the peplomer glycoprotein of coronavirus mouse hepatitis virus identify two subunits and detect a conformational change in the subunit released under mild alkaline conditions. J Virol 64:3051-5.

62. **Woo, P. C., S. K. Lau, C. M. Chu, K. H. Chan, H. W. Tsoi, Y. Huang, B. H. Wong, R. W. Poon, J. J. Cai, W. K. Luk, L. L. Poon, S. S. Wong, Y. Guan, J. S. Peiris, and K. Y. Yuen.** 2005. Characterization and complete genome sequence of a novel coronavirus, coronavirus HKU1, from patients with pneumonia. J Virol 79:884-95.

63. **Yu, G. Y., and M. M. Lai.** 2005. The ubiquitin-proteasome system facilitates the transfer of murine coronavirus from endosome to cytoplasm during virus entry. J Virol 79:644-8.

64. **Zavrski, I., L. Kleeberg, M. Kaiser, C. Fleissner, U. Heider, J. Sterz, C. Jakob, and O. Sezer.** 2007. Proteasome as an emerging therapeutic target in cancer. Curr Pharm Des 13:471-85.

65. **Zhang, Z., N. Torii, A. Furusaka, N. Malayaman, Z. Hu, and T. J. Liang.** 2000. Structural and functional characterization of interaction between hepatitis B virus X protein and the proteasome complex. J Biol Chem 275:15157-65.

Chapter 6

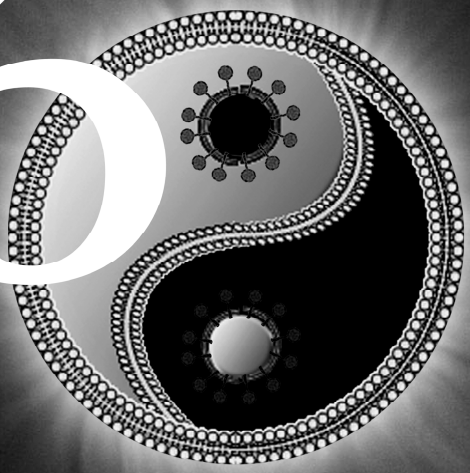

Cyclooxygenase Activity is Important for Efficient Replication of Mouse Hepatitis Virus at an Early Stage of Infection

Matthijs Raaben
Alexandra W.C. Einerhand
Lucas J.A. Taminiau
Michel van Houdt
Janneke Bouma
Rolien H. Raatgeep
Hans A. Büller
Cornelis A.M. de Haan
John W.A. Rossen

Virol Journal; 2007 Jun 7;4:55.

Abstract

Cyclooxygenases (COXs) play a significant role in many different viral infections with respect to replication and pathogenesis. Here we investigated the role of COXs in the mouse hepatitis coronavirus (MHV) infection cycle. Blocking COX activity by different inhibitors or by RNA interference affected MHV infection in different cells. The COX inhibitors reduced MHV infection at a post-binding step, but early in the replication cycle. Both viral RNA and viral protein synthesis were affected with subsequent loss of progeny virus production. Thus, COX activity appears to be required for efficient MHV replication, providing a potential target for anti-coronaviral therapy.

Introduction

Virus infections often cause acute inflammatory responses, which are mediated by several cellular effectors and soluble factors. Although these responses have an important protective role, they may also have deleterious effects on the host. The balance between these protective and deleterious effects may ultimately determine the course of disease after viral infection. Prostaglandins (PGs) are important regulators of this inflammatory reaction. They are synthesized by cyclooxygenases (COXs), converting arachidonic acid into PGH_2, which can then be isomerized to generate different biologically active forms of PGs. There are three known isoforms of COXs, with COX-1 and COX-2 being the best characterized. COX-1 is expressed in various cell types and PGs produced by COX-1 are predominantly involved in the regulation of various homeostatic processes (27). COX-2 is an immediate early response gene, which upon induction generates mainly hyperalgesic and proinflammatory PGs at sites of inflammation (17, 18). PGs from the E series, such as PGE_2, also exhibit immunomodulatory activities, preventing hyperactivation of the innate cellular immunity (4). Furthermore, they can inhibit the secretion of gamma interferon, a cytokine with antiviral activity (9). A direct role for COXs and PGs in controlling viral replication has been described for a wide range of virus infections, but their actions appear to be dependent on both the virus and cell type (28). For instance, COXs and/or PGs are required for efficient replication of herpesviruses (3, 11, 22, 25, 29, 30, 37), bovine leukemia virus (21), and rotavirus (23). In case of human cytomegalovirus, human T-lymphotropic virus type 1, and human immunodeficiency virus type-1 PGE_2 has been shown to stimulate virus replication by activating viral promotors (8, 12, 16). On the other hand, COXs/PGs negatively affect adenovirus replication, as well as replication of human immunodeficiency virus type 1 in macrophages (10, 19). The mechanisms by which COXs and PGs regulate viral replication are largely unclear.

Coronaviruses (CoVs) constitute a family of enveloped, positive-stranded RNA viruses. They are known pathogens in the veterinary field, causing severe diseases in several domestic species (34). Recently, their relevance has increased considerably with the discovery of several new human CoVs (HCoVs) such as the severe acute respiratory syndrome (SARS)-CoV (7), HCoV-NL63 (31), and HCoV-HKU1 (35). The role of COXs during CoV infection and pathogenesis is not well understood. MHV strain 3, which causes

fulminant hepatitis, was shown to induce the synthesis of PGE_2 in macrophages (20). However, the exogenous administration of PGE_2 could completely prevent the development of hepatic necrosis (1). More recently, two structural proteins from the SARS-CoV were shown to induce the expression of COX-2 *in vitro* (14, 15, 36), whereas elevated levels of PGE_2 were found in the blood of SARS-CoV-infected individuals (13), suggesting a role for COXs and PGs in CoV pathogenesis. However, the requirement for COX activity for CoV replication remains unexplored.

Results & Discussion

In the present study we investigated the role of COXs in the MHV replication cycle. To this end, Caco-2 cells, stably expressing the MHV receptor glycoprotein (Caco-MHVR) (24), were infected with MHV strain A59 (MHV-A59) at a multiplicity of infection (MOI) of 0.01 in the presence or absence of the COX-1 and COX-2 inhibitors indomethacin and curcumine.

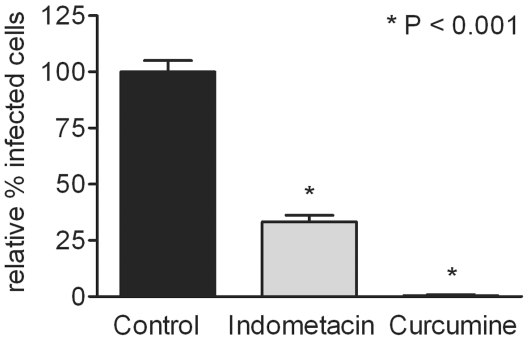

Fig.1. COX inhibitors are negatively affecting MHV infection. (A) Caco-MHVR cells were incubated with culture medium (containing a concentration of DMSO similar to that present in the inhibitor solutions), 20 μM indomethacin, or 30 μM curcumine 1 h prior to inoculation with MHV-A59 (MOI 0.01). The cells were maintained in the presence of the inhibitors until they were fixed at 6 h p.i. Infected cells were detected by an indirect IFA using an anti-MHV serum and Texas Red conjugated secondary antibodies. Fluorescence was viewed with a Nikon Eclipse E800 microscope. The numbers of MHV-infected cells in the drug-treated cells are presented as a percentage of the average number of infected cells in the mock-treated (control) cell cultures. Data are presented as mean ± standard error of mean (n = 6). For statistical analysis a one-way ANOVA with the Tukey-Kramer test was performed using GraphPad Prism version 3.00 for Windows (GraphPad Software). In all tests, $P < 0.05$ was considered statistically significant.

The cells were incubated 1 h prior to infection with the inhibitors, and were maintained in the presence of the inhibitors from 30 min post infection (p.i.). Cells were fixed at 6 h p.i. with ice-cold methanol, and the numbers of MHV-infected cells were determined by an indirect immunofluorescence assay (IFA) using anti-MHV antibodies (26). In the presence of 20 µM indomethacin, MHV infection was reduced by 57%, while curcumine reduced infection by 95% at a concentration of 30 µM (Fig.1). Both drugs affected MHV infection in a concentration-dependent manner (data not shown). The used concentrations of both drugs and of their solvent (DMSO) were non-toxic to the cells, as determined by cell proliferation assays (data not shown).

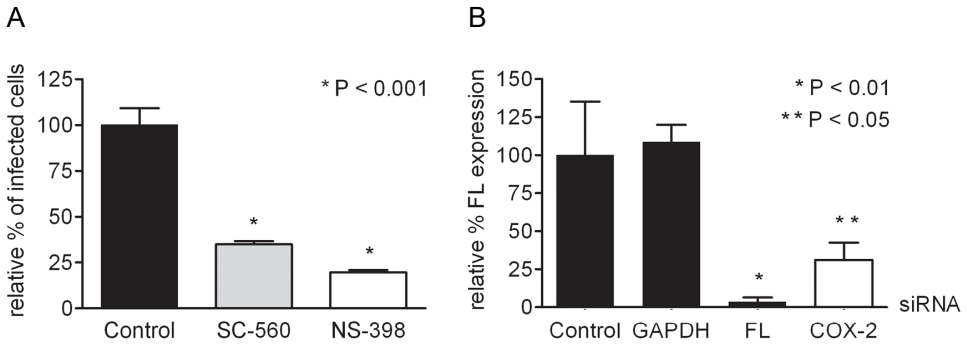

Fig.2. Blocking COX-1 or COX-2 activity by specific inhibitors, or by siRNAs targeting COX-2 mRNA reduce MHV infection. (A) Caco-MHVR cells were incubated with COX-1 (SC-560; 1 µM) or COX-2 (NS-398; 0.055 µM) inhibitor 1 h prior to inoculation with MHV-A59 (MOI 0.01) and were maintained in the presence of the inhibitors until they were fixed. The numbers of MHV-infected cells were determined with an indirect IFA and are presented as described in the legend of Figure 1. (B) HeLa cells were transfected with 10 nM siRNAs, targeting the indicated transcripts, 72 h prior to inoculation with MHV-FLSrec. Cell viability was measured for 30 min at 6 h p.i. using a WST-1 assay as described previously (33), after which the intracellular luciferase levels were determined as relative light units (RLU). Luciferase levels in siRNA-transfected cells are expressed as a percentage of the levels in the mock-transfected (control) cells and were corrected for the percentage of viable cells (n = 3).

Next, we determined the role of the different COX isoforms. The ability of specific COX-1 and COX-2 inhibitors to reduce MHV infection was determined in a similar way as described above. Both SC-560 and NS-398, which inhibit COX-1 and COX-2, respectively, reduced MHV infection by 65-75% at concentrations that were non-toxic to the cells (1 µM and 0.055 µM respectively) (Fig.2A). Apparently, the activity of both enzymes is required

for efficient MHV replication in Caco-MHVR cells. RNA interference technology was applied to confirm the observation that COX-2 activity is important for MHV replication. Parallel cultures of HeLa cells were transfected with siRNAs (purchased from Dharmacon, Inc.) targeting COX-2, firefly luciferase (FL) (positive control) or GAPDH (specificity control) transcripts for degradation. They were infected at 72 h posttransfection with MHV-FLSrec (5), a recombinant MHV expressing the FL reporter gene, the level of which is a reliable measure for MHV replication (6). Silencing of GAPDH, a cellular housekeeping gene, did not affect FL expression compared to mock-transfected (control) cells (Fig.2B). However, HeLa cells transfected with siRNAs targeting the FL or COX-2 transcripts showed a reduction in FL expression of more than 90% and 65%, respectively. A taqman reverse transcription (RT)-PCR targeting COX-2 mRNA revealed that in cells treated with COX-2 siRNAs, COX-2 mRNA levels were decreased with more than 70% compared to control cells (data not shown). Therefore, these data show the requirement of COX-2 activity for efficient MHV replication.

To determine which step of the MHV replication cycle was affected by the COX inhibitors, the production of infectious particles, of viral protein and of viral RNA was analyzed. For this purpose, Caco-MHVR cells were inoculated with MHV-A59 (MOI 1) in the presence or absence of indomethacin or curcumine. The amount of infectious viral progeny present in cells and culture media was monitored by determining the number of fluorescent focus-forming units (ffu) at different time-points p.i. Inhibition of COX activity by curcumine and indomethacin resulted in a significant decrease in the yield of infectious viral progeny by more than 95% and 85%, respectively (Fig.3A). In addition, the amount of N protein present in cell lysates was analyzed by Western blotting using a polyclonal anti-MHV serum. N protein expression levels were markedly reduced by curcumine (86% reduction), and to a lesser extent by indomethacin (24%) (Fig.3B). Consistent with these results, much smaller syncytia were observed after infection of Caco-MHVR cells in the presence of the COX inhibitors (Fig.3C). Reduced expression levels of the MHV S protein, which is responsible for cell-cell fusion in MHV-infected cells (32) are likely to explain the lack of syncytium formation after COXs inhibition. Finally, viral RNA synthesis was analyzed in the presence of COX inhibitors. At 6 h p.i., total RNA was isolated and viral RNA

synthesis was monitored by Taqman RT-PCR using a probe and primers that detect the N gene (details in legend Fig.3).

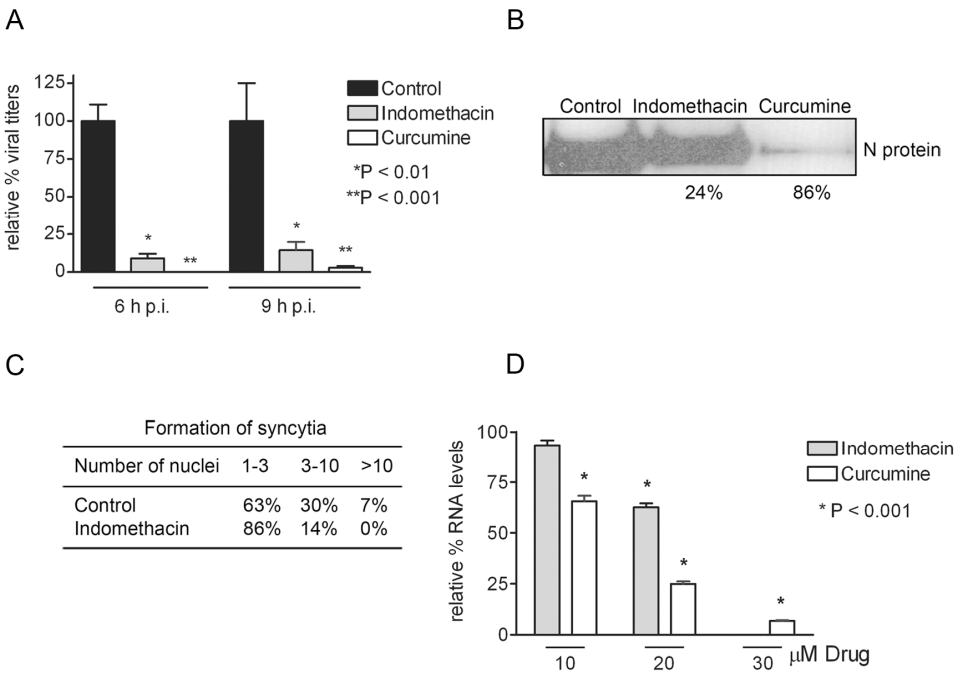

Fig.3. Indomethacin and curcumine inhibit MHV replication at the level of RNA synthesis. Caco-MHVR cells were incubated with and maintained in culture medium containing DMSO, 20 μM indomethacin, or 30 μM curcumine as described in figure legend 1. After 1 h, the cells were inoculated with MHV-A59 (MOI 1). At 6 and 9 h p.i., supernatants were collected and cells were harvested to isolate infectious viral particles, proteins and total RNA. (A) Caco-MHVR cells were inoculated with serial dilutions of combined supernatants and cleared cell homogenates from mock-treated (black bars), indomethacin-treated (grey bars) and curcumine-treated (white bars) cultures collected at 6 and 9 h p.i. The amount of ffu in the samples was determined with an indirect IFA as described in the legend of Figure 1 (n = 3). (B) Protein samples were analyzed on a SDS-15% polyacrylamide gel followed by Western blotting using the polyclonal anti-MHV serum. The N protein levels and the percentage of reduction (normalized for β-tubulin expression (data not shown)) in drug-treated cells compared to mock-treated cells are indicated. (C) The size of the observed syncytia was measured by counting the number of nuclei per syncytium of MHV-infected cells in the absence or presence of 20 μM indomethacin. (D) The expression levels of the N gene of MHV were determined by Taqman RT-PCR using primers 2915 (5'-GCCTCGCCAAAAGAGGACT-3') and 2916 (5'-GGGCCTCTCTTTCCAAAACAC-3') and a dual labeled probe (5'-6-FAM-CAAACAAGCAGTGCCCAGTGCAGC-TAMRA-3'). The relative amount of viral RNA in the drug-treated cells was expressed as a percentage of the average amount of viral RNA in the mock-treated cells.

Indomethacin and curcumine both inhibited viral RNA synthesis in a dose-dependent manner (Fig.3D). These results indicate that the COX inhibitors interfere with viral RNA and protein synthesis and consequently affect the production of infectious particles. In agreement with our findings, a recent study described the potent antiviral effect of indomethacin on SARS and canine coronavirus (CCoV) replication (2).

To study the kinetics of inhibition of MHV replication in more detail Caco-MHVR cells were inoculated with MHV-A59 (MOI 0.01) for 2 h at 4°C to allow binding of the virus to the cells without entry. After removing any unbound viral particles, the cells were placed at 37°C to induce virus entry and 20 μM indomethacin was added at the time-points indicated (Fig.4). MHV infection was significantly reduced, as measured by the indirect IFA described above, if indomethacin was added up to 1 h after the cells were placed at 37°C. The maximum inhibitory effect was obtained when indomethacin was added immediately after the cells were placed at 37°C. No significant inhibition of the infection was observed if indomethacin was added 2 h after the cells were placed at 37°C.

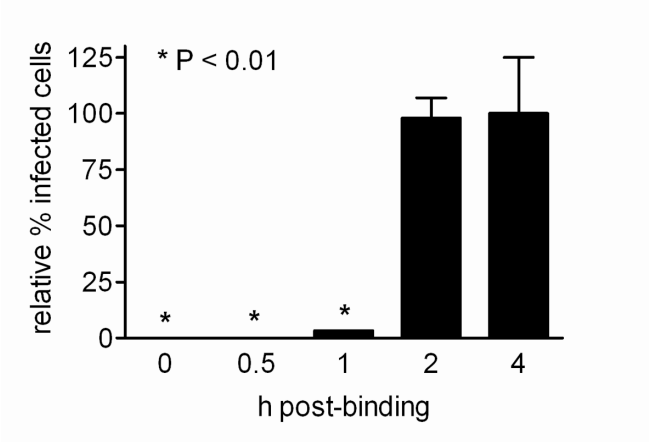

Fig.4. COX inhibition affects MHV infection at a post-binding step. Caco-MHVR cells were inoculated with MHV-A59 (MOI 0.01) at 4°C for 2 h. Subsequently, cells were placed at 37°C and 20 μM indomethacin was added to the culture medium immediately (t = 0 h post binding) or at the indicated times. Cells were maintained in culture medium containing indomethacin until they were fixed at 6 h post binding. The numbers of infected cells are presented as described in the legend of Figure 1 (n = 3).

This result demonstrates that COX activity plays an important role early in the virus infection cycle, at a post-binding step. Thus, COX activity might either be required for efficient entry or for an initial step in RNA replication. Similarly, rotavirus replication was also negatively affected by the addition of COX inhibitors early, but not late in the infection cycle (23). In conclusion, our results clearly show that COX activity is required for efficient virus replication *in vitro* early during MHV infection. These findings may offer new possibilities for anti-CoV therapy.

Acknowledgements

This work was supported by grants from the Sophia Foundation for Medical Research, Rotterdam, The Netherlands, and The Netherlands Organization for Scientific Research.

References

1. **Abecassis, M., J. Falk, V. Dindzans, W. Lopatin, L. Makowka, G. Levy, and R. Falk.** 1987. Prostaglandin E2 (PGE2) alters the pathogenesis of MHV-3 infection in susceptible BALB/cJ mice. Adv Exp Med Biol 218:465-6.

2. **Amici, C., A. Di Coro, A. Ciucci, L. Chiappa, C. Castilletti, V. Martella, N. Decaro, C. Buonavoglia, M. R. Capobianchi, and M. G. Santoro.** 2006. Indomethacin has a potent antiviral activity against SARS coronavirus. Antivir Ther 11:1021-30.

3. **Baker, D. A., J. Thomas, J. Epstein, D. Possilico, and M. L. Stone.** 1982. The effect of prostaglandins on the multiplication and cell-to-cell spread of herpes simplex virus type 2 *in vitro*. Am J Obstet Gynecol 144:346-9.

4. **Betz, M., and B. S. Fox.** 1991. Prostaglandin E2 inhibits production of Th1 lymphokines but not of Th2 lymphokines. J Immunol 146:108-13.

5. **de Haan, C. A., Z. Li, E. te Lintelo, B. J. Bosch, B. J. Haijema, and P. J. Rottier.** 2005. Murine coronavirus with an extended host range uses heparan sulfate as an entry receptor. J Virol 79:14451-6.

6. **de Haan, C. A., L. van Genne, J. N. Stoop, H. Volders, and P. J. Rottier.** 2003. Coronaviruses as vectors: position dependence of foreign gene expression. J Virol 77:11312-23.

7. **Drosten, C., S. Gunther, W. Preiser, S. van der Werf, H. R. Brodt, S. Becker, H. Rabenau, M. Panning, L. Kolesnikova, R. A. Fouchier, A. Berger, A. M. Burguiere, J. Cinatl, M. Eickmann, N. Escriou, K. Grywna, S. Kramme, J. C. Manuguerra, S. Muller, V. Rickerts, M. Sturmer, S. Vieth, H. D. Klenk, A. D. Osterhaus, H. Schmitz, and H. W. Doerr.** 2003. Identification of a novel coronavirus in patients with severe acute respiratory syndrome. N Engl J Med 348:1967-76.

8. **Dumais, N., B. Barbeau, M. Olivier, and M. J. Tremblay.** 1998. Prostaglandin E2 Up-regulates HIV-1 long terminal repeat-driven gene activity in T cells via NF-kappaB-dependent and -independent signaling pathways. J Biol Chem 273:27306-14.

9. **Hasler, F., H. G. Bluestein, N. J. Zvaifler, and L. B. Epstein.** 1983. Analysis of the defects responsible for the impaired regulation of EBV-induced B cell proliferation by rheumatoid arthritis lymphocytes. II. Role of monocytes and the increased sensitivity of rheumatoid arthritis lymphocytes to prostaglandin E. J Immunol 131:768-72.

10. **Hayes, M. M., B. R. Lane, S. R. King, D. M. Markovitz, and M. J. Coffey.** 2002. Prostaglandin E(2) inhibits replication of HIV-1 in macrophages through activation of protein kinase A. Cell Immunol 215:61-71.

11. **Janelle, M. E., A. Gravel, J. Gosselin, M. J. Tremblay, and L. Flamand.** 2002. Activation of monocyte cyclooxygenase-2 gene expression by human herpesvirus 6. Role for cyclic AMP-responsive element-binding protein and activator protein-1. J Biol Chem 277:30665-74.

12. **Kline, J. N., G. M. Hunninghake, B. He, M. M. Monick, and G. W. Hunninghake.** 1998. Synergistic activation of the human cytomegalovirus major immediate early promoter by prostaglandin E2 and cytokines. Exp Lung Res 24:3-14.

13. **Lee, C. H., R. F. Chen, J. W. Liu, W. T. Yeh, J. C. Chang, P. M. Liu, H. L. Eng, M. C. Lin, and K. D. Yang.** 2004. Altered p38 mitogen-activated protein kinase expression in different leukocytes with increment of immunosuppressive mediators in patients with severe acute respiratory syndrome. J Immunol 172:7841-7.

14. **Liu, M., C. Gu, J. Wu, and Y. Zhu.** 2006. Amino acids 1 to 422 of the spike protein of SARS associated coronavirus are required for induction of cyclooxygenase-2. Virus Genes 33:309-17.

15. **Liu, M., Y. Yang, C. Gu, Y. Yue, K. K. Wu, J. Wu, and Y. Zhu.** 2007. Spike protein of SARS-CoV stimulates cyclooxygenase-2 expression via both calcium-dependent and calcium-independent protein kinase C pathways. Faseb J.

16. **Moriuchi, M., H. Inoue, and H. Moriuchi.** 2001. Reciprocal interactions between human T-lymphotropic virus type 1 and prostaglandins: implications for viral transmission. J Virol 75:192-8.

17. **Newton, R., L. M. Kuitert, M. Bergmann, I. M. Adcock, and P. J. Barnes.** 1997. Evidence for involvement of NF-kappaB in the transcriptional control of COX-2 gene expression by IL-1beta. Biochem Biophys Res Commun 237:28-32.

18. **Newton, R., D. A. Stevens, L. A. Hart, M. Lindsay, I. M. Adcock, and P. J. Barnes.** 1997. Superinduction of COX-2 mRNA by cycloheximide and interleukin-1beta involves increased transcription and correlates with increased NF-kappaB and JNK activation. FEBS Lett 418:135-8.

19. **Ongradi, J., A. Telekes, J. Farkas, I. Nasz, and M. Bendinelli.** 1994. The effect of prostaglandins on the replication of adenovirus wild-types and temperature-sensitive mutants. Acta Microbiol Immunol Hung 41:173-88.

20. **Pope, M., O. Rotstein, E. Cole, S. Sinclair, R. Parr, B. Cruz, R. Fingerote, S. Chung, R. Gorczynski, L. Fung, and et al.** 1995. Pattern of disease after murine hepatitis virus strain 3 infection correlates with macrophage activation and not viral replication. J Virol 69:5252-60.

21. **Pyeon, D., F. J. Diaz, and G. A. Splitter.** 2000. Prostaglandin E(2) increases bovine leukemia virus tax and pol mRNA levels via cyclooxygenase 2: regulation by interleukin-2, interleukin-10, and bovine leukemia virus. J Virol 74:5740-5.

22. **Ray, N., M. E. Bisher, and L. W. Enquist.** 2004. Cyclooxygenase-1 and -2 are required for production of infectious pseudorabies virus. J Virol 78:12964-74.

23. **Rossen, J. W., J. Bouma, R. H. Raatgeep, H. A. Buller, and A. W. Einerhand.** 2004. Inhibition of cyclooxygenase activity reduces rotavirus infection at a postbinding step. J Virol 78:9721-30.

24. **Rossen, J. W., G. J. Strous, M. C. Horzinek, and P. J. Rottier.** 1997. Mouse hepatitis virus strain A59 is released from opposite sides of different epithelial cell types. J Gen Virol 78 (Pt 1):61-9.

25. **Rott, D., J. Zhu, M. S. Burnett, Y. F. Zhou, A. Zalles-Ganley, J. Ogunmakinwa, and S. E. Epstein.** 2003. Effects of MF-tricyclic, a selective cyclooxygenase-2 inhibitor, on atherosclerosis progression and susceptibility to cytomegalovirus replication in apolipoprotein-E knock-out mice. J Am Coll Cardiol 41:1812-9.

26. **Rottier, P. J., M. C. Horzinek, and B. A. van der Zeijst.** 1981. Viral protein synthesis in mouse hepatitis virus strain A59-infected cells: effect of tunicamycin. J Virol 40:350-7.

27. **Spencer, A. G., J. W. Woods, T. Arakawa, Singer, II, and W. L. Smith.** 1998. Subcellular localization of prostaglandin endoperoxide H synthases-1 and -2 by immunoelectron microscopy. J Biol Chem 273:9886-93.

28. **Steer, S. A., and J. A. Corbett.** 2003. The role and regulation of COX-2 during viral infection. Viral Immunol 16:447-60.

29. **Symensma, T. L., D. Martinez-Guzman, Q. Jia, E. Bortz, T. T. Wu, N. Rudra-Ganguly, S. Cole, H. Herschman, and R. Sun.** 2003. COX-2 induction during murine gammaherpesvirus 68 infection leads to enhancement of viral gene expression. J Virol 77:12753-63.

30. **Thiry, E., B. Mignon, F. Thalasso, and P. P. Pastoret.** 1988. Effect of prostaglandins PGE2 and PGF alpha 2 on the mean plaque size of bovine herpesvirus 1. Ann Rech Vet 19:291-3.

31. **van der Hoek, L., K. Pyrc, M. F. Jebbink, W. Vermeulen-Oost, R. J. Berkhout, K. C. Wolthers, P. M. Wertheim-van Dillen, J. Kaandorp, J. Spaargaren, and B. Berkhout.** 2004. Identification of a new human coronavirus. Nat Med 10:368-73.

32. **Vennema, H., L. Heijnen, A. Zijderveld, M. C. Horzinek, and W. J. Spaan.** 1990. Intracellular transport of recombinant coronavirus spike proteins: implications for virus assembly. J Virol 64:339-46.

33. **Verheije, M. H., T. Wurdinger, V. W. van Beusechem, C. A. de Haan, W. R. Gerritsen, and P. J. Rottier.** 2006. Redirecting coronavirus to a nonnative receptor through a virus-encoded targeting adapter. J Virol 80:1250-60.

34. **Weiss, S. R., and S. Navas-Martin.** 2005. Coronavirus pathogenesis and the emerging pathogen severe acute respiratory syndrome coronavirus. Microbiol Mol Biol Rev 69:635-64.

35. Woo**, P. C., S. K. Lau, C. M. Chu, K. H. Chan, H. W. Tsoi, Y. Huang, B. H. Wong, R. W. Poon, J. J. Cai, W. K. Luk, L. L. Poon, S. S. Wong, Y. Guan, J. S. Peiris, and K. Y. Yuen.** 2005. Characterization and complete genome sequence of a novel coronavirus, coronavirus HKU1, from patients with pneumonia. J Virol 79:884-95.

36. **Yan, X., Q. Hao, Y. Mu, K. A. Timani, L. Ye, Y. Zhu, and J. Wu.** 2006. Nucleocapsid protein of SARS-CoV activates the expression of cyclooxygenase-2 by binding directly to regulatory elements for nuclear factor-kappa B and CCAAT/enhancer binding protein. Int J Biochem Cell Biol 38:1417-28.

37. **Zhu, H., J. P. Cong, D. Yu, W. A. Bresnahan, and T. E. Shenk.** 2002. Inhibition of cyclooxygenase 2 blocks human cytomegalovirus replication. Proc Natl Acad Sci U S A 99:3932-7.

Chapter 7

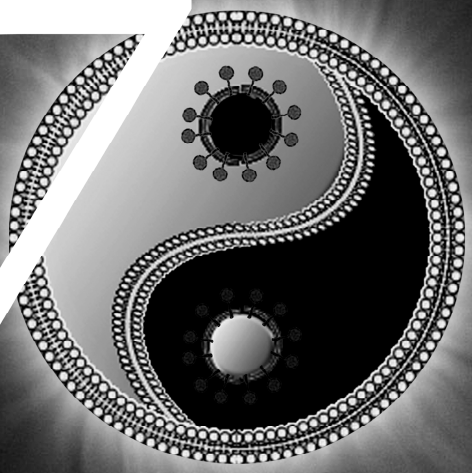

Non-Invasive Imaging of Mouse Hepatitis Coronavirus Infection Reveals Determinants of Viral Replication and Spread *in Vivo*

Matthijs Raaben
Henk-Jan Prins
Peter J.M. Rottier
Anton C. Martens
Cornelis A.M. de Haan

Cellular Microbiology; 2009 May;11:825–41.

Abstract

Bioluminescence imaging (BLI) is a powerful new method to study virus dissemination in the live animal. Here we used this method to monitor the spatial and temporal progression of mouse hepatitis coronavirus (MHV) infection in mice using luciferase-expressing viruses. Upon intranasal inoculation, virus replication could initially be observed in the nasal cavity and the cervical lymph nodes, after which the infection spread to the brain and frequently to the eyes. The kinetics of virus spread to and clearance from the brain appeared to depend on the inoculation dose. After intraperitoneal inoculation, virus replication was predominantly observed in the liver and occasionally in the intestines, but interestingly also in the tail and paws. BLI thus elucidated new anatomic locations of virus replication. Furthermore, MHV dissemination was shown to be critically dependent on the viral spike protein, but also on the mouse strain used. Widespread dissemination was observed in mice lacking a functional type I interferon response. The importance of the type I interferon system in limiting viral spread was also demonstrated by the administration of type I interferons to mice. Our results provide new insights in coronavirus pathogenesis and demonstrate the potential of BLI to study coronavirus-host interactions *in vivo*.

Introduction

Current insights into infection processes of pathogens in their hosts and into the dynamics of their spread are largely based on studies using conventional methodologies. These methods have, however, many limitations. They require the experimental animals to be sacrificed in order to identify the sites of infection and to quantify the replication of the pathogens. They hence require large numbers of animals and are costly. They do not allow the real-time monitoring of spatial and temporal progression of infection in the same animal. Important variations in host–pathogen interactions might therefore be overlooked, while dissemination of a pathogen to unexpected anatomical locations might be missed, simply because the infected tissue is not harvested and analysed (24, 38). As of recently many of these limitations of the conventional techniques can be overcome by powerful new methods that involve non-invasive imaging of pathogen replication and spread in infected live animals.

As a member of the Coronavirus (CoV) family, the mouse hepatitis virus (MHV) provides a practical model system for studying CoV-induced pathogenesis in mice. Depending on the inoculation route, the virus strain, and the genetic background of the host, MHV infection can result in a variety of pathological disorders (5). The most commonly used laboratory strains primarily infect the liver and the brain, thereby providing animal models for studying encephalitis and hepatitis as well as for immune-mediated demyelinating disease that sometimes develop during a later stage of infection (51). Inoculation of susceptible mice, either intracranially or intranasally, with neurotropic MHV strains can result in a number of different outcomes, ranging from acute encephalomyelitis to chronic demyelinating disease (23). Besides a mild encephalitis, MHV strain A59 also causes enteric disease and moderate hepatitis (30). The differences in pathogenesis between various MHV strains have been linked mainly to the spike protein which mediates virus-cell attachment and subsequent membrane fusion (53). However, other viral genes have been shown to also significantly contribute to pathogenesis (13, 25, 62).

The role of the immune system in response to MHV infection has been extensively studied. Both humoral and cellular immune reactions are essential to guard against MHV infections (1, 42, 46). Clearance of virus during acute infection is predominantly regulated by a

typical expression pattern of proinflammatory chemokines that attract CD8+ and CD4+ T lymphocytes to sites of infection (18, 29, 63). Also interferon (IFN)- and perforin-mediated mechanisms are involved in the clearance of MHV from different cell types (68). The kinetics and the extent of the host immune response, which aims to limit the production of infectious virus and viral spread without inducing extensive deleterious effects, is important in determining survival of the host. Infectious virus is usually cleared from MHV-infected mice within two weeks. Most animals, however, do not appear to obtain complete sterile immunity, since viral RNA is often found to persist within the central nervous system (CNS).

Recent biotechnological advances now allow the real-time imaging of pathogen replication and spread in living animals by making use of bioluminescence imaging (BLI). To this end, light emitted by luciferase reporter proteins is detected by a cooled charge-coupled device (CCD) camera (8, 69). Important advantages of BLI are an intrinsically low background combined with a very high sensitivity for monitoring light emission *in vivo* (6, 24). Furthermore, the substrate for firefly luciferase (FL), D-luciferin, is able to cross cellular membranes as well as the intact blood-brain barrier, thereby allowing the imaging of any anatomic location. In addition, D-luciferin is non-toxic, allowing the monitoring of individual mice over time through consecutive imaging. Thus, fewer animals are typically needed to acquire statistically meaningful data at multiple time-points as compared to conventional approaches (24). Initially, BLI was used to identify sites of bacterial replication in intact animals (7). Nowadays, this technique is widely used to study the formation and spread of cancer metastases and to visualize the effect of chemotherapy (61). BLI has also been used to study the dissemination of herpes simplex virus, Sindbis virus, Vaccinia virus, and Infectious hematopoietic necrosis virus (9, 20, 35, 55).

All previous studies describing MHV infections and pathogenesis in mouse models have been relying on the sacrifice of infected mice in order to determine virus distribution and titers in various organs over time. Although these conventional approaches have defined important factors that dictate replication and virulence of MHV *in vivo* as described above, non-invasive whole-body imaging of MHV infection in living mice is likely to offer new insights into virus replication, dissemination and pathogenesis. Here, we have taken

advantage of BLI to study the replication and spread of firefly luciferase-expressing MHV (10, 16) in mice in real-time. We were also able to demonstrate differences in virus replication and spread, resulting either from differences in virus doses, mutations in the spike gene, differences in host susceptibility or from the administration of antiviral compounds. In addition, we identified new anatomic sites of virus replication. Our results provide new insights in coronavirus pathogenesis and demonstrate the potential of BLI to study CoV-host interactions *in vivo*.

Results

The Characteristics of Reporter MHVs *in Vitro* and *in Vivo*

In our previous studies we extensively characterized various recombinant MHVs expressing luciferase reporter genes. The insertion of a FL expression cassette at different positions in the viral RNA genome was shown not to appreciably affect virus multiplication *in vitro*, while the FL expression levels were demonstrated to be a reliable measure for virus replication (16, 65). To verify the feasibility of detecting MHV infection *in vivo* with BLI, we compared two recombinant MHVs containing the luciferase gene at different positions in the viral genome with a recombinant wild-type MHV-A59 with respect to virus replication. Therefore, we prepared new stocks of MHV-EFLM (containing the FL gene as an additional expression cassette between the E and M gene), MHV-2aFLS (containing the FL expression cassette at the position of the hemagglutinin esterase pseudo gene) and wild-type MHV-A59 (Fig.1A). In agreement with the previous studies we observed that the growth characteristics of the luciferase-expressing viruses in tissue culture were highly similar to that of the parental MHV-A59 (Fig.1B), with the FL reporter gene being expressed at high levels for both MHV-EFLM and MHV-2aFLS. For the characterization of the FL-expressing viruses *in vivo* we used BALB/c mice, which have been shown to be susceptible to MHV infection (48). Since the inoculation route largely determines the dissemination of virus infection in an animal, we made use of both intranasal and intraperitoneal injection. 6-8 weeks old mice were inoculated with 10^6 $TCID_{50}$ of virus or with PBS (control) and sacrificed at 5 days post inoculation, at which day virus titres peak (40).

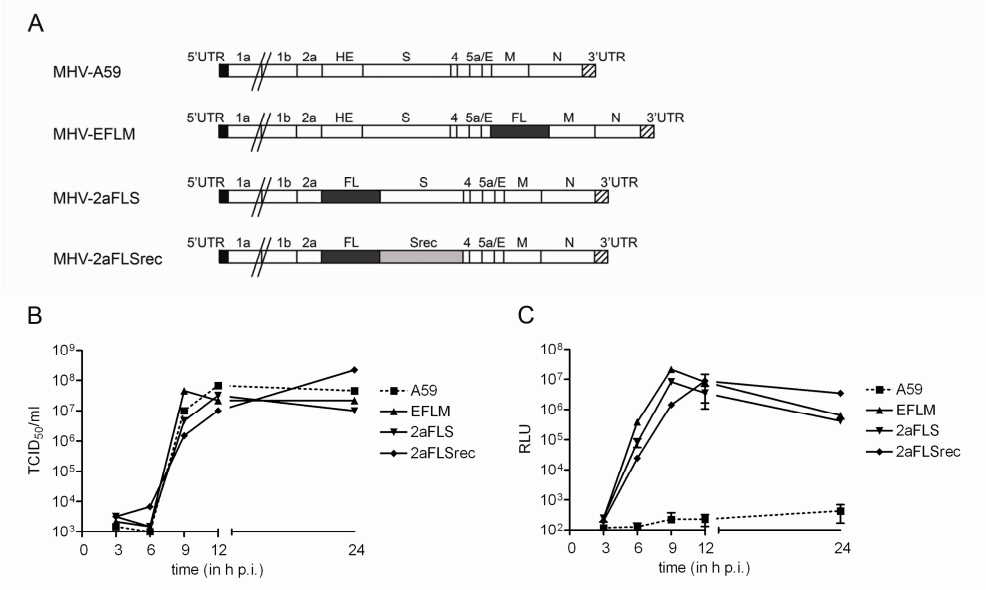

Fig.1. Recombinant viruses with an FL expression cassette at different genomic locations. (A) The genomic organization of the recombinant wild-type MHV (MHV-A59) and of the recombinant viruses carrying a FL expression cassette. The numbers designate the genes encoding the non-structural proteins, while genes encoding the spike (S) protein, envelope (E) protein, membrane (M) protein, hemagglutinin-esterase (HE) protein, and nucleocapsid (N) protein are indicated by their abbreviations. Srec indicates the S gene carrying the mutations that are responsible for the extended host range. The 5'- and 3'- untranslated regions (UTR) are also designated. (B) The growth kinetics of the MHV recombinants. LR7 cells were infected with each recombinant MHV at an MOI of 1. Viral infectivity in the cell culture media at different times p.i. was determined by a quantal assay on LR7 cells, and $TCID_{50}$ values were calculated. (C) In parallel, the intracellular expression of luciferase in relative light units (RLU) was determined as described in the *Material & Methods* section. Standard deviations (n = 3) are indicated.

Since MHV-A59 mainly targets the liver and brain (19, 31), these organs were taken for analyses. Tissue homogenates were prepared and subsequently tested for virus titres, RNA levels, and FL activity. In intranasally inoculated animals, we detected high virus titres in the brains of all infected mice, with no disparity between the wild-type and FL-expressing viruses (Fig.2A). Infectious virus could not be recovered from the liver homogenates. Also the viral RNA levels in the brains of the animals, as determined by quantitative RT-PCR, were indistinguishable between groups. However, viral RNA in the liver could only be detected in wild-type MHV-infected mice (Fig.2B).

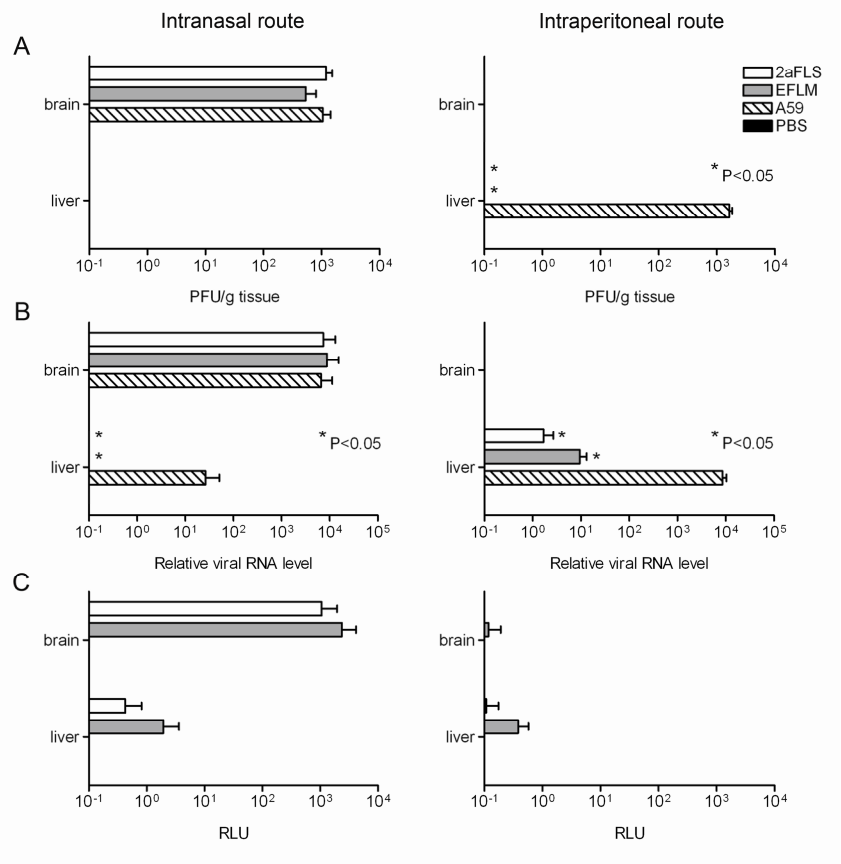

Fig.2. Replication of MHV-EFLM and MHV-2aFLS *in vivo*. 6-8 weeks old female BALB/c mice were inoculated either intranasally or intraperitoneally with PBS or with 10^6 $TCID_{50}$ of wild-type MHV-A59, MHV-EFLM or MHV-2aFLS. At 5 days post inoculation, all mice were sacrificed and brains and livers were collected. Homogenates were prepared as described in the *Material & Methods* section. (A) Viral infectivity in the homogenates was determined by performing a plaque assay on LR7 cells. The viral titers are expressed as plaque-forming units per gram (PFU/g) tissue. (B) The amounts of viral genomic RNA relative to total RNA, isolated from the liver and brain homogenates, were determined by quantitative Taqman RT-PCR. (C) Luciferase activities (in RLU) in each of the homogenates were determined by using a luminometer as described above. Standard deviations (n = 4) are indicated in all graphs.

All mice infected with the FL-expressing recombinants showed high FL activity in the brain, as well as some FL activity in the liver (Fig.2C). Although not statistically significant, the FL expression levels of MHV-2aFLS were somewhat lower than those of MHV-EFLM, which is consistent with the relative expression levels observed *in vitro* (16). After intraperitoneal inoculation, infectious virus could only be recovered from the livers of

wild-type MHV-A59-infected animals (Fig.2A). Although viral RNA was detected in the livers of all groups, the levels were approximately a 1,000-fold lower for the FL-expressing MHV recombinants (Fig.2B). Furthermore, only in some livers of MHV-EFLM- and MHV-2aFLS-infected mice FL activity above background level could be detected. Overall, these data show that the introduction of the FL expression cassette into the genome of MHV-A59 affected virus multiplication in the liver but, importantly, not in the brain of 6-8 weeks old BALB/c mice. High levels of FL activity were measured in the brains of MHV-EFLM- and MHV-2aFLS-infected mice at 5 days post infection (p.i.), indicating that these viruses are attractive candidates to be used for BLI after intranasal inoculation.

Bioluminescence Imaging of MHV-EFLM- and MHV-2aFLS-Infected Mice

Thus, we applied whole body BLI to study the replication and spread of the two firefly luciferase-expressing MHVs. To this end, BALB/c mice were inoculated intranasally with 10^6 $TCID_{50}$ of virus after which virus replication was followed over time in individual mice. In general, very similar patterns of virus dissemination were observed for both viruses. At 2 days post inoculation, a strong signal was observed, apparently emanating from the nasal cavity, when the mice were imaged at their dorsal side (Fig.3A). When imaged from the ventral side, replication additionally could be observed in two distinct spots, probably representing the cervical lymph nodes of the animal. At this time point, no signal coming from the brain could yet be detected. Three days later, dissemination of virus replication to the brain was apparent, while replication in the cervical lymph nodes was no longer observed. At 7 days post inoculation, the signal coming from the brain appeared more dispersed, while its intensity was clearly declining. At 9 days post inoculation, signal from the brain was scarcely detectable in most mice, while it could no longer be detected at day 12 (data not shown). With BLI, it is important to note that the measurable photon flux decreases with increasing depth of the target tissue (36). Thus, the signal coming from the brain is significantly attenuated when compared to the signal from the olfactory epithelium, since photons emitted from brain cells must penetrate considerably more tissue to be detected (Fig.3B). As a consequence, signal intensities should only be compared when photons emanate from the same tissue. Photon quantification of the head regions demonstrated that mice infected with MHV-EFLM showed significantly higher signal intensities than mice infected with MHV-2aFLS at 2 days post inoculation (Fig.3B).

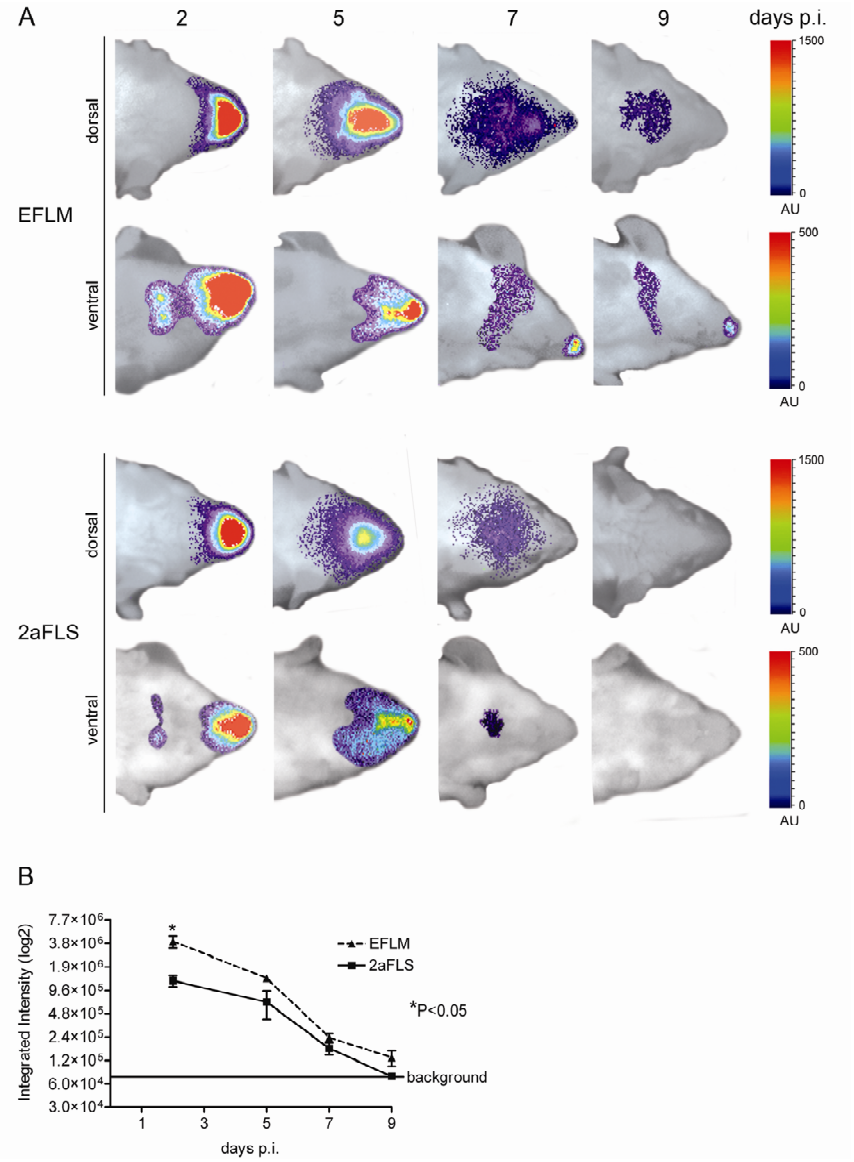

Fig.3. BLI of MHV-EFLM and MHV-2aFLS: spatial and temporal progression of infection. 6-8 weeks old female BALB/c mice were inoculated intranasally with 10^6 $TCID_{50}$ of either MHV-EFLM or MHV-2aFLS. At the indicated times post inoculation (days p.i.), mice were processed for BLI as described in the *Material & Methods* section. (A) Dorsal and ventral images of a representative mouse, either infected with MHV-EFLM or with MHV-2aFLS, are shown. The emitted photons were measured by a CCD-camera and are displayed as a heat map in an overlay image. Note that the scaling (in arbitrary units (AU)) differs between the dorsal and ventral images. (B) The total amounts of emitted photons from the dorsal head regions at the different time-points were quantified and are expressed as integrated intensities on a $\log^2$ scale with standard deviations (n = 4).

In conclusion, with BLI the temporal and spatial spread of MHV replication could be readily visualized in living mice. While mice infected with different luciferase-expressing viruses displayed very similar patterns of virus dissemination, BLI allowed the quantitative detection of relatively small differences in FL-expression levels between MHV-EFLM and MHV-2aFLS, which is consistent with our earlier observations (16).

Virus Inoculation Dose Strongly Affects Intensity and Spread of the Infection

We next analyzed whether we could visualize virus inoculation dose-dependent effects. To this end, BALB/c mice were infected with two different doses of MHV-EFLM, a high dose of $5x10^6$ and a low dose of $2x10^3$ $TCID_{50}$, and progression of infection was subsequently monitored by BLI at different time-points post inoculation (Fig.4A). As expected, photon quantification of the head regions at 2 days post inoculation demonstrated a clear correlation between the virus inoculation dose and the total signal produced from the olfactory epithelium (Fig.4B). In addition, spread of virus replication from the nasal cavity into the CNS was more rapidly observed for the mice inoculated with the higher dose. This effect was quantified by dividing the head region into two sections (i.e. anterior versus posterior) after which the relative amount of photons emitted from these sections was determined (Fig.4C). With a high virus inoculation dose, approximately 50% of the total amount of photons was coming from the posterior part at day 5, while with the low virus dose this degree of dissemination was delayed until around day 7. Consistently, while mice that received the high dose showed virus replication in the cervical lymph nodes after 2 days, this was apparent in the mice inoculated with the low dose only after 5 days (Supplemental table S1A). Interestingly, mice infected with the higher dose appeared to clear the virus infection faster than animals infected with the low dose. MHV replication was easily detectable at day 9 in mice inoculated with the low dose, whereas the luciferase signal of the high dose-inoculated group was almost undetectable at this time point. In some mice infected with a high virus dose, we could additionally visualize infection of the liver and lungs after 2 days, whereas at later time-points (9 days), strong signals from the eyes were occasionally detectable. For a summary of the results see Supplemental table S1.

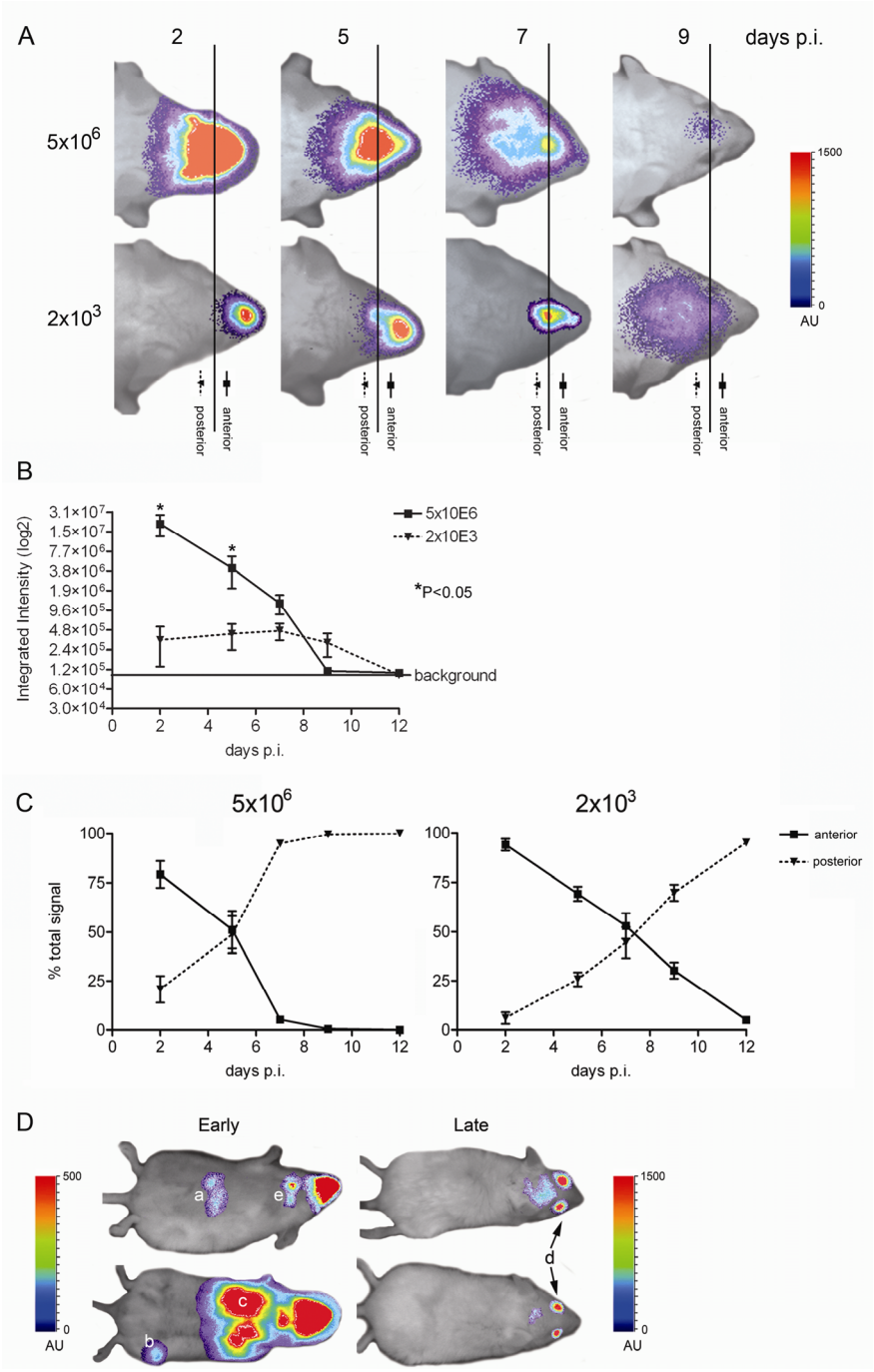
A
2
5
7
9
days p.i.
5x10^6
2x10^3
1500
0
AU
posterior
anterior
B
Integrated Intensity (log2)
3.1×10^7
1.5×10^7
7.7×10^6
3.8×10^6
1.9×10^6
9.6×10^5
4.8×10^5
2.4×10^5
1.2×10^5
6.0×10^4
3.0×10^4
5x10E6
2x10E3
*P<0.05
background
0 2 4 6 8 10 12
days p.i.
C
5x10^6
2x10^3
% total signal
100
75
50
25
0
anterior
posterior
days p.i.
D
Early
Late
500
0
AU
1500
a
e
c
b
d

Fig.4. The inoculation dose affects virus dissemination. BALB/c mice were inoculated intranasally with $5x10^6$ or $2x10^3$ $TCID_{50}$ of MHV-EFLM. At the indicated times post inoculation (days p.i.), mice were processed for BLI. (A) Dorsal images of a representative mouse are portrayed. The emitted photons were measured at the indicated time-points and are displayed as a heat map in an overlay representation. Scaling (in arbitrary units (AU)) is similar in all depicted images. The vertical line in all panels represents the arbitrary border between the anterior (nose) and posterior (brain) regions of the head, which were selected for photon quantification. (B) The total amounts of emitted photons from the complete head regions at the different time-points were quantified and are expressed as integrated intensities on a $\log^2$ scale with standard deviations (n = 4). (C) The relative amounts of emitted photons from the anterior and posterior regions of the head (i.e. brain versus nasal epithelium) at the different time-points were quantified and are expressed as percentage of the total signal, with standard deviations for both virus doses (n = 4). (D) Interesting phenotypes of mice at early (i.e. 2 days; ventral images portrayed) or late (i.e. 9 days; dorsal images portrayed) times post inoculation with $5x10^6$ $TCID_{50}$ of MHV-EFLM are shown: (a) liver, (b) paw, (c) lung, (d) eye, and (e) cervical lymph nodes. Note that the scaling (in arbitrary units (AU)) differs between the ventral and dorsal images.

In conclusion, virus dissemination was shown to differ in mice infected with a low or a high dose. In mice that received the low dose virus replication was initially restricted to the nasal cavity, while much faster dissemination of virus infection was observed after inoculation with a high dose. Strikingly, and counter intuitively, this rapid dissemination appeared to come at a cost, as these mice were able to clear the infection faster than the mice that received the low dose.

In Vitro Adaptation of MHV to Heparan Sulfate Reduces Viral Replication and Spread *in Vivo*

We next analyzed the essential contribution of the S protein to virus dissemination by using BLI. The S protein of MHV is a major determinant of pathogenesis and tropism (53). It mediates virus-cell attachment and fusion via binding of the MHV receptor CEACAM1a both *in vitro* and *in vivo* (2, 21). Schickli and coworkers (60) described a limited set of mutations in the S protein of an MHV-A59 variant that had been acquired after extensive passaging in cell culture. We recently showed that these mutations enable the virus to use heparan sulfate as an additional attachment/entry factor. As a result, viruses carrying these mutations appeared to have acquired an extended host range as they were capable of entering cells also in a CEACAM1a-independent manner (12, 60). The physiological consequences of this adaptation *in vivo*, however, remain to be elucidated. Here, we examined the infection of mice by an MHV with such an extended host range.

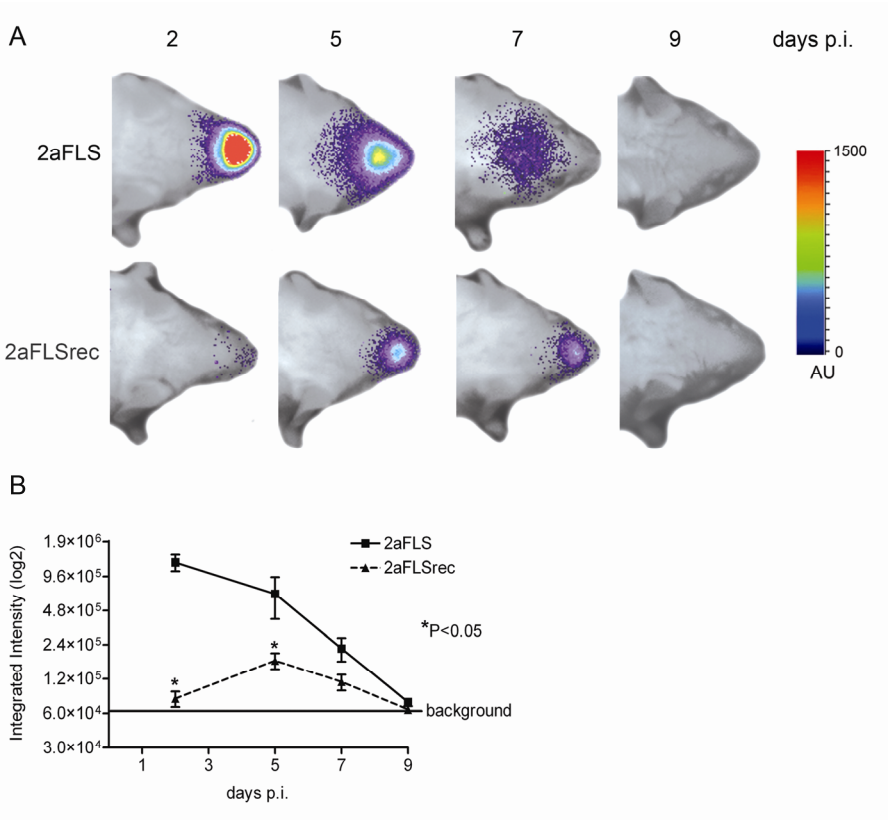

Fig.5. Adaptation to heparan sulfate affects virus replication and spread. 6-8 weeks old female BALB/c mice were inoculated intranasally with 10^6 $TCID_{50}$ of MHV-2aFLS or MHV-2aFLSrec. At the indicated times post inoculation (days p.i.), mice were processed for BLI. (A) The dorsal side of the head region of a representative mouse, infected with either MHV-2aFLS or MHV-2aFLSrec is shown. The emitted photons were measured at the indicated time-points and are displayed as a heat map in an overlay image. (B) The total amounts of emitted photons from the head regions at the different time-points were quantified and are expressed as integrated intensities on a log^2 scale with standard deviations (n = 4).

Therefore we made use of a previously described recombinant virus (12), which contains the mutant spike gene (Srec) and the FL reporter gene. Thus, this recombinant virus MHV-2aFLSrec only differs from its control virus MHV-2aFLS in its spike protein. Both viruses replicated to comparable titers in murine LR7 cells as demonstrated by the one-step growth curve shown in Fig.1B and displayed similar FL expression kinetics (Fig.1C). Next, BALB/c mice were inoculated via the intranasal route with these viruses. Clearly, MHV-2aFLSrec replicated to a lower extent than the parental virus MHV-2aFLS at all time-points

measured (Fig 5A and B). Although the luciferase signal exhibited by the virus with the extended host range increased until 5 days p.i., the infection did not progress towards the CNS as was observed for the control virus. Apparently, the acquisition of a heparan sulfate-dependent tropism significantly attenuated the ability of the virus to replicate and spread *in vivo*.

Replication and Spread of MHV in Mice of Different Genetic Background

Replication of viruses *in vivo* is not only dependent on the genetic make-up of the virus, but also that of its host. It has been observed that the susceptibility of inbred mouse strains to different virus infections can vary significantly (26, 50, 64). In order to comparatively evaluate the MHV infection process in mice, we infected three commonly used mouse strains with MHV-EFLM. To this end, BALB/c, C57BL/6, and 129SvEv mice were inoculated in parallel each with 10^6 $TCID_{50}$ via the intranasal route after which virus replication was monitored over time. Clearly, at 5 days post inoculation BALB/c mice displayed the highest signal in the brain, followed by C57BL/6 mice (Fig.6A and B). Interestingly, 129SvEv mice were significantly less susceptible to MHV-EFLM infection. In contrast to BALB/c and C57BL/6 mice, virus replication was no longer detectable from 7 days post inoculation in these animals (data not shown). To confirm these observations, we inoculated mice also with MHV-A59 wild-type virus and determined the viral RNA load in the brain by quantitative RT-PCR at 5 days post inoculation. In agreement with the BLI results, BALB/c mice showed the highest viral RNA levels, while the brains from C57BL/6 and 129SvEv mice contained considerably less viral RNA (Fig.6B).

Next we studied virus replication and spread of the FL-expressing virus after intraperitoneal inoculation of BALB/c and C57BL/6 mice. To this end 4 week-old mice were inoculated intraperitoneally with 10^6 $TCID_{50}$ of MHV-EFLM (Fig.6C). At 2 days post inoculation we could visualize virus replication in the liver, with no apparent difference between the two mouse strains. In some mice, infection of the intestine was also observed. Interestingly, in all mice we could observe infection of the tail and paws, hitherto unidentified sites of infection. The signal rapidly decreased in time, with infection no longer being visible at 5-7 days post inoculation (data not shown). These results show that although replication of FL gene-containing viruses is decreased in 6-8 weeks old mice (Fig.2), which hardly enabled

the detection of MHV replication by BLI (data not shown), the infection could easily be monitored in younger mice, which are known to be more susceptible to infection. In addition, the technology allowed the identification of new anatomic sites of MHV replication that had been missed with the conventional techniques (Supplemental table S1B).

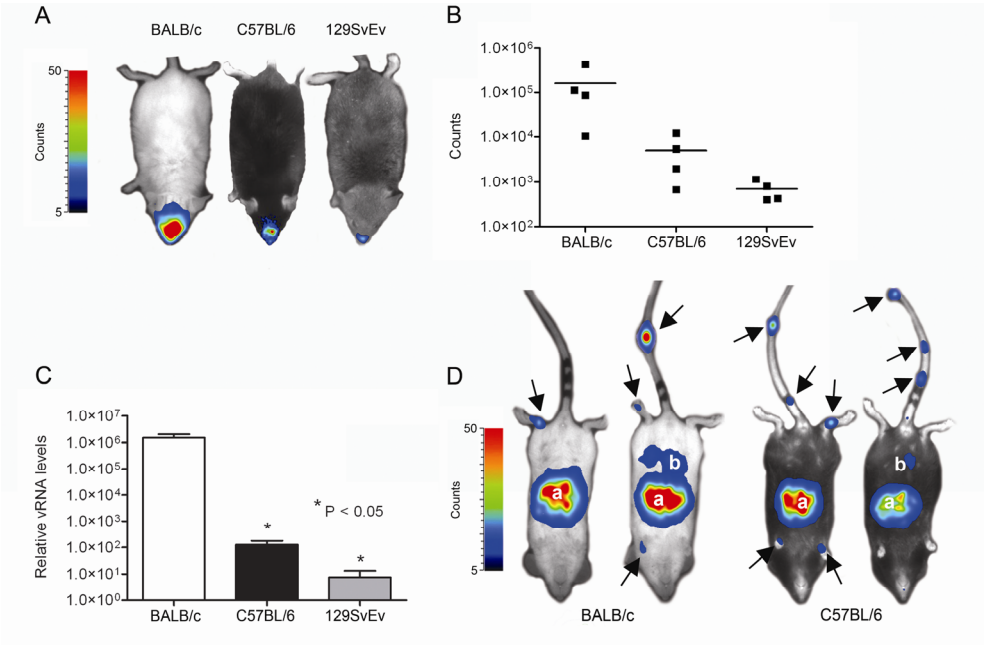

Fig.6. Replication of MHV-EFLM in mice of different genetic background. 6-8 weeks old female BALB/c, C57BL/6, and 129SvEv mice were inoculated intranasally with 10^6 $TCID_{50}$ of MHV-EFLM. (A) BLI was performed at 5 days post inoculation as described in the *Material & Methods* section. Here, the Biospace photon imager was used as detector for reporter gene expression. The emitted photon counts were measured and are displayed as a heat map in an overlay image. A representative dorsal image is shown for the different mouse strains. (B) The emitted photons from the head regions of each individual mouse were quantified and are expressed as the total number of counts measured within the 10-minute imaging period. Data are corrected for the background values (signal from uninfected mice). (C) Mice infected with wild-type MHV-A59 were sacrificed at day 5 p.i., after which the individual brains were collected. Total RNA was isolated and Taqman RT-PCR was performed targeting MHV genomic RNA sequences. The relative viral RNA (vRNA) levels and standard deviations are depicted (n = 4). (D) 4 weeks old BALB/c and C57BL/6 mice were inoculated intraperitoneally with 10^6 $TCID_{50}$ of MHV-EFLM. BLI was performed at 2 days post inoculation. Also here, the Biospace photon imager was used. The emitted photons were measured and are displayed as a heat map in an overlay image. Two representative ventral images are shown for the two different mouse strains. The anatomic locations displaying virus replication are indicated and include: (a) liver, and (b) intestine. The arrows point to sites of virus replication in the tail and paws of the mice.

Enhanced Spread of MHV in IFNAR$^{-/-}$ Mice

Next, BLI was used to investigate the importance of the antiviral type I IFN system in controlling acute MHV infection. To this end, the effect of IFN alpha receptor knock-out (IFNAR$^{-/-}$) was studied using 129SvEv mice. Wild-type and knock-out mice were inoculated via the intranasal route with 10^6 $TCID_{50}$ of MHV-EFLM and the infection process was monitored as before. Already at 2 days p.i. a significant difference between the IFNAR$^{-/-}$ and wild-type mice was apparent when the animals were examined from the ventral side (Fig.7A). A much higher signal was emitted from the nasal cavity in the IFNAR$^{-/-}$ mice compared to the wild-type mice while, in addition, infection of the cervical lymph nodes was only detected in the knock-out mice. At later time-points, infection was rapidly cleared from the wild-type mice, whereas dissemination to other organs, including liver and intestine, was manifest in the IFNAR$^{-/-}$ mice. Virus dissemination was accompanied by severe clinical signs, which included a significant decrease in body weight (Fig.7B). Mice had to be euthanized at 7 days p.i. Interestingly, virus replication in the tail and paws could again be detected in the IFNAR$^{-/-}$ mice, similar to what we had observed after inoculation of BALB/c and C57BL/6 mice via the intraperitoneal route (Fig.5C). *Ex vivo* imaging of the abdominal region of the IFNAR$^{-/-}$ mice clearly identified the liver as the major site of MHV-EFLM replication (Fig.7C), the organ showing a focal pattern of luciferase expression. This observation was confirmed by the histological analysis of liver sections, as focal lesions were only observed in IFNAR$^{-/-}$ mice, but not in the control mice (Fig.7D). Overall, these results indicate that mice lacking a functional type I IFN response exhibit disseminated infection after intranasal inoculation with MHV-A59, which could be readily visualized using BLI. In view of the increasing availability of all kinds of mutant mice, BLI is an attractive approach to investigate the role of a particular host protein or pathway in virus replication and dissemination *in vivo*.

Recombinant Type I IFN Blocks Virus Spread

As apparently uncontrolled virus dissemination was observed in mice lacking a functional type I IFN response, we next evaluated the anti-coronaviral effect of exogenous administration of type I IFN. Thus, a cocktail of IFNα/β was applied to BALB/c mice intranasally. It has been established before that IFN can bypass the blood-brain barrier after intranasal delivery (56).

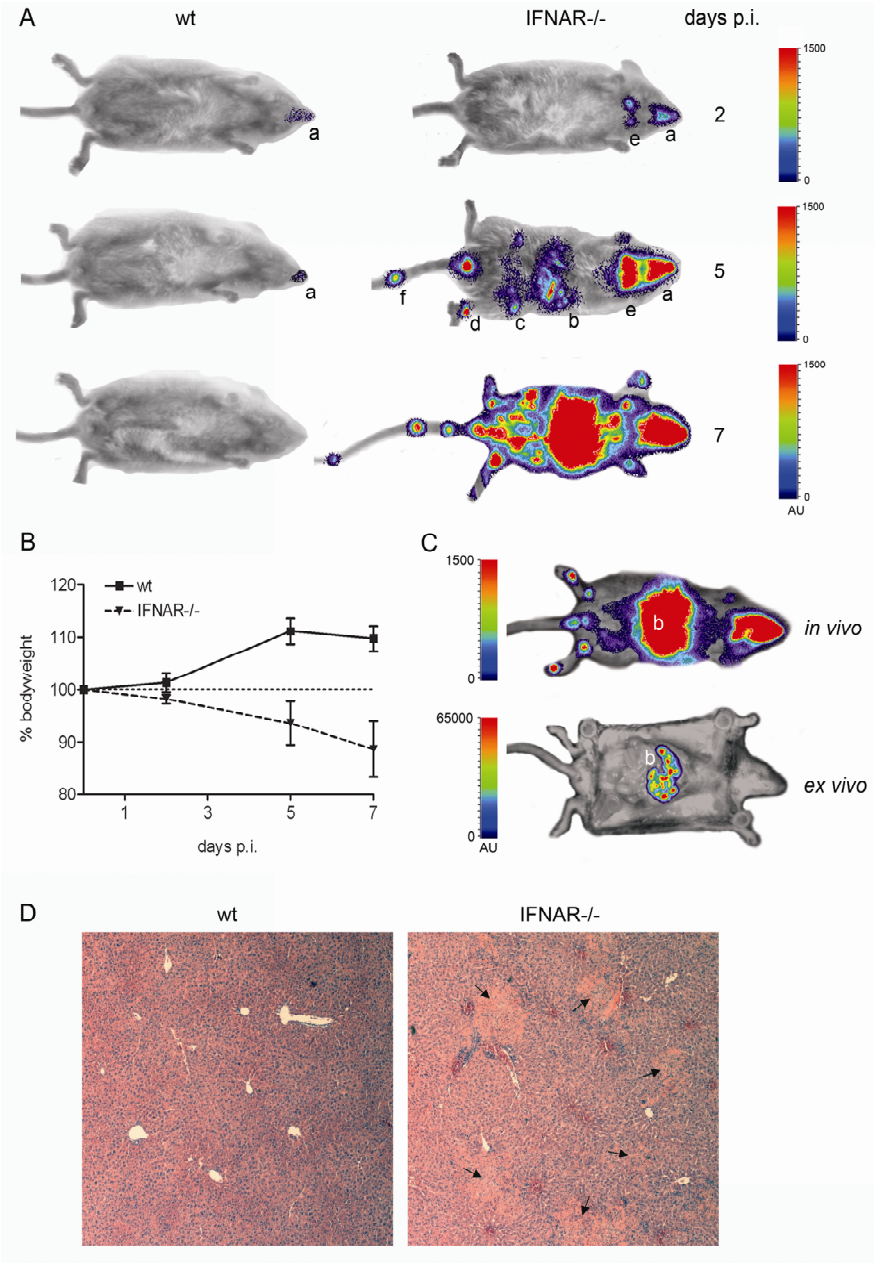

Fig.7. IFNAR$^{-/-}$ mice are highly susceptible to MHV-EFLM infection. IFNAR$^{-/-}$ or the parental 129SvEv mice were inoculated intranasally with 1x10^{6} $TCID_{50}$ of MHV-EFLM. At the indicated times post inoculation (days p.i.), mice were processed for BLI. (A) Ventral images of a representative mouse are shown. The emitted photons were measured at the indicated time-points and are displayed as a heat map in an overlay image: (a) nasal cavity, (b) liver, (c) intestine, (d) paws, (e) cervical lymph nodes, and (f) tail. (B) The average body weight of both groups

of mice is shown as the percentage relative to the initial weight at the beginning of the experiment. Standard deviations are indicated (n = 4). (C) *In vivo* versus *ex vivo* imaging of an IFNAR$^{-/-}$ mouse infected with MHV-EFLM at 7 days post inoculation. After the standard BLI procedure, this mouse was sacrificed and immediately processed for imaging of the internal organs. Note that the scaling (in arbitrary units (AU)) in both images is different in order to visualize the focal infection pattern in the liver after *ex vivo* imaging. (D) The liver of the IFNAR$^{-/-}$ mouse in panel C was subsequently processed for histology as described in the *Material & Methods* section. As a control, a liver section of a MHV-EFLM infected 129SvEv wild-type mouse is shown. Typical focal lesions resulting from infection with MHV are indicated by the black arrows.

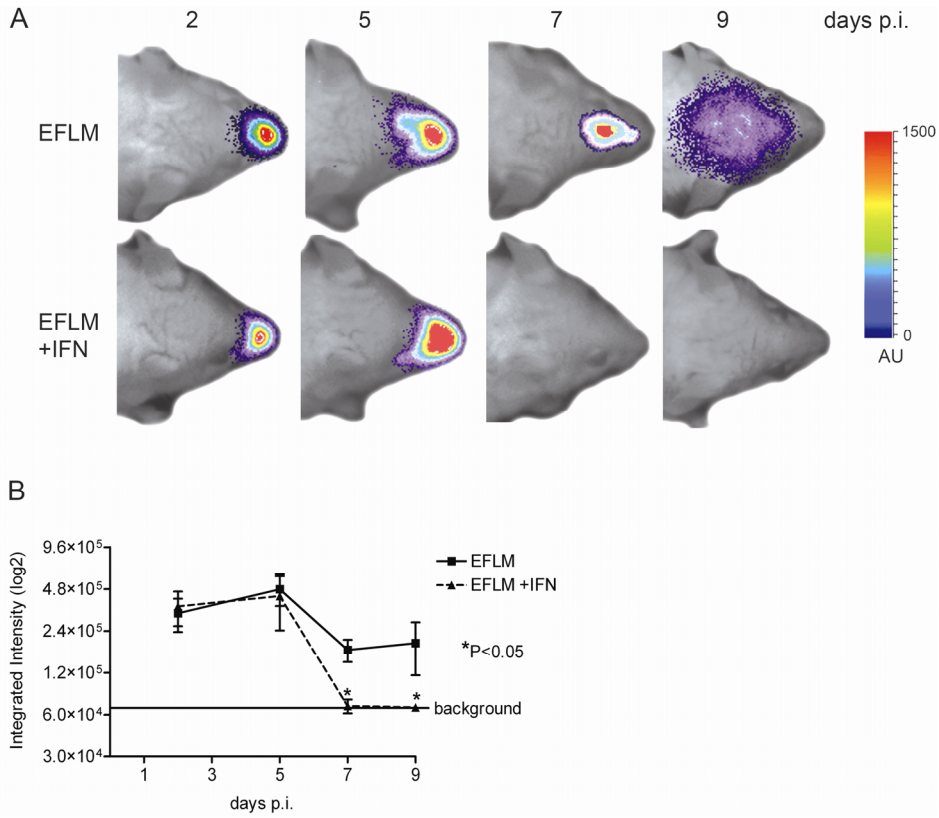

Fig.8. Recombinant IFNα/β inhibits spread of MHV-EFLM. 6-8 weeks old female BALB/c mice were given either 1,000 U of recombinant mouse IFN-α/β in PBS or PBS alone on each of days -2, -1, 0, 1, and 2 relative to inoculation with MHV-EFLM. At the indicated times post inoculation, mice were processed for BLI. (A) Dorsal images of a representative mouse, inoculated with $2x10^3$ $TCID_{50}$ MHV-EFLM, are indicated. The emitted photons were measured at the indicated time-points and are displayed as a heat map in an overlay image. (B) The total amounts of emitted photons from the head regions at the different time-points were quantified and are expressed as integrated intensities on a log^2 scale with standard deviations (n = 4).

Following subsequent intranasal inoculation with $2x10^3$ $TCID_{50}$ of MHV-EFLM, mice were processed for BLI at the indicated time-points as described above (Fig.8A). At day 2, replication of MHV was not significantly affected by the application of IFN. However, while virus replication spread to the brains of the mock-treated animals, this was not observed in the IFN-treated mice. Rather, the luciferase signal was lost by day 7. These observations were confirmed by the photon quantification of the head regions of the individual mice (Fig.8B). Thus, exogenous delivery of type I IFN did not prevent the initial replication in the nose, but prevented dissemination of virus infection to the CNS. The results also indicate that BLI is a promising technique for non-invasive screening of antiviral compounds, the major advantage being that this system allows detection of virus replication and spread after application of an antiviral compound over time within the same animal.

Discussion

Mouse models are essential for defining factors that regulate replication and virulence of viruses. However, the conventional approaches for studying viral infections in mouse models are frequently limited by the need to sacrifice large numbers of animals to quantify viral titers, and establish the complete pattern of virus dissemination. The application of non-invasive imaging methods for the monitoring of virus infections in living animals can significantly facilitate studies on determinants of viral spread and pathogenesis (24). We used BLI for the real-time monitoring of MHV infection by using recombinant MHV viruses that express FL reporter proteins. We confirm and extend previous observations by demonstrating that MHV dissemination is critically dependent on the virus inoculation route and dose, the viral spike protein, the genetic background of the host, and the type I IFN system. In addition, the technology provided insights into the kinetics and dynamics of the infection process under these different conditions. Furthermore, BLI revealed an animal-to-animal variation in viral spread and elucidated new anatomic locations of virus replication.

Despite its many attractive features for studying MHV replication and spread, the BLI technology has also some inherent limitations. First of all, photon transmission is affected by hair and organ pigmentation. Thus, photon flux from the surface of an animal will be

superior to that from an internal organ, since light is attenuated about 10-fold for every centimeter of tissue through which it has to pass (6). As a consequence it is impossible to quantitatively compare bioluminescent signals derived from different anatomic locations. This phenomenon also explains why the photon flux from the head region at 2 days p.i. is much higher than at later time-points as the signal initially originates from the nasal cavity but thereafter increasingly derives from the CNS, where it is much more shielded by surrounding tissue. To partly overcome this limitation, we routinely imaged the mice from both the ventral and the dorsal side. Second, the introduction of a foreign gene into the viral genome may affect virus replication *in vivo*. Interestingly, no significant differences could be observed between the replication of wild-type and FL-expressing viruses in the brain of intranasally-infected mice, indicating that introduction of the foreign gene did not affect replication *in vivo* per se. However, after intraperitoneal application the replication of reporter gene expressing viruses in the liver was clearly much lower. The cause of this apparent discrepancy is currently unknown. Importantly, however, FL expression was found at all the known sites of MHV replication (22, 27, 39, 43, 52, 54).

The MHV spike protein is an important determinant of pathogenesis (53). Using BLI, we monitored virus replication and spread of a recombinant virus that carried mutations in the spike gene shown to result in an extended host range *in vitro* due to the virus' ability to enter cells in a CEACAM1a-independent but heparan sulfate-dependent manner (12, 15, 60). Although it has been suggested that host range variants might arise *in vivo* during persistent infection of tissues that express low levels of the native MHV receptor (59, 60), this particular host range extension was obtained after serial passaging *in vitro*. Clearly, the mutant virus replicated to a much lower extent *in vivo* and was not able to spread to the brain. Many viruses adapt to heparan sulfate as an entry receptor upon propagation of the virus in cell culture (32, 41, 49). Often, but not always (11, 34), this adaptation results in a reduction of virulence in living animals, consistent with our results.

Inbred mouse strains are known to differ in their susceptibility to many virus infections (5, 26, 50, 64). In our experiments we monitored the replication of MHV in three different mouse strains. C57BL/6 and 129SvEv mice appeared to be less susceptible to infection compared to BALB/c mice after intranasal inoculation. Similar results were obtained when

mice were infected with wild-type MHV-A59 and viral RNA load monitored using quantitative RT-PCR. Strikingly, MHV replicated to approximately the same extent in BALB/c and C57BL/6 mice after intraperitoneal inoculation. Previously, mouse susceptibility to MHV infection was found to be linked to the viral receptor genotype (48). However, quantitative RT-PCR analysis of the CEACAM1a expression levels in brain and liver revealed only relatively small differences in the MHV receptor levels between the different mice strains, which did not correlate with the observed differences in viral replication (data not shown). Apparently, other yet unknown host factors contribute to or limit the dissemination of MHV. The resistance of 129SvEv mice to infection is not restricted to MHV, since also vesicular stomatitis virus replicated much more efficiently in BALB/c than in 129SvEv mice after intranasal inoculation (17). The difference in MHV replication between BALB/c and C57BL/6 mice might be associated with the mouse strain variation in immune responses which have been described for other virus infections (3, 33, 58, 64, 67). In general, C57BL/6 mice have a propensity to elicit a predominant T helper cell 1 response, while BALB/c mice have a tendency to elicit a predominant T helper cell 2 response.

Our results confirm and extend previous observations that dissemination of MHV infection is determined both by the route and by the dose of inoculation. Interestingly, clear differences in the spatio-temporal dissemination of the infection could be observed after intranasal inoculation with different virus doses. As expected, the virus inoculation dose correlated with the luminescent signal at two days p.i. However, inoculation with a low virus dose resulted in delayed spreading of the infection to the CNS and subsequent delayed clearance. This result suggests that a certain level of replication in the nasal epithelium is required for subsequent dissemination. Strikingly, at 9 days p.i. higher levels of virus replication could be observed after inoculation with the low dose compared with the high dose. Thus after inoculation with the high dose, virus was cleared faster from the brain. Apparently, clearance of the virus is triggered by the extent of virus replication in the brain. Probably high levels of virus replication more effectively induce an antiviral innate immune response. These results are corroborated by the observation that the expression levels of type I IFN and other cytokines positively correlate with the viral load in the brain of MHV-infected mice (unpublished results).

Type I IFN is a fundamental component of the innate immune response, which upon induction elicit an important antiviral signaling cascade that controls and orchestrates the outcome of numerous virus infections (71). Here, we analyzed the full extent of MHV dissemination in mice lacking a functional type I IFN response. These mice appeared to be highly susceptible to MHV and showed severe spread of the infection throughout the body when analyzed with BLI after intranasal inoculation. In contrast, the parental 129SvEv animals only showed some low levels of viral replication in the nasal cavity. These results confirm and extend recent studies in which MHV-A59 infected IFNAR$^{-/-}$ mice were also shown to be highly susceptible to infection, both after intraperitoneal (4) and after intracranial inoculation (57). We additionally demonstrated the importance of the type I IFN system in controlling MHV dissemination by administration of type I IFNs. Intranasal delivery of recombinant type I IFNs inhibited the spread of the infection to the brain, consistent with a previous study using the MHV strain JHM (44). It was interesting to observe that, while the spread to the brain was affected, the initial replication in the nasal epithelium was not decreased by the intranasally administered IFNs. The experiments demonstrate the power of the BLI technology for studying the effects of antiviral agents on virus replication and dissemination in animal models as was also illustrated earlier (35, 37).

Our observations show that virus dissemination in an organism is a multifactorial process in which the genetic make-up of pathogen and host, the inoculation dose and route, and the status of the immune system play important roles. In addition, through the application of BLI it has now become evident that, besides the typical, reproducible dissemination characteristics of MHV in mice, clear animal-to-animal variation also occurs. Thus, while the infection invariably targets organs like brain, cervical lymph nodes and liver, depending on the inoculation route/dose, other anatomical sites of replication are less frequently detected (see Supplemental table S1 for an overview). Occasionally, MHV replication was measured in the lungs, in the intestine or in the eyes. Quite frequently infection was also detected in the tail and paws, body parts not described earlier as sites of MHV replication. These results suggest that MHV can spread to and replicate in bone marrow *in vivo*, consistent with earlier *in vitro* studies demonstrating infection of bone marrow-derived macrophages and dendritic cells (57, 70). Strikingly, MHV replication in tail and paws was never observed throughout the entire length of these extremities, but occurred only in

distinct sites that differed between animals. In this respect, the dissemination of MHV is reminiscent of cancer metastases, which often also occur at distinct anatomical locations (45). Similar to the importance of microenvironmental host factors in determining the non-random pattern of tumor localization, replication of MHV may also be enabled by local conditions in a specific microenvironment.

Material & Methods

Cells and viruses

LR7 mouse fibroblast cells (28), were maintained in Dulbecco's Modified Eagle's Medium (DMEM; Cambrex Bio Science) containing 10% (v/v) fetal calf serum (Bodinco B.V.), 100 U/ml Penicillin, and 100 μg/ml Streptomycin, supplemented with Geneticin G418 (250 μg/ml). MHV strain A59 and the derivates expressing the FL reporter gene (MHV-EFLM, MHV-2aFLS, and MHV-2aFLSrec) have been described previously (12, 16). All viruses were grown in LR7 cells. Virus stocks were concentrated by pelleting through sucrose-cushion centrifugation, and subsequently resuspended in phosphate-buffered saline (PBS).

Mice

BALB/c and C57BL/6 mice at different ages were obtained from Charles River, while type I IFN receptor knock-out mice ($IFNAR^{-/-}$) (47) and the parental 129SvEv mice were obtained from B&K Universal Ltd. Mice were inoculated either intraperitoneally or intranasally with various doses of the different viruses. Infected mice were either processed for BLI, or sacrificed at the indicated time-points for organ dissection. When indicated, mice were (pre)-treated with 1,000 U of a cocktail of recombinant mouse IFN alpha/beta (IFNα/β; Sigma-Aldrich). The cytokines were applied intranasally on each of days -2, -1, 0, 1, and 2 relative to the inoculation with MHV-EFLM. Control animals were treated with PBS.

Tissue homogenization and histology

Whole brains and livers were dissected from the MHV-infected and control mice. The tissues were added to Lysing Matrix D tubes (MP Biomedical), containing 1 ml of PBS, and processed using a FastPrep instrument (MP Biomedical). The tissues were homogenized at 6,000 rpm for 40 sec and immediately placed on ice. Subsequently, the homogenates were centrifuged at 14,000 rpm for 10 min at 4°C and supernatants were harvested, aliquoted and stored at -80°C. The aliquots were processed for the different assays as described below. When indicated, whole livers from MHV-infected mice were harvested, fixed in phosphate-buffered formalin, embedded in paraffin, sectioned, and stained with hematoxylin.

Total RNA isolation and quantitative RT-PCR

Total RNA was isolated from brain and liver homogenates using the TRIzol reagent (Invitrogen) according to the manufacturer's protocol. RNA was further purified using the RNeasy mini-kit with subsequent DNaseI treatment on the column (Qiagen). The relative amounts of viral genomic RNA were determined by quantitative Taqman RT-PCR as described before (14).

Virus titration

Titration of virus stocks was performed by determination of the tissue culture 50% infectious dose ($TCID_{50}$) in LR7 cells (66). The viral titers in tissue homogenates were determined by plaque assays. Briefly, LR7 cells in 6-well microplates were inoculated with 4-fold serial dilutions of the homogenates. At 1 h post inoculation, medium was replaced with an agar overlay. At approximately 48 h post inoculation, the LR7 cell monolayers were fixed

and stained with crystal violet, after which the total amount of plaques was counted. The viral titers are expressed as plaque-forming units per gram (PFU/g) tissue.

Luciferase assays

Monolayers of MHV-infected LR7 cells were lysed with 1x Passive Lysis Buffer (Promega). Luciferase expression was measured according to the manufacturer's instructions, and relative light units (RLU) were determined in a Turner Designs TD-20/20 luminometer. In case of the tissue homogenates, 40 µl was mixed with 40 µl 2x Passive Lysis Buffer and incubated for 5 min at room temperature after which the luciferase expression was measured as described above.

Bioluminescence imaging

When indicated, MHV replication in mice was assessed by *in vivo* BLI with a highly sensitive, cooled charge-coupled device (CCD) camera (VersArray 1300B, Roper Scientific Inc.) mounted in a light-tight imaging chamber (Roper Scientific Inc.). Imaging and quantification of signals was controlled by the acquisition software MetaVue (Universal Imaging Corporation). Prior to imaging, mice were anesthetized by intraperitoneal injection of KXA: ketamine hydrochloride (100 mg/kg; Vétoquinol BV) plus xylazine (10 mg/kg; Eurovet Animal Health BV) and atropine (0.05 mg/kg; Pharmachemie BV). The substrate D-luciferin sodium salt (Synchem Laborgemeinschaft OHG) dissolved in PBS was injected intraperitoneal at a dose of ~125 mg/kg. Mice were positioned in a specially designed box and placed onto the stage inside the light-tight camera box. Four mice were imaged simultaneously exactly 5 min after the injection of D-luciferin. The integrated light intensity of a stack of sequential 1-minute exposures (10 from the dorsal side, and 10 from the ventral side) was used to calculate the amount of emitted light from the animals. A low intensity visible light image was made and used to create overlay-images. Images were further analyzed with Metamorph Imaging software (Universal Imaging Corporation). In some BLI experiments, the detection of emitted photons was performed by the equally sensitive photon imager from Biospace Lab. BLI images obtained with the Biospace CCD camera were analyzed by Photovision software (Biospace Lab).

Acknowledgements

This work was supported by grants from the M.W. Beijerinck Virology Fund, Royal Netherlands Academy of Arts and Sciences, and The Netherlands Organization for Scientific Research (NWO-VIDI-700.54.421) to C.A.M. de Haan. We thank Monique Oostra, Marne Hagemeijer, and Mijke Vogels for stimulating discussions.

Supplementary Data

Supplemental table S1A. Anatomical sites of MHV-EFLM infection in BALB/c mice inoculated with different doses (i.e. $2x10^3$ and $5x10^6$ $TCID_{50}$). The numbers of mice from a group of 4 which showed infection at the indicated anatomical sites are indicated at the different time-points p.i.

Viral dose:	**$2x10^3$ $TCID_{50}$**					**$5x10^6$ $TCID_{50}$**				
Days p.i.:	2	5	7	9	12	2	5	7	9	12
Anatomic site:										
Nasal cavity	4/4	4/4	4/4	3/4	0/4	4/4	4/4	4/4	4/4	0/4
Brain	0/4	3/4	3/4	3/4	1/4	3/4	4/4	4/4	2/4	0/4
Cervical lymph node	0/4	2/4	0/4	0/4	0/4	4/4	0/4	0/4	0/4	0/4
Eye	0/4	0/4	0/4	0/4	0/4	0/4	0/4	0/4	2/4	1/4
Liver	0/4	0/4	1/4	1/4	0/4	1/4	1/4	0/4	0/4	0/4
Intestine	0/4	0/4	0/4	0/4	0/4	0/4	0/4	0/4	0/4	0/4
Paw	0/4	0/4	0/4	0/4	0/4	1/4	1/4	0/4	0/4	0/4
Tail	0/4	0/4	0/4	0/4	0/4	0/4	0/4	0/4	0/4	0/4
Lung	0/4	0/4	0/4	0/4	0/4	1/4	1/4	0/4	0/4	0/4

Supplemental table S1B. Anatomical sites of infection in MHV-EFLM infected mice of different genetic background (i.e. BALB/c, C57BL/6, 129SvEv, and $IFNAR^{-/-}$). Note that mice were inoculated intranasally (i.n.) or intraperitoneally (i.p.) with 10^6 $TCID_{50}$ of MHV-EFLM and subsequently imaged at different time-points post inoculation. The numbers of mice from a group of 8 or 4 animals which showed infection at the indicated anatomical sites at any time point post inoculation are indicated.

Strain:	**BALB/c**		**C57BL/6**		**129SvEv**		**$IFNAR^{-/-}$**	
Inoculation route:	i.n.	i.p.	i.n.	i.p.	i.n.	i.p.	i.n.	i.p.
Anatomic site:								
Nasal cavity	8/8	0/8	8/8	0/8	4/4	-	4/4	-
Brain	8/8	0/8	6/8	0/8	1/4	-	4/4	-
Cervical lymph node	8/8	0/8	6/8	0/8	0/4	-	4/4	-
Eye	4/8	0/8	0/8	0/8	0/4	-	4/4	-
Liver	2/8	7/8	0/8	7/8	0/4	-	4/4	-
Intestine	0/8	2/8	0/8	4/8	0/4	-	4/4	-
Paw	0/8	6/8	0/8	7/8	0/4	-	4/4	-
Tail	1/8	5/8	0/8	8/8	0/4	-	4/4	-
Lung	1/8	0/8	0/8	0/8	0/4	-	4/4	-

References

1. **Bergmann, C. C., N. W. Marten, D. R. Hinton, B. Parra, and S. A. Stohlman.** 2001. CD8 T cell mediated immunity to neurotropic MHV infection. Adv Exp Med Biol 494:299-308.

2. **Blau, D. M., C. Turbide, M. Tremblay, M. Olson, S. Letourneau, E. Michaliszyn, S. Jothy, K. V. Holmes, and N. Beauchemin.** 2001. Targeted disruption of the Ceacam1 (MHVR) gene leads to reduced susceptibility of mice to mouse hepatitis virus infection. J Virol 75:8173-86.

3. **Brenner, G. J., N. Cohen, and J. A. Moynihan.** 1994. Similar immune response to nonlethal infection with herpes simplex virus-1 in sensitive (BALB/c) and resistant (C57BL/6) strains of mice. Cell Immunol 157:510-24.

4. **Cervantes-Barragan, L., R. Zust, F. Weber, M. Spiegel, K. S. Lang, S. Akira, V. Thiel, and B. Ludewig.** 2007. Control of coronavirus infection through plasmacytoid dendritic-cell-derived type I interferon. Blood 109:1131-7.

5. **Compton, S. R., S. W. Barthold, and A. L. Smith.** 1993. The cellular and molecular pathogenesis of coronaviruses. Lab Anim Sci 43:15-28.

6. **Contag, C. H., and M. H. Bachmann.** 2002. Advances in *in vivo* bioluminescence imaging of gene expression. Annu Rev Biomed Eng 4:235-60.

7. **Contag, C. H., P. R. Contag, J. I. Mullins, S. D. Spilman, D. K. Stevenson, and D. A. Benaron.** 1995. Photonic detection of bacterial pathogens in living hosts. Mol Microbiol 18:593-603.

8. **Contag, C. H., S. D. Spilman, P. R. Contag, M. Oshiro, B. Eames, P. Dennery, D. K. Stevenson, and D. A. Benaron.** 1997. Visualizing gene expression in living mammals using a bioluminescent reporter. Photochem Photobiol 66:523-31.

9. **Cook, S. H., and D. E. Griffin.** 2003. Luciferase imaging of a neurotropic viral infection in intact animals. J Virol 77:5333-8.

10. **de Haan, C. A., B. J. Haijema, D. Boss, F. W. Heuts, and P. J. Rottier.** 2005. Coronaviruses as vectors: stability of foreign gene expression. J Virol 79:12742-51.

11. **de Haan, C. A., B. J. Haijema, P. Schellen, P. W. Schreur, E. te Lintelo, H. Vennema, and P. J. Rottier.** 2008. Cleavage of group 1 coronavirus spike proteins: how furin cleavage is traded off against heparan sulfate binding upon cell culture adaptation. J Virol 82:6078-83.

12. **de Haan, C. A., Z. Li, E. te Lintelo, B. J. Bosch, B. J. Haijema, and P. J. Rottier.** 2005. Murine coronavirus with an extended host range uses heparan sulfate as an entry receptor. J Virol 79:14451-6.

13. **de Haan, C. A., P. S. Masters, X. Shen, S. Weiss, and P. J. Rottier.** 2002. The group-specific murine coronavirus genes are not essential, but their deletion, by reverse genetics, is attenuating in the natural host. Virology 296:177-89.

14. **de Haan, C. A., K. Stadler, G. J. Godeke, B. J. Bosch, and P. J. Rottier.** 2004. Cleavage inhibition of the murine coronavirus spike protein by a furin-like enzyme affects cell-cell but not virus-cell fusion. J Virol 78:6048-54.

15. **de Haan, C. A., E. Te Lintelo, Z. Li, M. Raaben, T. Wurdinger, B. J. Bosch, and P. J. Rottier.** 2006. Cooperative involvement of the S1 and S2 subunits of the murine coronavirus spike protein in receptor binding and extended host range. J Virol 80:10909-18.

16. **de Haan, C. A., L. van Genne, J. N. Stoop, H. Volders, and P. J. Rottier.** 2003. Coronaviruses as vectors: position dependence of foreign gene expression. J Virol 77:11312-23.

17. **Durbin, R. K., S. E. Mertz, A. E. Koromilas, and J. E. Durbin.** 2002. PKR protection against intranasal vesicular stomatitis virus infection is mouse strain dependent. Viral Immunol 15:41-51.

18. **Glass, W. G., B. P. Chen, M. T. Liu, and T. E. Lane.** 2002. Mouse hepatitis virus infection of the central nervous system: chemokine-mediated regulation of host defense and disease. Viral Immunol 15:261-72.

19. **Haring, J., and S. Perlman.** 2001. Mouse hepatitis virus. Curr Opin Microbiol 4:462-6.

20. **Harmache, A., M. LeBerre, S. Droineau, M. Giovannini, and M. Bremont.** 2006. Bioluminescence imaging of live infected salmonids reveals that the fin bases are the major portal of entry for Novirhabdovirus. J Virol 80:3655-9.

21. **Hemmila, E., C. Turbide, M. Olson, S. Jothy, K. V. Holmes, and N. Beauchemin.** 2004. Ceacam1a$^{-/-}$ mice are completely resistant to infection by murine coronavirus mouse hepatitis virus A59. J Virol 78:10156-65.

22. **Holmes, K. V., and M. M. C. Lai.** 1996. Coronaviruses. In: Fields Virology, 3rd edn. (ed. Fields, B. N., D. M. Knipe, and P. M. Howley, Philadelphia, Lippincott-Raven Publishers), pp. 1075–1094.

23. **Houtman, J. J., and J. O. Fleming.** 1996. Pathogenesis of mouse hepatitis virus-induced demyelination. J Neurovirol 2:361-76.

24. **Hutchens, M., and G. D. Luker.** 2007. Applications of bioluminescence imaging to the study of infectious diseases. Cell Microbiol 9:2315-22.

25. **Iacono, K. T., L. Kazi, and S. R. Weiss.** 2006. Both spike and background genes contribute to murine coronavirus neurovirulence. J Virol 80:6834-43.

26. **Jubelt, B., S. L. Ropka, S. Goldfarb, C. Waltenbaugh, and R. P. Oates.** 1991. Susceptibility and resistance to poliovirus-induced paralysis of inbred mouse strains. J Virol 65:1035-40.

27. **Komurasaki, Y., C. N. Nagineni, Y. Wang, and J. J. Hooks.** 1996. Virus RNA persists within the retina in coronavirus-induced retinopathy. Virology 222:446-50.

28. **Kuo, L., G. J. Godeke, M. J. Raamsman, P. S. Masters, and P. J. Rottier.** 2000. Retargeting of coronavirus by substitution of the spike glycoprotein ectodomain: crossing the host cell species barrier. J Virol 74:1393-406.

29. **Lane, T. E., J. L. Hardison, and K. B. Walsh.** 2006. Functional diversity of chemokines and chemokine receptors in response to viral infection of the central nervous system. Curr Top Microbiol Immunol 303:1-27.

30. **Lavi, E., D. H. Gilden, M. K. Highkin, and S. R. Weiss.** 1986. The organ tropism of mouse hepatitis virus A59 in mice is dependent on dose and route of inoculation. Lab Anim Sci 36:130-5.

31. **Lavi, E., D. H. Gilden, M. K. Highkin, and S. R. Weiss.** 1984. Persistence of mouse hepatitis virus A59 RNA in a slow virus demyelinating infection in mice as detected by in situ hybridization. J Virol 51:563-6.

32. **Lee, E., R. A. Hall, and M. Lobigs.** 2004. Common E protein determinants for attenuation of glycosaminoglycan-binding variants of Japanese encephalitis and West Nile viruses. J Virol 78:8271-80.

33. **Leipner, C., K. Grun, I. Schneider, B. Gluck, H. H. Sigusch, and A. Stelzner.** 2004. Coxsackievirus B3-induced myocarditis: differences in the immune response of C57BL/6 and BALB/c mice. Med Microbiol Immunol 193:141-7.

34. **Liu, J., and S. C. Thorp.** 2002. Cell surface heparan sulfate and its roles in assisting viral infections. Med Res Rev 22:1-25.

35. **Luker, G. D., J. P. Bardill, J. L. Prior, C. M. Pica, D. Piwnica-Worms, and D. A. Leib.** 2002. Noninvasive bioluminescence imaging of herpes simplex virus type 1 infection and therapy in living mice. J Virol 76:12149-61.

36. **Luker, G. D., and K. E. Luker.** 2008. Optical imaging: current applications and future directions. J Nucl Med 49:1-4.

37. **Luker, K. E., M. Hutchens, T. Schultz, A. Pekosz, and G. D. Luker.** 2005. Bioluminescence imaging of vaccinia virus: effects of interferon on viral replication and spread. Virology 341:284-300.

38. **Luker, K. E., and G. D. Luker.** 2008. Applications of bioluminescence imaging to antiviral research and therapy: multiple luciferase enzymes and quantitation. Antiviral Res 78:179-87.

39. **MacNamara, K. C., S. J. Bender, M. M. Chua, R. Watson, and S. R. Weiss.** 2008. Priming of CD8+ T cells during central nervous system infection with a murine coronavirus is strain dependent. J Virol 82:6150-60.

40. **MacNamara, K. C., M. M. Chua, J. J. Phillips, and S. R. Weiss.** 2005. Contributions of the viral genetic background and a single amino acid substitution in an immunodominant CD8+ T-cell epitope to murine coronavirus neurovirulence. J Virol 79:9108-18.

41. **Mandl, C. W., H. Kroschewski, S. L. Allison, R. Kofler, H. Holzmann, T. Meixner, and F. X. Heinz.** 2001. Adaptation of tick-borne encephalitis virus to BHK-21 cells results in the formation of multiple heparan sulfate binding sites in the envelope protein and attenuation *in vivo*. J Virol 75:5627-37.

42. **Marten, N. W., S. A. Stohlman, and C. C. Bergmann.** 2001. MHV infection of the CNS: mechanisms of immune-mediated control. Viral Immunol 14:1-18.

43. **McIntosh, K.** 1996. Coronaviruses. In: Fields Virology, 3rd edn. (ed. Fields, B. N., D. M. Knipe, and P. M. Howley, Philadelphia, Lippincott-Raven Publishers), pp. 401-430.

44. **Minagawa, H., A. Takenaka, S. Mohri, and R. Mori.** 1987. Protective effect of recombinant murine interferon beta against mouse hepatitis virus infection. Antiviral Res 8:85-95.

45. **Molloy, T., and L. J. van 't Veer.** 2008. Recent advances in metastasis research. Curr Opin Genet Dev 18:35-41.

46. **Morales, S., B. Parra, C. Ramakrishna, D. M. Blau, and S. A. Stohlman.** 2001. B-cell-mediated lysis of cells infected with the neurotropic JHM strain of mouse hepatitis virus. Virology 286:160-7.

47. **Muller, U., U. Steinhoff, L. F. Reis, S. Hemmi, J. Pavlovic, R. M. Zinkernagel, and M. Aguet.** 1994. Functional role of type I and type II interferons in antiviral defense. Science 264:1918-21.

48. **Ohtsuka, N., and F. Taguchi.** 1997. Mouse susceptibility to mouse hepatitis virus infection is linked to viral receptor genotype. J Virol 71:8860-3.

49. **Olmsted, R. A., R. S. Baric, B. A. Sawyer, and R. E. Johnston.** 1984. Sindbis virus mutants selected for rapid growth in cell culture display attenuated virulence in animals. Science 225:424-7.

50. **Parker, J. C., M. D. Whiteman, and C. B. Richter.** 1978. Susceptibility of inbred and outbred mouse strains to Sendai virus and prevalence of infection in laboratory rodents. Infect Immun 19:123-30.

51. **Perlman, S.** 1998. Pathogenesis of coronavirus-induced infections. Review of pathological and immunological aspects. Adv Exp Med Biol 440:503-13.

52. **Perlman, S. R., T.E. Lane, and M.J. Buchmeier.** 1999. Coronaviruses: hepatitis, hepatitis, and central nervous system disease. In: Effects of Microbes on the Immune System 1:331-348.

53. **Phillips, J. J., M. M. Chua, E. Lavi, and S. R. Weiss.** 1999. Pathogenesis of chimeric MHV4/MHV-A59 recombinant viruses: the murine coronavirus spike protein is a major determinant of neurovirulence. J Virol 73:7752-60.

54. **Robbins, S. G., B. Detrick, and J. J. Hooks.** 1990. Retinopathy following intravitreal injection of mice with MHV strain JHM. Adv Exp Med Biol 276:519-24.

55. **Rodriguez, J. F., D. Rodriguez, J. R. Rodriguez, E. B. McGowan, and M. Esteban.** 1988. Expression of the firefly luciferase gene in vaccinia virus: a highly sensitive gene marker to follow virus dissemination in tissues of infected animals. Proc Natl Acad Sci U S A 85:1667-71.

56. **Ross, T. M., P. M. Martinez, J. C. Renner, R. G. Thorne, L. R. Hanson, and W. H. Frey, 2nd.** 2004. Intranasal administration of interferon beta bypasses the blood-brain barrier to target the central nervous system and cervical lymph nodes: a non-invasive treatment strategy for multiple sclerosis. J Neuroimmunol 151:66-77.

57. **Roth-Cross, J. K., S. J. Bender, and S. R. Weiss.** 2008. Murine coronavirus mouse hepatitis virus is recognized by MDA5 and induces type I interferon in brain macrophages/microglia. J Virol 82:9829-38.

58. **Scalzo, A. A., N. A. Fitzgerald, C. R. Wallace, A. E. Gibbons, Y. C. Smart, R. C. Burton, and G. R. Shellam.** 1992. The effect of the Cmv-1 resistance gene, which is linked to the natural killer cell gene complex, is mediated by natural killer cells. J Immunol 149:581-9.

59. **Schickli, J. H., L. B. Thackray, S. G. Sawicki, and K. V. Holmes.** 2004. The N-terminal region of the murine coronavirus spike glycoprotein is associated with the extended host range of viruses from persistently infected murine cells. J Virol 78:9073-83.

60. **Schickli, J. H., B. D. Zelus, D. E. Wentworth, S. G. Sawicki, and K. V. Holmes.** 1997. The murine coronavirus mouse hepatitis virus strain A59 from persistently infected murine cells exhibits an extended host range. J Virol 71:9499-507.

61. **Shah, K., A. Jacobs, X. O. Breakefield, and R. Weissleder.** 2004. Molecular imaging of gene therapy for cancer. Gene Ther 11:1175-87.

62. **Sperry, S. M., L. Kazi, R. L. Graham, R. S. Baric, S. R. Weiss, and M. R. Denison.** 2005. Single-amino-acid substitutions in open reading frame (ORF) 1b-nsp14 and ORF 2a proteins of the coronavirus mouse hepatitis virus are attenuating in mice. J Virol 79:3391-400.

63. **Stiles, L. N., J. L. Hardison, C. S. Schaumburg, L. M. Whitman, and T. E. Lane.** 2006. T Cell Antiviral Effector Function Is Not Dependent on CXCL10 Following Murine Coronavirus Infection. J Immunol 177:8372-80.

64. **Thach, D. C., T. Kimura, and D. E. Griffin.** 2000. Differences between C57BL/6 and BALB/cBy mice in mortality and virus replication after intranasal infection with neuroadapted Sindbis virus. J Virol 74:6156-61.

65. **Verheije, M. H., M. Raaben, M. Mari, E. G. Te Lintelo, F. Reggiori, F. J. van Kuppeveld, P. J. Rottier, and C. A. de Haan.** 2008. Mouse hepatitis coronavirus RNA replication depends on GBF1-mediated ARF1 activation. PLoS Pathog 4:e1000088.

66. **Verheije, M. H., T. Wurdinger, V. W. van Beusechem, C. A. de Haan, W. R. Gerritsen, and P. J. Rottier.** 2006. Redirecting coronavirus to a nonnative receptor through a virus-encoded targeting adapter. J Virol 80:1250-60.

67. **Weinberg, J. B., M. L. Lutzke, R. Alfinito, and R. Rochford.** 2004. Mouse strain differences in the chemokine response to acute lung infection with a murine gammaherpesvirus. Viral Immunol 17:69-77.

68. **Weiss, S. R., and S. Navas-Martin.** 2005. Coronavirus pathogenesis and the emerging pathogen severe acute respiratory syndrome coronavirus. Microbiol Mol Biol Rev 69:635-64.

69. **Wu, J. C., G. Sundaresan, M. Iyer, and S. S. Gambhir.** 2001. Noninvasive optical imaging of firefly luciferase reporter gene expression in skeletal muscles of living mice. Mol Ther 4:297-306.

70. **Zhou, H., and S. Perlman.** 2006. Preferential infection of mature dendritic cells by mouse hepatitis virus strain JHM. J Virol 80:2506-14.

71. **Zuniga, E. I., B. Hahm, and M. B. Oldstone.** 2007. Type I interferon during viral infections: multiple triggers for a multifunctional mediator. Curr Top Microbiol Immunol 316:337-57.

Chapter 8

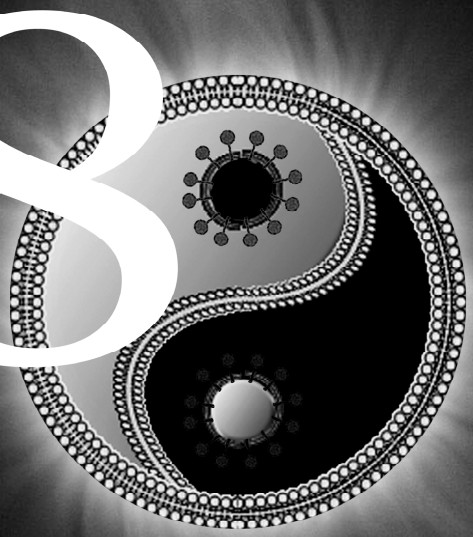

Type I Interferon Receptor –Independent and –Dependent Host Transcriptional Responses to Mouse Hepatitis Coronavirus Infection *in Vivo*

Matthijs Raaben
Marian J.A. Groot Koerkamp
Peter J.M. Rottier
Cornelis A.M. de Haan

BMC Genomics; 2009 Aug 3;10:350.

Abstract

The role of type I IFNs in protecting against coronavirus (CoV) infections is not fully understood. While CoVs are poor inducers of type I IFNs in tissue culture, several studies have demonstrated the importance of the type I IFN response in controlling MHV infection in animals. The protective effectors against MHV infection are, however, still unknown. In order to get more insight into the antiviral gene expression induced in the brains of MHV-infected mice, we performed whole-genome expression profiling. Three different mouse strains, differing in their susceptibility to infection with MHV, were used. In BALB/c mice, which display high viral loads but are able to control the infection, 57 and 121 genes were significantly differentially expressed (≥1.5 fold change) upon infection at 2 and 5 days post infection, respectively. Functional association network analyses demonstrated a strong type I IFN response, with Irf1 and Irf7 as the central players. At 5 days post infection, a type II IFN response also becomes apparent. Both the type I and II IFN response, which were more pronounced in mice with a higher viral load, were not observed in 129SvEv mice, which are much less susceptible to infection with MHV. 129SvEv mice lacking the type I interferon receptor ($IFNAR^{-/-}$), however, were not able to control the infection. Gene expression profiling of these mice identified type I IFN-independent responses to infection, with IFN-γ as the central player. As the BALB/c and the $IFNAR^{-/-}$ 129SvEv mice demonstrated very similar viral loads in their brains, we also compared their gene expression profiles upon infection with MHV in order to identify type I IFN-dependent transcriptional responses. Many known IFN-inducible genes were detected, several of which have previously been shown to play an important protective role against virus infections. We speculate that the additional type I IFN-dependent genes that we discovered may also be important for protection against MHV infection. Transcriptional profiling of mice infected with MHV demonstrated the induction of a robust IFN response, which correlated with the viral load. Profiling of $IFNAR^{-/-}$ mice allowed us to identify type I IFN–independent and –dependent responses. Overall, this study broadens our present knowledge of the type I and II IFN-mediated effector responses during CoV infection *in vivo*.

Introduction

Cytokines are key regulators that dictate many aspects of innate and adaptive immunity. Induction of type I interferons (IFNs), a well-known subset of cytokines with antiviral activity, is triggered by a selection of cellular pattern recognition receptors, including TLRs (Toll-like receptors), RIG-I (retinoic acid-inducible gene I), and MDA5 (melanoma differentiation-associated protein 5). These receptors are activated in response to a range of pathogen-specific factors, which includes double-stranded RNA produced during virus infection (21, 46). Secreted type I IFNs (i.e. IFN-α and IFN-β), subsequently induce an antiviral transcription program in the infected cell as well as in adjacent cells, thereby magnifying the "danger" signal and protecting against the infection.

The role of type I IFNs in controlling coronavirus (CoV) infections is not well understood. A number of studies has shown that CoVs, like the mouse hepatitis virus (MHV) and the severe acute respiratory syndrome (SARS)-CoV, are poor inducers of type I IFNs in cell culture, and even escape from detection by cytoplasmic pattern recognition receptors (33, 43, 51, 52, 57, 58). Consistently, virus-encoded IFN antagonistic functions have been described for both MHV and SARS-CoV (28, 56). *In vivo*, however, MHV infection appeared to induce the production of IFN-α in plasmacytoid dendritic cells (pDCs) by a TLR7-dependent mechanism (3). Moreover, MHV infections of primary neuronal cultures and of the central nervous system (CNS) induced IFN-β gene expression, indicating that the production of type I IFNs *in vivo* is not limited to pDCs (35, 39). Furthermore, neuronal cultures infected with MHV exhibited increased expression of several type I IFN-induced transcription factors (36). More recently, Roth-Cross and co-workers reported that macrophages and macrophage-like microglia cells produce IFN-β in the CNS of MHV-infected mice in a MDA5-dependent manner (38).

Several studies have demonstrated the importance of the type I IFN response in controlling MHV infection *in vivo*. The exogenous delivery of type I IFNs was shown to inhibit MHV infection of and spread to the mouse brain (26, 34). Consistently, infection of mice lacking the functional type I IFN receptor ($IFNAR^{-/-}$) with MHV resulted in increased viral replication and extended tissue tropism (3, 17, 34). Although many type I IFN-responsive

genes have been identified (40), the protective effectors against MHV infection are yet unknown (47).

In order to get more insight into the antiviral gene expression induced in the brains of MHV-infected mice, we performed whole-genome expression profiling. Three different mouse strains (BALB/c, 129SvEv and IFNAR$^{-/-}$ 129SvEv mice), differing in their susceptibility to infection with MHV, were used. Previously, we have observed that 129SvEv mice are significantly more resistant to infection via the intranasal route than BALB/c mice (34). The reason for the significant difference in susceptibility is not known, but may be related to different antiviral immune responses in these two mouse strains. Furthermore, gene expression profiling of 129SvEv mice lacking the type I IFN receptor, which are not able to control the MHV infection (3), allowed us to identify type I IFN-independent transcriptional responses.

Results & Discussion

We started by comparing the whole-genome expression profiles in the brains of the BALB/c and the 129SvEv mice upon infection with MHV. To this end, mice were inoculated intranasally with 10^6 $TCID_{50}$ of MHV strain A59 or with PBS (control). Groups of mice (n = 4) were sacrificed at 2 and 5 days post inoculation after which the brains were harvested and total RNA was isolated. The extent of virus replication was determined by quantitative reverse transcriptase (RT)-PCR targeting MHV-specific RNA sequences as described earlier (32). Previously, we demonstrated that the viral RNA load correlates well with viral infectivity in tissue homogenates (34). While no viral RNA could be detected yet at 2 days post inoculation (data not shown), viral RNA was observed in the brain of both mouse strains at day 5 (Fig.1A). As expected, the BALB/c mice displayed a much higher viral RNA load than the 129SvEv mice.

Fig.1. Genome-wide expression profiling of the brains of BALB/c and 129SvEv mice infected with MHV. BALB/c and 129SvEv mice were intranasally inoculated with PBS (control) or with MHV-A59. At day 2 and 5, mice (n = 4) were sacrificed and the brains and livers were harvested. The PBS-groups (n = 4) were also sacrificed at 5 days post inoculation. (A) Viral RNA (vRNA) levels within the brain were determined at 5 days post inoculation by quantitative RT-PCR targeting MHV-specific sequences. Standard deviations are indicated (*P<0.0001).

(B) Microarray analysis was performed as described in the *Material & Methods* section. The PBS-inoculated BALB/c or 129SvEv mice were taken as reference. Based on the significant alterations in gene expression (≥1.5 fold change cut-off) within the brains of BALB/c mice at 5 days post infection, a cluster analysis (standard correlation) was performed resulting in the indicated gene tree (n = 121). The different conditions (i.e. mouse strains and day post infection) are indicated. (C-D) From the the gene tree shown in panel B, clusters representing "early" and "late" genes could be identified. For detailed information see the text and Supplemental table 1. (E) The IFN-α4, IFN-β1, and IFN-γ mRNA levels were determined by quantitative RT-PCR. The fold changes after infection with MHV relative to the PBS-inoculated animals are shown. Standard deviations are indicated.

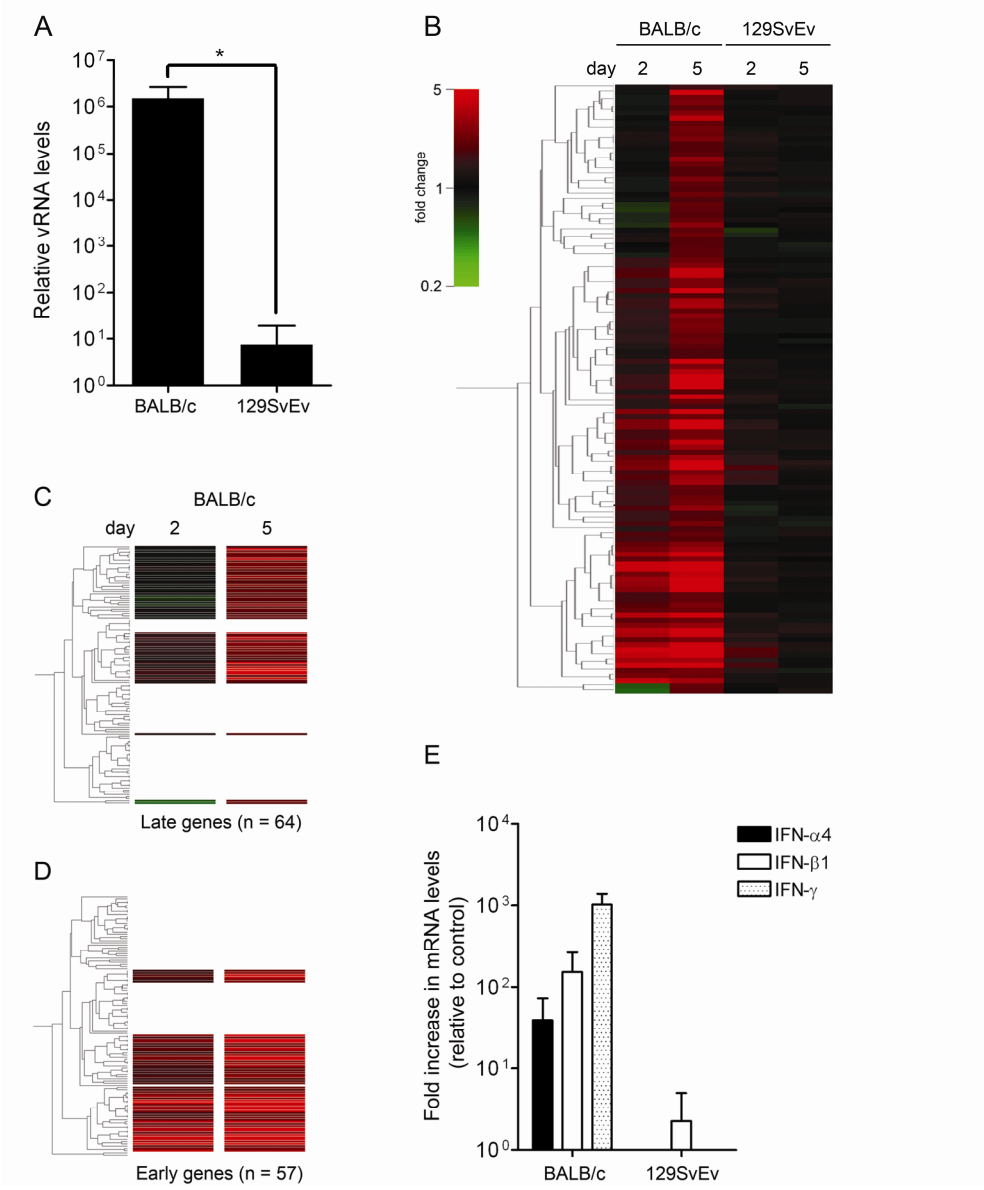

Next, the RNA extracts were processed for microarray analysis using the PBS-inoculated groups as the reference. In total, 57 and 121 genes were significantly differentially expressed (≥1.5 fold change) in BALB/c mice at 2 and 5 days post infection, respectively. In contrast, in the 129SvEv mice, no significant induction of gene expression was observed. The results are depicted in Fig.1B as a gene tree that was built based on the genes with a significantly altered expression level in BALB/c mice at 5 days post infection (i.e. expression-based cluster analysis). From these data we were able to identify host genes, the increased expression (≥1.5 fold) of which could already be detected at day 2 (i.e. early genes; Fig.1C) or only at day 5 (i.e. late genes; Fig.1D). The group of early-induced transcripts contained many IFN-inducible genes, including the well-known interferon regulatory factor 7 (*Irf7*), signal transducer and activator of transcription 1 (*Stat1*), and 2'-5' oligoadenylate synthetase (*Oas*) genes (Supplemental table 1A). Within the cluster of "late" genes (Supplemental table 1B) several chemokines (i.e. *Ccl2*, *Ccl5*, *Ccl7*, *Cxcl9*, and *Cxcl10*) could be identified.

Next, in order to construct a functional association network, we applied the STRING 8.0 software (18) to the list of proteins encoded by the "early" and "late" genes. We also included known interactors of our hits in this analysis, while proteins that did not demonstrate any known interactions were excluded for clarity. The results are shown in Fig.2A and 2B. Functional association network analysis of the proteins encoded by the "early" genes revealed two main modules. One module contained several proteins involved in antigen presentation, while the other module contained numerous proteins involved in the type I IFN response. The key player in this latter module appeared to be Irf7, which is the master regulator of type I IFN-dependent responses (15).

Fig.2. Early and late transcriptional responses to infection with MHV. (A) The early gene expression network. The "early" genes listed in Supplemental table 1A (n = 57) were subjected to functional association network analysis by using the public STRING 8.0 database (www.string.embl.de). Indicated is the confidence view of the analysis. Stronger associations are symbolized by thicker lines. (B) The late gene expression network. The "late" genes listed in Supplemental table 1B (n = 64) were subjected to functional association network analysis as described above. In both panels, the key players in the network (i.e. Irf7 for panel A and IFN-γ, Irf1, and Irf8 for panel B) are indicated in red.

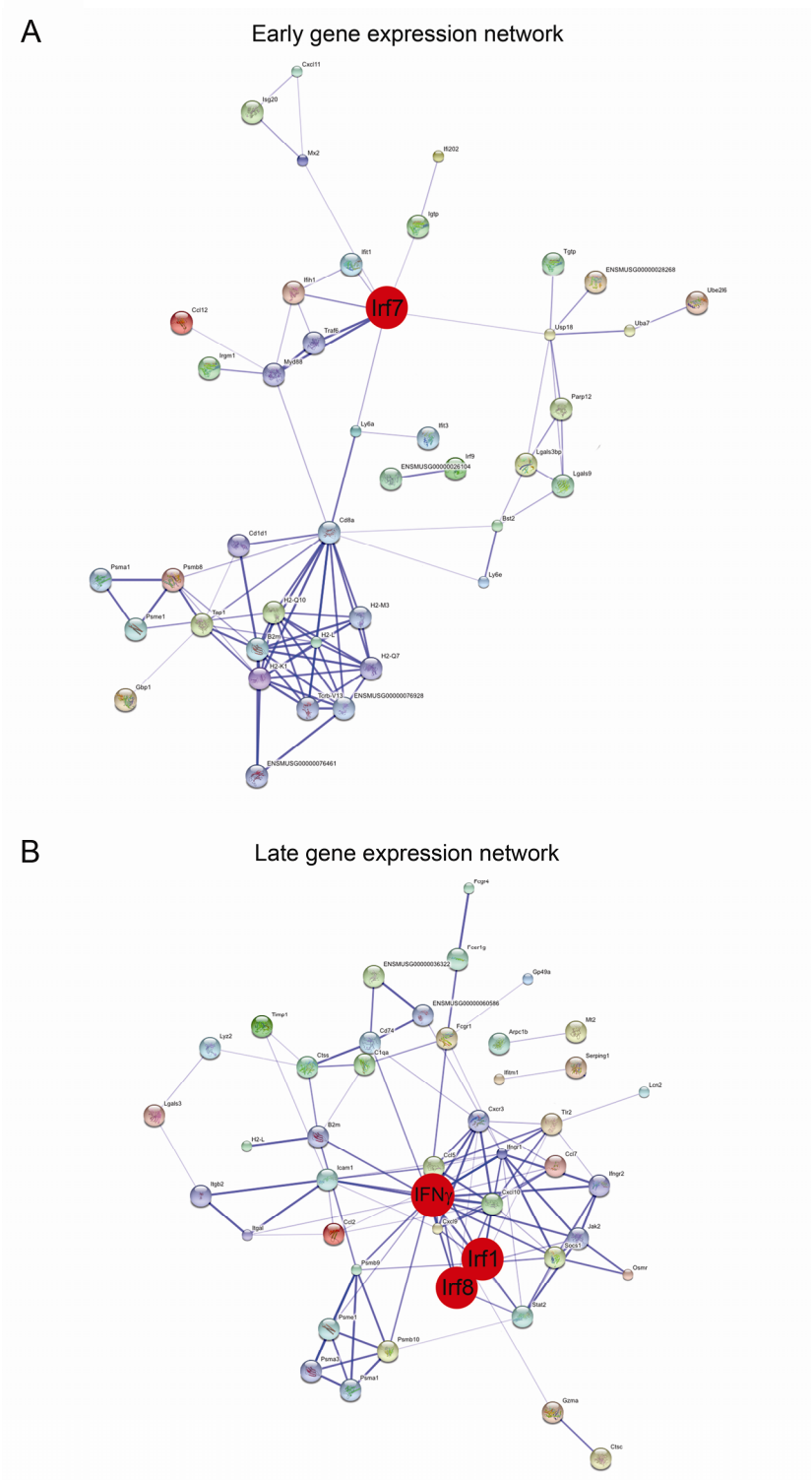
A
Early gene expression network
Irf7
B
Late gene expression network
IFNγ
Irf1
Irf8

Functional association network analysis of the proteins encoded by the "late" genes revealed a large network of proteins involved in host-pathogen interactions. Although the microarray analyses did not reveal the induction of IFN-γ gene expression itself, IFN-γ appeared at a central position in the network. In addition, the induction of a type I IFN response was also evident from this network as demonstrated by the presence of the transcription factors Irf1 and Irf8, both of which demonstrated elevated mRNA levels upon MHV infection. In conclusion, these results demonstrate that MHV infection induces a robust IFN response both at 2 and 5 days post infection, in which the transcription factors Irf7, Irf1, and Irf8 appear to be the key players. At 5 days post infection, a type II IFN response also becomes apparent.

To confirm and extend these observations, we next analyzed the induction of type I and II IFN gene expression (i.e. IFN-α4 and IFN-β1, and IFN-γ, respectively) by using quantitative RT-PCR. In agreement with the microarray expression profiles, significant induction of these type I and II IFNs could only be detected in the MHV-infected BALB/c animals (Fig.1E). The observation that the BALB/c mice, unlike the 129SvEv mice, exhibited abundant expression of IFN-responsive genes upon MHV infection appears counter intuitive as the 129SvEv mice are much more resistant to the infection than the BALB/c mice. Apparently, the resistance of 129SvEv mice to MHV infection is not controlled by a more robust IFN response. The reason for the observed difference in susceptibility between the different mouse strains after intranasal inoculation is not known. MHV-A59 was recently shown to replicate efficiently in the liver of 129SvEv mice after intraperitoneal inoculation (3). Interestingly, the resistance of 129SvEv mice after intranasal inoculation is not restricted to infection with MHV, as it was also observed for vesicular stomatitis virus (5).

The microarray expression profiles described above suggested that the induction of an IFN response correlates with the viral load within the brain. To confirm this, we examined the data of the individual BALB/c mice at 5 days post infection in more detail. Clearly, the animals with the highest viral loads (mouse 2 and 4; Fig.3A), also displayed significantly higher levels of induction of type I and II IFN expression (Fig.3B). Likewise, the amplitude of the gene expression profiles (Fig.3C and Supplemental table 2) of the individual mice

also correlated with the viral loads in the brain. These observations are in agreement with results obtained by the profiling of SARS-CoV-infected macaques (4). Also in that study a positive correlation between virus load and the induction of gene expression was observed. A few genes (n = 6), including *ISG20*, showed an inverse correlation with the viral load. We currently have no explanation for this observation as expression of *ISG20* is known to be induced by type I IFNs (12, 13). Interestingly, ISG20 has been shown to exhibit antiviral activity against other viruses (6, 19).

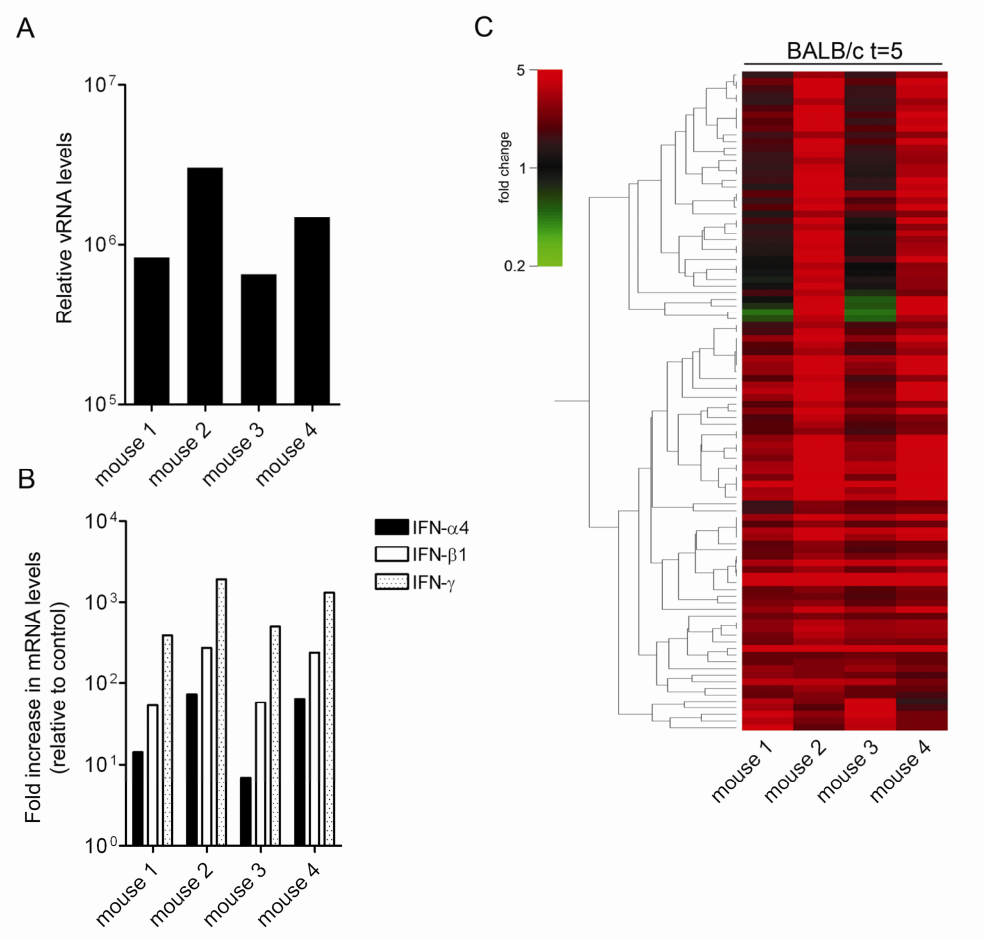

Fig.3. Induction of gene expression correlates with the viral load. vRNA (panel A) and IFN-α4, IFN-β1, and IFN-γ mRNA (panel B) levels within the brains of the individual BALB/c mice (mouse 1-4) at 5 days post infection were determined as described in the legend of Figure 1. (C) Microarray data analysis of the individual BALB/c mice (mouse 1-4). The gene tree shown (n = 96) is based on the significant alterations at 5 days post infection while applying an expression cut-off (≥2.0 fold). For detailed information see Supplemental table 2.

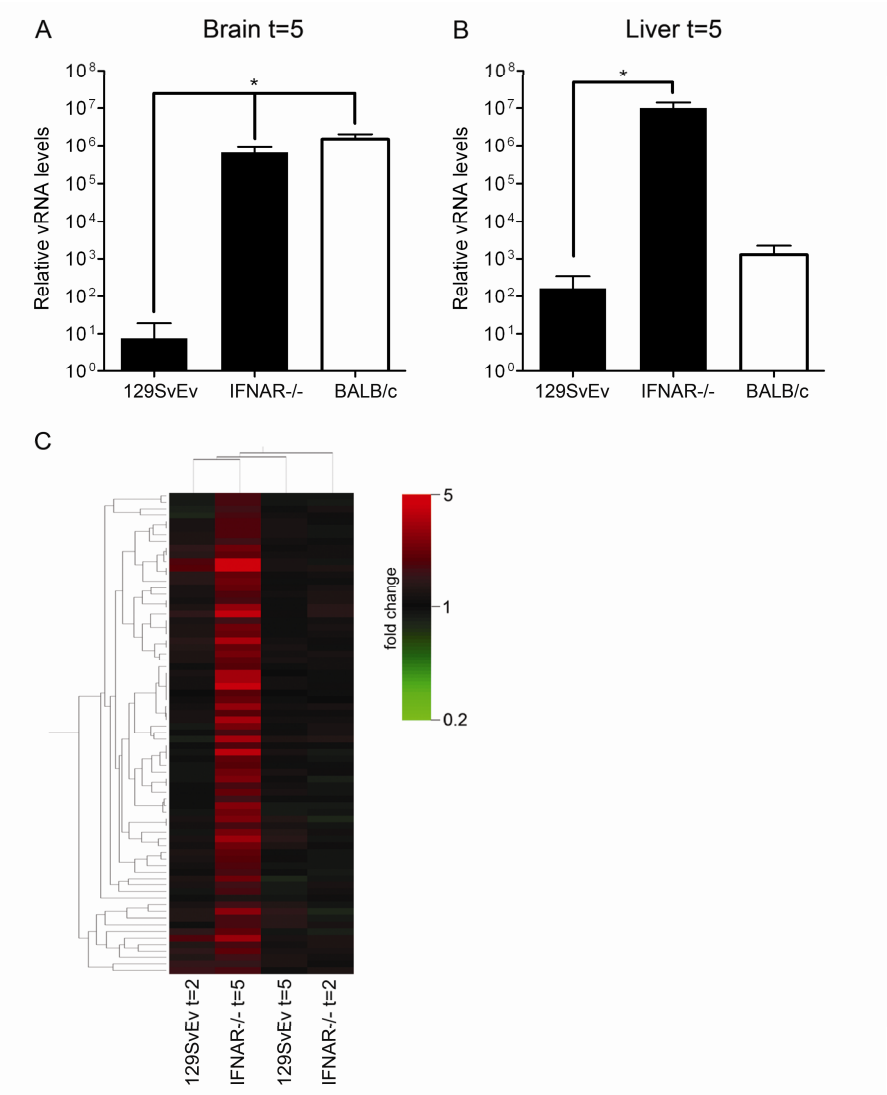

Fig.4. The type I IFN receptor-independent expression profile within the brains of IFNAR$^{-/-}$ mice after MHV infection. IFNAR$^{-/-}$ 129SvEv mice were intranasally inoculated with 10^6 $TCID_{50}$ of MHV-A59 or treated with PBS (control). At day 5, mice (n = 4) were sacrificed and the brains and livers were harvested. (A and B) The vRNA levels within brains and livers were determined as described in the legend of Figure 1. Standard deviations are indicated (*P<0.0001). Also depicted are the vRNA levels for the parental 129SvEv mice and BALB/c mice. (C) Total RNA samples obtained from the brains of PBS- or MHV-inoculated IFNAR$^{-/-}$ mice were processed for microarray analysis as described in the legend to Figure 1. Based on the significant alterations (≥1.5 fold change cut-off) in gene expression within the brains of the IFNAR$^{-/-}$ mice at 5 days post infection (n = 73) a gene tree was build. The different conditions (i.e. mouse strain and day post infection) are indicated. See Supplemental table 3 for details. Note that the different conditions are also clustered according to their similarities in the complete gene expression profile.

To study the role of type I IFN–independent and –dependent gene expression in the control of MHV infection *in vivo* in more detail, we next made use of the IFNAR$^{-/-}$ mice (27). These mice are highly susceptible to MHV infection as compared to the parental 129SvEv mice (3, 34). Indeed, when these mice were inoculated intranasally with 10^6 $TCID_{50}$ of MHV-A59, viral RNA levels in their brains became much higher than in animals from the parental strain at 5 days post infection (Fig.4A). Interestingly, at this time point the viral RNA levels in the IFNAR$^{-/-}$ mice were comparable to those in the brains of the BALB/c mice. However, efficient dissemination of the infection, resulting in high viral loads in the liver as determined by quantitative RT-PCR, was only observed in the IFNAR$^{-/-}$ mice and not in the wild-type mice, which displayed viral RNA levels just above background (Fig.4B). Thus, in agreement with previous studies, a type I IFN-dependent response is required to inhibit virus dissemination (3, 38).

Whole-genome expression profiling of brains of the IFNAR$^{-/-}$ mice revealed the significantly induced expression of 73 genes (≥1.5 fold) at 5 days post infection. In contrast, at day 2, hardly any alterations in gene expression could be detected in these knock-out mice (Supplemental table 3). Fig.4C shows an expression-based cluster analysis of these 73 genes for the wild-type and IFNAR$^{-/-}$ mice. Comparison of the complete expression profiles of these mice revealed that the transcriptional profile at day 5 in the IFNAR$^{-/-}$ mice has a larger similarity with the profile at day 2 of the parental 129SvEv mice than with that of the knock-out mice at day 2 post infection (Fig.4C). This observation may suggest the presence of an early host response to infection with MHV in the parental mice, even though no significant induction (≥1.5 fold) of gene expression could be detected (Fig.1B). Such a response, may not be evident in transcriptional profiles of whole organs, but might only be apparent at the cellular level. We speculate that early decisive events are happening in initial target cell populations such as DCs and macrophages (2). These responses could prevent extensive viral replication very early after infection, thereby reducing subsequent type I IFN responses.

As the knock-out mice lack a functional type I IFN receptor, the upregulation of gene expression observed in these mice apparently occurs independently of type I IFN signalling. Not much is known yet about type I IFN-independent responses to infection. The

observation that the transcriptional upregulation of *Irf1* was independent of type I IFN signalling is consistent with the notion that IFN-γ can also induce expression of this gene (7, 20). Likewise, we also observed increased transcription of *Ifitm1* and *Ifitm3* independent of type I IFN signalling, again corresponding with the literature (23, 54). Interestingly, the expression of various genes encoding proteins involved in antigen presentation (i.e. *H2*, *B2m*, *Psmb8*, *Psmb9*, and *Ctss*) was also increased in the absence of type I IFN signalling. *Psmb8* and *Psmb9* encode immunoproteasome subunits which facilitate antigen presentation to CD8+ T cells after virus infection, a process that is primarily regulated by IFN-γ (50). Furthermore, also the expression of the major histocompatibility complex class II (MHC II) invariant chain, also called CD74 (1), was increased upon infection of the knock-out mice. These data are in agreement with the observation that the induction of genes involved in antigen processing is independent of STAT1 activation by IFN-α (59). We also observed the transcriptional upregulation of the 3 isoforms of metallothionein (*Mt1*, *Mt2*, and *Mt3*), which encode proteins known to scavenge toxic metals (22). The induction of these genes, which was not apparent in either wild-type mice, could reflect an acute-phase reaction in the brain of MHV-infected IFNAR$^{-/-}$ mice, which likely contributes to pathogenesis as has been shown for other viruses (9, 10, 16).

We constructed a functional association network by applying the STRING 8.0 software (18) to the list of proteins encoded by the type I IFN-independent genes (Supplemental table 3). We also included known interactors of our hits in this analysis, while proteins that did not demonstrate any interactions were again excluded for clarity. The result is shown in Fig.5. The analysis revealed IFN-γ as the central player in the type I IFN-independent antiviral network as this protein appeared to link a number of smaller modules. The induction of IFN-γ gene expression could be confirmed using quantitative RT-PCR (data not shown). The finding that IFN-γ-mediated transcriptional responses are not dramatically affected in the absence of type I IFN signalling is in agreement with reports referred to above and with a recent publication by Ireland et al. (17), which shows that IFN-γ expression is significantly induced in the CNS of MHV-infected IFNAR$^{-/-}$ mice. While the production of IFN-γ by NK cells plays a major role in the protection against infection with MHV (24, 41, 42, 48, 49), the IFN-γ-mediated transcriptional responses that we observed were not protective against acute MHV infection in the IFNAR$^{-/-}$ mice.

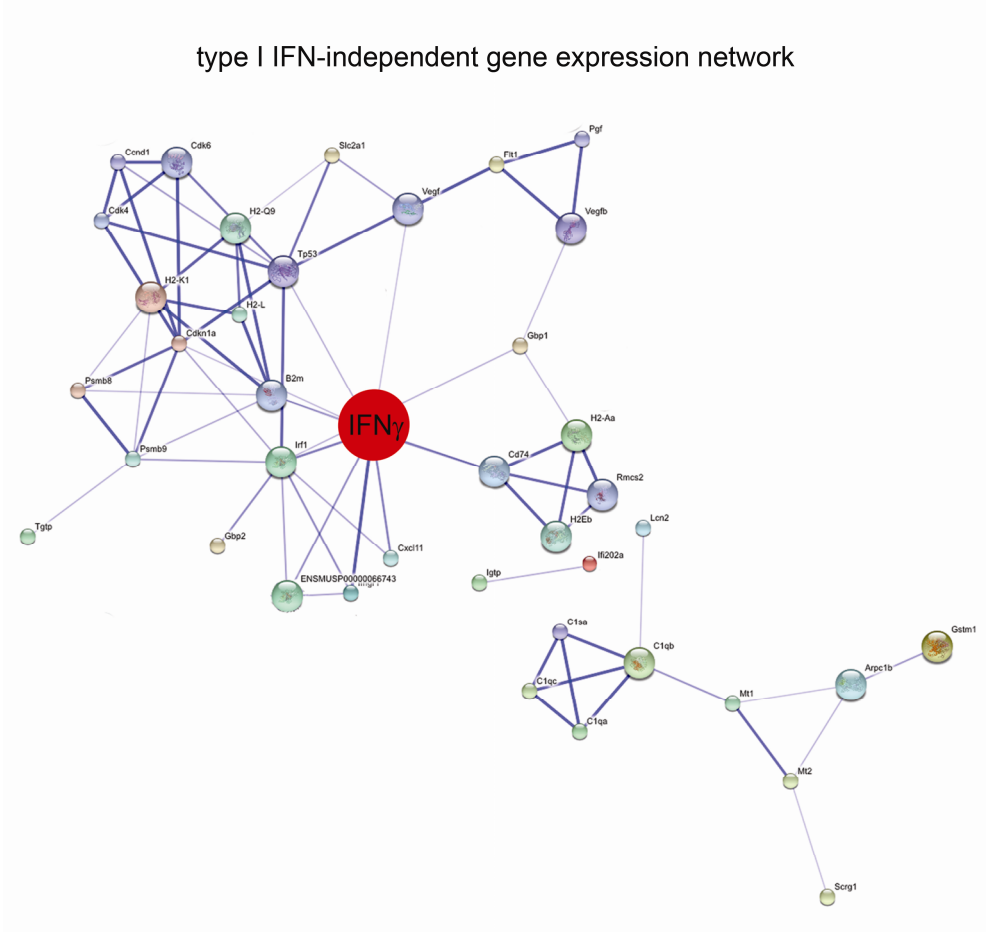

Fig.5. The type I IFN-independent gene expression network. The genes listed in the Supplemental table 3 (n = 73) were subjected to functional association network analysis by using the STRING 8.0 database as described in the legend of Figure 2. The key player in the network, IFN-γ, is indicated in red.

Several studies have shown that MHV [(3, 34, 38), and this study] as well as several other viruses (8, 29, 45) replicate to much higher levels (up to 10^5 fold difference) in IFNAR$^{-/-}$ mice than in their wild-type counterparts. In this study we show that a strong correlation exists between the amplitude of type I and II IFN host responses with the viral load. The huge differences in virus replication between wild-type and IFNAR$^{-/-}$ mice therefore do not permit a fair comparison between gene expression profiles of these mice, with the aim of identifying type I IFN-dependent responses. Indeed, as no significant gene expression is observed in the wild-type 129SvEv mice, a comparison with the expression profile of the IFNAR$^{-/-}$ mice only provides information about type I IFN-independent and not IFN-

dependent responses. We now observe, in agreement with our previous study, that the brain of BALB/c and IFNAR$^{-/-}$ 129SvEv mice contain very similar MHV loads at day 2 and 5 post infection (34). Since the type I IFN-responsive pathway is very well conserved among many different species (31), we considered it acceptable to compare the gene expression profiles of these mice with the aim of identifying type I IFN-dependent responses, although comparing transcriptional profiles of wild-type and IFNAR$^{-/-}$ mice from a different genetic background should obviously be done very cautiously. Ideally, a comparison between wild-type BALB/c and IFNAR$^{-/-}$ BALB/c mice would have been more accurate. While the induced expression of a number of genes was similar for the two mouse strains (i.e. type I IFN signalling-independent gene-expression), that of other genes was only observed in the BALB/c mice (i.e. tentative type I IFN signalling-dependent gene expression). The expression of yet other genes appeared to be partially dependent of type I IFN signalling: increased expression of these genes was observed in the IFNAR$^{-/-}$ mice, but much more so in the BALB/c mice.

Genes, the expression of which was upregulated (≥1.5 fold) in the BALB/c mice but not significantly changed in the IFNAR$^{-/-}$ mice upon infection with MHV, were tentatively designated as type I IFN-dependent. Genes, the transcriptional upregulation of which was at least 2 times higher in the BALB/c mice than in the IFNAR$^{-/-}$ mice, were also added to the list of tentative type I IFN-dependent genes. As expected, this set of genes (n = 82) contained many known IFN-responsive genes like *Isg20*, *Ifit1*, *Ifit3*, *Isgf3g*, *Mx2* and *Ube1l* (Supplemental table 4). Functional association network analyses showed Irf1 and Irf7 to be the key players in the network (Supplemental Fig.1). Several of the tentative type I IFN-dependent genes (including *Mx2* and *Ube1l*) have previously been shown to play an important protective role against virus infections (11, 14, 25, 30, 44). We speculate that other genes present in this list may also be important for full protection against MHV infection.

In conclusion, Transcriptional profiling of mice infected with MHV demonstrated the induction of a robust IFN response, which correlated with the viral load. Profiling of IFNAR$^{-/-}$ mice allowed us to identify type I IFN–independent and –dependent responses.

Overall, this study broadens our present knowledge of the type I IFN-mediated effector responses during CoV infection *in vivo*.

Material & Methods

Mouse infection experiments

6-8 week old BALB/c were obtained from Charles River Laboratories, while type I IFN receptor knock-out mice ($IFNAR^{-/-}$) (27) and the parental 129SvEv mice were obtained from B&K Universal Ltd. Mice were inoculated intranasally with 10^6 $TCID_{50}$ of MHV strain A59 and sacrificed at the indicated time-points for organ dissection. Control animals were treated with PBS. The study protocol was approved by the animal ethics committee of the Utrecht University, and all experiments were performed in accordance with accepted institutional and governmental policies.

Tissue homogenization and isolation of total RNA

Whole brains and livers were dissected from the MHV-infected and control mice. The tissues were added to Lysing Matrix D tubes (MP Biomedical), containing 1 ml of RNApro™ solution (Q-BIOgene), and processed using a FastPrep instrument (MP Biomedical). The tissues were homogenized at 6,000 rpm for 40 sec and immediately placed on ice. Subsequently, the homogenates were centrifuged at 14,000 rpm for 10 min at 4°C and supernatants were harvested and stored at -80°C. Total RNA was isolated from the homogenates using the TRIzol reagent (Invitrogen) according to the manufacturer's protocol. RNA was further purified using the RNeasy mini-kit with subsequent DNaseI treatment on the column (Qiagen). RNA integrity was determined by spectrometry and by a microfluidics-based platform using a UV-mini1240 device (Shimadzu) and a 2100 Bioanalyzer (Agilent Technologies), respectively.

Quantitative RT-PCR

1 µg of total RNA was reverse transcribed into cDNA using 0.5 µM oligo(dT) primers and 20U of M-MuLV-Reverse transcriptase (Fermentas) in a total reaction volume of 20 µl for 1 h at 37°C. Subsequently, gene expression levels of type I and II IFNs (i.e. IFN-α4 [NM_010504.2], IFN-β1 [NM_010510.1], and IFN-γ [NM_008337.3], respectively), were measured by quantitative PCR using Assay-On-Demand reagents and equipment (PE Applied Biosystems), according to the manufacturer's instructions. The quantitative PCR reactions were performed in a total reaction volume of 20 µl containing 10 µl Taqman® Universal PCR Master Mix (2x), 5 µl cDNA, 1 µl TaqMan® Gene Expression Assay Mix (20x), and 4 µl water using an ABI Prism 7000 sequence detection system under the following conditions: 95°C for 10 min, followed by 40 cycles of 95°C for 15 secs and 60°C for 1 min. For all assays, we performed "no-RT" (reaction using total RNA as the substrate) and "no template" (reaction using water as the substrate) controls. In both cases, omitting cDNA from the reaction resulted in a lack of PCR product generation. All assays were analyzed with ABI Prism 7000 Software v1.2.3f2 (PE Applied Biosystems). The comparative Ct-method was used to determine the fold change for each gene (primer efficiencies were similar for both the endogenous control primer set and genes of interest primer sets [data not shown]). Note that the Ct values of all samples were within the limits of the standard curves (data not shown). The housekeeping gene GAPDH (NM_008084.2) was used as a reference in all experiments, since expression of this gene was found constant among samples. The amounts of viral RNA were determined by quantitative RT-PCR as described before (32).

Microarray hybridizations

The microarray experiments were performed as described previously (33). Briefly, mRNA was amplified from 1 µg of total RNA by cDNA synthesis with oligo(dT) double-anchored primers, followed by in vitro transcription using a T7 RNA polymerase kit (Ambion). During transcription, 5-(3-aminoallyl)-UTP was incorporated into the single stranded cRNA. Cy3 and Cy5 NHS-esters (Amersham Biosciences) were coupled to 2 µg cRNA. RNA quality was monitored after each successive step using the equipment described above. Corning UltraGAPS slides, printed with a Mouse Array-Ready Oligo set (Operon; 35,000 spots), were hybridized with 1 µg of each alternatively labeled cRNA target at 42°C for 16-20 h. Two independent dye-swap hybridizations (4 arrays) were performed for each experimental group. After hybridization the slides were washed extensively and scanned using the Agilent G2565AA DNA Microarray Scanner.

Statistical analysis

After data extraction using Imagene 5.6 Software (BioDiscovery), Lowess normalization (55) was performed on mean spot-intensities in order to correct for dye and print-tip biases (37). The microarray data was analysed using ANOVA (R version 2.2.1/MAANOVA version 0.98-7) (http://www.r-project.org) (53). Briefly, in a fixed effect analysis, sample, array and dye effects were modelled. P-values were determined by a permutation F2-test, in which residuals were shuffled 5,000 times globally. Genes with $P<0.05$ after family wise error correction were considered significantly changed. Cluster analysis (standard correlation) was performed with GeneSpring GX 7.2 software (Silicon Genetics). When indicated, the confidence level was increased by applying a fold change cut-off. The resulting genelists were subjected to Genespring 7.2 software for further analysis.

ArrayExpress accession numbers

MIAME-compliant data in MAGE-ML format as well as complete descriptions of protocols have been submitted to the public microarray database ArrayExpress (http://www.ebi.ac.uk/arrayexpress/) with the following accession numbers: microarray layout, P-UMCU-8; gene expression data of MHV-infected mice, E-MEXP-2081; protocols for total RNA isolation and mRNA amplification, P-MEXP-34397; cRNA labeling, P-MEXP-34400 and P-MEXP-35534; hybridization and washing of slides, P-MEXP-34401; scanning of slides, P-MEXP-34430; data normalization, P-MEXP-34431.

Acknowledgements

This work was supported by grants from the M.W. Beijerinck Virology Fund, Royal Netherlands Academy of Arts and Sciences, and The Netherlands Organization for Scientific Research (NWO-VIDI-700.54.421) to C.A.M. de Haan. We thank Connie Bergmann for advice and Monique Oostra, Marne Hagemeijer, and Mijke Vogels for stimulating discussions.

Supplementary Data

Supplemental table 1. Gene expression profiles in the brain of MHV-infected mice. (A) Early genes (n = 57), and (B) Late genes (n = 64). The induction of expression for each gene in infected animals relative to the PBS-inoculated animals is indicated for the different conditions (i.e. mouse strain and day post infection).

Table 1A. Early genes (n = 57)

GeneID	Common Name	RefSeq	BALB/c t=2	BALB/c t=5	129Sv t=2	129Sv t=5
MMAA300004126	69717	XM_001003852	**1,6**	**2,8**	1,0	1,0
MMAA300002620	1810023F06 Rik	NM_029803	**4,4**	**10,4**	1,1	1,0
MMAA300008745	B2m	NM_009735	**2,2**	**5,4**	1,3	1,2
MMAA300017604	Bst2	NM_198095	**1,6**	**2,1**	1,0	1,0
MMAA200001340	C1qc	NM_007574	**1,5**	**1,9**	1,1	1,0
MMAA300009870	Ccl12	NM_011331	**1,7**	**9,3**	1,2	1,1
MMAA200009050	Cxcl11	NM_019494	**1,5**	**6,1**	1,0	1,0
MMAA300012414	D11Ertd759e	NM_001040005	**1,6**	**2,9**	1,4	1,0
MMAA200000807	D12Ertd647e	NM_026790	**2,7**	**3,0**	1,1	1,2
MMAA300004057	ENSMUSES TG00003733 703		**1,8**	**2,6**	1,0	1,0
MMAA300012450	ENSMUSG0 0000039955		**1,9**	**3,2**	1,3	1,0
MMAA300012693	Fbxo39	NM_001037713	**2,0**	**2,8**	1,1	1,0
MMAA200000089	Gbp1	NM_010259	**2,7**	**6,1**	1,1	1,0
MMAA200004765	Gbp2	NM_010260	**2,4**	**4,1**	1,1	1,0
MMAA200000729	Gbp3	NM_018734	**3,5**	**5,5**	1,3	1,1
MMAA300006597	Gbp4	NM_029509	**5,3**	**4,8**	1,1	1,1
MMAA300017406	genomic:17-45870359-45870428		**6,1**	**8,3**	1,1	1,0
MMAA300011983	H28	NM_031367	**1,9**	**2,1**	1,1	1,0
MMAA300004062	H2-K1	NM_019909	**7,2**	**4,9**	1,1	1,2
MMAA300012864	H2-Q1		**1,7**	**3,2**	1,1	1,1
MMAA300010152	H2-Q10	NM_010391	**2,3**	**3,3**	0,9	1,0
MMAA300010147	H2-Q8	NM_023124	**1,6**	**2,2**	1,0	1,0
MMAA300006884	Herc5	XM_978982	**1,5**	**2,4**	1,0	1,0
MMAA300005162	Ifi202b	NM_008327	**2,2**	**7,2**	1,5	1,2
MMAA300005166	Ifi204	NM_008329	**1,5**	**5,2**	1,2	1,0
MMAA200006998	Ifi44	NM_133871	**4,3**	**6,4**	1,2	1,1
MMAA200004157	Ifih1	NM_027835	**1,6**	**2,8**	1,1	1,1
MMAA200002418	Ifit1	NM_008331	**3,7**	**3,4**	1,2	1,0
MMAA300016271	Ifit3	NM_010501	**5,9**	**7,6**	1,6	1,0
MMAA200009330	Ifitm3	NM_025378	**2,3**	**5,4**	1,8	1,1
MMAA200000303	Iigp2	NM_018738	**1,6**	**5,1**	1,2	1,0
MMAA200001244	Irf7	NM_016850	**1,6**	**2,2**	1,1	1,0
MMAA200006739	Irgm	NM_008326	**3,0**	**7,2**	1,1	1,0
MMAA200003721	Isg20	NM_020583	**2,4**	**3,3**	1,0	1,0

MMAA200000773	Isgf3g	NM_008394	**2,3**	**2,1**	1,0	1,0
MMAA200001213	Lgals3bp	NM_011150	**3,3**	**5,9**	1,4	1,1
MMAA200003577	Lgals9	NM_010708	**1,5**	**1,8**	1,0	1,0
MMAA200002687	Ly6c	NM_010738	**4,2**	**8,2**	1,8	1,0
MMAA200000279	Ly6e	NM_008529	**1,7**	**2,0**	0,9	1,1
MMAA200014954	Ly6f	NM_008530	**3,1**	**6,8**	1,2	1,0
MMAA200003282	Mx2	NM_013606	**2,0**	**2,6**	1,2	0,9
MMAA300000160	Oas1g	NM_011852	**2,4**	**6,2**	1,2	1,0
MMAA300006738	Oasl2	NM_011854	**2,8**	**4,5**	1,0	1,0
MMAA200004993	Olfr56	NM_010999	**2,5**	**6,9**	1,2	1,0
MMAA300011591	Parp12	NM_172893	**1,6**	**2,2**	1,1	1,0
MMAA200003254	Psmb8	NM_010724	**1,9**	**4,4**	1,1	1,1
MMAA200000293	Psme1	NM_011189	**4,0**	**2,1**	1,0	1,0
MMAA300018571	Samd9l	XM_983894	**1,8**	**4,1**	1,5	1,0
MMAA200002695	Stat1	NM_009283	**3,4**	**5,2**	1,1	1,0
MMAA300010868	Tap1	NM_013683	**1,7**	**5,3**	1,1	1,0
MMAA200003398	Tgtp	NM_001045540	**7,3**	**17,5**	1,9	1,1
MMAA200005563	Tor3a	NM_023141	**1,5**	**2,0**	1,0	1,0
MMAA200002067	Trim25	NM_009546	**1,9**	**2,6**	1,2	1,0
MMAA200000426	Ube1l	NM_023738	**2,1**	**2,9**	1,0	1,0
MMAA300005461	Ube2l6	NM_019949	**1,5**	**2,3**	1,0	0,9
MMAA200005576	Usp18	NM_011909	**1,9**	**3,9**	1,0	1,0
MMAA300005673	Zbp1	NM_021394	**2,7**	**6,2**	1,1	1,0

Table 1B. Late genes (n = 64)

GeneID	**Common Name**	**RefSeq**	**BALB/c t=2**	**BALB/c t=5**	**129Sv t=2**	**129Sv t=5**
MMAA300004129	15040	XM_992574	1,4	**1,9**	1,0	1,0
MMAA300007721	665536		1,1	**1,8**	1,1	1,0
MMAA300002618	1810023F06 Rik	NM_029803	1,4	**2,1**	1,1	0,9
MMAA200003525	6620401K05 Rik	NM_172774	1,1	**1,8**	1,1	1,0
MMAA300012210	AI481105	XM_989905	1,4	**1,7**	0,9	1,0
MMAA300006778	Arpc1b	NM_023142	0,9	**1,9**	1,0	1,1
MMAA200000131	C1qa	NM_007572	1,3	**2,3**	1,0	1,0
MMAA200000049	Ccl2	NM_011333	1,0	**7,5**	1,0	1,0
MMAA300009668	Ccl5	NM_013653	0,9	**2,8**	1,0	1,0
MMAA200003414	Ccl7	NM_013654	0,9	**2,8**	1,0	1,1
MMAA300004234	Cd74	NM_001042605	1,0	**2,0**	1,0	0,9
MMAA300000452	Cp	NM_007752	1,3	**2,8**	1,1	1,0
MMAA200000242	Ctsc	NM_009982	1,1	**2,5**	1,1	1,0
MMAA200001409	Ctss	NM_021281	1,2	**2,0**	1,1	1,0
MMAA200000311	Cxcl10	NM_021274	1,4	**13,0**	1,1	1,0
MMAA200000272	Cxcl9	NM_008599	1,0	**2,2**	1,0	1,0
MMAA300009934	D14Ertd668e	NM_199015	1,2	**2,4**	1,0	1,0
MMAA300018596	ENSMUSG0 0000063388		1,1	**2,7**	1,1	1,0

MMAA200004470	Fcer1g	NM_010185	1,0	**2,5**	1,1	1,1
MMAA200000053	Fcgr1	NM_010186	1,4	**2,1**	1,0	1,0
MMAA300021278	Fcgr3a	NM_144559	1,0	**2,1**	1,0	1,0
MMAA200003376	Gzma	NM_010370	0,9	**2,5**	1,0	1,0
MMAA200003391	H2-Ea	NM_010381	1,1	**2,1**	1,1	1,0
MMAA200014858	H2-Q1		1,1	**1,9**	1,0	1,1
MMAA300010153	H2-Q9	NM_010394	1,4	**2,4**	1,1	1,1
MMAA200000255	Hck	NM_010407	1,1	**1,9**	1,0	1,0
MMAA300010905	Icam1	NM_010493	1,0	**2,7**	1,0	1,0
MMAA300005165	Ifi205	NM_001033450	1,2	**2,1**	1,1	1,0
MMAA300004660	Ifitm1	NM_026820	1,0	**2,3**	1,0	1,0
MMAA200000196	Ifngr1	NM_010511	1,0	**1,6**	1,1	1,0
MMAA200000461	Irf1	NM_008390	1,4	**6,5**	1,1	1,0
MMAA200001229	Irf8	NM_008320	1,1	**1,7**	1,0	1,0
MMAA300015119	Krt18	NM_010664	1,2	**1,6**	0,9	1,1
MMAA300005306	Lcn2	NM_008491	1,4	**6,8**	1,0	1,1
MMAA300021034	Lgals3	NM_010705	1,3	**1,8**	1,0	1,0
MMAA300001891	Lilrb4	NM_013532	1,2	**1,8**	1,1	1,0
MMAA300002751	Ly86	NM_010745	0,8	**1,9**	1,0	1,0
MMAA300002048	Lyzs	NM_017372	0,9	**2,5**	1,0	1,0
MMAA300004266	Ms4a4b	NM_021718	0,9	**1,9**	1,0	1,0
MMAA200006504	Ms4a6b	NM_028595	1,1	**2,6**	0,9	1,0
MMAA200011666	Ms4a6d	NM_026835	1,1	**2,5**	1,1	1,0
MMAA200009417	Mt2	NM_008630	1,0	**1,7**	1,0	0,9
MMAA200007409	Myct1	NM_026793	0,9	**1,9**	1,1	1,0
MMAA200016125	Oasl1	NM_145209	1,4	**3,0**	1,1	1,0
MMAA200002994	Osmr	NM_011019	1,0	**1,7**	1,0	1,1
MMAA300009340	Parp14	NM_001039530	1,2	**2,2**	1,1	1,0
MMAA300015703	Phf11	NM_172603	1,4	**3,1**	1,2	1,0
MMAA200007618	Plac8	NM_139198	1,0	**2,9**	1,1	1,0
MMAA200013018	Plec1	XM_993494	1,3	**2,6**	1,0	1,0
MMAA200000278	Psmb10	NM_013640	1,2	**2,3**	1,0	1,0
MMAA200003424	Psmb9	NM_013585	1,4	**4,0**	1,1	1,0
MMAA300018890	Psme1	NM_011189	1,0	**2,1**	1,2	1,0
MMAA200003295	Saa3	NM_011315	1,0	**5,0**	1,0	1,0
MMAA200012660	Samhd1	NM_018851	1,3	**2,1**	1,0	1,0
MMAA200008133	Serping1	NM_009776	1,0	**2,2**	1,1	1,0
MMAA200000042	Socs1	NM_009896	1,1	**1,5**	1,2	1,0
MMAA200004256	Stat2	NM_019963	1,2	**1,9**	0,9	1,0
MMAA200003694	Tgm2	NM_009373	1,3	**2,5**	1,0	0,9
MMAA300000154	Timp1	NM_011593	1,0	**1,9**	1,0	1,0
MMAA200015882	Tlr2	NM_011905	1,0	**2,3**	1,1	1,0
MMAA200000616	Tspo	NM_009775	1,0	**2,0**	1,0	1,0
MMAA300002295	Tyki	NM_020557	1,4	**2,0**	1,0	1,0
MMAA300017681	XR_003396.1	XM_924014	1,3	**2,4**	1,1	1,1
MMAA300015120	XR_005070.1	XR_005070	1,1	**1,6**	1,0	1,0

Supplemental table 2. Differentially expressed genes per BALB/c mouse. The induction of gene expression at day 5 for 96 genes relative to the PBS-inoculated animals is indicated for the four individual BALB/c mice. Differential gene expression correlates with the viral load.

GeneID	Common Name	RefSeq	M1	M2	M3	M4
MMAA300004126	69717	XM_001003852	3,3	1,7	4,6	1,5
MMAA300002620	1810023F06Rik	NM_029803	3,3	20,8	3,4	14,1
MMAA300008745	B2m	NM_009735	2,5	10,0	2,7	6,4
MMAA300017604	Bst2	NM_198095	2,2	2,4	2,0	2,0
MMAA200000131	C1qa	NM_007572	2,3	2,7	1,8	2,3
MMAA300009870	Ccl12	NM_011331	2,9	15,1	2,4	16,8
MMAA200000049	Ccl2	NM_011333	3,7	14,5	2,1	9,7
MMAA300009668	Ccl5	NM_013653	1,5	5,0	1,4	3,3
MMAA200003414	Ccl7	NM_013654	1,4	5,2	0,9	3,8
MMAA300004234	Cd74	NM_001042605	1,1	3,0	1,4	2,5
MMAA300000452	Cp	NM_007752	0,6	5,3	0,6	4,5
MMAA200000242	Ctsc	NM_009982	1,3	4,3	1,3	3,0
MMAA200001409	Ctss	NM_021281	1,9	2,5	1,7	1,9
MMAA200000311	Cxcl10	NM_021274	6,6	22,5	6,0	17,1
MMAA200009050	Cxcl11	NM_019494	3,2	9,8	2,9	8,3
MMAA200000272	Cxcl9	NM_008599	1,2	3,6	1,0	2,7
MMAA300012414	D11Ertd759e	NM_001040005	1,4	4,6	1,4	4,1
MMAA200000807	D12Ertd647e	NM_026790	3,6	2,3	4,1	2,2
MMAA300009934	D14Ertd668e	NM_199015	1,2	4,3	1,1	3,2
MMAA300004057	ENSMUSESTG00003733703		1,7	4,1	1,9	2,6
MMAA300012450	ENSMUSG00000039955		2,7	3,9	3,1	3,2
MMAA300018596	ENSMUSG00000063388		1,6	4,2	1,7	3,3
MMAA300012693	Fbxo39	NM_001037713	1,6	4,7	1,4	3,7
MMAA200004470	Fcer1g	NM_010185	2,1	3,1	2,0	2,6
MMAA200000053	Fcgr1	NM_010186	1,9	2,5	1,7	2,2
MMAA300021278	Fcgr3a	NM_144559	1,3	3,0	1,3	2,8
MMAA200000089	Gbp1	NM_010259	3,4	10,5	4,1	6,2
MMAA200004765	Gbp2	NM_010260	2,9	4,2	3,2	6,2
MMAA200000729	Gbp3	NM_018734	3,0	8,9	2,8	7,3
MMAA300006597	Gbp4	NM_029509	1,0	10,6	1,5	6,1
MMAA300017406	genomic:17-45870359-45870428		7,0	10,1	9,4	6,6
MMAA200003376	Gzma	NM_010370	1,0	5,2	1,1	2,8
MMAA300011983	H28	NM_031367	1,8	2,7	1,6	2,3
MMAA200003391	H2-Ea	NM_010381	0,9	3,8	1,1	2,6
MMAA300004062	H2-K1	NM_019909	3,1	7,8	3,5	5,3
MMAA300012864	H2-Q1		2,7	3,7	2,9	3,3
MMAA300010152	H2-Q10	NM_010391	3,7	2,4	5,8	1,3
MMAA300010147	H2-Q8	NM_023124	2,8	2,4	2,0	1,6
MMAA300010153	H2-Q9	NM_010394	2,0	3,0	2,4	2,2

MMAA300006884	Herc5	XM_978982	1,3	4,5	1,1	2,8
MMAA300010905	Icam1	NM_010493	2,9	2,3	3,1	2,4
MMAA300005162	Ifi202b	NM_008327	0,8	15,3	0,7	11,9
MMAA300005166	Ifi204	NM_008329	1,4	9,2	1,3	8,7
MMAA300005165	Ifi205	NM_001033450	1,5	3,7	0,8	2,2
MMAA200006998	Ifi44	NM_133871	2,1	11,9	1,8	10,1
MMAA200004157	Ifih1	NM_027835	1,2	4,6	1,3	4,0
MMAA200002418	Ifit1	NM_008331	2,4	4,6	2,3	4,5
MMAA300016271	Ifit3	NM_010501	2,9	13,3	2,7	11,3
MMAA300004660	Ifitm1	NM_026820	2,1	3,1	2,0	1,9
MMAA200009330	Ifitm3	NM_025378	3,4	7,9	4,0	6,3
MMAA200000303	Iigp2	NM_018738	3,2	7,4	3,1	6,5
MMAA200000461	Irf1	NM_008390	2,8	12,5	2,5	8,0
MMAA200001244	Irf7	NM_016850	2,0	2,4	2,5	2,0
MMAA200006739	Irgm	NM_008326	2,9	13,7	2,8	9,6
MMAA200003721	Isg20	NM_020583	5,3	1,9	3,8	2,2
MMAA200000773	Isgf3g	NM_008394	1,8	2,8	1,9	2,0
MMAA300005306	Lcn2	NM_008491	1,8	13,2	2,8	9,4
MMAA200001213	Lgals3bp	NM_011150	3,4	8,2	3,9	8,0
MMAA200002687	Ly6c	NM_010738	5,0	13,2	5,2	9,3
MMAA200000279	Ly6e	NM_008529	2,2	2,1	1,7	2,1
MMAA200014954	Ly6f	NM_008530	3,4	11,7	3,7	8,3
MMAA300002048	Lyzs	NM_017372	2,0	3,0	2,2	2,7
MMAA200006504	Ms4a6b	NM_028595	1,1	5,0	1,0	3,5
MMAA200011666	Ms4a6d	NM_026835	1,7	4,1	1,5	2,7
MMAA200003282	Mx2	NM_013606	1,3	4,4	1,1	3,5
MMAA300000160	Oas1g	NM_011852	3,2	9,9	3,9	7,7
MMAA200016125	Oasl1	NM_145209	1,7	4,9	1,4	4,0
MMAA300006738	Oasl2	NM_011854	5,8	2,7	7,2	2,3
MMAA200004993	Olfr56	NM_010999	3,2	13,3	1,9	9,3
MMAA300011591	Parp12	NM_172893	1,3	3,4	1,2	2,9
MMAA300009340	Parp14	NM_001039530	1,4	3,1	1,4	2,7
MMAA300015703	Phf11	NM_172603	1,0	5,8	0,7	4,8
MMAA200007618	Plac8	NM_139198	2,2	3,6	2,9	3,0
MMAA200013018	Plec1	XM_993494	1,4	4,0	1,6	3,4
MMAA200000278	Psmb10	NM_013640	1,8	3,4	1,7	2,2
MMAA200003254	Psmb8	NM_010724	3,0	7,2	3,1	4,3
MMAA200003424	Psmb9	NM_013585	1,6	7,4	1,7	5,2
MMAA200000293	Psme1	NM_011189	1,7	2,7	1,8	2,1
MMAA200003295	Saa3	NM_011315	1,7	9,8	2,2	6,2
MMAA300018571	Samd9l	XM_983894	1,5	8,8	1,1	5,1
MMAA200012660	Samhd1	NM_018851	0,7	3,9	0,6	3,2
MMAA200008133	Serping1	NM_009776	1,0	4,2	1,0	2,8
MMAA200002695	Stat1	NM_009283	2,4	8,4	2,7	7,5
MMAA300010868	Tap1	NM_013683	2,0	10,4	1,7	7,2
MMAA200003694	Tgm2	NM_009373	1,3	4,2	1,2	3,3
MMAA200003398	Tgtp	NM_001045540	10,1	26,7	10,7	22,5

MMAA200015882	Tlr2	NM_011905	1,3	3,4	1,3	3,1
MMAA200005563	Tor3a	NM_023141	1,4	2,4	2,0	2,2
MMAA200002067	Trim25	NM_009546	1,7	3,8	1,7	3,4
MMAA200000616	Tspo	NM_009775	2,0	2,6	1,9	1,6
MMAA300002295	Tyki	NM_020557	2,0	2,0	2,1	1,9
MMAA200000426	Ube1l	NM_023738	1,5	4,5	1,4	4,1
MMAA300005461	Ube2l6	NM_019949	1,6	3,2	1,5	2,8
MMAA200005576	Usp18	NM_011909	2,8	5,9	2,2	4,7
MMAA300017681	XR_003396.1	XM_924014	1,7	3,7	1,8	2,6
MMAA300005673	Zbp1	NM_021394	2,2	12,2	1,7	8,6

Supplemental table 3. Type I IFN-independent genes. The induction of differential gene expression (≥1.5 fold) in the brain of MHV-infected IFNAR$^{-/-}$ mice at day 5 relative to the PBS-inoculated animals is indicated. The relative expression of these genes in the parental 129SvEv mice after infection with MHV is also shown.

GeneID	Common Name	RefSeq	129Sv t=2	129Sv t=5	IFNAR t=2	IFNAR t=5
MMAA300018417	665509		1,1	1,0	1,1	**1,5**
MMAA200000796	Apod	NM_007470	1,2	1,0	1,0	**2,0**
MMAA300006778	Arpc1b	NM_023142	1,0	1,1	1,0	**1,6**
MMAA200004830	Arrdc2	NM_027560	1,0	1,0	1,0	**1,8**
MMAA300008745	B2m	NM_009735	1,3	1,2	1,0	**4,1**
MMAA200000131	C1qa	NM_007572	1,0	1,0	0,9	**2,1**
MMAA200000979	C1qb	NM_009777	1,0	1,0	1,0	**3,1**
MMAA200001340	C1qc	NM_007574	1,1	1,0	1,0	**2,0**
MMAA300004234	Cd74	NM_001042605	1,0	0,9	1,0	**3,8**
MMAA200007578	Cdkn1a	NM_007669	1,0	1,0	1,0	**2,1**
MMAA300012869	Chi3l3	XM_889251	1,1	1,0	1,0	**3,3**
MMAA300000452	Cp	NM_007752	1,1	1,0	0,9	**2,3**
MMAA200009050	Cxcl11	NM_019494	1,0	1,0	1,0	**1,6**
MMAA300001385	Cyp2j9	NM_028979	0,9	0,9	1,0	**1,6**
MMAA300012450	ENSMUSG00000039955		1,3	1,0	1,0	**2,1**
MMAA200001345	Flt1	NM_010228	1,1	1,1	1,0	**1,6**
MMAA200000089	Gbp1	NM_010259	1,1	1,0	1,0	**3,2**
MMAA200004765	Gbp2	NM_010260	1,1	1,0	1,0	**2,3**
MMAA200000729	Gbp3	NM_018734	1,3	1,1	1,1	**1,9**
MMAA200005744	Gdpd3	NM_024228	1,1	1,0	1,0	**1,6**
MMAA200000881	Glul	NM_008131	1,0	1,0	0,9	**1,6**
MMAA300020817	Grrp1	XM_485455	0,9	1,0	1,0	**1,5**
MMAA200000761	Gstm1	NM_010358	1,0	0,9	1,0	**1,5**
MMAA300010457	H2-Aa	NM_010378	1,3	0,9	1,0	**1,9**
MMAA300004076	H2-Eb1	NM_010382	1,1	1,0	1,0	**1,7**
MMAA300004062	H2-K1	NM_019909	1,1	1,2	1,0	**2,8**
MMAA300012864	H2-Q1		1,1	1,1	1,0	**1,7**
MMAA300010153	H2-Q9	NM_010394	1,1	1,1	1,0	**1,6**
MMAA200005712	Hexb	NM_010422	1,1	1,0	1,1	**1,5**
MMAA300017926	Hspb1	NM_013560	1,1	1,0	1,1	**1,6**

MMAA300005162	Ifi202b	NM_008327	1,5	1,2	1,3	**1,5**
MMAA300004660	Ifitm1	NM_026820	1,0	1,0	1,1	**2,2**
MMAA200009330	Ifitm3	NM_025378	1,8	1,1	1,1	**3,0**
MMAA200000196	Ifngr1	NM_010511	1,0	1,0	1,0	**1,6**
MMAA200000191	Igfbp7	NM_008048	1,0	1,0	1,1	**2,1**
MMAA200000303	Iigp2	NM_018738	1,2	1,0	1,0	**1,8**
MMAA200000461	Irf1	NM_008390	1,1	1,0	1,1	**1,9**
MMAA300015119	Krt18	NM_010664	0,9	1,1	1,0	**2,2**
MMAA300005306	Lcn2	NM_008491	1,0	1,1	1,1	**2,9**
MMAA200001213	Lgals3bp	NM_011150	1,4	1,1	1,0	**1,5**
MMAA200011815	Lrg1	NM_029796	1,0	1,0	1,1	**1,6**
MMAA200002687	Ly6c	NM_010738	1,8	1,0	1,0	**6,6**
MMAA200014954	Ly6f	NM_008530	1,2	1,0	1,0	**3,4**
MMAA300002048	Lyzs	NM_017372	1,0	1,0	1,0	**4,2**
MMAA300002047	Lzp-s	NM_013590	1,0	1,0	1,0	**1,8**
MMAA300007075	Mgp	NM_008597	1,1	1,0	1,0	**1,9**
MMAA200006504	Ms4a6b	NM_028595	0,9	1,0	1,0	**1,6**
MMAA300007885	Mt1	NM_013602	1,0	0,9	1,1	**2,5**
MMAA200009417	Mt2	NM_008630	1,0	0,9	1,0	**2,3**
MMAA300007883	Mt3	NM_013603	1,1	0,9	1,2	**1,5**
MMAA200004993	Olfr56	NM_010999	1,2	1,0	1,0	**2,2**
MMAA300000072	Phyhd1	NM_177725	1,0	1,0	1,2	**3,1**
MMAA200007618	Plac8	NM_139198	1,1	1,0	1,0	**1,5**
MMAA200016029	Podxl	NM_013723	1,1	1,0	1,1	**1,6**
MMAA200003254	Psmb8	NM_010724	1,1	1,1	1,0	**2,1**
MMAA200003424	Psmb9	NM_013585	1,1	1,0	1,0	**2,0**
MMAA300005843	S100a11	NM_016740	1,0	1,1	1,2	**1,6**
MMAA200003295	Saa3	NM_011315	1,0	1,0	1,1	**2,0**
MMAA200003167	Scrg1	NM_009136	1,0	1,0	1,0	**1,5**
MMAA200003360	Serpina3g	NM_009251	1,0	1,0	1,0	**1,8**
MMAA300001921	Sgk	NM_011361	0,9	1,1	1,0	**1,5**
MMAA300006210	Slc2a1	NM_011400	1,0	1,0	1,0	**1,6**
MMAA300004422	Sorbs1	NM_178362	1,1	1,0	1,0	**1,5**
MMAA200002695	Stat1	NM_009283	1,1	1,0	1,0	**1,5**
MMAA200003495	Sult1a1	NM_133670	0,9	1,1	1,1	**3,3**
MMAA200003694	Tgm2	NM_009373	1,0	0,9	1,0	**2,5**
MMAA200003398	Tgtp	NM_001045540	1,9	1,1	1,0	**13,1**
MMAA200006098	Tm2d2	NM_027194	1,1	0,9	1,3	**2,7**
MMAA300007712	Tsc22d3	NM_010286	1,0	1,0	1,0	**2,0**
MMAA200009290	Ubd	NM_023137	1,0	1,0	1,0	**1,8**
MMAA300017681	XR_003396.1	XM_924014	1,1	1,1	1,0	**1,9**
MMAA300015120	XR_005070.1	XR_005070	1,0	1,0	1,0	**1,8**
MMAA200003752	Zfp113	NM_019747	1,0	1,0	1,0	**1,5**

Supplemental table 4. Tentative type I IFN-dependent genes. List of genes the expression of which was upregulated (≥1.5 fold) in the BALB/c mice but not significantly changed in the IFNAR$^{-/-}$ mice upon infection with MHV. Genes, the transcriptional upregulation of which was at least 2 times higher in the BALB/c mice than in the IFNAR$^{-/-}$ mice, were also added to the list.

GeneID	Common Name	RefSeq	BALB/c t=5	IFNAR t=5	Ratio
MMAA300004129	15040	XM_992574	**1,9**	1,0	1,8
MMAA300004126	69717	XM_001003852	**2,5**	1,0	2,5
MMAA300002618	1810023F06Rik	NM_029803	**1,8**	1,1	1,6
MMAA200003525	6620401K05Rik	NM_172774	**1,7**	1,1	1,6
MMAA300012210	AI481105	XM_989905	**1,7**	0,9	1,8
MMAA300017604	Bst2	NM_198095	**2,1**	1,0	2,1
MMAA300009870	Ccl12	NM_011331	**6,5**	1,4	4,6
MMAA200000049	Ccl2	NM_011333	**5,8**	1,1	5,1
MMAA300009668	Ccl5	NM_013653	**2,4**	1,1	2,1
MMAA200003414	Ccl7	NM_013654	**2,3**	1,0	2,3
MMAA200000242	Ctsc	NM_009982	**2,2**	1,3	1,7
MMAA200000311	Cxcl10	NM_021274	**11,1**	1,3	8,6
MMAA200009050	Cxcl11	NM_019494	**6,1**	**1,6**	3,7
MMAA200000272	Cxcl9	NM_008599	**1,9**	1,1	1,7
MMAA300012414	D11Ertd759e	NM_001040005	**2,4**	1,2	2,1
MMAA200000807	D12Ertd647e	NM_026790	**2,9**	1,0	2,8
MMAA300009934	D14Ertd668e	NM_199015	**2,0**	1,0	2,0
MMAA300004057	ENSMUSESTG00003733703		**2,4**	1,4	1,8
MMAA300012693	Fbxo39	NM_001037713	**2,5**	1,0	2,4
MMAA200000053	Fcgr1	NM_010186	**2,1**	1,1	1,9
MMAA300021278	Fcgr3a	NM_144559	**2,0**	1,1	1,8
MMAA200000729	Gbp3	NM_018734	**5,5**	**1,9**	2,9
MMAA300006597	Gbp4	NM_029509	**3,1**	1,2	2,7
MMAA300017406	genomic:17-45870359-45870428		**8,1**	1,1	7,3
MMAA200003376	Gzma	NM_010370	**2,0**	1,0	2,0
MMAA300011983	H28	NM_031367	**2,0**	1,0	2,0
MMAA200003391	H2-Ea	NM_010381	**1,8**	1,1	1,6
MMAA300004061	H2-K1	NM_019909	**3,3**	1,2	2,7
MMAA300010152	H2-Q10	NM_010391	**2,9**	1,2	2,5
MMAA300010147	H2-Q8	NM_023124	**2,2**	1,0	2,2
MMAA300006884	Herc5	XM_978982	**2,1**	1,1	1,9
MMAA300010905	Icam1	NM_010493	**2,7**	1,4	1,8
MMAA300005162	Ifi202b	NM_008327	**7,2**	1,5	4,8
MMAA300005166	Ifi204	NM_008329	**3,5**	1,1	3,2
MMAA300005165	Ifi205	NM_001033450	**1,8**	1,1	1,7
MMAA200006998	Ifi44	NM_133871	**4,6**	1,1	4,2
MMAA200004157	Ifih1	NM_027835	**2,3**	1,0	2,2
MMAA200002418	Ifit1	NM_008331	**3,3**	1,2	2,7

MMAA300016271	Ifit3	NM_010501	**5,9**	1,2	4,8
MMAA200000303	Iigp2	NM_018738	**5,1**	**1,8**	2,8
MMAA200000461	Irf1	NM_008390	**6,5**	**1,9**	3,5
MMAA200001244	Irf7	NM_016850	**2,2**	1,1	2,1
MMAA200003721	Isg20	NM_020583	**3,0**	1,0	3,1
MMAA200000773	Isgf3g	NM_008394	**2,1**	1,1	1,9
MMAA300005306	Lcn2	NM_008491	**6,8**	**2,9**	2,3
MMAA300021034	Lgals3	NM_010705	**1,8**	1,1	1,7
MMAA200001213	Lgals3bp	NM_011150	**5,9**	1,5	3,8
MMAA200003577	Lgals9	NM_010708	**1,8**	1,1	1,6
MMAA300001891	Lilrb4	NM_013532	**1,7**	1,1	1,5
MMAA200000279	Ly6e	NM_008529	**2,0**	1,2	1,7
MMAA200014954	Ly6f	NM_008530	**6,8**	**3,4**	2,0
MMAA300004266	Ms4a4b	NM_021718	**1,9**	1,0	1,8
MMAA200006504	Ms4a6b	NM_028595	**2,6**	1,6	1,7
MMAA200011666	Ms4a6d	NM_026835	**2,3**	1,1	2,1
MMAA200003282	Mx2	NM_013606	**2,2**	1,0	2,2
MMAA200007409	Myct1	NM_026793	**1,7**	1,0	1,7
MMAA300000160	Oas1g	NM_011852	**5,5**	1,1	5,0
MMAA200016125	Oasl1	NM_145209	**2,6**	1,0	2,7
MMAA300006738	Oasl2	NM_011854	**4,0**	1,0	4,1
MMAA200004993	Olfr56	NM_010999	**6,9**	**2,2**	3,2
MMAA300011591	Parp12	NM_172893	**2,0**	1,1	1,8
MMAA300009340	Parp14	NM_001039530	**2,0**	1,1	1,8
MMAA300015703	Phf11	NM_172603	**2,1**	1,2	1,7
MMAA200007618	Plac8	NM_139198	**2,9**	1,5	2,0
MMAA200013018	Plec1	XM_993494	**2,3**	1,3	1,8
MMAA200000278	Psmb10	NM_013640	**2,2**	1,0	2,1
MMAA200003254	Psmb8	NM_010724	**4,4**	**2,1**	2,1
MMAA200003424	Psmb9	NM_013585	**4,0**	**2,0**	2,0
MMAA300003147	Psme1	NM_011189	**1,9**	1,0	1,8
MMAA200003295	Saa3	NM_011315	**5,0**	**2,0**	2,5
MMAA300018571	Samd9l	XM_983894	**3,0**	1,2	2,5
MMAA200002695	Stat1	NM_009283	**5,2**	**1,5**	3,6
MMAA200004256	Stat2	NM_019963	**1,9**	1,0	1,9
MMAA300000154	Timp1	NM_011593	**1,9**	1,0	1,8
MMAA200015882	Tlr2	NM_011905	**2,1**	1,1	1,9
MMAA200005563	Tor3a	NM_023141	**2,0**	1,1	1,9
MMAA200002067	Trim25	NM_009546	**2,5**	1,2	2,1
MMAA200000616	Tspo	NM_009775	**2,0**	1,2	1,6
MMAA300002295	Tyki	NM_020557	**2,0**	0,9	2,1
MMAA200000426	Ube1l	NM_023738	**2,5**	1,1	2,3
MMAA300005461	Ube2l6	NM_019949	**2,2**	1,1	2,1
MMAA200005576	Usp18	NM_011909	**3,6**	0,9	3,8
MMAA300005673	Zbp1	NM_021394	**4,4**	1,2	3,6

Supplemental Fig.1. Tentative type I IFN-dependent gene expression network. The genes listed in the Supplemental table 4 (n = 82) were subjected to functional association network analysis by using the public STRING 8.0 database (www.string.embl.de). Indicated is the confidence view of the analysis. Stronger associations are symbolized by thicker lines. The central players in the network (i.e. Irf1 and Irf7) are indicated in red.

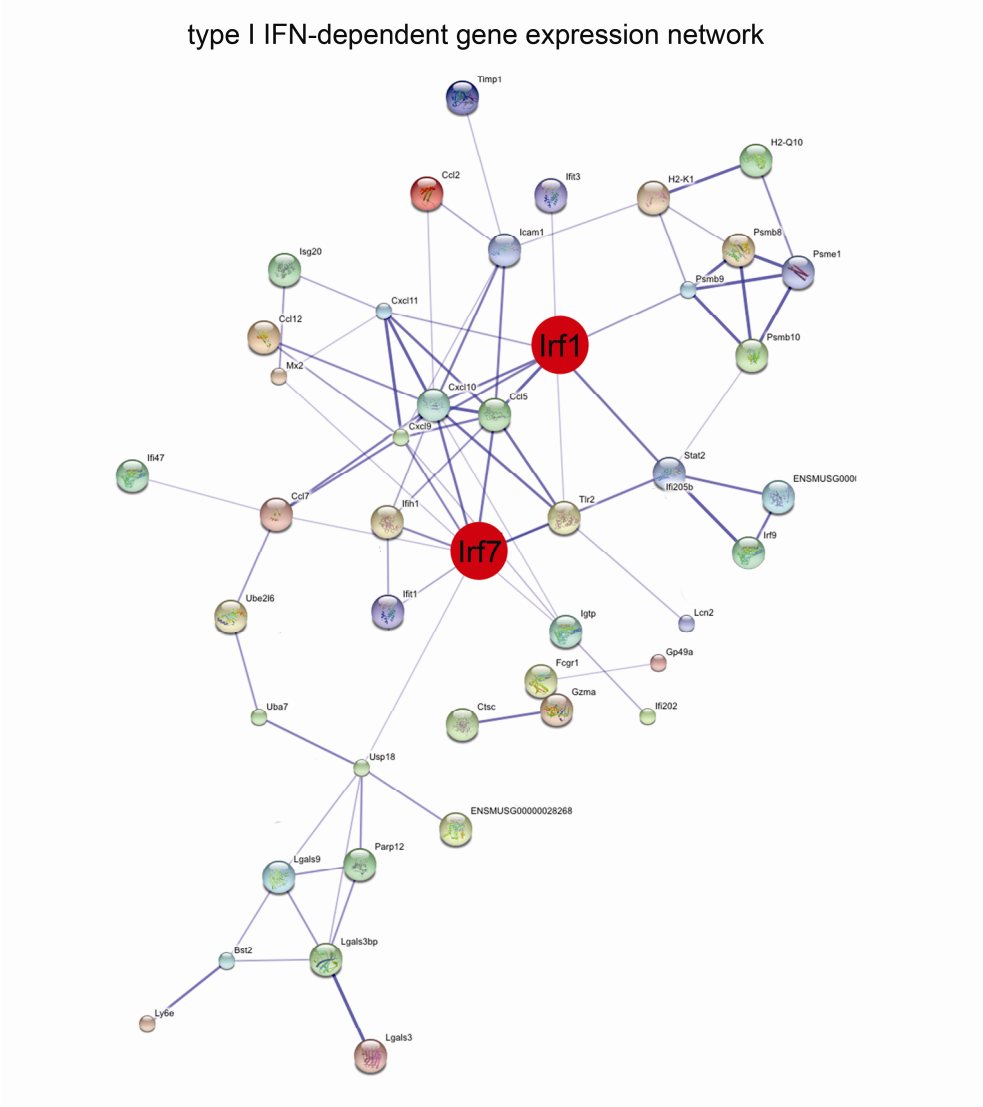

References

1. **Becker-Herman, S., G. Arie, H. Medvedovsky, A. Kerem, and I. Shachar.** 2005. CD74 is a member of the regulated intramembrane proteolysis-processed protein family. Mol Biol Cell 16:5061-9.

2. **Cervantes-Barragan, L., U. Kalinke, R. Zust, M. Konig, B. Reizis, C. Lopez-Macias, V. Thiel, and B. Ludewig.** 2009. Type I IFN-mediated protection of macrophages and dendritic cells secures control of murine coronavirus infection. J Immunol 182:1099-106.

3. **Cervantes-Barragan, L., R. Zust, F. Weber, M. Spiegel, K. S. Lang, S. Akira, V. Thiel, and B. Ludewig.** 2007. Control of coronavirus infection through plasmacytoid dendritic-cell-derived type I interferon. Blood 109:1131-7.

4. **de Lang, A., T. Baas, T. Teal, L. M. Leijten, B. Rain, A. D. Osterhaus, B. L. Haagmans, and M. G. Katze.** 2007. Functional genomics highlights differential induction of antiviral pathways in the lungs of SARS-CoV-infected macaques. PLoS Pathog 3:e112.

5. **Durbin, R. K., S. E. Mertz, A. E. Koromilas, and J. E. Durbin.** 2002. PKR protection against intranasal vesicular stomatitis virus infection is mouse strain dependent. Viral Immunol 15:41-51.

6. **Espert, L., G. Degols, Y. L. Lin, T. Vincent, M. Benkirane, and N. Mechti.** 2005. Interferon-induced exonuclease ISG20 exhibits an antiviral activity against human immunodeficiency virus type 1. J Gen Virol 86:2221-9.

7. **Flodstrom, M., and D. L. Eizirik.** 1997. Interferon-gamma-induced interferon regulatory factor-1 (IRF-1) expression in rodent and human islet cells precedes nitric oxide production. Endocrinology 138:2747-53.

8. **Fragkoudis, R., L. Breakwell, C. McKimmie, A. Boyd, G. Barry, A. Kohl, A. Merits, and J. K. Fazakerley.** 2007. The type I interferon system protects mice from Semliki Forest virus by preventing widespread virus dissemination in extraneural tissues, but does not mediate the restricted replication of avirulent virus in central nervous system neurons. J Gen Virol 88:3373-84.

9. **Frisk, P., J. Tallkvist, I. L. Gadhasson, J. Blomberg, G. Friman, and N. G. Ilback.** 2007. Coxsackievirus B3 infection affects metal-binding/transporting proteins and trace elements in the pancreas in mice. Pancreas 35:e37-44.

10. **Ghoshal, K., S. Majumder, Q. Zhu, J. Hunzeker, J. Datta, M. Shah, J. F. Sheridan, and S. T. Jacob.** 2001. Influenza virus infection induces metallothionein gene expression in the mouse liver and lung by overlapping but distinct molecular mechanisms. Mol Cell Biol 21:8301-17.

11. **Giannakopoulos, N. V., E. Arutyunova, C. Lai, D. J. Lenschow, A. L. Haas, and H. W. Virgin.** 2009. ISG15 Arg151 and the ISG15-conjugating enzyme UbE1L are important for innate immune control of Sindbis virus. J Virol 83:1602-10.

12. **Gongora, C., G. David, L. Pintard, C. Tissot, T. D. Hua, A. Dejean, and N. Mechti.** 1997. Molecular cloning of a new interferon-induced PML nuclear body-associated protein. J Biol Chem 272:19457-63.

13. **Gongora, C., G. Degols, L. Espert, T. D. Hua, and N. Mechti.** 2000. A unique ISRE, in the TATA-less human Isg20 promoter, confers IRF-1-mediated responsiveness to both interferon type I and type II. Nucleic Acids Res 28:2333-41.

14. **Haller, O., P. Staeheli, and G. Kochs.** 2007. Interferon-induced Mx proteins in antiviral host defense. Biochimie 89:812-8.

15. **Honda, K., H. Yanai, H. Negishi, M. Asagiri, M. Sato, T. Mizutani, N. Shimada, Y. Ohba, A. Takaoka, N. Yoshida, and T. Taniguchi.** 2005. IRF-7 is the master regulator of type-I interferon-dependent immune responses. Nature 434:772-7.

16. **Ilback, N. G., A. W. Glynn, L. Wikberg, E. Netzel, and U. Lindh.** 2004. Metallothionein is induced and trace element balance changed in target organs of a common viral infection. Toxicology 199:241-50.

17. **Ireland, D. D., S. A. Stohlman, D. R. Hinton, R. Atkinson, and C. C. Bergmann.** 2008. Type I interferons are essential in controlling neurotropic coronavirus infection irrespective of functional CD8 T cells. J Virol 82:300-10.

18. **Jensen, L. J., M. Kuhn, M. Stark, S. Chaffron, C. Creevey, J. Muller, T. Doerks, P. Julien, A. Roth, M. Simonovic, P. Bork, and C. von Mering.** 2009. STRING 8--a global view on proteins and their functional interactions in 630 organisms. Nucleic Acids Res 37:D412-6.

19. **Jiang, D., H. Guo, C. Xu, J. Chang, B. Gu, L. Wang, T. M. Block, and J. T. Guo.** 2008. Identification of three interferon-inducible cellular enzymes that inhibit the replication of hepatitis C virus. J Virol 82:1665-78.

20. **Kano, A., T. Haruyama, T. Akaike, and Y. Watanabe.** 1999. IRF-1 is an essential mediator in IFN-gamma-induced cell cycle arrest and apoptosis of primary cultured hepatocytes. Biochem Biophys Res Commun 257:672-7.

21. **Kawai, T., and S. Akira.** 2006. Innate immune recognition of viral infection. Nat Immunol 7:131-7.

22. **Kelly, E. J., and R. D. Palmiter.** 1996. A murine model of Menkes disease reveals a physiological function of metallothionein. Nat Genet 13:219-22.

23. **Kelly, J. M., C. S. Gilbert, G. R. Stark, and I. M. Kerr.** 1985. Differential regulation of interferon-induced mRNAs and c-myc mRNA by alpha- and gamma-interferons. Eur J Biochem 153:367-71.

24. **Kyuwa, S., Y. Tagawa, K. Machii, S. Shibata, K. Doi, K. Fujiwara, and Y. Iwakura.** 1998. MHV-induced fatal peritonitis in mice lacking IFN-gamma. Adv Exp Med Biol 440:445-50.

25. **Lai, C., J. J. Struckhoff, J. Schneider, L. Martinez-Sobrido, T. Wolff, A. Garcia-Sastre, D. E. Zhang, and D. J. Lenschow.** 2008. Mice lacking the ISG15 E1 enzyme, UbE1L, demonstrate increased susceptibility to both mouse adapted and non-adapted influenza B virus infection. J Virol.

26. **Minagawa, H., A. Takenaka, S. Mohri, and R. Mori.** 1987. Protective effect of recombinant murine interferon beta against mouse hepatitis virus infection. Antiviral Res 8:85-95.

27. **Muller, U., U. Steinhoff, L. F. Reis, S. Hemmi, J. Pavlovic, R. M. Zinkernagel, and M. Aguet.** 1994. Functional role of type I and type II interferons in antiviral defense. Science 264:1918-21.

28. **Narayanan, K., C. Huang, K. Lokugamage, W. Kamitani, T. Ikegami, C. T. Tseng, and S. Makino.** 2008. Severe acute respiratory syndrome coronavirus nsp1 suppresses host gene expression, including that of type I interferon, in infected cells. J Virol 82:4471-9.

29. **Ohka, S., H. Igarashi, N. Nagata, M. Sakai, S. Koike, T. Nochi, H. Kiyono, and A. Nomoto.** 2007. Establishment of a poliovirus oral infection system in human poliovirus receptor-expressing transgenic mice that are deficient in alpha/beta interferon receptor. J Virol 81:7902-12.

30. **Okumura, A., P. M. Pitha, and R. N. Harty.** 2008. ISG15 inhibits Ebola VP40 VLP budding in an L-domain-dependent manner by blocking Nedd4 ligase activity. Proc Natl Acad Sci U S A 105:3974-9.

31. **Pennings, J. L., T. G. Kimman, and R. Janssen.** 2008. Identification of a common gene expression response in different lung inflammatory diseases in rodents and macaques. PLoS ONE 3:e2596.

32. **Raaben, M., A. W. Einerhand, L. J. Taminiau, M. van Houdt, J. Bouma, R. H. Raatgeep, H. A. Buller, C. A. de Haan, and J. W. Rossen.** 2007. Cyclooxygenase activity is important for efficient replication of mouse hepatitis virus at an early stage of infection. Virol J 4:55.

33. **Raaben, M., M. J. Groot Koerkamp, P. J. Rottier, and C. A. de Haan.** 2007. Mouse hepatitis coronavirus replication induces host translational shutoff and mRNA decay, with concomitant formation of stress granules and processing bodies. Cell Microbiol 9:2218-29.

34. **Raaben, M., H. J. Prins, A. C. Martens, P. J. Rottier, and C. A. de Haan.** 2009. Non-invasive imaging of mouse hepatitis coronavirus infection reveals determinants of viral replication and spread *in vivo*. Cell Microbiol.

35. **Rempel, J. D., S. J. Murray, J. Meisner, and M. J. Buchmeier.** 2004. Differential regulation of innate and adaptive immune responses in viral encephalitis. Virology 318:381-92.

36. **Rempel, J. D., L. A. Quina, P. K. Blakely-Gonzales, M. J. Buchmeier, and D. L. Gruol.** 2005. Viral induction of central nervous system innate immune responses. J Virol 79:4369-81.

37. **Roepman, P., L. F. Wessels, N. Kettelarij, P. Kemmeren, A. J. Miles, P. Lijnzaad, M. G. Tilanus, R. Koole, G. J. Hordijk, P. C. van der Vliet, M. J. Reinders, P. J. Slootweg, and F. C. Holstege.** 2005. An expression profile for diagnosis of lymph node metastases from primary head and neck squamous cell carcinomas. Nat Genet 37:182-6.

38. **Roth-Cross, J. K., S. J. Bender, and S. R. Weiss.** 2008. Murine coronavirus mouse hepatitis virus is recognized by MDA5 and induces type I interferon in brain macrophages/microglia. J Virol 82:9829-38.

39. **Roth-Cross, J. K., L. Martinez-Sobrido, E. P. Scott, A. Garcia-Sastre, and S. R. Weiss.** 2007. Inhibition of the alpha/beta interferon response by mouse hepatitis virus at multiple levels. J Virol 81:7189-99.

40. **Samarajiwa, S. A., S. Forster, K. Auchettl, and P. J. Hertzog.** 2008. INTERFEROME: the database of interferon regulated genes. Nucleic Acids Res.

41. **Schijns, V. E., C. M. Wierda, M. van Hoeij, and M. C. Horzinek.** 1996. Exacerbated viral hepatitis in IFN-gamma receptor-deficient mice is not suppressed by IL-12. J Immunol 157:815-21.

42. **Smith, A. L., S. W. Barthold, M. S. de Souza, and K. Bottomly.** 1991. The role of gamma interferon in infection of susceptible mice with murine coronavirus, MHV-JHM. Arch Virol 121:89-100.

43. **Spiegel, M., A. Pichlmair, L. Martinez-Sobrido, J. Cros, A. Garcia-Sastre, O. Haller, and F. Weber.** 2005. Inhibition of Beta interferon induction by severe acute respiratory syndrome coronavirus suggests a two-step model for activation of interferon regulatory factor 3. J Virol 79:2079-86.

44. **Staeheli, P., M. A. Horisberger, and O. Haller.** 1984. Mx-dependent resistance to influenza viruses is induced by mouse interferons alpha and beta but not gamma. Virology 132:456-61.

45. **Steinhoff, U., U. Muller, A. Schertler, H. Hengartner, M. Aguet, and R. M. Zinkernagel.** 1995. Antiviral protection by vesicular stomatitis virus-specific antibodies in alpha/beta interferon receptor-deficient mice. J Virol 69:2153-8.

46. **Stetson, D. B., and R. Medzhitov.** 2006. Type I interferons in host defense. Immunity 25:373-81.

47. **Thiel, V., and F. Weber.** 2008. Interferon and cytokine responses to SARS-coronavirus infection. Cytokine Growth Factor Rev 19:121-32.

48. **Thirion, G., and J. P. Coutelier.** 2009. Production of protective gamma interferon by natural killer cells during early mouse hepatitis virus infection. J Gen Virol 90:442-7.

49. **Trifilo, M. J., and T. E. Lane.** 2004. The CC chemokine ligand 3 regulates CD11c+CD11b+CD8alpha- dendritic cell maturation and activation following viral infection of the central nervous system: implications for a role in T cell activation. Virology 327:8-15.

50. **Van den Eynde, B. J., and S. Morel.** 2001. Differential processing of class-I-restricted epitopes by the standard proteasome and the immunoproteasome. Curr Opin Immunol 13:147-53.

51. **Versteeg, G. A., P. J. Bredenbeek, S. H. van den Worm, and W. J. Spaan.** 2007. Group 2 coronaviruses prevent immediate early interferon induction by protection of viral RNA from host cell recognition. Virology 361:18-26.

52. **Versteeg, G. A., O. Slobodskaya, and W. J. Spaan.** 2006. Transcriptional profiling of acute cytopathic murine hepatitis virus infection in fibroblast-like cells. J Gen Virol 87:1961-75.

53. **Wu, H., Kerr MK, Cui X, Churchill GA.** 2002. MAANOVA: a software package for the analysis of spotted cDNA microarray experiments. In: The analysis of gene expression data: methods and software http://research.jax.org/faculty/churchill/.

54. **Yang, G., Y. Xu, X. Chen, and G. Hu.** 2007. IFITM1 plays an essential role in the antiproliferative action of interferon-gamma. Oncogene 26:594-603.

55. **Yang, Y. H., S. Dudoit, P. Luu, D. M. Lin, V. Peng, J. Ngai, and T. P. Speed.** 2002. Normalization for cDNA microarray data: a robust composite method addressing single and multiple slide systematic variation. Nucleic Acids Res 30:e15.

56. **Ye, Y., K. Hauns, J. O. Langland, B. L. Jacobs, and B. G. Hogue.** 2007. Mouse hepatitis coronavirus A59 nucleocapsid protein is a type I interferon antagonist. J Virol 81:2554-63.

57. **Zhou, H., and S. Perlman.** 2007. Mouse hepatitis virus does not induce Beta interferon synthesis and does not inhibit its induction by double-stranded RNA. J Virol 81:568-74.

58. **Zhou, H., and S. Perlman.** 2006. Preferential infection of mature dendritic cells by mouse hepatitis virus strain JHM. J Virol 80:2506-14.

59. **Zimmerer, J. M., G. B. Lesinski, M. D. Radmacher, A. Ruppert, and W. E. Carson, 3rd.** 2007. STAT1-dependent and STAT1-independent gene expression in murine immune cells following stimulation with interferon-alpha. Cancer Immunol Immunother 56:1845-52.

Chapter 9

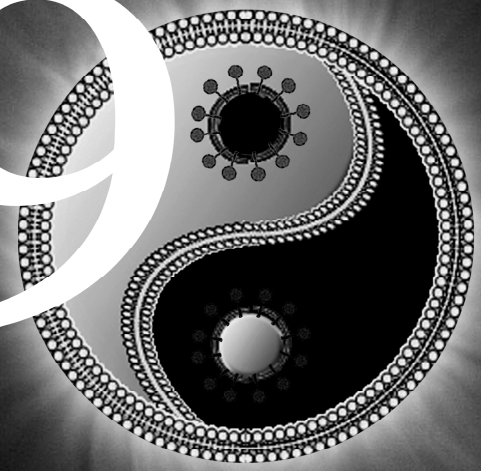

Summarizing Discussion

Summarizing discussion

Viruses are completely dependent on their host for their reproduction. The intimate relationship with its host implies a constant molecular battle between the virus and host defence systems. All through their co-evolution, virus-host interactions have shaped the immune system. Concomitantly, viruses have developed sophisticated mechanisms to evade and to manipulate the host defences and to exploit cellular pathways to facilitate their own propagation. Since numerous conserved cellular pathways are targeted by viral proteins, viral gene functions offer important insights into the molecular mechanisms functioning in cell biology and immunology. In this thesis we portray different aspects of the interactions between coronaviruses (CoVs) and their host. We have applied diverse techniques such as genome-wide microarray analysis and bioluminescence imaging (BLI) to investigate some of these interactions, both in cultured cells and in living animals. In this final chapter I will discuss the implications of our results and our current knowledge about CoV-host interactions.

Coronavirus-Host Interactions at a Cellular Level

Translational Regulation During Virus Infection

The control of mRNA translation, both viral and cellular, is an important aspect of the interplay between virus and host. Since viruses depend completely on the host translational machinery for the expression of their proteome, two potentially contradictory requirements need to be met. On the one hand, the viral mRNAs need to be efficiently translated. On the other, however, the ability of the host cell to synthesize antiviral proteins needs to be restricted in order to provide the virus with a competitive advantage. A variety of mechanisms exists by which viruses ensure the shut-down of cellular translation while maintaining the synthesis of their own gene products.

In chapter 3 we describe the course of host translational inhibition and the associated cellular processes that are activated during MHV infection, including phosphorylation of eukaryotic initiation factor (eIF)2α, induction of cytoplasmic mRNA containing stress granules and processing bodies, and large scale mRNA degradation. The latter was discovered by performing genome-wide microarray analysis of MHV-infected cells in the presence of a transcriptional inhibitor. The induction of eIF2α phosphorylation can be

considered an antiviral defence pathway for cells to cope with the infection, since many viruses, including CoVs, replicate to higher levels in cells that express inactive eIF2α or in cells that are deficient for one of the kinases (i.e. PKR, PERK, GCN2, and HRI) responsible for this phosphorylation event (6, 10, 23, 39, 62, 69). Interestingly, reoviruses appear to be the only viruses observed so far to benefit from the induction of this stress response pathway (73). Since PKR, which is normally triggered by dsRNA, does not seem to be activated during MHV infection, we hypothesized in chapter 3 that PERK could be responsible for eIF2α phosphorylation during MHV infection, since this kinase is activated by ER stress (e.g. the unfolded protein response [UPR]). Indeed, Bechill *et al.* recently showed that MHV infection induces the UPR and PERK activation, with subsequent phosphorylation of eIF2α accompanied by prolonged translational inhibition (8). Nevertheless, CoV protein synthesis is quite robust in the presence of phosphorylated eIF2α.

The mechanism(s) by which CoVs sustain the production of viral proteins under these harsh conditions is still not known. The extensive degradation of mRNAs that we observed during MHV infection is likely to contribute effectively to the competition between host and viral mRNAs for the translational apparatus, but it is expected that other, yet unidentified (viral) factors play a significant role in the translational regulation during CoV infection. For example, signals within the untranslated regions (UTRs) of the viral genome and mRNAs may provide these templates a translational advantage over cellular mRNAs as has been shown for other viruses (15, 16, 29, 87). Although secondary RNA structures within the CoV UTRs have been identified which facilitate transcription (30, 44, 45), we were not yet able to detect translational enhancers when using reporter RNAs containing a luciferase gene flanked by the viral UTRs (unpublished observation).

The Role of the Early Secretory Pathway in the Formation of Viral Replication Complexes

Positive-strand RNA viruses require cellular membranes to anchor their replication complexes (RCs) (68). Replication of CoVs, and also of arteriviruses (i.e. another virus family within the order of the *Nidovirales*), induce the formation of double-membrane vesicles (DMVs) on which the replication takes place (26, 37, 60, 74, 75). The membrane association of the viral RC is likely to be beneficial for the virus, since it may facilitate the

recruitment of components involved in RNA replication and may shield viral RNA replication intermediates (i.e. double-stranded RNA) from recognition by the host cell (81). The induction of similar membrane structures is also seen when cells are infected with picornaviruses, alphaviruses, and flaviviruses (7, 11, 12, 40, 70, 80). Although the membrane origin of most virus-induced replication structures was found to be the endoplasmic reticulum (ER), for some alphaviruses it has been shown that the membranes at the sites of replication are derived from endosomal and lysosomal compartments (21, 46, 56). In contrast, flock house virus appears to replicate on the outer membrane of mitochondria (49).

For CoVs the ER is thought to be the donor of the replication structures (37, 54). Studies trying to unravel the cellular pathways that lead to the induction of the virus replication structures are still ongoing. In chapter 4 we describe that replication of CoVs is sensitive to Brefeldin A (BFA) treatment and that the replication is severely inhibited when cells are depleted for GBF1 and its effector Arf1 (82). These two proteins are involved in the formation of secretory vesicles, which indicates that this pathway is required for CoV replication. Likewise, replication of poliovirus replication is also sensitive to BFA; in this case the replication vesicles are formed at the ER via the COPII budding machinery (32, 48, 67). Intriguingly, however, whereas poliovirus infection results in a redistribution of Arf1 to sites of RNA replication (9), this is not the case during CoV infection (see Chapter 4). Therefore, the mechanism by which the CoV RCs are formed is not completely understood. It is still possible that the secretory pathway simply facilitates CoV replication by delivering lipids to the RCs. Supporting this hypothesis, an inhibitor of phospholipid biosynthesis (i.e. cerulenin) appeared to reduce MHV replication considerably (unpublished observation). RNA replication of poliovirus, vesicular stomatitis virus, and Semliki Forest virus, was also markedly inhibited by cerulenin throughout the infection, suggesting that the synthesis of viral RNA is dependent on the continuous synthesis of lipids (28, 57, 58). The role of lipid metabolism and transport during CoV infection is still an interesting unexplored research area.

The structural resemblance of the CoV-induced DMVs with autophagosomes, membrane-bound structures involved in the turnover of protein aggregates and cytoplasmic organelles

during stress (47, 50), suggests that the autophagy pathway might also play a role in the formation of the RCs. There have been contradicting observations regarding the involvement of autophagy during MHV infection (19, 60, 89) and it is still unclear what the relevance of this pathway is in the formation of the sites of RNA replication. Obviously, further investigations are needed to unravel the exact mechanism(s) by which the secretory and/or autophagy pathway contribute to the biogenesis of functional CoV RCs.

The Role of the Ubiquitin-Proteasome System During Viral Infection

The ubiquitin proteolytic pathway plays a vital function in the proteasomal degradation of short-lived and regulatory proteins important for maintaining cellular homeostasis. The processes involved include controlling the cell cycle and division, cellular stress response pathways, modulation of cell surface receptors, the secretory pathway, biogenesis of organelles, and antigen processing (72). Degradation by the ubiquitin-proteasome pathway involves two major steps: [1] covalent attachment of multiple ubiquitin moieties to the protein substrate, and [2] degradation of the targeted protein by the 20S proteasomal core complex.

In chapter 5 we show that proteasome inhibitors (i.e. MG132, epoxomicin, and Velcade) can block the entry and replication of CoVs from different groups. Previously, Yu and co-workers reported the inhibitory effect of MG132 on the entry of MHV. They found that the virus can enter cells in the absence of a functional proteasome, but stays trapped within an endosomal compartment (88). Similar results were obtained for infection with influenza virus (35). As ubiquitination is not required for entry of MHV (see Chapter 5), we hypothesize that proteasomal degradation is necessary as a late step in the entry phase. Comparable results were recently obtained with Herpes Simplex Virus (20). Here, Delboy and co-workers propose that proteasomal degradation of virion and/or host proteins is required for efficient delivery of incoming HSV capsids to the nucleus. Though further studies are needed, proteasome-mediated degradation of CoV virion proteins during virus cell entry might be essential for establishing an infection. Also, there are examples of substrates that are targeted for proteasomal degradation independently of ubiquitin (24, 31, 33). Sumoylation is one of the ubiquitin-like post-translational modifications which can target specific proteins for degradation (34). Recently it has been shown that the

nucleocapsid protein of SARS-CoV becomes sumoylated (43). It would be of interest to see if this modification is a prerequisite for virion disassembly. Importantly, in our studies, both ubiquitination and proteasomal activity were shown to be required for efficient CoV replication, revealing a potential drug target for antiviral therapy. Supporting this latter idea, the application of a proteasome inhibitor was found to significantly reduce coxsackievirus-induced myocardial damage in mice (22). Furthermore, proteasome inhibitors (including Velcade) are already being used in the clinic for the treatment of certain cancers, including multiple myeloma (14, 25, 41, 53).

Coronavirus-Host Interactions in the Natural Host

A Bioluminescence-Based Mouse Model for Studying MHV Infection

In order to study virus-host interactions in living animals, we have developed a mouse model based on BLI technology. This technique is frequently being used to study the formation and spread of malignancies and to visualize the effect of chemotherapy (52). In addition, BLI allows for the real-time monitoring of spatial and temporal progression of infection in the same animal.

In chapter 7 we made use of luciferase-expressing recombinant MHV viruses in order to follow virus replication and spread in different mouse strains (63). After intranasal infection of BALB/c mice with these viruses, replication could initially (at day 2) be detected in the nasal cavity and the cervical lymph nodes, after which the infection had spread to the brain by day 5. Infection, as determined by quantification of the luciferase signal, was detected until approximately day 12. Occasionally, virus infection of the eyes, liver, and lungs was observed, but in general the infection was mainly restricted to the brain. A drawback of BLI is the current limitation of planar display, as compared to the tomographic or 3D images typically revealed by Positron Emission Tomography (PET) or Magnetic Resonance Imaging (MRI). Since BLI lacks this depth information, we could not pinpoint the exact location of MHV replication within the brains of our mice. However, recent technological advances with rotating mirrors may enable tomographic BLI (38, 59). In addition, ongoing research is trying to combine multiple *in vivo* imaging methods (i.e. multimodality imaging) to provide greater resolution and 3D images. For example, the development of PET combined with Computer Tomography (CT) offers high anatomical resolution with

functional information, resulting in a bimodal image (78, 79). PET imaging relies on probes/tracers known as isotopes that can be administered to animals to create a specific image. Furthermore, the development of Optical PET (OPET) detectors may allow simultaneous capture of PET and bioluminescence images (2, 3, 61). When used for studying virus-host interactions, one of these state-of-the-art techniques may be able to generate a 3D image of the sites of replication within a living animal, thereby providing additional information about the spatial localization of the infection, which might reveal important new insights. BLI also enables multichannel imaging through the use of multiple probes with differing spectral characteristics, which allow the detection of various processes within an individual animal (86). Thus, in principle it is possible to follow virus replication in time and to concurrently visualize a defined molecular process within an infected animal.

Overall, as described in chapter 7, we demonstrated that CoV dissemination in an organism is a multi-factorial process in which the genetic make-up of the virus and the host, the inoculation dose and route, and the status of the immune system play significant roles. With the use of BLI, it has become apparent that, besides the typical, reproducible dissemination features of MHV in mice, clear animal-to-animal variation also occurs. Quite frequently infection was also detected in the tail and paws, body parts not described earlier as sites of MHV replication. Apparently, MHV can spread to and replicate in bone marrow *in vivo*, consistent with earlier *in vitro* studies demonstrating infection of bone marrow-derived macrophages and dendritic cells (65, 91). Strikingly, MHV replication in tail and paws was never observed throughout the entire length of these extremities, but occurred only at distinct sites that differed between animals, suggesting that replication is enabled by local conditions in a specific microenvironment. In this respect, the dissemination of MHV is reminiscent of the bone metastases observed for prostate and breast cancer, as observed by using BLI (71, 90). These metastases are often found in areas with increased marrow cellularity and accelerated bone resorption, underscoring the importance of micro-environmental host factors in determining the non-random pattern of tumor localization in the skeleton. These and other observations support the ‘seed-and-soil’ hypothesis of cancer dissemination, which was already put forward by S. Paget in 1889 (55). It seems quite

possible that a similar 'seed-and-soil' theory might explain, at least in part, the dissemination of MHV infection *in vivo*.

Our BLI-based mouse model provides an ideal tool for the study of CoV-host interactions, which can be used to confirm the antiviral effects of compounds inhibiting MHV infection in tissue culture. These compounds include Velcade (as described in chapter 5) and cyclooxygenase (COX) inhibitors (as briefly described in chapter 6) which were shown to reduce CoV replication significantly in different cell types. Especially the proteasome inhibitor Velcade is an attractive candidate for use *in vivo*, since clinical trials with this drug for the treatment of diverse cancers are already ongoing. However, there have been reports which describe an immunomodulatory effect of Velcade (4, 51, 76), and patients who received Velcade for the treatment of multiple myeloma appeared to be prone to recurrent Varicella Herpes Zoster infection (36, 77). Therefore, the question remains whether proteasome inhibitors present a new class of antivirals. At least for CoVs, the answer seems doubtful in view of very recent observations which showed that MHV-induced pathogenesis in mice was enhanced rather than reduced in the presence of Velcade (unpublished observation).

Interestingly, the recombinant luciferase-expressing viruses replicated to similar levels as wild-type virus in cell culture and in the brains of infected mice after intranasal inoculation, but to considerably lower levels in the liver after intraperitoneal injection. These results indicate that virus replication in the liver might offer a particularly sensitive assay to detect changes in virus fitness *in vivo*. Since our reporter viruses have no mutations in any of the viral proteins, we hypothesize that the introduction of a foreign gene into the genome of MHV has a subtle effect on virus replication, the significance of which can only be detected in the liver of infected mice. Strikingly, the same organ-specific attenuation was recently also seen for recombinant MHV viruses which express a mutant accessory (group-specific) protein (66). Although the authors ascribe this effect to the specific mutation, it might as well have been the result of a minor defect in virus replication. Previously, our lab discovered that all the MHV group-specific gene clusters are dispensable for virus replication *in vitro*, but that the corresponding deletion mutant viruses were attenuated when inoculated into mice (18). We recently performed additional experiments with these

viruses and found that deletion of the group-specific gene clusters (either separately or in combination) did not affect replication in the brain, but severely affected virus replication in the liver (unpublished results). Altogether, further research will be necessary to verify whether the specific mutations are the actual cause of the organ-specific attenuation or that a slight defect in virus replication is the underlying reason for this remarkable phenotype.

Gene Expression Profiling of MHV-Infected Mice

We discovered that 129SvEv mice were significantly more resistant to MHV infection than BALB/c mice after intranasal inoculation. Yet, when type I interferon receptor knock-out ($IFNAR^{-/-}$) mice (in a 129SvEv genetic background) were infected with a luciferase-expressing MHV virus, widespread dissemination of the infection was observed, which is consistent with recent reports (13, 65). The type I IFN response is an essential component of the innate immunity. However, the search for effector genes that are activated by type I IFN signalling is still ongoing. Therefore, as described in chapter 8, we performed genome-wide microarray analysis of different mouse strains infected with MHV, in order to construct type I IFN-independent and -dependent gene expression networks. Interestingly, a comparison of the obtained gene expression data of CoV infection in tissue culture (see chapter 3) and of infection of mice (as described in chapter 8) revealed completely different expression profiles. Previous gene expression studies of CoV infections *in vitro* and *in vivo* showed the same discrepancy (1, 5, 17, 27, 42, 62, 64, 84, 85). While in tissue culture the induction of type I IFN-dependent genes was completely absent, in the brain of infected BALB/c mice we could readily detect the expression of type I IFN-dependent gene expression. These data can be explained by the fact that only certain cell types induce type I IFN in response to MHV infection. It has been reported that CoVs can evade recognition by host cells by shielding its RNA replication intermediates (i.e. dsRNA) from detection by pattern recognition receptors like Toll-like receptors (TLRs), RIG-I, and MDA-5 (83). Only certain cell types like plasmacytoid dendritic cells (pDCs) and macrophages can respond to CoV infection by producing type I IFN (13, 65). *In vivo*, these cells can trigger a typical type I IFN response in adjacent cells, the transcriptional response of which we could measure by gene expression profiling of MHV-infected brain tissue. The induced expression of many known type I IFN-responsive genes was detected, but also some new genes were identified, genes of which the induced expression was not seen in the highly

susceptible IFNAR$^{-/-}$ mice. It would be of interest to construct knock-out mice of each of these genes and to determine the susceptibility of these mice to MHV or other virus infections.

One of the main conclusions from chapter 8 is that the induction of a type I IFN response by MHV in mice strongly correlates with the viral load. This is an important observation, and should be taken into account when performing these types of microarray studies. In addition to the work described in this chapter, we also performed genome-wide microarray analysis of the mRNA expression levels within the brains of BALB/c mice infected with recombinant MHV viruses lacking some or all group-specific genes. The rational behind this approach was to find potential differences in immune responses which can be attributed to these accessory genes. Using this approach we were, however, not able to detect any differences in the transcriptome of animals infected with wild-type MHV-A59 or recombinant virus (unpublished observation). As described above, the replication of these viruses in the brain was comparable to wild-type levels. Therefore, it might be interesting to perform expression profiling of the mRNA content in the liver, where replication of the recombinant viruses was shown to be attenuated. However, a fair comparison of transcriptional profiles in the liver would be extremely difficult since the induction of host gene expression strongly correlates with the virus load. Thus, the question still remains whether the group-specific genes of MHV do possess immunomodulatory properties and, if so, whether these functions are organ-specific.

Final Remarks

Virus-host interactions take place at multiple levels. In this thesis we have described several CoV-host interactions that occur at the cellular, as well as at the level of the organism. Knowledge about the interactions on a molecular/cellular level is of the utmost importance to gain more insight into the fundamental processes of the virus infection cycle, including virus cell entry, replication, and assembly. The introduction of novel high-throughput genomics tools to virus research, like siRNA-library screening, genome-wide yeast-two-hybrid screens, and microarray gene expression profiling, has already resulted in an enormous amount of new information about the role and function of host genes in virus–host interactions. However, the success of these applications critically depends on our ability to correctly integrate the obtained data with functional assays to get a better understanding of the molecular basis of virus–host interactions. As new insights into the virus-host interactions at the molecular level may lead to new therapeutic avenues, the challenge will then be to translate these findings to the level of the organism. Moreover, some research questions can only be investigated properly in living animals, for instance when analyzing the role of the immune system and the accessory genes during CoV infections. In this age of genomics, one might think of performing high-throughput screens using living animals to directly assess the effect of any genetic perturbation *in vivo*. Considering the increasing availability of libraries of knock-out mice, one can think of performing large-scale screenings by using a BLI-based approach as described in this thesis. Altogether, these kinds of studies will support the rational design of novel intervention strategies for viral infections.

References

1. **Aich, P., H. L. Wilson, R. S. Kaushik, A. A. Potter, L. A. Babiuk, and P. Griebel.** 2007. Comparative analysis of innate immune responses following infection of newborn calves with bovine rotavirus and bovine coronavirus. J Gen Virol 88:2749-61.

2. **Alexandrakis, G., F. R. Rannou, and A. F. Chatziioannou.** 2006. Effect of optical property estimation accuracy on tomographic bioluminescence imaging: simulation of a combined optical-PET (OPET) system. Phys Med Biol 51:2045-53.

3. **Alexandrakis, G., F. R. Rannou, and A. F. Chatziioannou.** 2005. Tomographic bioluminescence imaging by use of a combined optical-PET (OPET) system: a computer simulation feasibility study. Phys Med Biol 50:4225-41.

4. **Arpinati, M., G. Chirumbolo, B. Nicolini, C. Agostinelli, and D. Rondelli.** 2009. Selective apoptosis of monocytes and monocyte-derived DCs induced by bortezomib (Velcade). Bone Marrow Transplant 43:253-9.

5. **Baig, E., and E. N. Fish.** 2008. Distinct signature type I interferon responses are determined by the infecting virus and the target cell. Antivir Ther 13:409-22.

6. **Baltzis, D., L. K. Qu, S. Papadopoulou, J. D. Blais, J. C. Bell, N. Sonenberg, and A. E. Koromilas.** 2004. Resistance to vesicular stomatitis virus infection requires a functional cross talk between the eukaryotic translation initiation factor 2alpha kinases PERK and PKR. J Virol 78:12747-61.

7. **Barton, D. J., S. G. Sawicki, and D. L. Sawicki.** 1991. Solubilization and immunoprecipitation of alphavirus replication complexes. J Virol 65:1496-506.

8. **Bechill, J., Z. Chen, J. W. Brewer, and S. C. Baker.** 2008. Coronavirus infection modulates the unfolded protein response and mediates sustained translational repression. J Virol 82:4492-501.

9. **Belov, G. A., M. H. Fogg, and E. Ehrenfeld.** 2005. Poliovirus proteins induce membrane association of GTPase ADP-ribosylation factor. J Virol 79:7207-16.

10. **Berlanga, J. J., I. Ventoso, H. P. Harding, J. Deng, D. Ron, N. Sonenberg, L. Carrasco, and C. de Haro.** 2006. Antiviral effect of the mammalian translation initiation factor 2alpha kinase GCN2 against RNA viruses. Embo J 25:1730-40.

11. **Bienz, K., D. Egger, and T. Pfister.** 1994. Characteristics of the poliovirus replication complex. Arch Virol Suppl 9:147-57.

12. **Bienz, K., D. Egger, T. Pfister, and M. Troxler.** 1992. Structural and functional characterization of the poliovirus replication complex. J Virol 66:2740-7.

13. **Cervantes-Barragan, L., U. Kalinke, R. Zust, M. Konig, B. Reizis, C. Lopez-Macias, V. Thiel, and B. Ludewig.** 2009. Type I IFN-mediated protection of macrophages and dendritic cells secures control of murine coronavirus infection. J Immunol 182:1099-106.

14. **Cheriyath, V., B. S. Jacobs, and M. A. Hussein.** 2007. Proteasome inhibitors in the clinical setting: benefits and strategies to overcome multiple myeloma resistance to proteasome inhibitors. Drugs R D 8:1-12.

15. **Chiu, W. W., R. M. Kinney, and T. W. Dreher.** 2005. Control of translation by the 5'- and 3'-terminal regions of the dengue virus genome. J Virol 79:8303-15.

16. **Chizhikov, V., and J. T. Patton.** 2000. A four-nucleotide translation enhancer in the 3'-terminal consensus sequence of the nonpolyadenylated mRNAs of rotavirus. Rna 6:814-25.

17. **Dar, A., S. Munir, S. Vishwanathan, A. Manuja, P. Griebel, S. Tikoo, H. Townsend, A. Potter, V. Kapur, and L. A. Babiuk.** 2005. Transcriptional analysis of avian embryonic tissues following infection with avian infectious bronchitis virus. Virus Res 110:41-55.

18. **de Haan, C. A., P. S. Masters, X. Shen, S. Weiss, and P. J. Rottier.** 2002. The group-specific murine coronavirus genes are not essential, but their deletion, by reverse genetics, is attenuating in the natural host. Virology 296:177-89.

19. **de Haan, C. A., and F. Reggiori.** 2008. Are nidoviruses hijacking the autophagy machinery? Autophagy 4:276-9.

20. **Delboy, M. G., D. G. Roller, and A. V. Nicola.** 2008. Cellular proteasome activity facilitates herpes simplex virus entry at a postpenetration step. J Virol 82:3381-90.

21. **Froshauer, S., J. Kartenbeck, and A. Helenius.** 1988. Alphavirus RNA replicase is located on the cytoplasmic surface of endosomes and lysosomes. J Cell Biol 107:2075-86.

22. **Gao, G., J. Zhang, X. Si, J. Wong, C. Cheung, B. McManus, and H. Luo.** 2008. Proteasome inhibition attenuates coxsackievirus-induced myocardial damage in mice. Am J Physiol Heart Circ Physiol 295:H401-8.

23. **Garcia, M. A., E. F. Meurs, and M. Esteban.** 2007. The dsRNA protein kinase PKR: virus and cell control. Biochimie 89:799-811.

24. **Glass, J. R., and E. W. Gerner.** 1987. Spermidine mediates degradation of ornithine decarboxylase by a non-lysosomal, ubiquitin-independent mechanism. J Cell Physiol 130:133-41.

25. **Goranov, S. E., and V. S. Goranova-Marinova.** 2005. Bortezomib (Velcade)--a new therapeutic strategy for patients with refractory multiple myeloma. Folia Med (Plovdiv) 47:11-9.

26. **Gosert, R., A. Kanjanahaluethai, D. Egger, K. Bienz, and S. C. Baker.** 2002. RNA replication of mouse hepatitis virus takes place at double-membrane vesicles. J Virol 76:3697-708.

27. **Gruslin, E., S. Moisan, Y. St-Pierre, M. Desforges, and P. J. Talbot.** 2005. Transcriptome profile within the mouse central nervous system and activation of myelin-reactive T cells following murine coronavirus infection. J Neuroimmunol 162:60-70.

28. **Guinea, R., and L. Carrasco.** 1990. Phospholipid biosynthesis and poliovirus genome replication, two coupled phenomena. Embo J 9:2011-6.

29. **Holden, K. L., and E. Harris.** 2004. Enhancement of dengue virus translation: role of the 3' untranslated region and the terminal 3' stem-loop domain. Virology 329:119-33.

30. **Hsue, B., and P. S. Masters.** 1997. A bulged stem-loop structure in the 3' untranslated region of the genome of the coronavirus mouse hepatitis virus is essential for replication. J Virol 71:7567-78.

31. **Hwang, J., and R. F. Kalejta.** 2007. Proteasome-dependent, ubiquitin-independent degradation of Daxx by the viral pp71 protein in human cytomegalovirus-infected cells. Virology 367:334-8.

32. **Irurzun, A., L. Perez, and L. Carrasco.** 1992. Involvement of membrane traffic in the replication of poliovirus genomes: effects of brefeldin A. Virology 191:166-75.

33. **Kalejta, R. F., and T. Shenk.** 2003. Proteasome-dependent, ubiquitin-independent degradation of the Rb family of tumor suppressors by the human cytomegalovirus pp71 protein. Proc Natl Acad Sci U S A 100:3263-8.

34. **Kerscher, O., R. Felberbaum, and M. Hochstrasser.** 2006. Modification of proteins by ubiquitin and ubiquitin-like proteins. Annu Rev Cell Dev Biol 22:159-80.

35. **Khor, R., L. J. McElroy, and G. R. Whittaker.** 2003. The ubiquitin-vacuolar protein sorting system is selectively required during entry of influenza virus into host cells. Traffic 4:857-68.

36. **Kim, S. J., K. Kim, B. S. Kim, H. J. Lee, H. Kim, N. R. Lee, S. H. Nam, J. H. Kwon, H. J. Kim, S. K. Sohn, J. H. Won, J. H. Lee, C. Suh, S. S. Yoon, H. J. Kim, I. Kim, Y. R. Do, W. S. Lee, Y. D. Joo, and H. J. Shin.** 2008. Bortezomib and the increased incidence of herpes zoster in patients with multiple myeloma. Clin Lymphoma Myeloma 8:237-40.

37. **Knoops, K., M. Kikkert, S. H. Worm, J. C. Zevenhoven-Dobbe, Y. van der Meer, A. J. Koster, A. M. Mommaas, and E. J. Snijder.** 2008. SARS-coronavirus replication is supported by a reticulovesicular network of modified endoplasmic reticulum. PLoS Biol 6:e226.

38. **Koo, V., P. W. Hamilton, and K. Williamson.** 2006. Non-invasive *in vivo* imaging in small animal research. Cell Oncol 28:127-39.

39. **Krishnamoorthy, J., Z. Mounir, J. F. Raven, and A. E. Koromilas.** 2008. The eIF2alpha kinases inhibit vesicular stomatitis virus replication independently of eIF2alpha phosphorylation. Cell Cycle 7:2346-51.

40. **Kujala, P., A. Ikaheimonen, N. Ehsani, H. Vihinen, P. Auvinen, and L. Kaariainen.** 2001. Biogenesis of the Semliki Forest virus RNA replication complex. J Virol 75:3873-84.

41. **Kyle, R. A., and S. Vincent Rajkumar.** 2006. Treatment of multiple myeloma: an emphasis on new developments. Ann Med 38:111-5.

42. **Leong, W. F., H. C. Tan, E. E. Ooi, D. R. Koh, and V. T. Chow.** 2005. Microarray and real-time RT-PCR analyses of differential human gene expression patterns induced by severe acute respiratory syndrome (SARS) coronavirus infection of Vero cells. Microbes Infect 7:248-59.

43. **Li, F. Q., H. Xiao, J. P. Tam, and D. X. Liu.** 2005. Sumoylation of the nucleocapsid protein of severe acute respiratory syndrome coronavirus. FEBS Lett 579:2387-96.

44. **Lin, Y. J., X. Zhang, R. C. Wu, and M. M. Lai.** 1996. The 3' untranslated region of coronavirus RNA is required for subgenomic mRNA transcription from a defective interfering RNA. J Virol 70:7236-40.

45. **Liu, P., L. Li, J. J. Millership, H. Kang, J. L. Leibowitz, and D. P. Giedroc.** 2007. A U-turn motif-containing stem-loop in the coronavirus 5' untranslated region plays a functional role in replication. Rna 13:763-80.

46. **Magliano, D., J. A. Marshall, D. S. Bowden, N. Vardaxis, J. Meanger, and J. Y. Lee.** 1998. Rubella virus replication complexes are virus-modified lysosomes. Virology 240:57-63.

47. **Mari, M., and F. Reggiori.** 2007. Shaping membranes into autophagosomes. Nat Cell Biol 9:1125-7.

48. **Maynell, L. A., K. Kirkegaard, and M. W. Klymkowsky.** 1992. Inhibition of poliovirus RNA synthesis by brefeldin A. J Virol 66:1985-94.

49. **Miller, D. J., M. D. Schwartz, and P. Ahlquist.** 2001. Flock house virus RNA replicates on outer mitochondrial membranes in Drosophila cells. J Virol 75:11664-76.

50. **Mizushima, N.** 2007. Autophagy: process and function. Genes Dev 21:2861-73.

51. **Nencioni, A., K. Schwarzenberg, K. M. Brauer, S. M. Schmidt, A. Ballestrero, F. Grunebach, and P. Brossart.** 2006. Proteasome inhibitor bortezomib modulates TLR4-induced dendritic cell activation. Blood 108:551-8.

52. **Nogawa, M., T. Yuasa, S. Kimura, J. Kuroda, K. Sato, H. Segawa, A. Yokota, and T. Maekawa.** 2005. Monitoring luciferase-labeled cancer cell growth and metastasis in different *in vivo* models. Cancer Lett 217:243-53.

53. **Onitilo, A. A., J. Engel, B. Olatosi, and S. Fagbemi.** 2007. Community experience with bortezomib in patients with multiple myeloma. Am J Hematol 82:637-9.

54. **Oostra, M., E. G. te Lintelo, M. Deijs, M. H. Verheije, P. J. Rottier, and C. A. de Haan.** 2007. Localization and membrane topology of coronavirus non-structural protein 4: involvement of the early secretory pathway in replication. J Virol 81:12323-36.

55. **Paget, S.** 1989. The distribution of secondary growths in cancer of the breast. 1889. Cancer Metastasis Rev 8:98-101.

56. **Peranen, J., P. Laakkonen, M. Hyvonen, and L. Kaariainen.** 1995. The alphavirus replicase protein nsP1 is membrane-associated and has affinity to endocytic organelles. Virology 208:610-20.

57. **Perez, L., and L. Carrasco.** 1991. Cerulenin, an inhibitor of lipid synthesis, blocks vesicular stomatitis virus RNA replication. FEBS Lett 280:129-33.

58. **Perez, L., R. Guinea, and L. Carrasco.** 1991. Synthesis of Semliki Forest virus RNA requires continuous lipid synthesis. Virology 183:74-82.

59. **Piwnica-Worms, D., D. P. Schuster, and J. R. Garbow.** 2004. Molecular imaging of host-pathogen interactions in intact small animals. Cell Microbiol 6:319-31.

60. **Prentice, E., W. G. Jerome, T. Yoshimori, N. Mizushima, and M. R. Denison.** 2004. Coronavirus replication complex formation utilizes components of cellular autophagy. J Biol Chem 279:10136-41.

61. **Prout, D. L., R. W. Silverman, and A. Chatziioannou.** 2004. Detector Concept for OPET-A Combined PET and Optical Imaging System. IEEE Trans Nucl Sci 51:752-756.

62. **Raaben, M., M. J. Groot Koerkamp, P. J. Rottier, and C. A. de Haan.** 2007. Mouse hepatitis coronavirus replication induces host translational shutoff and mRNA decay, with concomitant formation of stress granules and processing bodies. Cell Microbiol 9:2218-29.

63. **Raaben, M., H. J. Prins, A. C. Martens, P. J. Rottier, and C. A. de Haan.** 2009. Non-invasive imaging of mouse hepatitis coronavirus infection reveals determinants of viral replication and spread *in vivo*. Cell Microbiol.

64. **Reghunathan, R., M. Jayapal, L. Y. Hsu, H. H. Chng, D. Tai, B. P. Leung, and A. J. Melendez.** 2005. Expression profile of immune response genes in patients with Severe Acute Respiratory Syndrome. BMC Immunol 6:2.

65. **Roth-Cross, J. K., S. J. Bender, and S. R. Weiss.** 2008. Murine coronavirus mouse hepatitis virus is recognized by MDA5 and induces type I interferon in brain macrophages/microglia. J Virol 82:9829-38.

66. **Roth-Cross, J. K., H. Stokes, G. Chang, M. M. Chua, V. Thiel, S. R. Weiss, A. E. Gorbalenya, and S. G. Siddell.** 2009. Organ-Specific Attenuation of Murine Hepatitis Virus (MHV-A59) by Replacement of Catalytic Residues in the Putative Viral Cyclic Phosphodiesterase NS2. J Virol.

67. **Rust, R. C., L. Landmann, R. Gosert, B. L. Tang, W. Hong, H. P. Hauri, D. Egger, and K. Bienz.** 2001. Cellular COPII proteins are involved in production of the vesicles that form the poliovirus replication complex. J Virol 75:9808-18.

68. **Salonen, A., T. Ahola, and L. Kaariainen.** 2005. Viral RNA replication in association with cellular membranes. Curr Top Microbiol Immunol 285:139-73.

69. **Samuel, M. A., K. Whitby, B. C. Keller, A. Marri, W. Barchet, B. R. Williams, R. H. Silverman, M. Gale, Jr., and M. S. Diamond.** 2006. PKR and RNase L contribute to protection against lethal West Nile Virus infection by controlling early viral spread in the periphery and replication in neurons. J Virol 80:7009-19.

70. **Schlegel, A., T. H. Giddings, Jr., M. S. Ladinsky, and K. Kirkegaard.** 1996. Cellular origin and ultrastructure of membranes induced during poliovirus infection. J Virol 70:6576-88.

71. **Schneider, A., L. M. Kalikin, A. C. Mattos, E. T. Keller, M. J. Allen, K. J. Pienta, and L. K. McCauley.** 2005. Bone turnover mediates preferential localization of prostate cancer in the skeleton. Endocrinology 146:1727-36.

72. **Schwartz, A. L., and A. Ciechanover.** 1999. The ubiquitin-proteasome pathway and pathogenesis of human diseases. Annu Rev Med 50:57-74.

73. **Smith, J. A., S. C. Schmechel, A. Raghavan, M. Abelson, C. Reilly, M. G. Katze, R. J. Kaufman, P. R. Bohjanen, and L. A. Schiff.** 2006. Reovirus induces and benefits from an integrated cellular stress response. J Virol 80:2019-33.

74. **Snijder, E. J., Y. van der Meer, J. Zevenhoven-Dobbe, J. J. Onderwater, J. van der Meulen, H. K. Koerten, and A. M. Mommaas.** 2006. Ultrastructure and origin of membrane vesicles associated with the severe acute respiratory syndrome coronavirus replication complex. J Virol 80:5927-40.

75. **Stertz, S., M. Reichelt, M. Spiegel, T. Kuri, L. Martinez-Sobrido, A. Garcia-Sastre, F. Weber, and G. Kochs.** 2007. The intracellular sites of early replication and budding of SARS-coronavirus. Virology 361:304-15.

76. **Straube, C., R. Wehner, M. Wendisch, M. Bornhauser, M. Bachmann, E. P. Rieber, and M. Schmitz.** 2007. Bortezomib significantly impairs the immunostimulatory capacity of human myeloid blood dendritic cells. Leukemia 21:1464-71.

77. **Tong, Y., J. Qian, Y. Li, H. Meng, and J. Jin.** 2007. The high incidence of varicella herpes zoster with the use of bortezomib in 10 patients. Am J Hematol 82:403-4.

78. **Townsend, D. W.** 2001. A combined PET/CT scanner: the choices. J Nucl Med 42:533-4.

79. **Townsend, D. W., J. P. Carney, J. T. Yap, and N. C. Hall.** 2004. PET/CT today and tomorrow. J Nucl Med 45 Suppl 1:4S-14S.

80. **Uchil, P. D., and V. Satchidanandam.** 2003. Architecture of the flaviviral replication complex. Protease, nuclease, and detergents reveal encasement within double-layered membrane compartments. J Biol Chem 278:24388-98.

81. **van Hemert, M. J., S. H. van den Worm, K. Knoops, A. M. Mommaas, A. E. Gorbalenya, and E. J. Snijder.** 2008. SARS-coronavirus replication/transcription complexes are membrane-protected and need a host factor for activity *in vitro*. PLoS Pathog 4:e1000054.

82. **Verheije, M. H., M. Raaben, M. Mari, E. G. Te Lintelo, F. Reggiori, F. J. van Kuppeveld, P. J. Rottier, and C. A. de Haan.** 2008. Mouse hepatitis coronavirus RNA replication depends on GBF1-mediated ARF1 activation. PLoS Pathog 4:e1000088.

83. **Versteeg, G. A., P. J. Bredenbeek, S. H. van den Worm, and W. J. Spaan.** 2007. Group 2 coronaviruses prevent immediate early interferon induction by protection of viral RNA from host cell recognition. Virology 361:18-26.

84. **Versteeg, G. A., O. Slobodskaya, and W. J. Spaan.** 2006. Transcriptional profiling of acute cytopathic murine hepatitis virus infection in fibroblast-like cells. J Gen Virol 87:1961-75.

85. **Wang, X., A. J. Rosa, H. N. Oliverira, G. J. Rosa, X. Guo, M. Travnicek, and T. Girshick.** 2006. Transcriptome of local innate and adaptive immunity during early phase of infectious bronchitis viral infection. Viral Immunol 19:768-74.

86. **Weissleder, R.** 1999. Molecular imaging: exploring the next frontier. Radiology 212:609-14.

87. **Yang, A. D., M. Barro, M. I. Gorziglia, and J. T. Patton.** 2004. Translation enhancer in the 3'-untranslated region of rotavirus gene 6 mRNA promotes expression of the major capsid protein VP6. Arch Virol 149:303-21.

88. **Yu, G. Y., and M. M. Lai.** 2005. The ubiquitin-proteasome system facilitates the transfer of murine coronavirus from endosome to cytoplasm during virus entry. J Virol 79:644-8.

89. **Zhao, Z., L. B. Thackray, B. C. Miller, T. M. Lynn, M. M. Becker, E. Ward, N. N. Mizushima, M. R. Denison, and H. W. t. Virgin.** 2007. Coronavirus replication does not require the autophagy gene ATG5. Autophagy 3:581-5.

90. **Zheng, Y., H. Zhou, J. R. Modzelewski, R. Kalak, J. M. Blair, M. J. Seibel, and C. R. Dunstan.** 2007. Accelerated bone resorption, due to dietary calcium deficiency, promotes breast cancer tumor growth in bone. Cancer Res 67:9542-8.

91. **Zhou, H., and S. Perlman.** 2006. Preferential infection of mature dendritic cells by mouse hepatitis virus strain JHM. J Virol 80:2506-14.

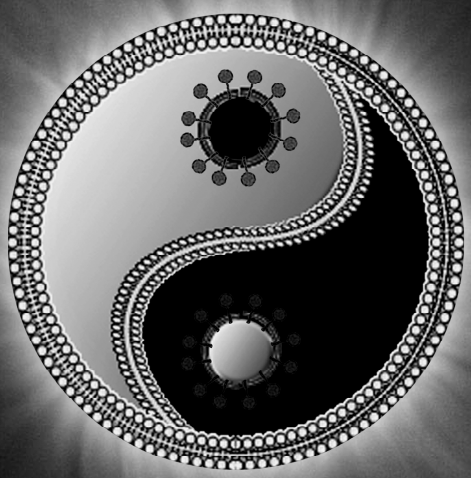

Nederlandse Samenvatting

Nederlandse Samenvatting

Virussen bestaan uit een hoeveelheid erfelijk materiaal (RNA of DNA), dat wordt omhuld door een mantel van eiwitten. Sommige virussen bevatten bovendien nog een membraanomhulsel (ook wel envelop genoemd), die ze verkrijgen van hun gastheercel. In tegenstelling tot de meeste bacteriën en parasieten zijn virussen compleet afhankelijk van een gastheer voor de vermenigvuldiging van hun genoom en voor de vorming van nieuwe virusdeeltjes. Door deze ziekteverwekkers te bestuderen kunnen we dus niet alleen veel te weten komen over de virussen zelf, maar ook over de biologische processen die zich afspelen in de gastheercel.

Er is in de natuur een enorme verscheidenheid aan virussen. Het in dit proefschrift beschreven onderzoek heeft zich specifiek gericht op de zogenaamde coronavirussen. Deze RNA virussen zijn al jaren bekend als de veroorzakers van luchtweg- en darminfecties bij diverse diersoorten, zoals kippen, katten, varkens, en ook muizen. Echter, tijdens de SARS uitbraak in 2003 hebben deze virussen meer bekendheid gekregen toen duidelijk werd dat een coronavirus (het SARS-coronavirus) de veroorzaker was van deze infectieziekte die uiteindelijk ruim 800 slachtoffers heeft geëist. Om eventuele nieuwe uitbraken van SARS dan wel van andere coronavirussen in de toekomst beter te kunnen bestrijden is meer kennis over deze groep van virussen noodzakelijk. In dit proefschrift is vooral gekeken naar de interacties die plaatsvinden tussen coronavirussen en hun gastheer, zowel op cellulair niveau als op het niveau van het complete organisme. Het muizen hepatitis coronavirus (MHV) is gebruikt als model systeem. Het voordeel van dit virus is dat de biologie ervan goed bekend is en dat de natuurlijke gastheer (de muis) een geschikt en geaccepteerd proefdier is.

MHV heeft een RNA genoom dat de genetische code bevat voor de productie van verschillende soorten virale eiwitten. Het nucleocapside (N) eiwit bindt aan het RNA genoom en vormt de kern van het virusdeeltje (het nucleocapside). Deze kern wordt omringd door een envelop, waarin 3 eiwitten verankerd zitten: het membraan (M) eiwit, het envelop (E) eiwit en het spike (S) eiwit. Deze 4 eiwitten (N, M, E, en S) worden ook wel de structurele eiwitten genoemd, aangezien ze de bouwstenen van het virus vormen. M en E zijn belangrijk voor de vorming van de envelop, terwijl het S eiwit belangrijk is voor de

penetratie van het virus in de doelcel door te zorgen voor de binding van het virusdeeltje aan de gastheercel en voor de fusie van de virale envelop met een cellulair membraan.

Door de fusie van de virale envelop met een membraan van de gastheercel belandt het virale RNA genoom in de cel, waar de niet-structurele eiwitten (nsp's) worden afgelezen (ook wel translatie genoemd). Eerst worden er 2 grote voorloper-eiwitten gemaakt die daarna op specifieke plaatsen worden geknipt, wat uiteindelijk 16 mature nsp's oplevert. Deze nsp's vormen samen een groot eiwitcomplex dat betrokken is bij de replicatie (vermenigvuldiging) van het virale RNA genoom. Voor de productie van de structurele eiwitten moeten eerst kortere RNA kopieën van het virale genoom worden gemaakt, een proces dat transcriptie wordt genoemd. Ook hiervoor zijn de nsp's verantwoordelijk. Naast de RNAs die coderen voor de structurele eiwitten worden er ook nog RNAs gemaakt die coderen voor eiwitten die niet essentieel zijn in de levenscyclus van het virus, de zogenaamde accessoire eiwitten. De functies van deze eiwitten zijn niet goed bekend, maar er zijn goede aanwijzingen dat sommige een rol spelen bij het onderdrukken van het afweersysteem van de gastheer.

Voor replicatie van het virale genoom, transcriptie van de kortere RNAs, translatie van virale RNAs in virale eiwitten, en de productie van nieuwe virusdeeltjes (ook wel assemblage genoemd), is MHV volledig afhankelijk van de machinerie van de gastheercel. In hoofdstuk 3 t/m 6 wordt de betrokkenheid van enkele cellulaire processen tijdens de levenscyclus van MHV nader onder de loep genomen. Een bekend verschijnsel gedurende een infectie met MHV is bijvoorbeeld dat de productie van eiwitten van de gastheercel volledig wordt geremd. In hoofdstuk 3 hebben we onderzocht welke cellulaire processen tijdens een MHV infectie met dit fenomeen te maken hebben. Met behulp van microarrays (microchips waarop we de complete transcriptie [van genomisch DNA naar RNA dat codeert voor eiwitten] van een gastheercel kunnen meten: zie hoofdstuk 2) hebben we bestudeerd welke RNAs in een MHV-geïnfecteerde cel meer of minder gemaakt worden op verschillende tijden na infectie. Hieruit kwam naar voren dat er in de gastheercel tijdens een infectie een stress respons wordt geïnitieerd die leidt tot de afbraak van cellulair RNA. Hierdoor krijgt het virus de translatie-machinerie van de gastheercel gaandeweg steeds meer voor zichzelf ter beschikking, wat zou kunnen verklaren waarom er later in de infectie

vooral virale eiwitten worden gemaakt en amper nog eiwitten van de gastheer. De stress respons bleek nochtans niet voordelig voor het virus, aangezien MHV beter vermenigvuldigde in cellen die deze stress respons niet kunnen aanzetten.

De replicatie/transcriptie van coronavirussen vindt plaats op speciale structuren in de gastheercel, die door het virus worden aangemaakt. Hoe deze structuren (die bestaan uit een dubbel membraan afkomstig van een bestaand cellulair compartiment) precies tot stand komen is tot nu toe niet goed bekend. Aangenomen wordt dat de virale eiwitten nsp3, nsp4, en nsp6 belangrijk zijn voor de formatie van deze structuren, omdat deze eiwitten meerdere domeinen bezitten waarmee ze zich in een membraan van de gastheercel kunnen nestelen. Het dubbele membraan waaruit deze replicatiestructuren zijn opgebouwd, is waarschijnlijk afkomstig vanuit het endoplasmatisch reticulum (ER), het compartiment van de cel waar de productie van de virale membraan-gebonden eiwitten plaatsvindt. Deze eiwitten kunnen vervolgens via een transportroute naar andere locaties in de cel worden vervoerd. In hoofdstuk 4 hebben we in verschillende experimenten laten zien dat deze specifieke transportroute erg belangrijk is voor coronavirus infectie, aangezien remming van deze route de replicatie van MHV kan stoppen.

Het eiwitmetabolisme in een cel is een belangrijk proces dat goed gereguleerd moet worden. De aanmaak en afbraak van eiwitten moeten dus goed in balans zijn. Het proteasoom is het belangrijkste complex in de cel dat de afbraak van eiwitten voor zijn rekening neemt. Eiwitten in de cel die bestemd zijn voor afbraak worden voorzien van een modificatie; er wordt een klein eiwit, ubiquitine genaamd, aan gekoppeld door een cellulair enzym. Deze modificatie wordt herkend door het proteasoom waarna het gehele eiwit kan worden afgebroken tot losse componenten die vervolgens weer kunnen worden gebruikt voor de productie van nieuwe eiwitten. Uit onderzoek is gebleken dat het proteasoom ook belangrijk is in de levenscyclus van verschillende virussen. In hoofdstuk 5 laten we zien dat de activiteit van het proteasoom belangrijk is voor zowel het binnendringen van MHV in een cel als voor de replicatie van het virus, maar niet voor virusassemblage; vorming van nieuw virus bleek niet geremd te worden wanneer de activiteit van het proteasoom met verschillende remmers werd geblokkeerd. Verder hebben we aan kunnen tonen dat, wanneer de koppeling van ubiquitine aan eiwitten wordt voorkomen, dit een remmend

effect heeft op de replicatie van MHV. Het zou interessant zijn om te kijken of remmers van het proteasoom ook coronavirus infecties kunnen bestrijden in levende dieren, bijvoorbeeld in muizen in het geval van MHV. Aangezien remmers van het proteasoom al gebruikt worden in de kliniek voor het bestrijden van bepaalde tumoren, moet het mogelijk zijn om dit nader te bestuderen.

Cellulaire cyclooxygenase (COX) enzymen zijn belangrijk voor de productie van prostaglandine, een eiwit dat ontstekingsreacties kan reguleren. Voor verschillende soorten virussen is beschreven dat remming van deze COXs een negatief effect kan hebben op virus replicatie. In hoofdstuk 6 wordt kort beschreven dat de activiteit van COXs belangrijk is voor een efficiënte replicatie van MHV, vooral vroeg in de infectiecyclus. Dit hebben we kunnen aantonen door gebruik te maken van COX remmers, maar ook door middel van RNA interferentie (RNAi) technologie (RNAi wordt toegepast om RNA dat in een cel codeert voor een bepaald eiwit te laten afbreken, waardoor uiteindelijk dat eiwit niet meer gemaakt kan worden). Uit onze proeven is gebleken dat MHV niet meer goed repliceert in cellen die geen COXs meer kunnen produceren. Het mechanisme hierachter hebben we nog niet kunnen achterhalen.

Sommige processen die tijdens virus infecties optreden kunnen alleen bestudeerd worden in een levend organisme, aangezien virussen daar te maken krijgen met het afweersysteem van de gastheer. In hoofdstuk 7 wordt de ontwikkeling van een nieuw muizenmodel beschreven, waarin we replicatie van MHV kunnen volgen in levende dieren. We hebben gebruik gemaakt van genetisch gemodificeerde (recombinant) virussen die een eiwit (het luciferase enzym van een vuurvliegje) maken dat licht (fotonen) uitzendt op het moment dat het toegediende substraat wordt omgezet. Muizen die geïnjecteerd worden met het substraat gaan dus licht uitzenden (bioluminescentie) op die plaatsen waar virus replicatie plaatsvindt. Dit licht kan worden gedetecteerd met een zeer gevoelige camera. Het voordeel van deze methode is dat je dezelfde muis in de tijd kunt volgen, aangezien je meerdere keren kunt meten. Een intrigerende waarneming was dat de recombinant virussen even goed vermenigvuldigden als wildtype virus in de hersenen van geïnfecteerde muizen, maar dat infectie van de lever veel minder ernstig was dan die van het wildtype virus. Blijkbaar zijn de recombinante virussen toch iets verzwakt ten opzichte van het wildtype virus. Toen

we echter genetisch gemodificeerde muizen met een verminderde aangeboren afweer gebruikten (in dit geval muizen die de type I interferon (IFN) receptor niet produceren [IFN receptor knock-out]), dan werd duidelijk dat de recombinant virussen wel in staat waren om deze muizen te doden. In deze muizen was ook te zien dat veel meer organen in de muis geïnfecteerd werden, aangezien er op meerder plaatsen fotonen te detecteren waren. Verder hebben we met deze bioluminescentiemethode verschillen in de gevoeligheid van bepaalde muizenstammen voor infectie kunnen aantonen en het belang van variabelen als virus dosering en besmettingsroute voor het orgaantropisme van MHV kunnen vaststellen. Met deze techniek is het nu ook mogelijk om o.a. snel verschillende (nieuwe) antivirale middelen te testen en de werking van deze middelen te volgen in individuele muizen.

De aangeboren afweer is een belangrijke component van het immuunsysteem voor de bescherming tegen allerlei virusinfecties. Vooral de zogenaamde IFN respons speelt een cruciale rol. Onderzoek heeft uitgewezen dat ook voor coronavirussen deze respons enorm belangrijk is voor het onder controle houden van de infectie. De IFN respons wordt door een geïnfecteerde cel geïnduceerd op het moment dat specifieke virale structuren worden herkend. Een cel (in het bijzonder sommige cellen van het immuunsysteem zoals macrofagen en dendritische cellen) maakt verschillende soorten eiwitten die deze ‘lichaamsvreemde’ structuren kunnen detecteren. Bij herkenning van dergelijke structuren door de cel vindt er productie en uitscheiding van IFN plaats. IFN kan dan binden aan de IFN receptor van dezelfde cel dan wel van naburige cellen en daarin een transcriptieprogramma opstarten dat de replicatie van het virus probeert tegen te gaan. In celkweek is MHV echter nauwelijks in staat om een IFN respons te induceren, wat waarschijnlijk te maken heeft met het feit dat de virale structuren niet goed herkend worden in de meeste celtypen doordat ze worden afgeschermd door de replicatiestructuren (zie hoofdstuk 4). In muizen is daarentegen wel een sterke inductie van IFN waar te nemen. Het transcriptieprogramma dat in gang wordt gezet in de hersenen van MHV-geïnfecteerde muizen is nader bestudeerd in hoofdstuk 8. Ook hierbij hebben we gebruik gemaakt van microarray technologie (zie hoofdstuk 2 en 3) om het complete transcriptieprogramma te kunnen analyseren. Door gebruik te maken van verschillende muizenstammen (wildtype versus IFN receptor knock-out muizen) zijn we meer te weten gekomen over de transcriptie van IFN-afhankelijke dan wel -onafhankelijke genen tijdens MHV infectie.

Het onderzoek zoals beschreven in dit proefschrift heeft interessante bijdragen geleverd aan onze kennis op gebied van coronavirus-gastheer interacties, zowel op het niveau van de cel als op het niveau van het organisme. Deze nieuwe inzichten bieden goede aanknopingspunten voor verdere fundamentele studies aan deze virussen en voor de ontwikkeling van antivirale middelen tegen deze potentieel ernstige ziekteverwekkers.

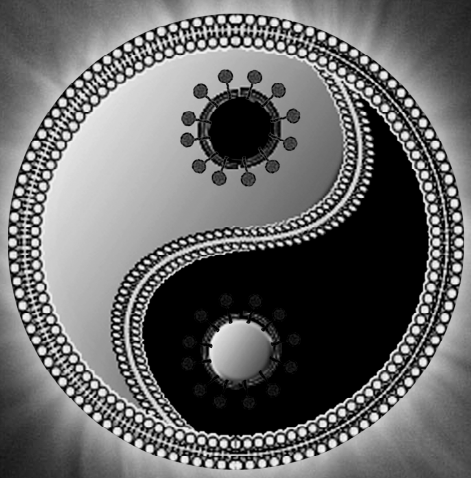

Dankwoord

Dankwoord

Dit proefschrift is tot stand gekomen door de inzet en steun van velen. Allereerst wil ik mijn promotor en co-promotor bedanken. Peter en Xander, ondanks het feit dat ik een maandje extra vakantie heb moeten opofferen, was ik erg vereerd met jullie aanbod om als AIO aan de slag te gaan op een nieuw project. Jullie enthousiasme gedurende mijn AIO-periode werkte aanstekelijk en vooral motiverend. Ook wil ik alle (ex)collega's van de afdeling virologie hartelijk bedanken voor alle hulp en vooral gezelligheid tijdens mijn AIO-jaren op het lab. Ik denk dat er maar weinig labs zijn waar een dergelijk goede sfeer heerst als op de 5de verdieping van het Androclus gebouw. In het bijzonder wil ik Tom en Hélène bedanken, mede door jullie ben ik gefascineerd geraakt door de virologie. Ik zal die vrijdagmiddag in december toen ons targeting-experimentje eindelijk gelukt was niet snel vergeten! Hélène, ook naast het werk zien we elkaar vrij regelmatig op de racefiets. Ik vind het erg leuk dat ik de afgelopen jaren een soort van "persoonlijke trainer" van je heb mogen zijn. Je vooruitgang is indrukwekkend te noemen! Ik sla mezelf dan ook graag op de borst. Uiteraard wil ik ook mijn (ex)collega-AIO's; Monique, Mijke, Marne, Martijn, Matthijn en Robbert ontzettend bedanken voor hun hulp/steun. De etentjes vond ik altijd erg gezellig. Monique, wij hebben elkaar pas echt leren kennen toen we bij elkaar op de kamer zijn beland. Ik heb veel van je kunnen leren en ik vond het dan ook jammer toen je vertelde dat je de afdeling ging verlaten. Gelukkig zien we elkaar nog af en toe. M3, M4, M5, M6, en Robbert: Veel succes met het afronden van jullie promotie-traject. Ik heb er vertrouwen in! Ik heb ook een aantal studenten mogen begeleiden. Rob, Kazimier en Renske, jullie hebben ook in meer of mindere mate meegeholpen aan de totstandkoming van dit proefschrift. Bedankt daarvoor en veel succes met jullie verdere wetenschappelijke carrière! Bert-Jan, Berend-Jan en Tom, wanneer gaan we weer eens biljarten en Turkse pizza eten? Als alternatief kunnen we natuurlijk ook naar Parijs gaan en daar de Tour de France bekijken.

Zonder "collaborations" kom je in de wetenschap niet ver. Daarom wil ik graag de groep van Frank Holstege, en in het bijzonder Marian Groot Koerkamp, ontzettend bedanken voor al hun hulp tijdens mijn microarray experimenten. Uiteindelijk heeft deze samenwerking toch maar mooi bijgedragen aan 3 hoofdstukken van mijn proefschrift! Ook wil ik het lab van Eric Snijder in het LUMC, en in het bijzonder Clara Posthuma, bedanken voor al hun

hulp en advies. Ik denk dat de proeven die jullie hebben gedaan (en nog steeds doen) erg belangrijk zijn en zeker een meerwaarde geven aan hoofdstuk 5 van dit proefschrift.

Uiteraard wil ik al mijn vrienden buiten het lab bedanken voor hun steun de afgelopen jaren. Een aantal van jullie moet zelf nog promoveren en ik vind het stiekem wel mooi dat ik de eerste van de club ben die zich in een apen-pakkie mag steken. Jan-Willem, super dat je mijn paranimf wilt zijn! Als dank zal ik zelf ook maar secondant komen spelen op 29 september. Robbert, Michael, Kees, Madelon, Frank, Henk-Jan: Succes met de laatste loodjes! Eefje, Nicoline, Sanne, Jeroen, Joost en Jorinde, bedankt voor alle mooie momenten en vooral jullie geduld tijdens al dat geouwehoer over wetenschap. Arjan en Mark, we kennen elkaar al vanaf de kleuterschool en zien elkaar nog steeds regelmatig. Ik vind dat heel bijzonder, en hoop dan ook dat we in de toekomst nog steeds onze avondjes kunnen plannen. Mark, wij zien elkaar bovendien nog vaak op de racefiets tijdens een koers of training. Als een echte regelneef kan ik jou de taak als paranimf wel toevertrouwen. Niet dat je veel hoeft te doen overigens.

Nu we het toch over fietsen hebben komen we gelijk bij mijn grootste passie (verslaving mag je het ook noemen). Een aantal mede-verslaafden wil ik graag bedanken voor de vele tochten die er in binnen- en buitenland gemaakt zijn. Als eerste: De ONZE-ploeg dan wel ‘Grupetto’. Bedankt voor alle intensieve kilometers! Ook UWTC de Domrenner, de studentenclub waar ik de laatste jaren mijn wedstrijdjes voor rijd, wil ik bedanken voor de vele mooie (sportieve) momenten. Dan hebben we ook nog het dinsdagavondje-clubje met in wisselende samenstelling: Hélène, Gerco, Ragna, Jeroen, Jasper, Wanda en Jan-Willem. Het was altijd leuk om met jullie na het werk nog even lekker door de polder te rossen.

Tot slot natuurlijk nog mijn familie. Paps en Mams, bedankt voor jullie onvoorwaardelijke steun en liefde. Zonder jullie was ik nooit zover gekomen. Tegen de rest van de familie zou ik willen zeggen: “Ai d'r niet uut goat dan kom iej ok nerges”. Of te wel: Kom lekker een biertje drinken op mijn feest! Ook mijn schoonfamilie mag ik natuurlijk niet vergeten. Kees en Gonny, François en Astrid, de Brabantse gezelligheid die jullie altijd meebrengen wordt erg gewaardeerd!

Uiteraard moet ik nog 1 persoon in het bijzonder bedanken, mijn vriendin Kristan. Ik ben er trots op dat jij straks achter me staat tijdens mijn openbare verdeding. We hebben samen al vele leuke dingen meegemaakt, maar dit wordt toch ook weer een hoogtepuntje, net zoals jouw promotie volgend jaar. Ik hoop dat we samen een mooie (wetenschappelijke) toekomst tegemoet gaan!

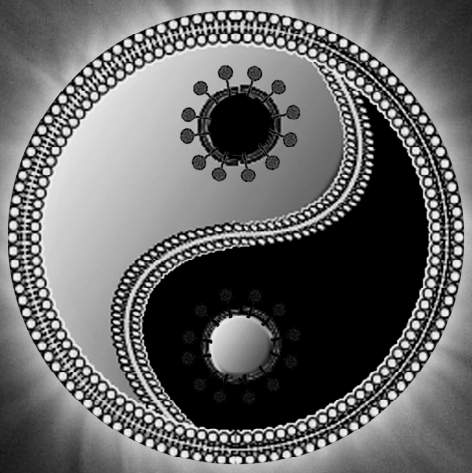

Curriculum Vitae

Matthijs Raaben werd geboren op 13 oktober 1980 te Groenlo. In 1999 behaalde hij het VWO diploma aan het Erfgooiers College in Huizen. Datzelfde jaar begon hij met de studie Medische Biologie aan de Universiteit Utrecht. Na het behalen van het propedeuse in 2000, werden tijdens zijn opvolgende master studie “Biology of Disease” wetenschappelijke stages uitgevoerd aan de Universiteit van Utrecht bij achtereenvolgens; de vakgroep Virologie van de Veterinaire Faculteit onder begeleiding van T. Würdinger en Dr. M.H. Verheije, en de vakgroep Biochemie van Membranen, Faculteit Scheikunde onder begeleiding van H.A. Boumann en Dr. A.I.P.M. de Kroon. In oktober 2004 werd de master titel behaald. Vanaf november 2004 werkte hij als assistent in opleiding bij de afdeling Virologie aan de Veterinaire Faculteit van de Universiteit Utrecht. Onder begeleiding van Dr. C.A.M. de Haan werd het onderzoek verricht zoals beschreven in dit proefschrift.

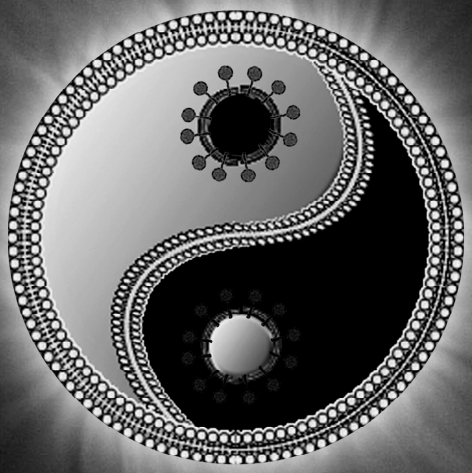

List of Publications

1. **de Haan, C. A., E. Te Lintelo, Z. Li, M. Raaben, T. Würdinger, B. J. Bosch, and P. J. Rottier.** Cooperative involvement of the S1 and S2 subunits of the murine coronavirus spike protein in receptor binding and extended host range. 2006, J Virol 80:10909-18.
2. **Raaben, M., A. W. Einerhand, L. J. Taminiau, M. van Houdt, J. Bouma, R. H. Raatgeep, H. A. Buller, C. A. de Haan, and J. W. Rossen.** Cyclooxygenase activity is important for efficient replication of mouse hepatitis virus at an early stage of infection. 2007, Virol J 4:55.
3. **Raaben, M., M. J. Groot Koerkamp, P. J. Rottier, and C. A. de Haan.** Mouse hepatitis coronavirus replication induces host translational shutoff and mRNA decay, with concomitant formation of stress granules and processing bodies. 2007, Cell Microbiol 9:2218-29.
4. **Raaben, M., M. J. Groot Koerkamp, P. J. Rottier, and C. A. de Haan.** Type I interferon receptor–independent and –dependent host transcriptional responses to mouse hepatitis coronavirus infection *in vivo*. 2009, BMC Genomics 10:350.
5. **Raaben, M., H. J. Prins, A. C. Martens, P. J. Rottier, and C. A. de Haan.** Non-invasive imaging of mouse hepatitis coronavirus infection reveals determinants of viral replication and spread *in vivo*. 2009, Cell Microbiol 5:825–841.
6. **Raaben, M., P. Whitley, D. Bouwmeester, R. A. Setterquist, P. J. Rottier, and C. A. de Haan.** 2008. Improved microarray gene expression profiling of virus-infected cells after removal of viral RNA. BMC Genomics 9:221.
7. **Verheije, M. H., M. Raaben, M. Mari, E. G. Te Lintelo, F. Reggiori, F. J. van Kuppeveld, P. J. Rottier, and C. A. de Haan.** Mouse hepatitis coronavirus RNA replication depends on GBF1-mediated ARF1 activation. 2008, PLoS Pathog 4:e1000088.
8. **Würdinger, T., M. H. Verheije, M. Raaben, B. J. Bosch, C. A. de Haan, V. W. van Beusechem, P. J. Rottier, and W. R. Gerritsen.** Targeting non-human coronaviruses to human cancer cells using a bispecific single-chain antibody. 2005, Gene Ther 12:1394-404.

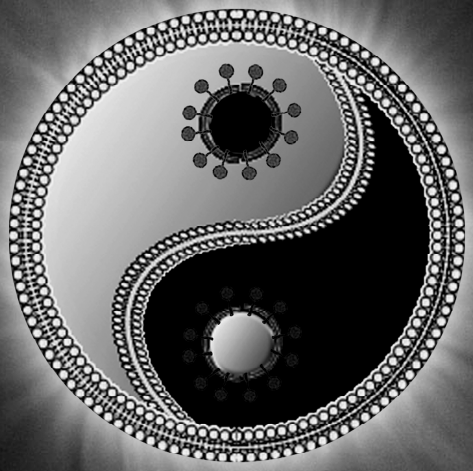

Conference Proceedings

Oral Presentations:

M.Raaben. **Bioluminescence Imaging of Coronavirus-Infected Mice.**
Dutch Annual Virology Symposium. 7 March 2008, Amsterdam, The Netherlands.

M.Raaben. **Bioluminescence Imaging of Coronavirus-Infected Mice.**
11th International Symposium on Nidoviruses. 22-27 June 2008, Oxford, UK.

M.Raaben. **Type I Interferon Receptor-Independent and -Dependent Host Transcriptional Responses to Mouse Hepatitis Coronavirus Infection *in Vivo*.**
28th Annual Meeting of the American Society for Virology.
11-15 July 2009, Vancouver, Canada.

Poster Presentations:

M. Raaben, L. Pelkmans, E. Krausz, E. Fava, P.J.M. Rottier, C.A.M. de Haan. **Functional Genomics of Coronavirus-Host Interactions Using a High-Throughput siRNA Strategy.**
The 5th major European Congress of the European Life Scientist Organization (ELSO).
3-6 September 2005, Dresden, Germany.

M. Raaben, M.J.A. Groot-Koerkamp, P.J.M. Rottier, C.A.M. de Haan. **Mouse Hepatitis Coronavirus Replication Induces Host Translational Shutoff and mRNA Decay, Concomitant with Formation of Stress Granules and Processing Bodies.**
The 3rd EMBL Biennial Symposium: From Functional Genomics to Systems Biology.
14-17 Oktober 2006, Heidelberg, Germany.

M. Raaben, M.J.A. Groot-Koerkamp, P.J.M. Rottier, C.A.M. de Haan. **Mouse Hepatitis Coronavirus Replication Induces Host Translational Shutoff and mRNA Decay, Concomitant with Formation of Stress Granules and Processing Bodies.**
The 8th International Symposia on Positive-Strand RNA Viruses.
26-30 May 2007, Washington, D.C., U.S.A.